# THERMALLY-REACTIVE CONJUGATED POLYMERS

by

Xu Han
B. E., Beijing University of Chemical Technology, 2001

THESIS SUBMITTED IN PARTIAL FULFILLMENT OF
THE REQUIREMENTS FOR THE DEGREE OF

DOCTOR OF PHILOSOPHY

In the
Department
of Chemistry



SIMON FRASER UNIVERSITY

Spring 2009

# APPROVAL

**Name:** **Xu Han**

**Degree:** **Doctor of Philosophy**

**Title of Thesis:** **Thermally-Reactive Conjugated Polymers**

**Examining Committee:**

**Chair:** **Dr. Erika Plettner**
Associate Professor, Department of Chemistry

---

**Dr. Steven Holdcroft**
Senior Supervisor

Professor, Department of Chemistry

---

**Dr. Zuo-Guang Ye**
Supervisor

Professor, Department of Chemistry

---

**Dr. David Vocadlo**
Supervisor

Associate Professor, Department of Chemistry

---

**Dr. Byron Gates**
Internal Examiner

Assistant Professor, Department of Chemistry

---

**Dr. Frederik C. Krebs**
External Examiner

Senior Scientist

Polymers for Energy Technology Programme

Technical University of Denmark

**Date Defended/Approved:** January 19, 2009

# Declaration of
# Partial Copyright Licence

# ABSTRACT

π-Conjugated polymers (πCPs) are promising active materials in application areas of organic microelectronics such as light-emitting devices (LEDs), thin-film transistors, and photovoltaic (PV) cells. A crucial requirement to implement this emerging technology is the reproducible deposition of active material in a spatially-controlled fashion. This thesis research concerns the study of thermally-reactive πCPs and 2D deposition of these materials. The technique of choice depends on the material under consideration, the substrate, and the intended application or research objective. Chemically-amplified soft lithography and direct thermal lithography were used to pattern polyfluorenes (PFs) to investigate their potential application as LEDs. Topographical control of active materials is also demonstrated using polymer blends for the application of PV cells.

Thermally-reactive PFs containing tetrahydropyran (THP) functional groups have been synthesized. The removal of the THP groups causes the polymers to become insoluble in normal organic solvent. Chemically-amplified soft lithography was used to pattern the luminescent polymers. However, these PFs may suffer from a degradation of fluorescence colour purity due to fluorenone defects, which are introduced by photo-oxidation and/or thermal oxidation process, or during device fabrication. Therefore, a series of thermally-reactive PFs exhibiting enhanced oxidative stability were synthesized. These

PFs, bearing aromatic groups directly attached to the 9-site carbon, eliminate the formation of fluorenone defects. Direct thermal lithography was used to pattern these PFs.

A facile method for preparing nano/micro-sized πCPs from polymers bearing thermally-cleavable THP groups is investigated. The feature size of the πCP formed is dependent on parameters such as choice of solvent, solution concentration, polymer blends composition, and the nature of the polymer(s) used. Features as small as 150 nm are demonstrated, and much smaller features are possible with further optimization of conditions. The insoluble nano-structured πCP has been exploited as a donor layer in polymeric PV cells following spin-casting an electron acceptor layer on top of the donor layer to form a nano-sized donor-acceptor heterojunction. The nano-structured πCP donor-acceptor layers provide an advantage over molecularly blended films in that electron acceptor is not isolated in the donor film, and vice versa, which may circumvent charge trapping and thus improve the device efficiency.

**Keywords:** π-conjugated polymers; polymeric photovoltaic devices; thermally-reactive polymers; luminescent polymers; polyfluorenes; polythiophenes.

**Subject Terms:** synthesis of π-conjugated polymers; thermally-reactive π-conjugated polymers; luminescent properties of π-conjugated polymers; patterning of π-conjugated polymers; photovoltaic properties of π-conjugated polymers.

*To my husband, Guangqing Jia,*

*my parents,*

*and my daughter, Siyue Jia*

# ACKNOWLEDGEMENTS

I would like to thank:

My senior supervisor Prof. Steven Holdcroft for providing the opportunity to study and work in his laboratory; for his supervision, research assistantships during my study; and for his guidance throughout the thesis research.

My supervisory committee Prof. Zuo-Guang Ye and Prof. David Vocadlo for serving on my supervisory committee and their great ideas to improve my thesis. My previous supervisory committee member Prof. Jason Clyburne for serving on my supervisory committee.

Dr. Jianfei Yu for preparing regioregular poly(3-(2-(2-tetrahydropyranyloxy)ethyl)thiophene).

Dr. Tim Peckham, Dr. Xiwen Chen, and Ms. Emily M. W. Tsang for proof-reading this manuscript.

Mrs. Marcy Tracey for her assistance with NMR training, Dr. Jusroop Mattu and Dr. Tianhong Xu for their assistance with atomic force microscopy, and Dr. Marianne Rodgers and Mr. Dave Edwards for there assistance in acquiring some of the thermal gravimetric analysis data.

Past and present members of the Holdcroft research group for their friendship and useful discussions.

Simon Fraser University and the Natural Sciences and Engineering Research Council of Canada for financial support.

Eastman Kodak Company for assistance in laser patterning of polymers.

# TABLE OF CONTENTS

# LIST OF FIGURES

# LIST OF SCHEMES

# LIST OF TABLES

# LIST OF ABBREVIATIONS

| | |
|---|---|
| **a** | Absorptivity |
| **A** | Absorbance |
| **Abs** | Absorbed |
| **ABS** | Photon absorbance |
| **AFM** | Atomic force microscopy |
| **AT** | Alkylthiophene |
| **b** | Path length of radiation |
| **BHJ** | Bulk heterojunction |
| **BPY** | 2,2’-Bipyridyl |
| **c** | Speed of light |
| **C** | Concentration |
| **CIE** | Commission internationale de l'eclairage |
| **COD** | 1,5-Cyclooctadiene |
| **CSA** | Camphorsulfonic acid |
| **d** | Distance of motion |
| **DC** | Direct current |
| **De- πCPs** | Deprotected πCPs |
| **De-PTHPEF** | Deprotected PTHPEF |
| **De-PTHPET** | Deprotected PTHPET |

| | |
|---|---|
| **diBrF** | 2,7-Dibromofluorene |
| **diBrHET** | 2,5-Dibromo-3-(2-hydroxy)ethylthiophene |
| **diBrTHPEF** | 2,7-Dibromo-9,9'-di(2-(2'-tetrahydropyranyloxy)ethyl)fluorene |
| **diBrTHPET** | 2,5-Dibromo-3-(2-(2-tetrahydropyranyl-2-oxy)ethyl)thiophene |
| **diHF** | 9,9'-Dihexylfluorene |
| **diHFTMB** | 9,9'-Dihexylfluorene-2,7-bis(trimethyleneborate) |
| **DMF** | Dimethylformamide |
| **dppp** | Diphenylphosphinopropane |
| **DTP** | Direct thermal patterning |
| **e** | Electron or electrical charge |
| **EDOT** | 3,4-Ethylenedioxythiophene |
| **Em** | Emitted |
| **EML** | Emissive layer |
| **ε** | Molar absorptivity |
| **EQE** | External quantum efficiency |
| **η** | Power conversion efficiency |
| **ETL** | Electron transport layer |
| **f** | Force |
| **FETs** | Field-effect transistors |
| **FF** | Fill factor |
| **FWHM** | Full width at half maximum height |
| **GPC** | Gel permeation chromatography |

| | |
|---|---|
| **GRIM** | Grignard Metathesis |
| **h** | Planck's constant |
| **HOMO** | Highest occupied molecular orbital |
| **HTL** | Hole transport layer |
| **I** | Integrated emission area under a peak |
| **IBPF** | 4,4'-Dimethyldiphenyliodonium hexafluorophosphate |
| $\mathbf{I_m}$ | Current at maximum power output |
| **IQE** | Internal quantum efficiency |
| **IR** | Infrared |
| $\mathbf{I_{sc}}$ | Short-circuit current |
| **ITO** | Indium-tin oxide |
| $\mathbf{J_m}$ | Current density at maximum power output |
| $\mathbf{J_{sc}}$ | Short-circuit current density |
| **k** | Force constant |
| **λ** | Wavelength |
| **LEDs** | Light-emitting devices |
| **LEP** | Light-emitting polymer |
| **LDA** | Lithium diisopropylamine |
| **LUMO** | Lowest unoccupied molecular orbital |
| **MALDI-TOF** | Matrix-assisted laser desorption/ionization time-of-flight mass spectroscopy |
| **MEH-PPV** | Poly(2-methoxy-5-(2'-ethylhexyloxy)-*p*-phenylenevinylene) |
| **MIMIC** | Micromolding in capillaries |

| | |
|---|---|
| **μCP** | Microcontact printing |
| **n** | Refractive index of the solvent |
| **NBS** | N-bromosuccinimide |
| **NIR** | Near-infrared |
| **NMR** | Nuclear magnetic resonance |
| **OLEDs** | Organic light-emitting devices |
| **p** | Phonon |
| **P, $P_1$** | Radiant power |
| **P3AT** | Poly(3-alkylthiophene) |
| **P3CT** | Poly-3-carboxydithiophene |
| **P3HT** | Poly(3-hexylthiophene) |
| **P3MHOCT** | Poly-(3-(2-methylhexan-2-yl)-oxy-carbonyldithiophene) |
| **PA** | Poly(acetylene) |
| **PAF** | Poly(9,9'-dialkylfluorene) |
| **PCBM** | [6,6]-Phenyl-$C_{61}$-butyric acid methyl ester |
| **[70]PCBM** | [6,6]-Phenyl-$C_{71}$-butyric acid methyl ester |
| **PCE** | Power conversion efficiency |
| **PCz** | Poly(carbazole) |
| **PDMS** | Polydimethylsiloxane |
| **PEDOT** | Poly-3,4-ethylenedioxythiophene polystyrenesulfonate |
| **PF** | Poly(fluorene) |
| **PFO** | Polydioctylfluorene |

| | |
|---|---|
| **p(HEMA)** | Poly(2-hydroxyethyl methacrylate) |
| **$\Phi_{EL}$** | External quantum efficiency |
| **$\Phi_{fl}$** | Fluorescence quantum yield |
| **$\Phi_{PL}$** | Quantum yield of photoluminescence |
| **πCP** | π-Conjugated polymer |
| **PL** | Photoluminescence |
| **PLEDs** | Polymer light-emitting devices |
| **$P_m$** | Maximum electrical power generation |
| **PMMA** | Poly(methylmethacrylate) |
| **$P_0$** | Incident optical power |
| **PPE** | Poly(*p*-phenylene ethynylene) |
| **$PPh_3$** | Triphenylphosphine |
| **PPP** | Poly(*p*-phenylene) |
| **PPV** | Poly(*p*-phenylene vinylene) |
| **PPy** | Poly(pyrole) |
| **PS** | Polystyrene |
| **PSS** | Polystyrenesulfonate |
| **PT** | Poly(thiophene) |
| **PTHPEF** | Poly[9,9'-di(2-(2-tetrahydropyranyloxy)ethyl)fluorene] |
| **PTHPEF-alt-diHF** | Poly[9,9'-di(2-(2-tetrahydropyranyloxy)ethyl) fluorene-alt-9,9'-dihexylfluorene] |
| **PTHPEF-alt-T** | Poly[9,9'-di(2-(2-tetrahydropyranyloxy)ethyl) fluorene-alt-thiophene] |

| | |
|---|---|
| **PTHPEF-co-THPET** | Poly[9,9'-di(2-(2-tetrahydropyranyloxy)ethyl) fluorene-co-(2-(2-tetrahydropyranyloxy)ethyl)thiophene] |
| **PTHPET** | Poly[3-(2-(2-tetrahydropyranyloxy)ethyl)thiophene)] |
| **PV** | Photovoltaic |
| **R** | Reflectance |
| **RGB** | Red, green, blue |
| **s** | Standard |
| **$S_0$** | Ground singlet state |
| **$S_1$** | First excited singlet state |
| **SSH** | Su-Schrieffer-Heeger |
| **T** | Transmittance |
| **$T_1$** | First excited triplet state |
| **TAG** | Thermal acid generator |
| **TGA** | Thermal gravimetric analysis |
| **THF** | Tetrahydrofuran |
| **THP** | Tetrahydropyran(yl) |
| **THPEF** | 9,9'-Di(2-(2-tetrahydropyranyloxy)ethyl)fluorene |
| **THPET** | 3-(2-(2-Tetrahydropyranyloxy)ethyl)thiophene) |
| **TMEBT** | 2,5-Bis(tetramethylethyleneborate)thiophene |
| **u** | Unknown |
| **UV-vis** | Ultraviolet - visible |
| **$V_{oc}$** | Open-circuit voltage |
| **$V_m$** | Voltage at maximum power output |

# CHAPTER 1:

# INTRODUCTION TO Π-CONJUGATED POLYMERS

## 1.1 Overview of π-Conjugated Polymers

Polymers have traditionally been considered as good electrical insulators. However, conjugated polymers possess extended systems containing delocalized electrons arising from their alternating structure of single and double bonds. In 1977, MacDiarmid, Shirakawa, and Heeger brought the unique properties of conjugated polymers to the fore when they discovered that chemical doping of polyacetylene with oxidizing agents (e.g., $I_2$, $FeCl_3$, and $AsF_5$) results in increased electronic conductivity by several orders of magnitude.[1] This work has led them to win the 2000 Nobel Prize in Chemistry. Since then, electronically conducting and semiconducting materials based on conjugated polymers have become the subject of multidisciplinary research.

The properties of conjugated polymers include non-linear optical behaviour, electronic conductivity, photoluminescence, electroluminescence, thermochromism, electrochromism, and exceptional mechanical properties, i.e., tensile strength.[2] Typical conjugated polymers include polyacetylene (PA), poly(*p*-phenylene) (PPP), polythiophene (PT), poly(*p*-phenylene vinylene) (PPV), polypyrole (PPy), polyfluorene (PF), polycarbazole (PCz), and poly(*p*-phenylene ethynylene) (PPE), as illustrated in **Figure 1.1**. Polymers composed of aromatic and heteroaromatic ring structures have been particularly outstanding from a material perspective. The early problem associated with the stability and solubility of such conducting and semiconducting polymers have largely been overcome using chemical intuition and experimentation. Conjugated polymers with improved solubility are suitable for structural

characterization and deposition using solution processing techniques, such as solution dipping, spin casting, drop casting, and printing methods.

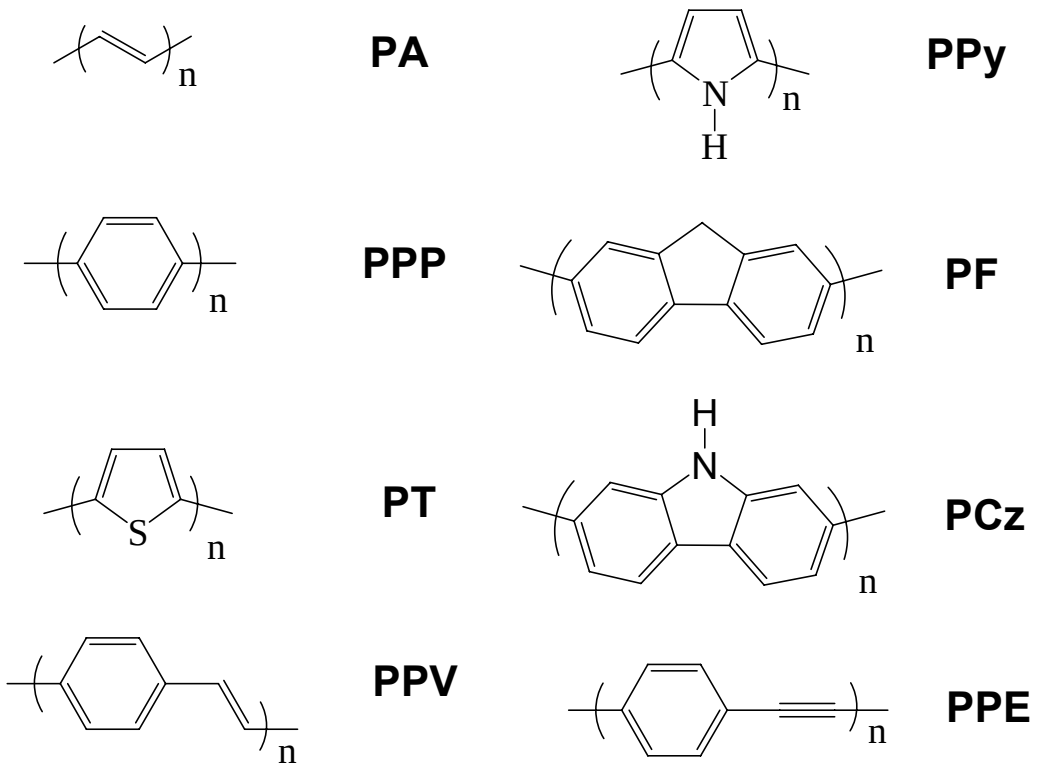


**Figure 1.1: Structures of typical conjugated polymers.**

Potential applications for conjugated polymers are primarily in the areas of organic electronics, opto-electronics, and electro-optics, including light-emitting devices (LEDs),[3] field-effect transistors (FETs),[4] photovoltaic (PV) devices,[5] polymer actuators,[6] and solid state lasers.[7] The field of organic electronic devices is rapidly expanding due to the promise of inexpensive materials, large-area, flexible, and lightweight devices, and device fabrication accompanied by

the wide variety of functionality of organic materials potentially available. Recently, polymer light-emitting devices (PLEDs) have reached commercial availability with improved performance. Significant progress has also been made in organic solar cells, for example, 5.0 % and 5.7 % of power conversion efficiency have been obtained for polymer (single junction)[8] and small molecule[9] based devices, respectively. However, considerable effort is still needed to optimize device architectures, enhance device efficiencies and overcome device degradation.

## 1.2 Structure of Conjugated Polymers

A chemically conjugated system is a system of atoms covalently bonded with alternating single and double or even triple bonds in a molecule of an organic compound. This system results in a general delocalization of the electrons across all of the adjacent parallel aligned p-orbitals of the atoms, which increases stability and thereby lowers the overall energy of the molecule. Conjugated polymers are characterized as an extended conjugated system containing delocalized π-electrons arising from their alternating structure of single and double bonds along polymer chains. The unique electric and optical properties of conjugated polymers are attributed to the overlap of p-orbitals and delocalized π-electrons. For example, strong absorption of light in the visible region is one of the special features of molecules containing conjugated repeat units, which is due to the lower energy required by the π-electrons to promote them to the excited state, since they are less tightly bound to the carbon nuclei.

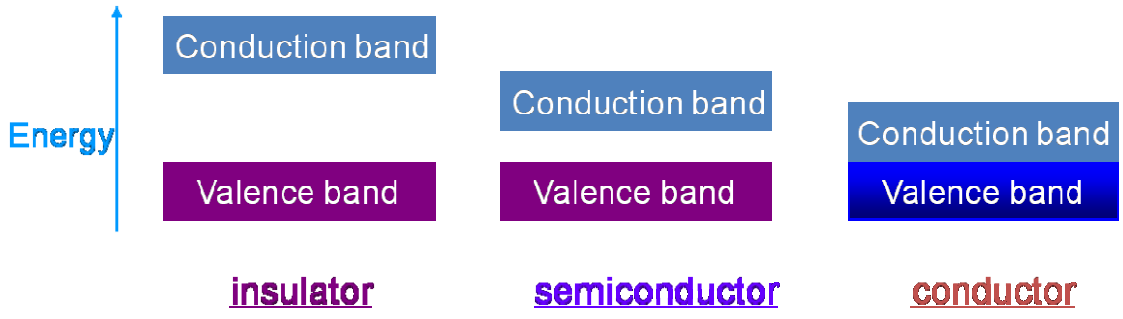


**Figure 1.2: Band structures of an insulator, semiconductor, and conductor.**

The diagram of band structures of an insulator, semiconductor, and conductor is shown in **Figure 1.2**. In general, the valence band is the lower band of allowed states. Since electrons have a tendency to fill the lowest available energy states, the valence band is always nearly completely filled with electrons, especially at temperatures near 0 K. As the temperature rises or light is introduced, electrons can absorb the energy and leave the valence band to rise up to the conduction band. When an electron gains enough energy to get to the upper band, it is free to move. It thus becomes a carrier and, therefore, conductivity increases. When electrons leave the valence band, they also leave behind a hole, which migrates in the material.

An insulator is a poor conductor as it requires a lot of energy >5 to 8 eV to promote the electrons into the conduction band. A metal is an excellent conductor because, at room temperature, it has electrons in its conduction band. This is due to a narrow or nonexistent band gap that results in the conduction band overlaps with the valence band. The reason semiconductors are so popular

is because they represent an intermediary position between a metal and an insulator. The band gap is wide enough such that current is not going through it at all times, but narrow enough so that it does not take much energy to move electrons into the conduction band in order to induce a current. In conducting polymers, the valence band represents the π band (the bonding orbitals) and the conduction band represents the π* band (the anti-bonding orbitals).

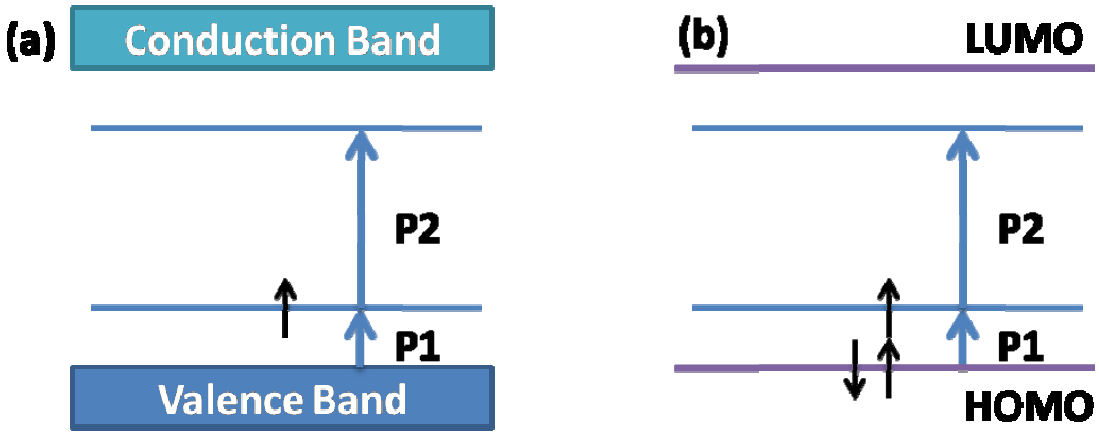


**Figure 1.3: Various models describing polaron levels and optical transitions for the positive polaron: (a) electron–phonon (SSH) model, (b) molecular orbital diagram.** [10]

It has been reported that chemical doping or electrical charge injection results in the formation of polarons in π-conjugated systems. The diagram of two models used to describe polarons in π-conjugated semiconductors is shown in **Figure 1.3**. **Figure 1.3(a)** depicts the electron–phonon (e–p) or Su-Schrieffer-Heeger (SSH) model.[10] The e–p coupling causes a gap to exist between valence

and conduction band. In the singly charged system, two localized polaron levels appear inside the gap. Two optical transitions, interpreted as the P1 and P2 transitions, were found experimentally.[11] **Figure 1.3(b)** depicts the molecular orbital diagram, where HOMO and LUMO are the highest occupied and lowest unoccupied molecular orbitals, respectively. These models are usually applied to a single, isolated chain. The effects of intrachain interaction on polarons are relatively easier to be understood. However, the effects of interchain interaction on polarons[12] in real sample films are not yet sufficiently understood.

## 1.3 Synthesis of Conjugated Polymers

Various π-conjugated polymers have been obtained using electrochemical and chemical polymerization. These polymers are electrochemically active, electrically conductive, and light-emitting. In this thesis, a selection of chemical polymerization methodologies are highlighted, since they are related to the work in the following chapters.

### 1.3.1 Chemical Oxidative Coupling Polymerization

Chemical oxidative coupling polymerization is generally referred to as the $FeCl_3$ method. This approach is a straightforward and versatile method for synthesizing conjugated polymers such as poly(3-alkylthiophene)s (P3ATs) and poly(9,9'-dialkylflourene)s (PAFs). It was developed by Yoshino and co-workers,[13] for the large-scale synthesis of P3ATs, using Lewis acids catalysts, such as $FeCl_3$, $MoCl_3$, and $RuCl_3$. In this approach, the 3-alkylthiophene monomer is dissolved in a suspension of $FeCl_3$ in $CHCl_3$ or other appropriate

solvents. $FeCl_3$ oxidizes the 3-alkylthiophene monomer to produce radical centers, predominantly in the 2- and 5- positions of the thiophene, which propagates to form a black P3AT precipitate. The resulting polymer is in its doped form which can be reduced by subsequent treatment with reducing agents, such as ammonia. The molecular weights of P3ATs are reasonably high, but with a wide polydispersity. However, this approach suffers from producing polymers with structural defects which may be undesirable for some applications.[14] It has been reported that these structural defects may be minimized by performing the reactions at lower temperatures, or using vanadium-based oxidants.[15] Nevertherless, it is still not suitable for the preparation of polythiophenes or polyfluorenes bearing acid-labile functionalities, since HCl is a product of the oxidation reaction.

### 1.3.2 Yamamoto Coupling Polymerization

Yamamoto coupling polymerization[16] is a convenient and efficient approach to synthesize conjugated polymers. The Ni-promoted synthetic method was developed by using the polycondensation of dihaloaromatic compounds. When the polymerization is carried out using $Ni(0)L_m$, the polymerization is considered to proceed through the following fundamental reactions, as illustrated in **Scheme 1.1**.[17]

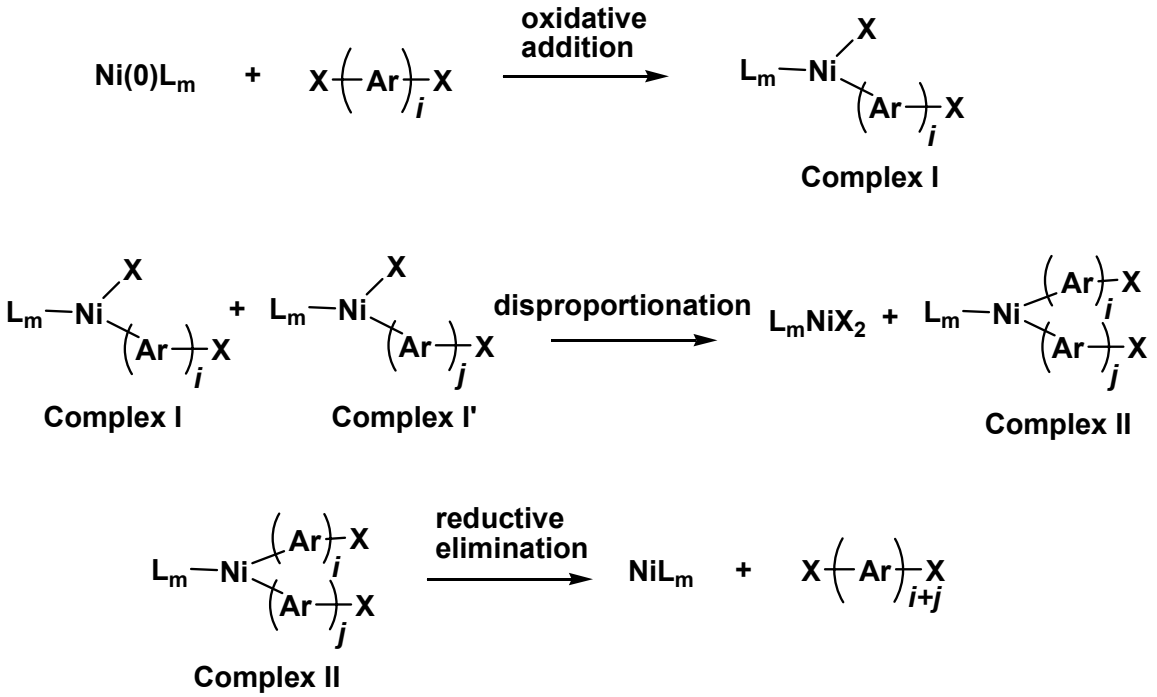


**Scheme 1.1: The mechanism of Yamamoto coupling polymerization.**

The first step is oxidative addition of C-X to Ni(0)$L_m$. The second step is disproportionation. Thirdly, diorganonickel (II) complexes $NiR_2L_m$ undergo reductive coupling (or reductive elimination) reactions to give R-R. The coordination of molecules, such as aromatic compounds, leading to the back-donation from the central metal facilitates the reductive elimination of R-R. When the Ni-C bond is highly stabilized, the complexes I and II as well as a complex of the type $L_m$(X)Ni-Ar-Ni(X)$L_m$ can be isolated. Thus, the mechanism of Yamamoto coupling polymerization for organometallic polycondensation is summarized as i) oxidative addition, ii) back-donation, and iii) reductive elimination.[18] A general example of dehalogenation coupling of fluorene monomer with a stoichiometric amount of $Ni(COD)_2$ (COD = 1,5-cyclooctadiene) is shown in **Scheme 1.2**.

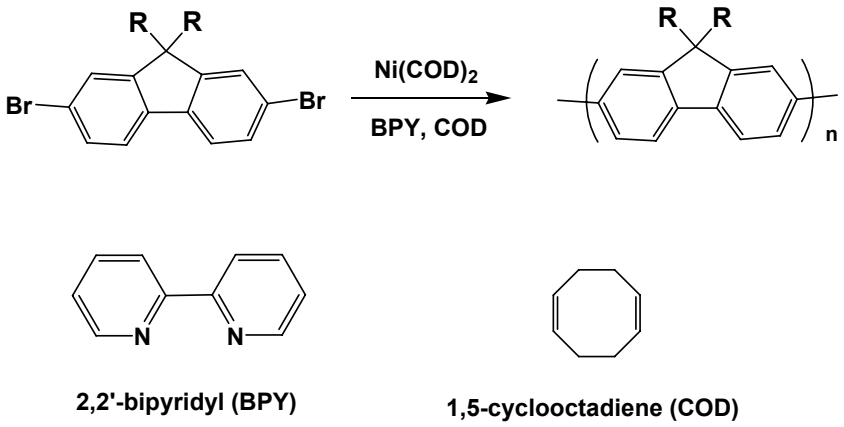


**Scheme 1.2: Synthesis of poly(9,9'-dialkylfluorene) via Yamamoto coupling polymerization.**

This organometallic polycondensation approach has been successfully used in polymerizing several classes of conjugated polymers, for example, PTs, PFs, PPPs, PPys, and polythiazoles. The Yamamoto coupling reaction employs a relatively large amount of Ni(0) complex (stoichiometric amount), since the Ni(0) complex works as a reagent instead of a catalyst in this reaction. The Ni(0) complex reagent is oxidized and then reduced during the reaction, but does not return to the Ni(0) state, so it loses the reactivity after the reaction. In addition, the Ni(0) complex is extremely sensitive to ambient air and moisture, so the reaction has to be prepared under a strictly inert atmosphere.

The molecular weight of the π-conjugated polymers prepared by Yamamoto coupling seems to be dependant on the solubility and crystallinity of the polymers.[18] There is a trend that crystalline polymers have a lower molecular weight whereas less crystalline species (especially those with an alkyl chain) propagate to form a higher molecular weight polymer.

### 1.3.3 Suzuki Coupling Polymerization

The Suzuki reaction is an organic reaction of an aryl- or vinyl-boronic acid with an aryl- or vinyl-halide catalyzed by a palladium(0) complex.[19] It is widely used to synthesize olefins, styrenes, and substituted biphenyls. First published in 1979 by Akira Suzuki, the Suzuki reaction couples boronic acids (containing an organic part) to halides.[20] **Scheme 1.3** shows the first published Suzuki Coupling, which is the palladium-catalyzed cross coupling between an organoboronic acid and an aryl halide. Recent catalyst and method developments have broadened the possible applications enormously, so that the scope of the reaction is not restricted to aryls, but also includes alkyls, alkenyls, and alkynyls. The reaction relies on a palladium catalyst such as tetrakis(triphenylphosphine)palladium(0) to effect part of the transformation. The palladium catalyst (more strictly a pre-catalyst) is 4-coordinate, and usually involves phosphine ligands. Potassium trifluoroborates and organoboranes or boronate esters may be used in place of boronic acids. Some pseudohalides (for example triflates) may also be used as coupling partners.

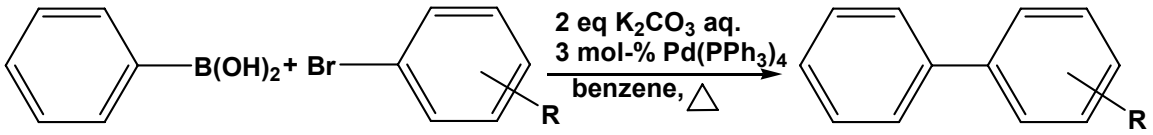


**Scheme 1.3: The first Suzuki reaction - the palladium-catalyzed cross coupling between organoboronic acid and halides.**

The mechanism of the Suzuki reaction viewed from the perspective of the

palladium catalyst, is shown in **Scheme 1.4**. The first step is the oxidative addition of palladium to the halide **2** to form the organo-palladium species **3**. Reaction with base gives intermediate **4**, which via transmetallation with the boronate complex **6** forms the organopalladium species **8**. Reductive elimination of the desired product **9** restores the original palladium catalyst **1**.

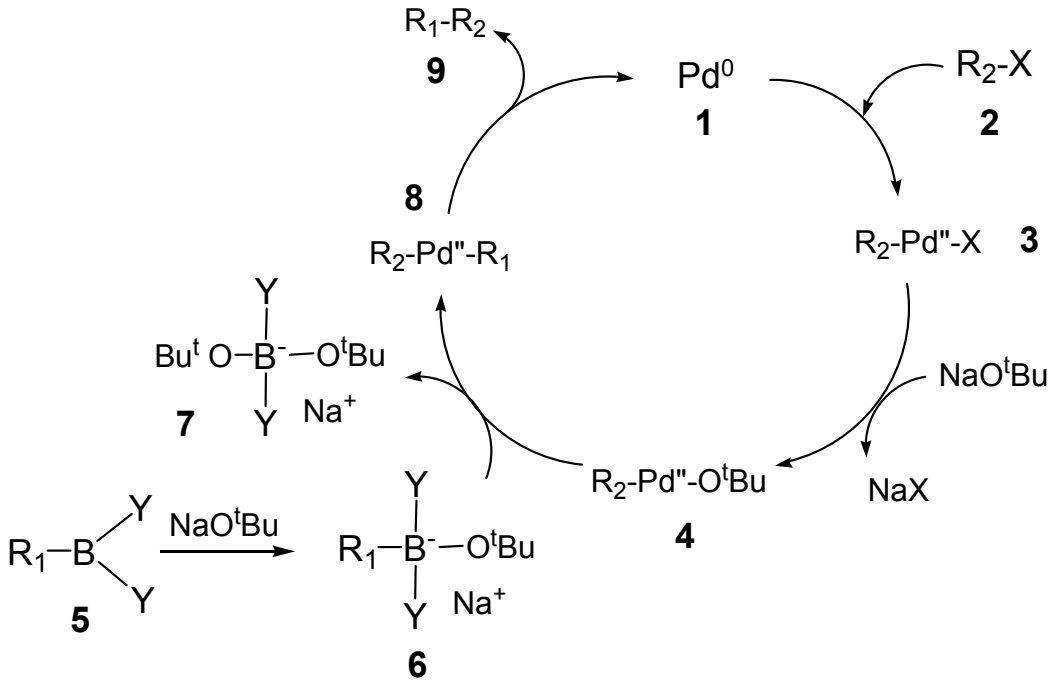


**Scheme 1.4: The mechanism of Suzuki reaction.**

Major advantages of the Suzuki reaction are the stability of the boron-reagents, the easy access to a broad variety boronic-acids through different synthetic pathways, the tolerance for different functional groups, and the less stringent experimental conditions (i.e., water insensitivity). The effects of the catalysts, ligands, solvents, and substrates have been investigated. The catalyst tetrakis(triphenylphosphine)palladium is the most common, but also other

homogeneous catalysts as well as immobilized or heterogeneous palladium-compounds have been used.

In a general Suzuki coupling polymerization, a diboronic acid (or ester) is coupled with a dibrominated aryl group in the presence of a base (i.e., $K_2CO_3$ or $Na_2CO_3$), as depicted in **Scheme 1.5**. Wegner and co-workers reported this approach in 1989 for the synthesis of well-defined, processable poly(p-phenylene)s.[21] This approach is quite easy and versatile, especially suited for the synthesis of alternating copolymers, such as flourene-based copolymers.

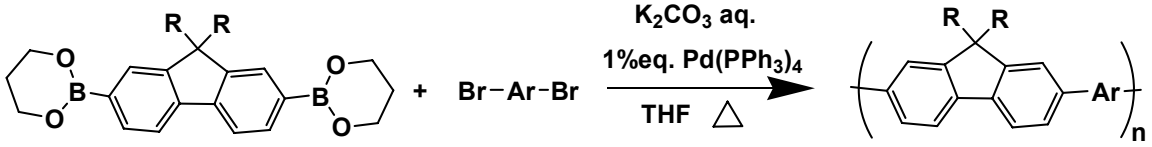


**Scheme 1.5: Synthesis of poly(9,9'-dialkylfluorene) copolymer via Suzuki coupling polymerization.**

### 1.3.4 Kumada Coupling Polymerization of Grignard Reagents

The Kumada Coupling or Corriu-Kumada coupling was the first Pd or Ni-catalyzed cross coupling reaction in organic chemistry between an alkyl or aryl Grignard reagent and an aryl or vinyl halocarbon.[22] This reaction is relevant to organic synthesis because it gives access to styrene containing compounds. The reaction type was reported independently by two groups in 1972, and was named after Makoto Kumada. The coupling of Grignard reagents with alkyl, vinyl or aryl halides under Ni-catalysis provides an economic transformation, but the reaction is limited to halide partners that do not react with organomagnesium

compounds. One example is in the industrial-scale production of styrene derivatives, and the Kumada Coupling is the method of choice for the low-cost synthesis of unsymmetrical biaryls.

The Nickel reaction mechanism for Ni(II) catalysts is a sequence of several steps [23]:

(i) Transmetallation: the dihalonickel catalyst reacts with the Grignard RMgX to form a diorganonickel intermediate $NiR_2L_2$ and a dihalonickel $NiX_2$.

(ii) Reductive elimination: reaction of $NiR_2L_2$ with the organohalide R'X forms the coupled product R-R together with the nickelorganohalide $NiR'XL_2$. In the overall reaction, this step is negligible because the active nickel compound is formed in catalytical amounts.

(iii) Transmetallation: in the first step of the catalytic cycle, nickelorganohalide $NiR'XL_2$ reacts with another equivalent of RMgX to mixed diorganonickel $NiRR'L_2$ compound and dihalonickel $NiX_2$.

(iv) Trans-cis isomerization: with substrates trans-dichloroethylene and phenylmagnesium chloride, the resulting stilbene is enriched in the cis isomer.

(v) Coordination: a new equivalent of organohalide R'-X adds face-on to the mixed dihalonickel complex.

(vi) Oxidative addition: The cross-coupled product R-R' is released with regeneration of nickelorganohalide $NiR'XL_2$.

The main steps in the mechanism for Ni(0) or Pd(0) catalysts are oxidative addition of the organohalide, transmetallation of the Grignard, and reductive elimination, as illustrated in **Scheme 1.6**. The advantage of this reaction is the direct coupling of Grignard reagents, which avoids additional reaction steps such as the conversion of Grignard reagents to zinc compounds for the starting materials in the Negishi Coupling.

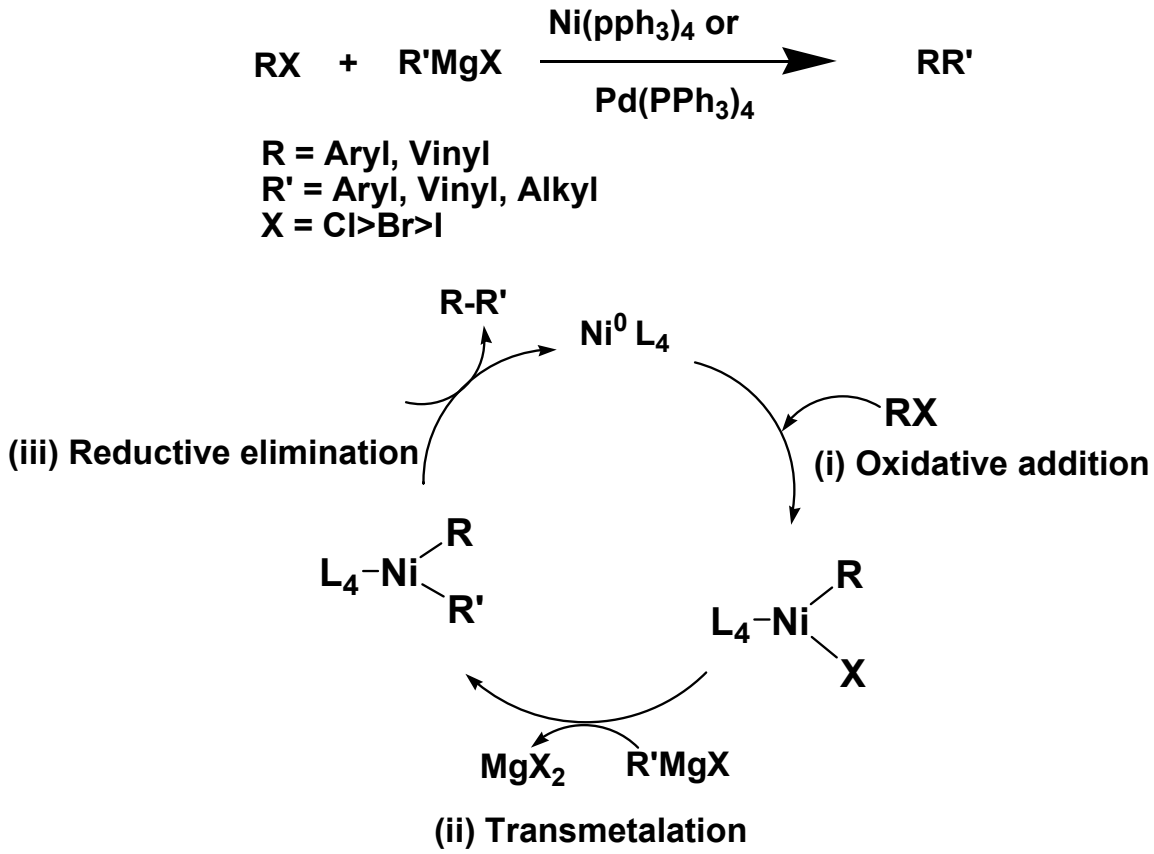


**Scheme 1.6: The mechanism of Kumada coupling reaction.**

In the past two decades, McCullough and co-workers investigated polymerization methods of P3ATs to prepare regio-regular P3ATs, where they discovered two methods which produced regio-regular (98 % head-to-tail

coupling) polymers: the McCullough method[24] and Grignard Metathesis.[25] These methods are illustrated in **Scheme 1.7** and are based on Kumada cross coupling reaction of 2-bromo-5-(magnesiobromo)-3-alkylthiophene (BrMgBrAT).

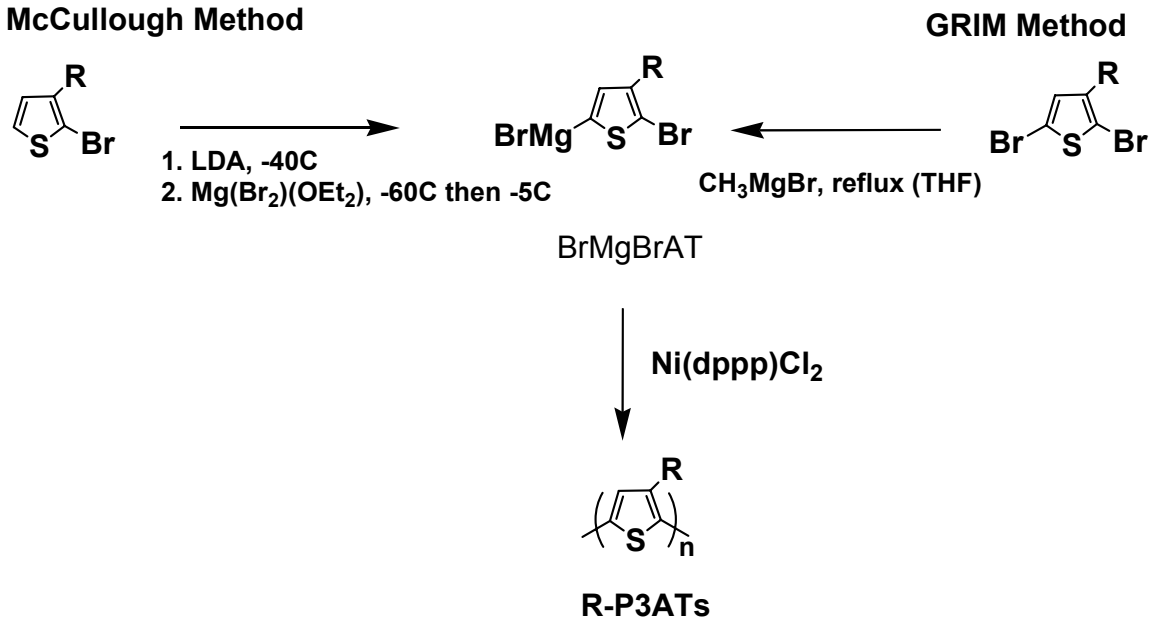


**Scheme 1.7: Synthesis of regio-regular P3ATs.**

## 1.4 Thermally-Reactive π-Conjugated Polymers

Thermally-reactive non-conjugated polymers have been the subject of interest in the last few decades due to their applications in adhesives, coating materials, medical devices, and especially microelectronics. Conventional microelectronic circuitry is often achieved by patterning polymer films by a technique known as chemical amplification. Acids released by the exposure radiation diffuse during the post-exposure bake step, thus the sensitivity of photoresists to the exposure energy can be increased.[26] This method can also be

employed in the design of thermally-reactive conjugated materials, but the electronic and optical properties of the conjugated polymer may be disrupted by the chemical amplification process. Thus, novel thermally-reactive conjugated materials and alternative methods of patterning need to be developed.

Thermally-reactive π-conjugated polymers are πCPs bearing thermally-cleavable groups, such as a carboxylic acid ester or tetrahydropyran (THP). These groups can be removed by thermal treatment or a catalyzed solid phase reaction to yield the corresponding deprotected π-conjugated polymer, which is insoluble in common organic solvents. In the context of thermally-reactive π-conjugated polymers, Yu *et al.* report the synthesis of several regioregular polythiophenes containing the 2-tetrahydropyranyl (THP) group.[27] In these polymers, THP groups are attached to the alkyl chain of a polythiophene. The deprotection temperature of these polymers is 200-300 °C. However, THP units can be cleaved at much lower temperature, ~130 °C, in the presence of a catalytic amount of acid. The acid-catalyzed elimination of dihydropyran from poly[3-(2-(2-tetrahydropyranyloxy)ethyl)thiophene)] (PTHPET) is illustrated in **Scheme 1.8**. Copolymers of PTHPET and 3-hexylthiophene were obtained to study the structure-property relationship of these thermally cleavable polymers. For the PTHPET homopolymer, an increased degree of conjugation persists upon removal of the thermally-cleavable THP group. However, copolymer films exhibit a melting transition and a subsequent decrease in coplanarity at high temperatures. This disorder prevails upon cooling due to either strong interchain H-bonding or the absence of crystallizable side chains. When the deprotection

reaction is carried out at lower temperatures, a high degree of π-delocalization is retained. A methodology reported to pattern thermally-reactive polythiophenes by soft lithography based on this chemistry is discussed in Section 1.6.3.

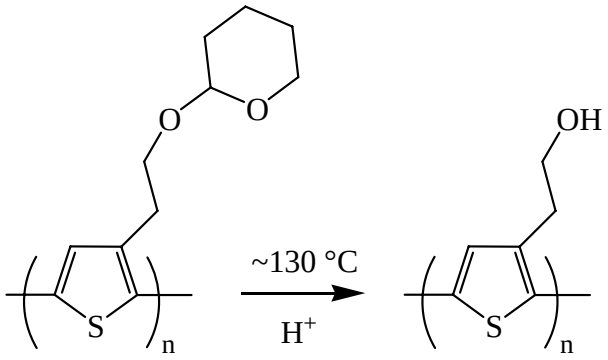


**PTHPET**
(soluble)

(insoluble)

**Scheme 1.8: Acid-catalyzed solid phase reaction of thermocleavable PTHPET.**

Thermally-reactive polymers are now being investigated in the fabrication of photovoltaic devices. Liu *et al.* reported the synthesis of a thermocleavable polythiophene carboxylic acid ester, poly-(3-(2-methylhexan-2-yl)-oxy-carbonyldithiophene) (P3MHOCT), which served as an interface layer between a $TiO_2$ electrode and poly-3-hexylthiophenes (P3HT) in a hybrid solar cell.[28] P3MHOCT was prepared by esterification of the carboxylic acid groups of thiophene with a tertiary alcohol and its subsequent polymerization. The polymer bearing alkyl ester groups is soluble in common organic solvents, thus solid thin films can be prepared by spin coating or drop casting. The ester groups can be removed to yield poly-3-carboxydithiophene (P3CT) by heating the film to ~200

°C, according to the reaction shown in **Scheme 1.9**, wherein the tertiary ester is removed, forming a free acid and an alkene as products. P3MHOCT was selected on the basis of several considerations: (i) the tertiary ester group can be removed at a relatively low temperature; (ii) the branched ester group contributes to a higher solubility, facilitating synthesis, purification, and processing; (iii) after thermal cleavage of the ester group, a polythiophene bearing electron withdrawing carboxylic acid groups remains, which allows tuning of the energy levels, enables the formation of a favorable interface between the polymer and $TiO_2$, and can potentially enhance the interfacial charge-transfer efficiency; (iv) the ability to change the solubility of P3MHOCT facilitates the preparation of multilayer devices. A hybrid solar cell device containing a layer of P3CT shows a 3-fold increase in photocurrent compared to the device without P3CT. The external quantum efficiency and power conversion efficiency of the device with P3CT are 12.6% and 1.10%, respectively. The enhancement in photocurrent of the device with P3CT may be attributed to several factors. The removal of solubilizing groups forms a higher chromophore density, manifesting in a higher light absorption coefficient of P3CT compared to that of P3HT. P3CT is likely to have a larger exciton diffusion length than P3HT, since the shorter average interchain distance in P3CT can contribute to a faster energy transfer from the excited polymer chain to the next. The possible chelation of -COOH groups to $TiO_2$ contributes to this enhancement by promoting forward interfacial electron transfer and eliminating sub-conduction band trap sites. It is also possible that

the enhancement in photocurrent is partially due to the cascade charge transfer along the LUMOs of P3HT, P3CT, and $TiO_2$.

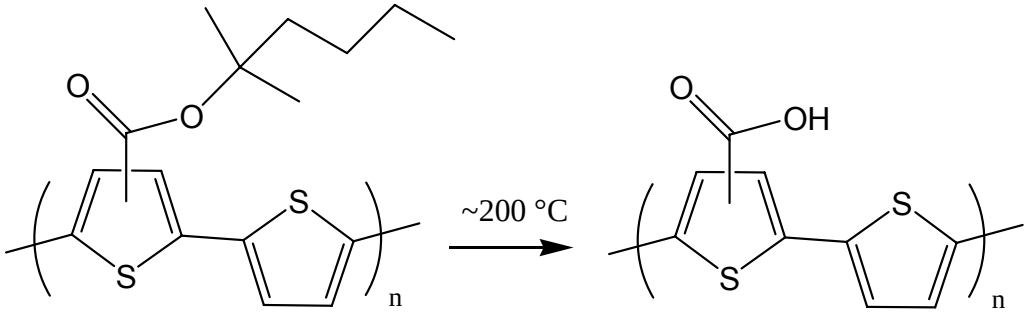


**P3MHOCT** (soluble) **P3CT** (insoluble)

**Scheme 1.9: Thermocleavable polythiophene carboxylic acid ester.**

Krebs *et al.* found that P3CT could be used to prepare stable solar cells with lifetimes in excess of 10,000 h under AM 1.5D illumination, at elevated temperatures but with exclusion of oxygen and moisture.[29] Recently, it was shown that P3CT can be converted to PT at temperature of ~300 °C upon decarboxylation, as shown in **Scheme 1.10**.[30] To study the device performance, the devices with a freshly spin-coated active layer containing P3MHOCT were annealed correspondingly at temperatures from 190 to 270 °C for ~30 s to obtain P3CT, and 310 °C for ~10 s to obtain PT. During the annealing, the color change of the sample from red to orange can be observed (conversion from P3MHOCT to P3CT) and then from orange to purple-red (conversion from P3CT to PT). UV-vis measurements confirm a significant change of the absorption coefficient at different temperatures. Also, a slight shift of the peaks (at 500 nm)

toward longer wavelengths can be seen when the samples were heated up to 310 °C. Efficiencies up to 1.5 % are reported for bulk heterojunctions based on the polythiophene via the thermal pathway and [6,6]-phenyl-$C_{71}$-butyric acid methyl ester ([70]PCBM). The stability of the devices was studied for more than 500 h.

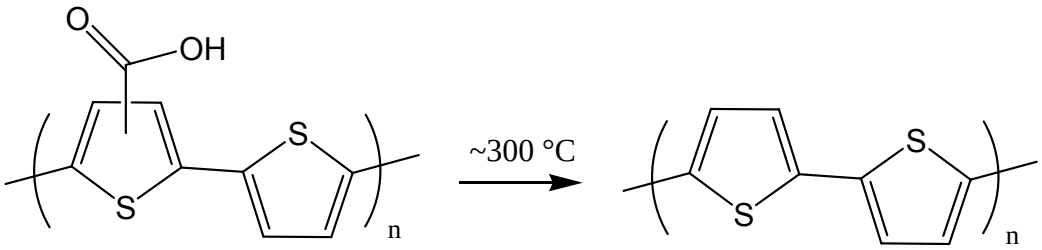


**P3CT**

(insoluble)

**PT**

(insoluble)

**Scheme 1.10: Chemical transformation of P3CT to PT.**

Very recently, Krebs *et al.* reported a new series of thermocleavable esters of low band gap monomers and polymers based on diphenyldithienylthienopyrazine.[31] The purposes of this study were to achieve a low temperature of elimination of the ester group for polymer preparation, and establish device stability performance when subjected to different conditions. A variety of ester groups were obtained and the temperature of elimination of the ester group was studied. The reaction to remove the thermocleavable ester group of the polymer materials is shown in **Scheme 1.11**. The lowest temperatures of elimination were observed in the range of 220 - 240 °C for tertiary esters giving the free acid. The highest temperatures of elimination were found for primary esters that lead to decomposition of the compound. Thus, only

for the tertiary esters thermal elimination can be controlled to yield a thermally-cleaved product. The onset wavelength of the absorption spectrum of this polymer film is ~950 nm. The band gap of this material from absorption measurements is ~1.3 eV. This film exhibits an even smaller band gap of ~1010 nm or 1.2 eV, but less intense absorption after thermal treatment at ~250 °C for 1 min. The photovoltaic performance of the polymers was tested and the best power conversion efficiency achieved was 0.4% in an indium-tin oxide (ITO)/poly-3,4-ethylenedioxythiophene polystyrenesulfonate (PEDOT)/polymer-/[6,6]-phenyl-$C_{61}$-butyric acid methyl ester (PCBM)/aluminum device. Lifetime studies were performed employing the best performing polymer material in four different atmospheres: dry nitrogen, dry oxygen, humid nitrogen, and the ambient atmosphere. The best stability (> hundreds of hours) was observed under nitrogen. In pure oxygen, the device decay was similar as under inert conditions. However, the devices were observed to decay rapidly in the presence of water.

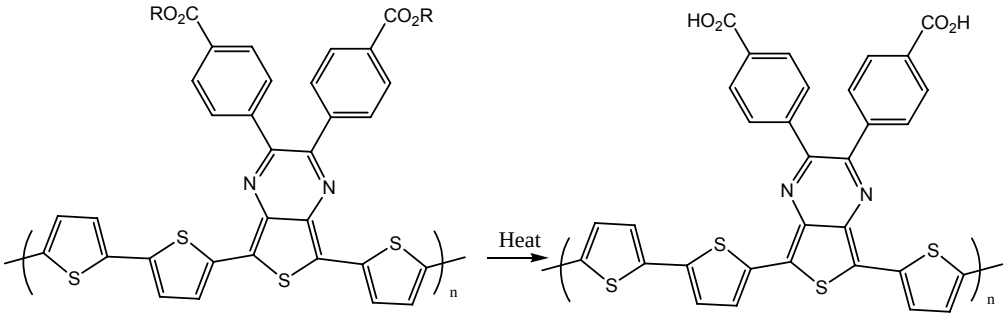


**Scheme 1.11: Thermocleavage of the polymer materials based on diphenyldithienylthienopyrazine.**

## 1.5 Characterization of Conjugated Polymers

In this thesis, $^{1}H$ nuclear magnetic resonance (NMR) spectroscopy, $^{13}C$ NMR spectroscopy, gel permeation chromatography (GPC), elemental analyses, mass spectroscopy, matrix-assisted laser desorption/ionization time-of-flight mass spectroscopy (MALDI-TOF), thermogravimetric analysis (TGA), infrared (IR) spectroscopy, ultra-violet-visible (UV-vis) absorption spectroscopy, photoluminescence (PL) spectroscopy, atomic force microscopy (AFM), fluorescence microscopy, and surface profilimetry were employed to study polymer properties. Characterization techniques discussed in the following sections include: UV-vis absorption spectroscopy, PL spectroscopy, TGA, and AFM measurements. These characterization tools are important for understanding the fundamental structure-property relationships of conjugated polymers.

### 1.5.1 UV-vis Absorption Spectroscopy

In general, absorption spectroscopy is based upon electromagnetic radiation, generally within the wavelength range of 160 to 780 nm. Absorption measurements based upon ultraviolet and visible radiation find widespread application for the quantitative determination of a large variety of inorganic and organic species. Molecular absorption spectroscopy is based on the measurement of the transmittance (T) or the absorbance (A) of solutions contained in transparent cells having a path length of b in cm. Ordinarily, the concentration (C) of an absorbing analyte is linearly related to absorbance as represented by **Equation 1.1**. This equation is a mathematical representation of

Beer's Law.[32] The variables in this equation are defined as absorbance (A), transmittance (T), radiant power (P, $P_1$), path length of radiation (b), absorptivity (a), molar absorptivity (ϵ).

$$A = -\log T = \log \frac{P_1}{P} = \epsilon b C$$

**Equation 1.1: Beer's law.**

Instruments for measuring the absorption of ultraviolet and visible radiation consist of one or more sources, wavelength selectors, sample containers, radiation transducers, and signal processors and readout devices. For the purpose of molecular absorption measurements, a continuum source whose power does not change sharply over a considerable range of wavelength is required. There are various types of instrument, such as single-beam, double-beam in space, double-beam in time, and multichannel. The spectroscopic instrument used in this thesis work is a double-beam in space instrument. Two beams are formed in space by a V-shaped mirror called a beam splitter. One beam passes through the reference solution to a phototransducer, and the second simultaneously traverses the sample to a second, matched transducer. The two outputs are amplified, and their ratio is determined electronically and displayed by readout devices.

Most applications of absorption spectroscopy to organic compounds are based upon transitions for n or π electrons to the π* excited state because the energies required for these processes bring the absorption peaks into an

experimentally convenient spectral region (200 to 700 nm). Both transitions require the presence of an unsaturated functional group to provide the π orbitals. In the molecular-orbital treatment, π electrons are considered to be further delocalized by conjugation. The orbital thus involves four (or more) atomic centers. The effect of this delocalization is to lower the energy level of the π* orbital and give it less antibonding character. Therefore, absorption maxima are shifted to longer wavelengths.

### 1.5.2 Photoluminescence Spectroscopy and Quantum Yield Measurement

The observed transitions in emission spectroscopy of conjugated polymers are attributed to the electronic π-π* transition emission. Upon electronic excitation of the polymer, the following photo-physical processes may occur: fluorescence, phosphorescence or radiationless decay, as shown in **Figure 1.4**.[33] Fluorescence is observed after singlet relaxation to the first excited state after excitation. If intersystem crossing occurs, a triplet excited state is generated, whereby relaxation will result in phosphorescence. If emission does not occur, then a non-radiative pathway is dominant, where the electronic excitation is converted into rotational or vibrational motion of the polymer or of its surroundings. The difference between the absorption and emission maxima is called the Stokes shift. This shift occurs when emission from the lowest vibrational excited state relaxes to various vibrational ground states.

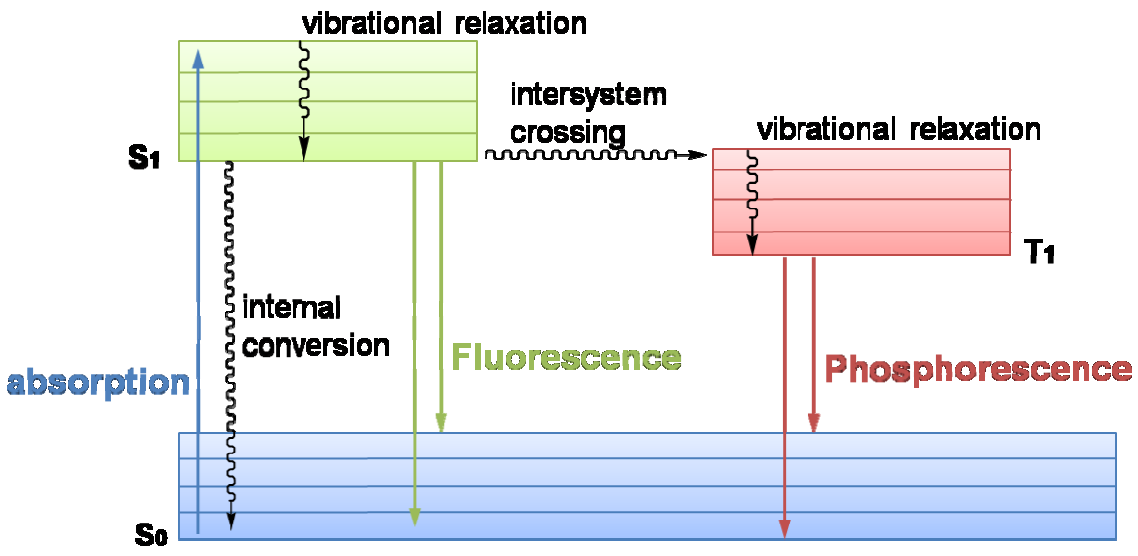


**Figure 1.4: The Jablonski diagram, where $S_0$ = ground singlet state, $S_1$ = first excited singlet state, $T_1$ = first excited triplet state.**

Quantitative analysis of the emission efficiency of the polymer is characterized by its quantum yield of luminescence ($\Phi_{pl}$). The $\Phi_{pl}$ is calculated as the ratio of the number of photons emitted over the number of photons absorbed, as depicted in **Equation 1.2**.

$$\Phi_{\mathrm{PL}} = \frac{\mathrm{Photons}_{\mathrm{Em}}}{\mathrm{Photons}_{\mathrm{Abs}}}$$

**Equation 1.2: Calculation of photoluminescence quantum yield, where $\mathrm{Photons}_{\mathrm{Em}}$ = photons emitted, $\mathrm{Photons}_{\mathrm{Abs}}$ = photons absorbed.**

Two classes of methods have been employed to obtain $\Phi_{pl}$, namely secondary and primary methods.[34] Regarding to the secondary method, $\Phi_{pl}$ is

related to that of a known standard, according to **Equation 1.3**. In this equation, $\Phi$ represents photoluminescence quantum yield, A is the absorbance at the excitation wavelength, I is the integrated emission area across the peak, and n is the refractive index of the solvent. The *u* subscript represents an unknown and the *s* subscript represents a standard. There are several standards, for example, 9,10-diphenylanthracene in cyclohexane ($\Phi_{pl}$ = 0.90),[35] quinine sulfate in 1 N $H_2SO_4$ ($\Phi_{pl}$ = 0.55),[36] and rhodamine 101 in ethanol ($\Phi_{pl}$ = 1.00)[37].

$$\Phi_u = \left( \frac{n_u^2 \times A_s \times I_u}{n_s^2 \times A_u \times I_s} \right) \Phi_s$$

**Equation 1.3: The photoluminescence quantum yield calculation by secondary method.**

The primary method was used in this thesis to obtain $\Phi_{pl}$. This method does not require any standard, but rather quantifies the number of photons absorbed and emitted simultaneously with an integrating sphere.[38] An integrating sphere is a device that gives as its output an unbiased and representative sample of all light deposited within the sphere regardless of the geometry of the deposition process. One of the advantages of this technique is for measurement of films. The large index of refraction of polymeric semi-conductors results in substantial waveguiding of the luminescence, which leads to an anisotropic distribution of the emission intensity. The integrating sphere circumvents this

effect, due to the collection of the light emitted in all directions. Thus, the photoluminescence quantum yield can be calculated by scanning over the excitation line with and without the sample. As shown in **Figure1.5**, the difference between the area of the excitation line is related to the number of photons absorbed and the area under the emission peak is related to the number of photons emitted.

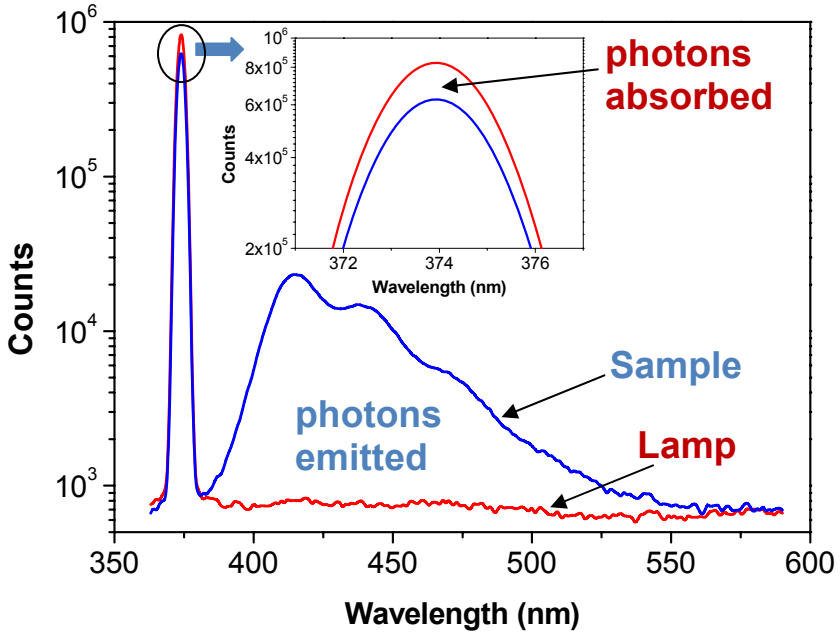


**Figure 1.5: An example of photoluminescence quantum yield measurement of a sample in an integrating sphere spectrofluorimeter.**

### 1.5.3 Thermogravimetric Analysis

Thermogravimetric analysis (TGA) is an analytical technique used to determine the thermal stability of materials and the fraction of volatile components. TGA measurements monitor the mass change of a specimen when

the sample is heated. The measurement is normally carried out in air or in an inert atmosphere, such as nitrogen, helium, or argon. The mass of the sample is recorded as a function of increasing temperature.

TGA instruments are of two types: vertical and horizontal balance. Vertical balance instruments have a specimen pan hanging from the balance or located above the balance on a sample stem. A calibration of these instruments is necessary to compensate for buoyancy effects. The reason of the buoyancy effects is due to the variation in the density of the purge gas with temperature. Vertical balance instruments do not have a reference pan. However, horizontal balance instruments normally have two pans (sample and reference). They do not have buoyancy effects, but require calibration to compensate for differential thermal expansion of balance arms. TGA instruments used in this thesis are of the vertical balance type. The details of the instruments used are summaried in the experimental section in each chapter. The onset temperature of decomposition of the sample is estimated from the point of intersection of two lines: one extrapolated from the slope of the curve just prior to the loss in mass and the second from the steepest part of the curve, as shown in **Figure1.6**.

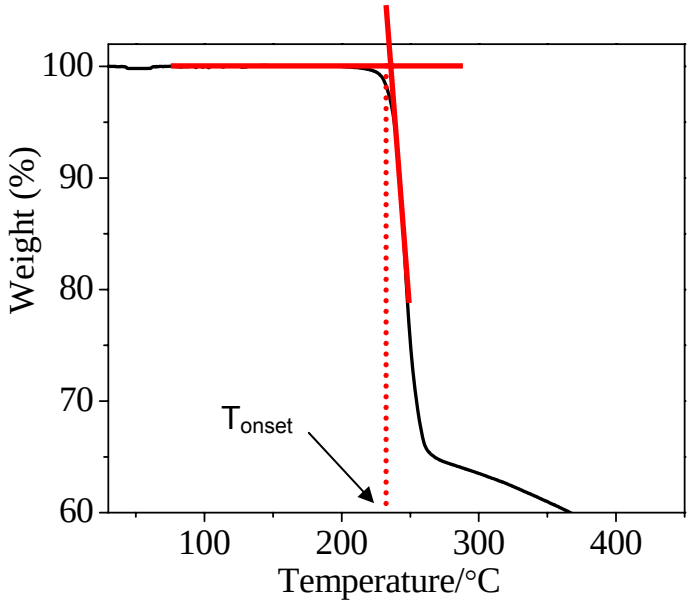


**Figure 1.6: An example of a thermogravimetric analysis measurement.**

### 1.5.4 Atomic Force Microscopy

Atomic force microscopy (AFM) allows scanning of non-conductive samples.[39] AFM can be divided into two primary scanning modes, contact and non-contact, which simply refers to whether or not the scanning probe actually comes into physical contact with the sample surface. Both primary modes have several variations for different applications.

In the contact AFM method, the probe tip (which is mounted to the end of the cantilever) scans across the sample surface, coming into direct physical contact with the sample. As the probe tip scans the surface, varying topographic features cause deflection of the tip and cantilever. A laser beam is bounced off of the cantilever and reflected onto a four-section photodetector. The amount of

deflection of the cantilever — or the force it applies to the sample — can then be calculated from the difference in light intensity on the sectors. Hooke's Law (f = -kd) gives the relationship between the cantilever's motion (d), and the force (f) required to generate the motion. It is possible to fabricate a cantilever with a force constant (k) of 1 N/m or less. Since motion of less than one angstrom can be measured, forces of less than 0.1 nanonewton are detectable.

As the cantilever moves across the sample surface in contact scanning, the lateral motion of the cantilever may cause damage to soft or fragile samples such as polymers. Because of this phenomenon as well as a number of other variables, non-contact mode (also called tapping mode) scanning is sometimes preferable. In non-contact operation, the cantilever is oscillated at its resonant frequency, as illustrated in **Figure 1.7**. In this mode, what is being detected are changes in force between the tip and sample, even though they are not in contact. These changes in force are also referred to as the force gradient. As the probe gets closer to the sample surface, the force gradient changes, thus changing both the oscillation amplitude and phase of the vibrating cantilever. Either the change in amplitude or the change in phase can be detected and used to control the tracking of the probe over the surface (i.e., the feedback-control loop). Amplitude detection is the non-contact method usually used for high-amplitude cantilever vibration. Phase detection is the method usually used when the cantilever vibration amplitude is relatively small (and/or higher sensitivity is needed for stable feedback).

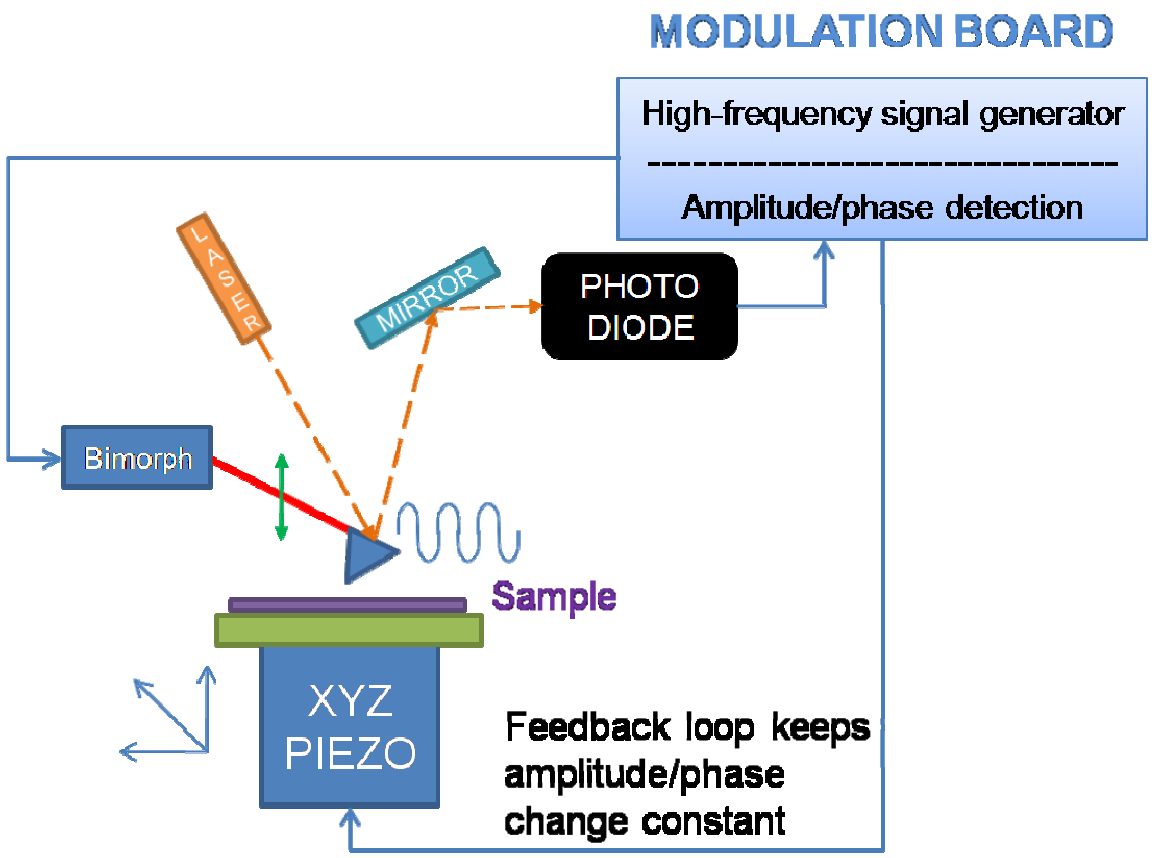


**Figure 1.7: Non-contact feedback loop.**

Because non-contact AFM takes place without any physical contact between the probe tip and the sample surface, it is ideal for scanning soft and/or adhesive samples such as polymers. Thus, the non-contact mode scanning was employed in this thesis to study the topology and morphology of the conjugated polymers and polymer blends.

## 1.6 Patterning of Conjugated Polymers

The ability to pattern functional polymers at different length scales is important for research fields including optics, electronics, cell biology, tissue

engineering, and medicinal science. Spatially controlled deposition of conjugated polymers as active components in organic devices is of interest in microelectronic devices and high resolution display applications, due to their inherent dependence on the formation of micron-sized circuitry.[40] Current trends in 2D deposition of conjugated polymers focus on three primary techniques: area-selected electropolymerization,[41] photochemical patterning,[42] and non-reactive techniques. The non-reactive techniques include screen printing,[43] inkjet printing,[44] and soft lithography,[45] such as microcontact printing (μCP),[46] and micromolding in capillaries (MIMIC).[47] The technique of choice depends on the material under consideration, the substrate, and the intended application or objective. Recently, for example, some methods such as photochemical cross-linking of the side groups to produce insoluble polymer networks in desired areas,[48] and laser-induced, thermal imaging[49] have been successfully used to manufacture devices. In the following sections, several methods developed for patterning of conjugated polymers are discussed, including photolithography, inkjet printing, soft lithography, and direct thermal patterning.

### 1.6.1 Photolithography

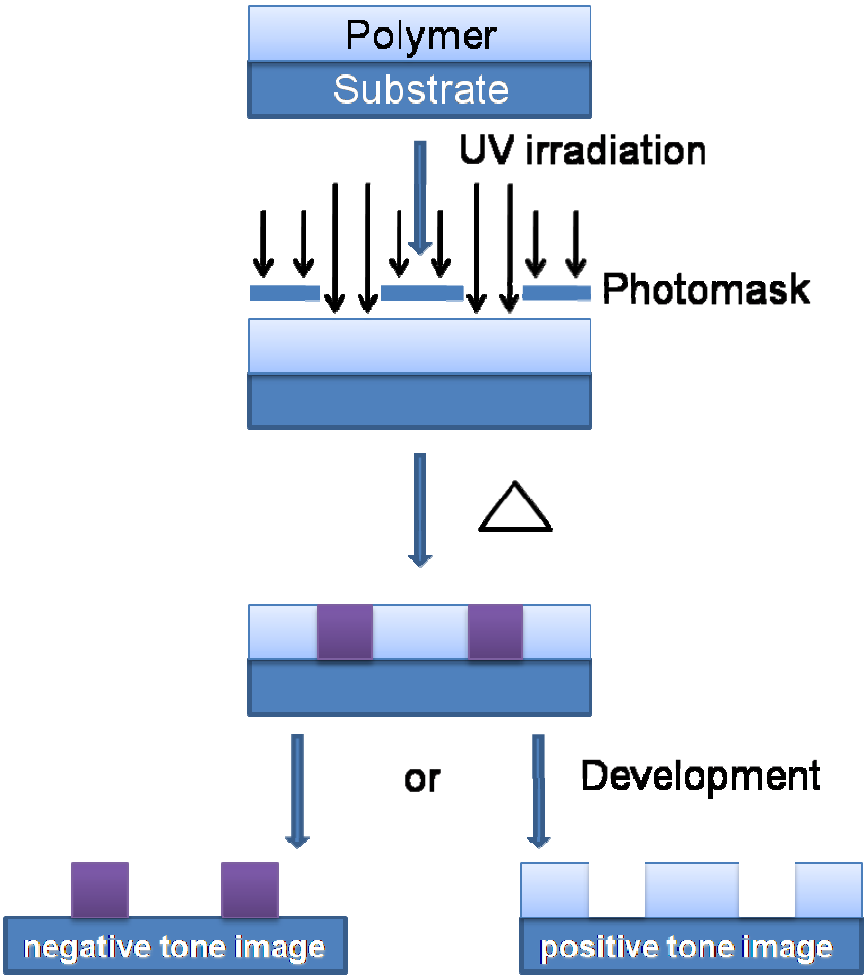


**Figure 1.8: Schematic diagram of a photolithographic process.**

Photolithography is a common patterning technique in the microelectronics and display industry. Photolithography is a process in which polymer films are patterned by photo-radiation through a photomask, as illustrated in **Figure 1.8**. In general, light is used to transfer a geometric pattern from the photomask to a light-sensitive photoresist on the substrate. A series of chemical treatments transfers the exposed pattern into the material underneath

the photoresist. For example, a polymer photoresist is coated onto a substrate. A photomask consisting of transparent and opaque regions, is placed (and aligned) over the polymer and the sample is irradiated. Finally, a negative image is formed after development, where the irradiated areas are insoluble, since insolubilization via cross-linking[50] or supra-molecular hydrogen bonding[27] occurs at exposed areas during photolysis. It is also possible to obtain a positive image using a positive photoresist. The positive photoresist becomes soluble in the basic developer after exposed to irradiation. These positive images are more commonly used in the electronics industry.

Photolithography is a cost-effective, high-throughput technique. It is used for large-area surface patterning with good alignment, controlled topography and a broad range of features. The lateral resolution of patterns arranges from micrometers to <100 nanometres. However, the intrinsic electronic property of the polymer resist may be damaged during the irradiation process, since high intensity incident light is used to change the solubility of the polymer under the irradiated regions. In addition, other effects may result due to structural defects and photoluminescent quenching. Thus, the patterned conjugated polymers may not retain their desired electronic and optical properties during device operation.

### 1.6.2 Ink-Jet Printing

Ink-jet printing is another common patterning technique in the microelectronics and display industry. Inkjet printing technology has been considered as the most promising for fabricating full colour, polymer light emitting diodes (PLEDs), since it allows a controlled number of drops of the polymer

solution (or ink) to be deposited at specified locations on the display substrate, as shown in **Figure 1.9**. After the solvent evaporates from the deposited polymer solution, a thin polymer film solidifies on the substrate. After years of materials, hardware, and process development, the ink-jet printing of PLED displays is on the verge of becoming a practical, commercial reality. Seiko-Epson was the first to demonstrate a prototype full-colour PLED display using inkjet printing, and currently holds the record for the largest organic light-emitting device (OLED) display, a 40-in.-diagonal panel. Other companies, including Toshiba, Samsung, and Philips have also demonstrated PLED prototype displays fabricated by ink-jet printing in a range of sizes and resolutions. Although they are in an advanced state of development in R&D laboratories over the world, full-colour PLED displays produced by this technique are not yet commercial products.

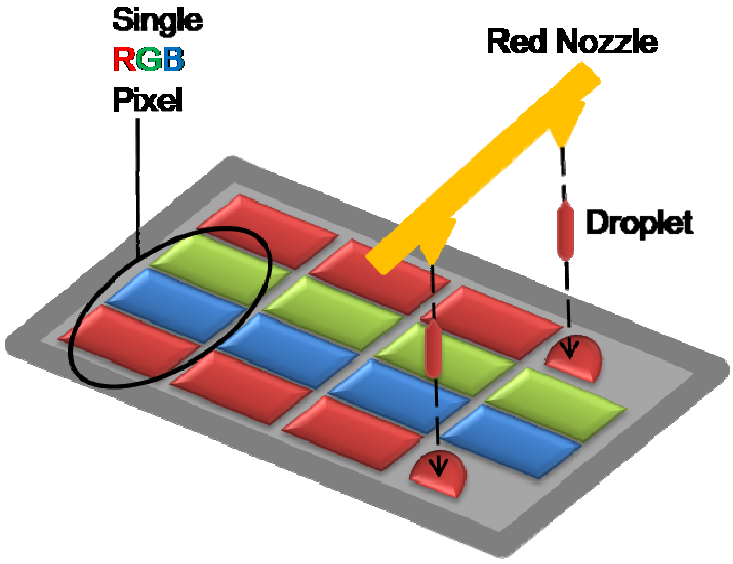


**Figure 1.9: The illustration of the ink-jet printing process as applied to PLED-display fabrication, the red-light-emitting-polymer ink is deposited following deposition of the blue and green materials.**

There are several critical aspects that affect the quality of printed films. First of all, the inks must be formulated to "jet" and be able to produce uniform films. The inks must be stable in solution and not precipitate, thus blocking the very small printhead nozzles. In addition, the correct volume of ink, typically a few tens of picoliters, must be deposited at the exact location on the substrate without overflowing and contaminating neighbouring pixels. Variations in ink-drop volume may be perceived as variations in brightness across the PLED display.

The resolution of an office printer can be as high as ~5 μm per pixel (4800 pdi). In principle, this resolution is more than enough for a full color PLED display, with a subpixel pitch ~50 μm. However, the challenge in printing displays is to have the printhead nozzles in register with accurate position on the substrate. An absolute positional accuracy of a few micrometers is required over the entire display surface. However, the absolute positional accuracy is not feasible. The resolution of a prototype PLED display is ~66 μm.[51]

### 1.6.3 Soft Lithography

In the context of photolithography and soft lithography, several regioregular polythiophenes containing 2-tetrahydropyranyl (THP) group were reported.[27] Yu *et. al.* reported a methodology to pattern thermally-reactive polythiophenes by soft lithography. Soft lithography is the collective name for a set of lithographic techniques that have been developed as an alternative to photolithography for micro- and nano-fabrication. In soft lithography, the key element for structure definition is a patterned elastomer which is used as a stamp

or mold. Common soft lithographic techniques include microcontact printing, micromolding in capillaries, replica molding, microtransfer molding, and solvent-assisted micromolding. The patterning technique of chemically-amplified soft lithography draws on concepts of chemical amplification and microcontact printing. In this method, THP groups are attached to the alkyl chain of polythiophene. TGA analysis showed deprotection of THP units at ~130 °C in the presence of a catalytic amount of acid. The deprotection temperature is much lower than that of the polymer in the absence of acid. The catalytic amount of acid was transferred from an "inked" polydimethylsiloxane (PDMS) stamp to the surface of the polymer, as depicted in **Figure 1.10**. An acid-catalyzed solid state reaction was employed to the thermally-reactive polythiophenes and resulted in the thermal cleavage of THP groups and the production of hydroxide functionalized polythiophene, dihydropyran, and acid, as shown in **Scheme 1.12**. The resulting deprotected polymer is insoluble. Compared with photolithography, the soft lithographic process is a low cost technique that circumvents the use of expensive lenses and eliminates possible damage to the conjugated polymer structure due to irradiation.[27] In addition, soft lithography can pattern flexible surfaces. This strategy would appear favorable for the patterning of photoluminescent conjugated polymers and flexible devices. This method has also been applied to the luminescent polyfluorenes. The details of this study are summarized in the second chapter of this thesis.

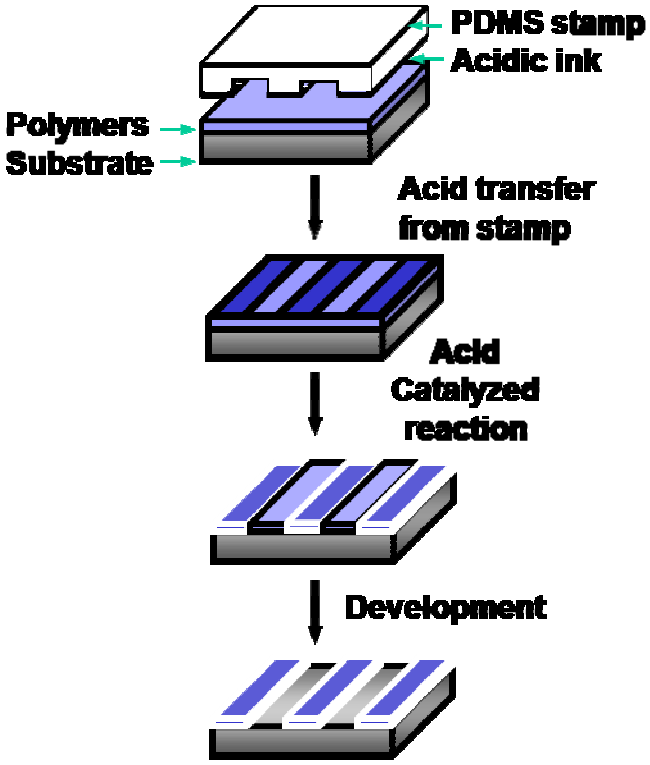


**Figure 1.10: Schematic diagram of a chemically amplified soft lithography process.**

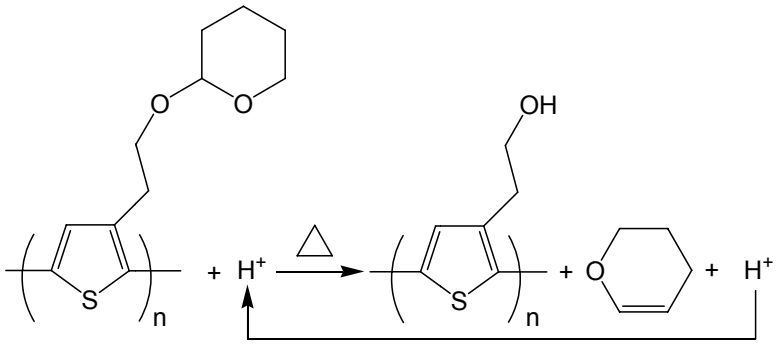


**Scheme 1.12: Acid catalyzed deprotection of THP-functionalized polythiophenes.**

### 1.6.4 Direct Thermal Patterning

Very recently, Gordon *et. al.* reported a novel, direct thermal patterning method for the pixilation of conjugated polymers.[52] The technique employs novel chemistry and state-of-the-art reprographic instrumentation. It has the potential for producing high resolution images with rapid throughput. The process of patterning single layer polymer-near infrared (NIR) dye films is illustrated in **Figure 1.11**. The materials used are the same thermally-reactive polythiophenes bearing THP groups. In the presence of a near-infrared (NIR) dye in the polythiophene film, the polymer film has a significant absorbance at 830 nm and undergoes thermal reaction at < 200 ºC. Polymer films were exposed to 830 nm irradiation from a portable 830 nm test laser and a Kodak NIR flat bed imaging laser scanner. The resulting polymer films were rendered insoluble, where the NIR light struck the surface. Also, this method has been applied to the luminescent polyfluorenes that bear THP groups. The details of this study are summarized in the third chapter of this thesis.

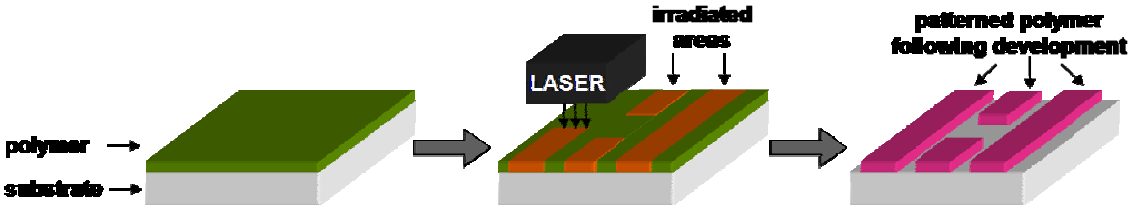


**Figure 1.11: Schematic diagram for the direct thermal patterning of thermally-reactive polymers using NIR laser irradiation.**

## 1.7 Applications, Device Fabrication, and Characterization of Conjugated Polymers

Organic semiconductors are a remarkable class of materials with present and potential applications in various optoelectronic devices. Device structures and performances based on electronically conducting, photoluminescent, or electroluminescent conjugated polymers are attracting considerable attention and investigation from both academic and industrial scientists. Various potential applications include PLEDs, polymer photovoltaic devices, and polymer field-effect transistors. Only polymer light emitting devices and polymer photovoltaic devices are considered in this thesis. Additional information on polymer photovoltaic cell devices is presented in Chapter 4.

### 1.7.1 Polymer Light Emitting Devices (PLED)

In general, two main classes of organic light emitting devices have been fabricated: small-molecule light-emitting devices (OLEDs) and polymer light emitting devices (PLEDs). A typical double-heterostructure small-molecule OLED consists of three organic layers sandwiched between electrodes. The organic layers adjacent to cathode and anode are the electron transport layer (ETL) and the hole transport layer (HTL), respectively. The emissive layer (EML) usually consists of light-emitting dyes or dopants dispersed in a suitable host material (often the same as the HTL or ETL material).

PLEDs consist of an electroluminescent conductive polymer that emits light when connected to an external voltage source. PLEDs have relatively simple architectures, with the light-emitting polymer (LEP) layer combining host,

emitter and charge transport functions in a single solution-processed layer of the device, as shown in **Figure 1.12**. This simple device structure consists of a transparent conducting anode (typically indium tin oxide (ITO) coated glass), an emitting polymer, and a low work function metal such as calcium. Upon application of an electric field, a hole and electron are simultaneously injected into opposite sides of the polymer layer. The hole-electron pair forms an exciton, which results in emission of light upon recombination. There are a wide selection of LEPs in several major chemical classes that have proved to be useful for PLED research, including poly(phenylene vinylene) (PPV) and polyfluorene (PF) polymers.

LEDs fabricated with an emitting polymer were first reported by Partridge in 1983, with the use of poly(vinylcarbazole).[53] Performances of these devices were poor, requiring high voltages and low operational lifetimes. Burroughes *et al.* were the first to report PLEDs based on poly(*p*-phenylenevinylene) in 1989.[54] These devices exhibited efficient light emission and led to a flood of research involved in the design and synthesis of new polymers as potential "plastic" emitters. One of the major applications is PLED-based, full-colour, flat panel displays. This is because PLEDs have several advantages over OLEDs, e.g., low cost due to solution processing, as well as advantages over liquid crystal displays in that they are visible over a much wider range of viewing angles. The thin film, full-spectrum, colour displays of PLEDs require a relatively small amount of power for the light produced. No vacuum is required, and the emissive materials can be applied on the substrate by a technique derived from

commercial ink-jet printing processes. The type of substrate used can also be mechanically flexible. An optimized PLED requires efficient and balanced charge injection, good and comparable mobilities for both holes and electrons, and high luminescence quantum yields.

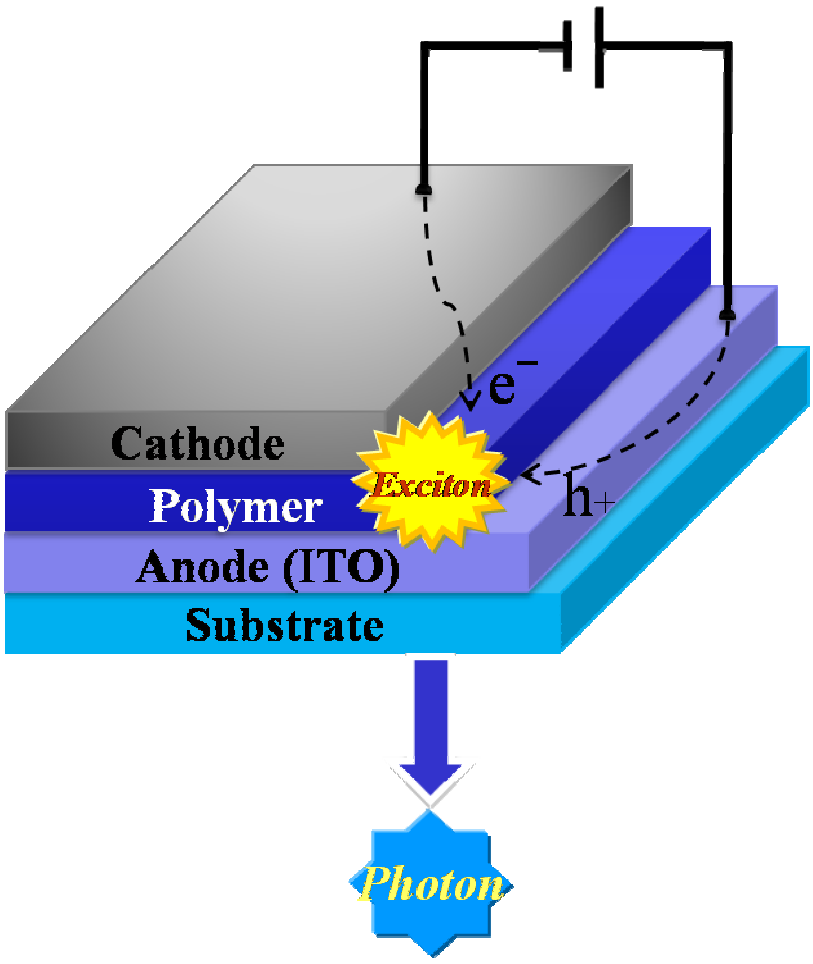


**Figure 1.12: A schematic illustration of the structure of a polymer light-emitting device (PLED).**

Electroluminescence in PLEDs is the emission observed upon the application of an electric field. Device efficiency is a measure of the number of

photons emitted through the transparent electrode per injected electron, commonly referred to as the external quantum efficiency ($\Phi_{EL}$). The $\Phi_{EL}$ of a LED is related to several factors including the solid state photoluminescence efficiency, the fraction of the photons which are emitted from the front surface of the device and the fraction of electrons and holes which recombine with each other.

### 1.7.2 Polymer Photovoltaic (PV) Devices

“Photovoltaic” is a term pertaining to the direct conversion of light into electricity. The word "photovoltaic," first used ca. 1890, is a combination of the Greek word for light and the name of the physicist and electricity pioneer Allesandro Volta. Thus, “photovoltaic" can be translated literally as "light-electricity." The conversion of sunlight to electricity using photovoltaic (PV) cells, also known as solar cells, is based on the photoelectric effect discovered by Alexander Bequerel in 1839. The photoelectric effect describes the release of positive and negative charge carriers in a solid state when light strikes its surface.

Photovoltaic systems have already played an important role of our lives. Simple PV systems provide power for many small consumer items, such as calculators and wristwatches. More complicated systems provide power for communications satellites, water pumps, and the lights, appliances, and machines at homes or workplaces. Many road and traffic signs along highways are now powered by PV. In many cases, PV power is the least expensive form of electricity for performing these tasks.

A photovoltaic device is an electrical device that converts light directly into DC electricity. The performance of a PV cell is a function of the characteristics of the light source, the materials used, and the design of the device. Photovoltaic efficiency is the ratio of electric power produced by a photovoltaic cell at any instant to the power of the sunlight striking the cell. The best efficiency reported recently is 40.8 % for III-V multijunction cells created by Spectrolab, [55] and about 5 % - 7 % for organic PV cells. [8,56]

Organic PV cells are divided into three major classes: small molecules, polymer, and hybrid devices. These classes are distinguished by the type of material and fabrication methods used. As depicted in **Figure 1.13**, polymer PV devices are generally prepared by solution processing. A typical device structure consists of blends of a conjugated polymer and an electron acceptor, or blends of two different conjugated polymers, sandwiched between transparent ITO anode and Al/Ca cathode layers. Such blends (e.g., polymer/[6,6]-phenyl-$C_{61}$-butyric acid methyl ester (PCBM)) have interfaces throughout the active layer, known as a bulk heterojunction. PPV, PT, PF, and their derivatives with different side chain substitution (e.g., alkyl side chains) have been most widely used in the active layers of polymer PV cells.

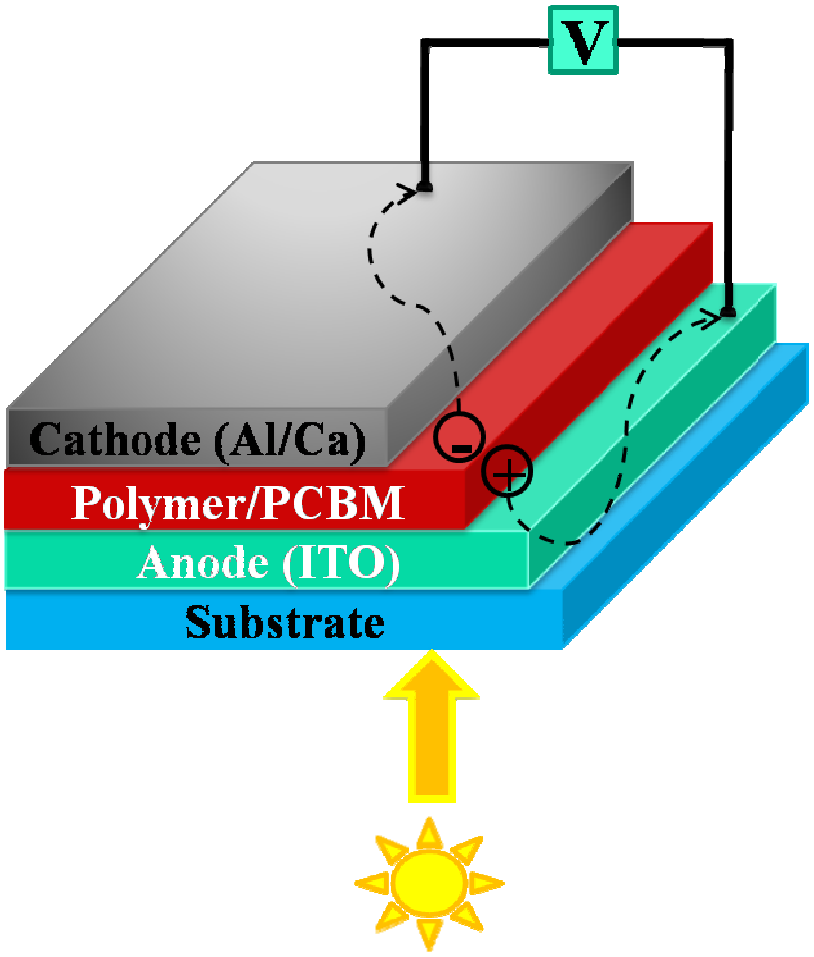


**Figure 1.13: A schematic illustration of the structure of a bulk heterojunction organic photovoltaic cell device.**

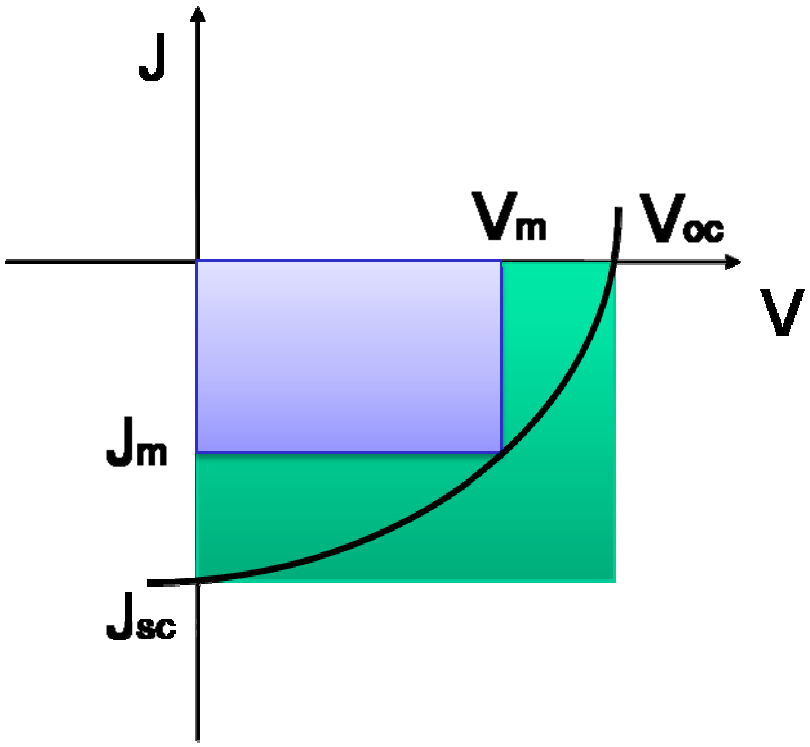


**Figure 1.14: Current-voltage response of photovoltaic device under illumination. The open-circuit voltage ($V_{oc}$), short-circuit current density ($J_{sc}$), and current density and voltage at maximum power output ($J_m$ and $V_m$, respectively) are defined.**

**Figure 1.14** shows a schematic diagram of the current-voltage curve of a PV device under illumination.[57] Devices are generally characterized by the open-circuit voltage ($V_{oc}$), the short-circuit current density ($J_{sc}$), and the fill factor (FF). $V_{oc}$ of a device is defined as the difference in electrical potential between two terminals of a device when there is no external load connected, i.e., the circuit is open. $J_{sc}$ of a device is defined as the highest electric current which can exist in a particular electrical system under short circuit conditions. The fill factor of a

device is defined as the ratio between the maximum power delivered to an external circuit and the potential power, as shown in **Equation 1.4**.

$$FF = \frac{P_m}{J_{sc}\, V_{oc}} = \frac{J_m\, V_m}{J_{sc}\, V_{oc}}$$

**Equation 1.4: Definition of fill factor.**

The fill factor is the ratio of the region defined by $J_m$ and $V_m$ (pink shaded region) to the region defined by $J_{sc}$ and $V_{sc}$ (blue shaded region) in **Figure 1.14**. The power conversion efficiency (η) of a device is defined as the ratio between the maximum electrical power generation ($P_m$) and the incident optical power $P_0$, as shown **in Equation 1.5**. $I_m$ is the current at maximum power output.

$$\eta = \frac{I_m\, V_m}{P_0}$$

**Equation 1.5: Definition of power conversion efficiency.**

The spectral response of PV devices is an important way to characterize such devices as well as optimize their performance. The device is illuminated by a monochromatic light source, generally consisting of a broadband illuminator dispersed through a monochromator. The photocurrent is measured as the function of wavelength and then compared to the light intensity or photon flux. The external quantum efficiency (EQE), also known as the incident photon

conversion efficiency, is given by the number of electrons generated per incident photon, as shown in **Equation 1.6**, where $I_{sc}$ is the short-circuit current, $P_0$ is the incident optical power, h is Planck's constant ($6.63\times10^{-34}$ J·s), c is the speed of light ($3\times10^{8}$ m/s), λ is the wavelength of light (in nm), and e is the electrical charge ($-1.602 \times 10^{-19}$ C, the absolute value is used in the formula). This generally follows the absorption spectrum of the materials consitituting the PV devices. The external quantum efficiency, also known as the photocurrent action spectrum, is given by the ratio of the photocurrent to the absorbed photon flux.

$$\mathrm{EQE} = \frac{\mathrm{N_e}}{\mathrm{N_{ph}}} = \frac{\mathrm{I_{sc}}}{\mathrm{P_0}}\frac{\mathrm{hc}}{\lambda \mathrm{e}}$$

**Equation 1.6: Definition of external quantum efficiency.**

In theory, the power efficiency of a solar cell can be calculated by integrating the EQE over the solar spectrum and multiplying by the monochromatic power efficiency. Such an approach fails because the fill factor depends on the wavelength, trapping states of materials, and non-linearity of solar cells. The best approach is to use a solar simulator that replicates the solar spectrum. The AM 1.5D spectrum is the solar spectrum reaching the surface of the earth after passing through the atmosphere, 48.2º from zenith, with a total intensity of approximately 90 mW/cm$^2$. In many cases, the solar simulator is not available and a white light sources is used instead, with the spectral mismatch taken into account in the calculations of the power conversion efficiencies of PV

devices. In this thesis, AM 1.5D solar spectrum source is used. The AM 1.5D solar spectrum is shown in **Figure 1.15**.

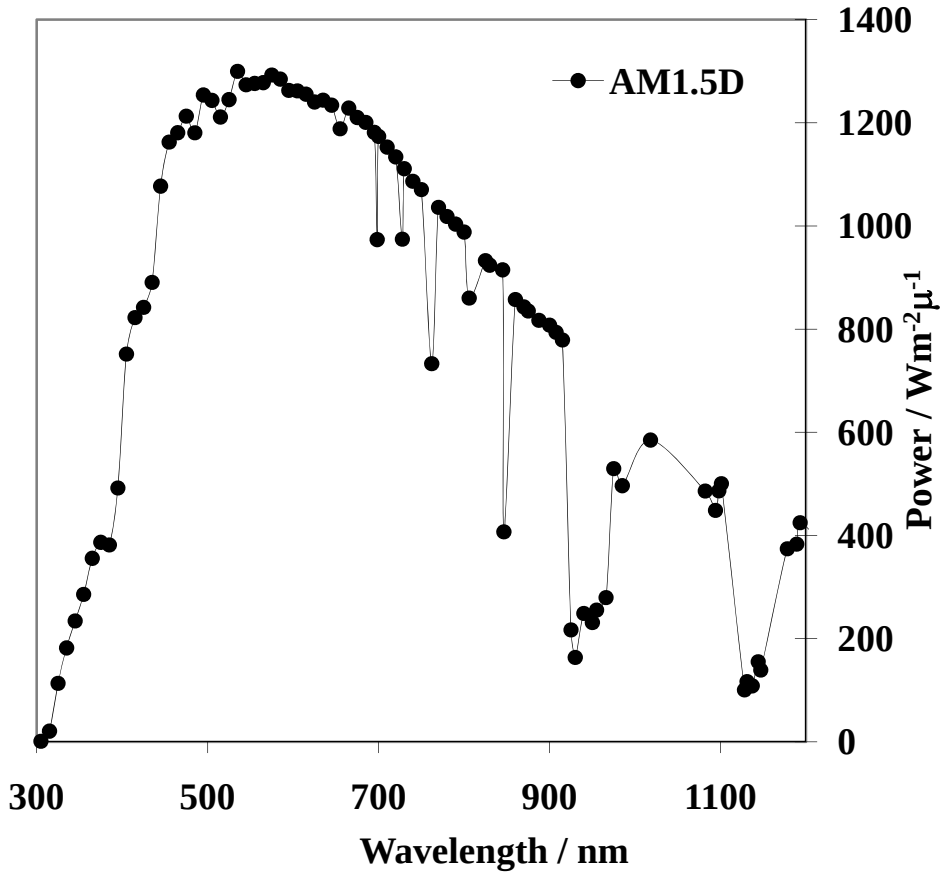


**Figure 1.15: AM 1.5D solar spectrum.**

The internal quantum efficiency (IQE) is given by the number of electrons generated per absorbed photon, as shown in **Equation 1.7**, where ABS is the photon absorbance, T is the transmittance, and R is the reflectance. T is calculated using Beer's law $T = 10^{-A}$, where A is optical absorbance measured from UV-vis absorption. R is determined by measuring the incident light intensity

with and without a piece of ITO-glass. The ratio of the incident light intensity with ITO-glass to the incident light intensity without ITO-glass is given to the value of R. In this work, R is a constant (R = (4.41 x $10^{-6}$) / (5.50 x $10^{-6}$) = 0.2) at the wavelength of 435 nm.

$$\mathrm{IQE} = \frac{\mathrm{EQE}}{\mathrm{ABS}} = \frac{\mathrm{EQE}}{1 - \mathrm{T} - \mathrm{R}}$$

**Equation 1.7: Definition of internal quantum efficiency.**

## 1.8 Project Overview

π-Conjugated polymers (πCPs) are attracting a great deal of interest, mainly due to their potential application in organic electronic devices, such as polymer light emitting displays, photovoltaic panels, and field-effect transistors. Different applications require different properties of the πCP. For example, emissive display technologies require highly photoluminescent πCPs, possessing relatively weak inter-chain interactions; while for photovoltaic and FET devices, strong inter-chain coupling, giving rise to high charge mobilities are required. Furthermore, a better understanding of how to control these properties via the deposition process needs to be addressed. It is also important that the πCPs retain their chemical and structural properties after patterning and development. It has been shown that current photolithographic and physical contact patterning methods have various limitations, such as degradation of fluorescent colour properties of the πCPs through photo or thermal oxidation processes. New

methods of spatial deposition of πCPs and novel πCPs with enhanced oxidative stability are under investigation. Soft lithography, direct thermal patterning, and patterning through the use of polymer blends is studied because these routes offer fast, reliable, high resolution, and high-throughout printing methods.

In Chapter 2 of this thesis, the structure-property relationships of thermally-reactive polyfluorenes are discussed. Polyfluorenes have recently received much attention due to their high charge mobility, electrochemical stability and high photoluminescent efficiency for the emission of blue light. Chemically-amplified soft lithography was used to pattern the luminescent polymers. The design of conjugated polymers bearing THP groups, or other protecting groups, is considered as a means for patterning luminescent polymers, without affecting the π-conjugation.

In Chapter 3, the preparation of a homopolymer of 9,9'-bis[4-(2-(2-tetrahydropyranyloxy)ethoxy)phenyl]fluorene and its copolymers with 3,4-benzothiadiazole and 4,7-di(3(4-n-octylphenyl)-2-thienyl)-2,1,3-benzothiadiazole to produce a series of thermally-reactive blue, green, and red luminescent polymers are discussed. These polymers were found applicable to patterning by NIR direct thermal lithography, in conjunction with a NIR dye and thermal acid generator. The presence of the phenyl groups at the 9-site carbon was found to be necessary to eliminate fluorenone formation, and to enhance the colour purity of the material.

In Chapter 4, a facile method for preparing nano/micro-sized topologies of π-conjugated polymers from πCP bearing thermally-cleavable solubilizing groups

is described. The dependence of feature size of the πCP formed on several parameters including solution concentration, type of solvent, and the nature of the polymer(s) is investigated. Nano-patterned PV devices were fabricated, characterized, and compared to bilayer, and bulk heterojunction devices. This facile patterning method is investigated as a route to prepare high surface area topographies for PV devices.

Chapter 5 contains a summary of the work and describes future studies and considerations related to the thesis topics.

## 1.9 References


(1) (a) H. Shirakawa, E. J. Louis, A. G. MacDiarmid, C. K. Chiang, A. J. Heeger, *J. Chem. Soc., Chem. Commun.* **1977**, 578. (b) C. K. Chiang, C. R. Fincher, Y. W. Park, A. J. Heeger, H. Shirakawa, E. J. Louis, S. C. Gau, A. G. MacDiarmid, *Phys. Rev. Lett.* **1977**, *39,* 1098.

(2) (a) T. A. Skotheim (ed.), in *Handbook of Conducting Polymers*, Marcel Dekker, New York, **1986**. (b) J. Roncali, *Chem. Rev.* **1992,** *92,* 9711. (c) J. Roncali, *Chem. Rev.* **1997,** *97,* 173. (d) J. A. Osaheni, S. A. Jenekhe, *Chem. Mater.* **1992,** *4,* 1282. (e) M. F. Roberts, S. A. Jenekhe, *Chem. Mater.* **1994,** *6,* 135. (f) M. Dotrong, R. Meheta, G. A. Balchin, R. C. Tomlinson, M. Sinksky, C. Y.-C. Lee, R. C. Evers, *J. Poly. Sci. Part A* **1993,** *31,* 723. (g) G. Q. Shi, S. Jin, G. Xue, C. Li, *Science* ***1995***, *267*, 994.

(3) (a) L. Akcelrud, *Prog. Polym. Sci*. **2003**, *28*, 875. (b) R. H. Friend, R. W. Gymer, A. B. Holmes, J. H. Burroughes, R. N. Marks, C. Taliani, D. D. C.

Bradley, D. A. dos Santos, J. L. Brédas, M. Löglund, W. R. Salaneck, *Nature* **1999**, *397*, 121. (c) A. Kraft, A. Grimsdale, A. B. Holmes, *Angew. Chem. Int*. **1998**, *37*, 402. (d) J. R. Sheats, Y. L. Chang, D. B. Roitman, A. Socking, *Acc. Chem. Res*. **1999**, *32*, 193. (e) S. Miyata, H. S. Nalwa (eds.), in *Organic Electroluminescent Materials and Devices*, Gordon & Breach, Amsterdam, **1997**. (f) X. Gong, J. C. Ostrowski, M. R. Robinson, D. Moses, G. C. Bazan, A. J. Heeger, *Adv. Mater.* **2002**, *14*, 581. (g) R. H. Partridge, *Polymer* **1983**, *24*, 733. (h) J. H. Burroughes, D. D. C. Bradley, A. R. Brown, R. N. Marks, K. MacKay, R. H. Friend, P. L. Burns, A. B. Holmes, *Nature* **1990**, *347*, 539.

(4) (a) C. D. Dimitrakopoulos, D. J. Mascaro, *Adv. Mater*. **2002**, *14*, 99. (b) F. Garnier, R. Hajlaoui, A. Yassar, P. Srivastava, *Science* **1994**, *265*, 1684. (c) Z. Bao, *Adv. Mater.* **2000**, *12*, 227. (d) G. H. Gelinck, T. C. T. Geuns, D. M. de Leeuw, *Appl. Phys. Lett.* **2000**, *77*, 1487. (e) H. E. A. Huitena, G. H. Gelinck, J. B. P. H. van der Putter, K. E. Kuijk, C. M. Hart, E. Cantatore, P. T. Herwig, A. J. J. M. van Breemen, D. M. de Leeuw, *Nature* **2001**, *414*, 599. (f) B. S. Ong, Y. Wu, P. Liu, S. Gardner *J. Am. Chem. Soc*. **2004**, *126*, 3378.

(5) (a) J. Christoph, J. Brabec, N. S. Sariciftci, J. C. Hummelen, *Adv. Funct. Mater.* **2001**, *11*, 15. (b) J. Xue, S. Uchida, B. P. Rand, S. R. Forrest, *Appl. Phys. Lett.* **2004**, *84*, 3013. (c) N. S. Sariciftci, L. Smilowitz, A. J. Heeger, F. Wudl, *Science* **1992**, *258*, 1474. (d) S. Morita, A. A. Zakhidov, K. Yoshino, *Solid State Commun*. **1992**, *82*, 249.

(6) (a) E. Smela, *Adv. Mater*. **2003**, *15*, 481. (b) E. Smela, in *Electroactive Polymer Actuators as Artificial Muscles: Reality, Potential and Challenges*, (Ed: Y. Bar-Cohen), SPIE Press, Bellingham, **2001**. (c) T. F. Otero, in *Conductive Polymers: Transport, Photophysics and Applications* (Ed: H. S. Nalwa), Vol. 4, John Wiley & Sons, New York, **1997**.

(7) N. Tessler, *Adv. Mater.* **1999**, *11*, 363.

(8) W. Ma, C. Yang, X. Gong, K. Lee, A. J. Heeger, *Adv. Funct. Mater.* **2005**, *15*, 1617.

(9) J. G. Xue, S. Uchida, B. P. Rand, S. R. Forrest, *Appl. Phys. Lett.* **2004,** *85*, 5757.

(10) (a) A. J. Heeger, S. Kivelson, J. R. Schrieffer, W.-P. Su, *Rev. Mod. Phys.* **1988**, *60*, 781. (b) D. K. Campbell, A. R. Bishop, K.Fesser, *Phys. Rev. B* **1982**, *26*, 6862. (c) K. Fesser, A. R. Bishop, D. K. Campbell, *Phys. Rev. B* **1983**, *27*, 4804.

(11) P. A. Lane, X. Wei, Z. V. Vardeny, *Phys. Rev. Lett.* **1996**, *77*, 1544.

(12) (a) J. A. Blackman, M. K. Sabra, *Phys. Rev. B* **1993**, *47*, 15437. (b) R. Österbacka, C.P. An, X.M. Jiang, Z.V. Vardeny, *Science* **2000**, *287*, 839. (c) J. Cornil, D. Beljonne, J.-P. Calbert, J.-L. Bredas, *Adv. Mater*. **2001**, *13*, 1053. (d) D. Beljonne, J. Cornil, H. Sirringhaus, P. J. Brown, M. Shkunov, R. H.. Friend, J. L. Bredas, *Adv. Funct. Mater.* **2001**, *11*, 229.

(13) (a) Y. Ohmori, M. Uchida, K. Muro, K. Yoshino, *Jpn. J. Appl. Phys*. **1991**, *30*, L1941. (b) R. Sugimoto, S. Takeda, H. B. Gu, K. Yoshino, *Chem. Express* **1986**, *1*, 635.

(14) H. Mao, B. Xu, S. Holdcroft, *Macromolecules* **1993**, *26*, 1163.

(15) (a) S. Amou, O. Haba, K. Shirato, T. Hayakawa, M. Ueda, K. Takeuchi, M. Asai, *J. Polym. Sci. Part A: Polym. Chem.* **1999**, *37*, 1943. (b) O. Haba, T. Hayakawa, M. Ueda, H. Kawaguchi, T. Kawazoe, *Reactive & Functional Polymers* **1998**, *37*, 163.

(16) T. Yamamoto, A. Morita, Y. Miyazaki, T. Maruyama, H. Wakayama, Z. -H. Zhou, Y. Nakamura, T. Kanbara, S. Sasaki, K. Kubota, *Macromolecules* **1992**, *25*, 1214.

(17) T. Yamamoto, T. Maruyama, Z.-H. Zhou, T. Ito, T. Fukuda, Y. Yoneda, F. Begum, T. Ikeda, S. Sasaki, H. Takezoe, A. Fukuda, K. Kubota, *J. Am. Chem. Soc.* **1994**, *116*, 4832.

(18) T. Yamamoto, *Synlett* **2003**, *4*, 425.

(19) N. Miyaura, A. Suzuki, *Chem. Rev.* **1995**, *95*, 2457.

(20) (a) N. Miyaura, K. Yamada, A. Suzuki, *Tetrahedron Letters* **1979**, 3437. (b) N. Miyaura, A. Suzuki *Chem. Commun.* **1979**, 866.

(21) M. Rehahn, A. D. Schluter, G. Wegner, W. J. Feast, *Polymer* **1989**, *30*, 1054.

(22) (a) K. Tamao, K. Sumitani, M. Kumada, *J. Am. Chem. Soc.* **1972**, *94*, 4374. (b) R. J. P. Corriu, J. P. J. Masse, *Chem. Soc., Chem. Commun.* **1972**, 144.

(23) L. Kürti, B. Czakó (eds.), in *Strategic Applications of Named Reactions in Organic Synthesis*, Elsevier Academic Press, Amsterdam, **2005**.

(24) (a) R. D. McCullough, R. D. Lowe, *J. Chem. Soc., Chem. Commun*. **1992**, 70. (b) R. D. McCullough, R. D. Lowe, M. Jayaraman, D. L. Anderson, *J. Org. Chem*. **1993**, *58*, 904.

(25) (a) R. S. Loewe, S. M. Khersonsky, R. D. McCullough, *Adv. Mater.* **1999**, *11*, 250. (b) R. S. Loewe, P. C. Ewbank, J. Liu, L. Zhai, R. D. McCullough, *Macromolecules* **2001**, *34*, 4324.

(26) Bratton, D. Yang, J. Dai, C. K. Ober, *Polym. Adv. Technol.* **2006**, *17*, 94.

(27) (a) J. Yu, S. Holdcroft, *Macromolecules* **2000**, *33*, 5073. (b) J. Yu, M. Abley, C. Yang, S. Holdcroft, *Chem. Commun*. **1998**, 1503. (c) J. Yu, S. Holdcroft, *Chem. Mater.* **2002**, *14*, 3705. (d) J. Yu, S. Holdcroft, *Chem. Mater.* **2001**, *13*, 526.

(28) J. S. Liu, E. N. Kadnikova, Y. X. Liu, M. D. McGehee, J. M. J. Fréchet, *J. Am. Chem. Soc.* **2004**, *126*, 9486.

(29) F. C. Krebs, *Proc. SPIE* **2005**, *5938*, 59380Y.

(30) S. A. Gevorgyan, F. C. Krebs, *Chem. Mater.* **2008**, *20*, 4386.

(31) M. H. Petersen, S. A. Gevorgyan, F. C. Krebs, *Macromolecules* **2008**, *41*, 8986.

(32) D. A. Skoog, F. J. Holler, T. A. Nieman, in *Principles of Instrumental Analysis*, fifth ed, Sauders College Publishing, New York, **1998**.

(33) J. Guillet, in *Photophysics and Photochemistry*, Cambridge University Press, London. **1985**, Pg 24.

(34) D. F. Eaton, *Pure Appl. Chem*. **1988**, *60*, 1107.

(35) (a) S. Hamai, F. Hirayama, *J. Phys. Chem*. **1983**, *87*, 83. (b) S. R. Meech, D. Phillips, *J. Photochem*. **1983**, *23*, 83.

(36) W. H. Melhuish, *J. Phys. Chem.* **1961**, *65*, 229.

(37) T. Karstens, K. Kobs, *J. Phys. Chem*. **1980**, *84*, 1871.

(38) (a) J. C. de Mello, H. F. Wittmann, R. H. Friend, *Adv. Mater*. **1997**, *9*, 230. (b) L. -O. Pålsson, A. P. Monkman, *Adv. Mater*. **2002**, *14*, 757.

(39) T. Marek, in *Thermo Microscopes Explorer Instrument Operation Manual*, ThermoMicroscopes Corporation, Sunnyvale, **1996**, Ch. 1.

(40) S. Holdcroft, *Adv. Mater.* **2001**,*13*,1753.

(41) C. B. Gorman, H. A. Biebuyck, G. M. Whitesides, *Chem. Mater.* **1995,** *7,* 526.

(42) (a) M. S. A. Abdou, S. Holdcroft, in *Encyclopedia of Conductive Molecules and Polymers* (Ed: H. S. Nalwa), Wiley, New York, **1996**, Ch. 4. (b) M. Angelopoulos, in *Handbook of Conducting Polymers*, 2nd ed. (Eds: T. A. Skotheim, R. L. Elsenbaumer, J. R. Reynolds), Marcel Dekker, New York, **1997**. (c) P. I. Clemonson, W. J. Feast, M. M. Ahmad, P. C. Allen, D. C. Bott, C. S. Brown, L. M. Connors, *Polymer* **1992,** *33,* 4711.

(43) Z. Bao, Y. Feng, A. Dodabalapur, V. R. Raju, A. J. Lovinger, *Chem. Mater.* **1997,** *9,* 1299. (b) Z. Bao, J. A. Rogers, H. E. Katz, *J. Mater. Chem.* **1999,** *9,* 1895.

(44) C. C. Wu, D. Marcy, M. H. Lu, J. C. Sturm, *Appl. Phys. Lett.* **1998,** *72,* 519.

(45) (a) Y. Xia, G. M. Whitesides, *Angew. Chem. Int. Ed.* **1998,** *37,* 550. (b) S. Brittain, K. Paul, X.-M. Zhao, G. Whitesides, *Phys. World* **1998,** *11,* 31. (c) T. Granlund, T. Nyberg, L. S. Roman, M. Svensson, O. Inganäs, *Adv. Mater.* **2000,** *12,* 269.

(46) J. A. Rogers, Z. Bao, A. Makhija, P. Braun, *Adv. Mater.* **1999,** *11,* 741.

(47) F. L. Zhang, T. Nyberg, O. Inganas, *Nano Lett.* **2002,** *2,* 1373.

(48) C. D. Müller, A. Falcou, N. Reckefuss, M. Rojahn, V. Wiederhirn, P. Rudati, H. Frohne, O. Nuyken, H. Becker, K. Meerholz, *Nature* **2003,** *421,* 829.

(49) J. Y. Lee, S. T. Lee, *Adv. Mater.* **2004**, *16*, 51.

(50) (a) M. S. A. Abdou, Z. W. Xie, A. Leung, S. Holdcroft, *Synth. Met*. **1992**, *52*,159. (b) M. S. A. Abdou, S. Holdcroft, *Macromolecules* **1993**, *26*, 2954. (c) M. S. A. Abdou, M. I. Arroyo, G. Diaz-Quijada, S. Holdcroft, *Chem. Mater.* **1991**, *3*, 1003.

(51) B-J. de Gans, P. C. Duineveld, U. S. Schubert, *Adv. Mater.* **2004**, *16*, 203.

(52) T. J. Gordon, J. Yu, C. Yang, S. Holdcroft, *Chem. Mater.* **2007**, *19*, 2155.

(53) R. H. Partridge, *Polymer* **1983**, *24*, 733.

(54) J. H. Burroughes, D. D. C. Bradley, A. R. Brown, R. N. Marks, K. MacKay, R. H. Friend, P. L. Burns, A. B. Holmes, *Nature* **1990**, *347*, 539.

(55) J. F. Geisz, D. J. Friedman, J. S. Ward, A. Duda, W. J. Olavarria, T. E. Moriarty, J. T. Kiehl, M. J. Romero, A. G. Norman, K. M. Jones, *Appl. Phys. Lett.* **2008,** *93,* 123505.

(56) (a) J. Peet, J. Y. Kim, N. E. Coates, W. L. Ma, D. Moses, A. J. Heeger, G. C. Bazan, *Nat. Mater.* **2007**, *6*, 497. (b) J. Y. Kim, K. Lee, N. E. Coates, D. Moses, T-Q. Nguyen, M. Dante, A. J. Heeger, *Science* **2007**, *317*, 222. (c) M. J. Currie, J. K. Mapel, T. D. Heidel, S. Goffri, M. A. Baldo, *Science* **2008**, *321*, 226.

(57) S.-S. Sun, N. S. Sariciftci (eds.), in *Organic Photovotaics Mechanisms, Mateials, and Devices*, CRC Press Taylor & Francis Group, Boca Raton, **2005**, Ch. 4.

# CHAPTER 2:

# SYNTHESIS, SOLID-PHASE REACTION, OPTICAL PROPERTIES AND PATTERNING OF THERMALLY-REACTIVE LUMINESCENT POLYFLUORENES

Sections of this chapter have been reproduced in part with permission from:

Xu Han, Xiwen Chen, George Vamvounis, and Steven Holdcroft,

*Macromolecules* **2005**, *38*, 1114-1122, Copyright 2005,

American Chemical Society

## 2.1 Introduction

Since the first report of polymer light-emitting devices (PLEDs) based on poly(*p*-phenylenevinylene) by Burroughes *et al.*,[1] research of photoluminescent and electroluminescent conjugated polymers has intensified. One of the technology drivers is PLED-based full-colour flat panel displays.[2] PLEDs have several advantages over small-molecule LEDs such as low cost due to solution processing and advantages over liquid crystal displays in that they are visible over a much wider range of angle.[3]

An optimized PLED requires efficient and balanced charge injection, good and comparable mobilities for both holes and electrons, and high luminescence quantum yields.[4] Polyfluorenes (PFs) and their derivatives have drawn much attention in this area, due to their good charge transport properties, high quantum yields of photoluminescence in the solid state, and exceptional electro-optical device efficiencies with long operational lifetimes. They have emerged as an attractive class of electroluminescent conjugated polymer that emit colours spanning the entire visible range with high efficiency and low operating voltage.[5] They have been much studied as active materials for potential applications such as PLEDs, organic field effect transistors (FET) [6] and organic photovoltaic cells.[7]

Critical features of this emerging technology are device fabrication and reproducible deposition of active material.[8] In the context of photolithography and soft lithography, several regioregular polythiophenes containing 2-tetrahydropyranyl (THP) group were reported recently.[9,10] Compared with acid-catalyzed photolithography, the soft lithographic process is a low cost technique

that circumvents the use of expensive equipment and eliminates possible damage to the conjugated polymer structure due to irradiation.[10] In addition, soft lithography can pattern flexible surfaces. The strategy of introducing THP groups to the side chain of the conjugated polymer, followed by deprotection would appear favorable for the patterning of photoluminescent polyfluorenes.

In this chapter, the synthesis of a soluble, acid-labile, blue luminescent fluorene-based polymer, poly[9,9'-di(2-(2-tetrahydropyranyloxy)ethyl)fluorene] (PTHPEF, **P1**), is reported. The synthesis route was designed by Dr. Xiwen Chen and Dr. George Vamvounis. This polymer undergoes the solid-state, acid-catalyzed reaction shown in **Scheme 2.1**. Moreover, a series of copolymers based on the fluorene unit were synthesized in order to develop an understanding of structure-property relationships. Thiophene, 3-(2-(2-tetrahydropyranyloxy)ethyl)thiophene (THPET), or 9,9'-dihexylfluorene (diHF) were incorporated into the main chain to obtain copolymers with emissions of different colour (blue, blue-green, green) and high emission intensity. The polymers were also found to retain their optical properties and quantum yields in the solid state after deprotection. Chemical amplified soft lithography was carried out to yield polymer patterns.

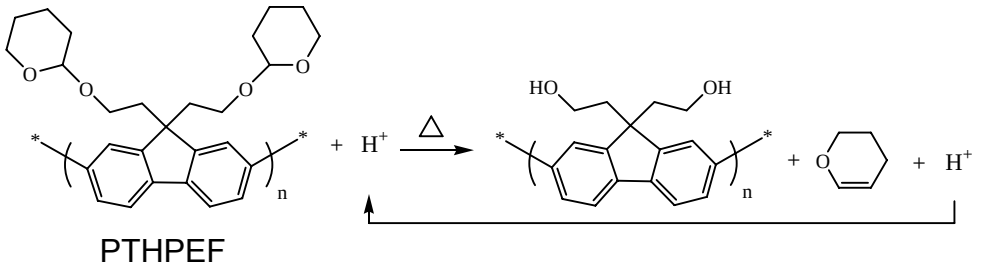


**Scheme 2.1: Acid-catalyzed elimination of dihydropyran from PTHPEF.**

## 2.2 Experimental

### 2.2.1 Measurements

400 MHz $^{1}H$ NMR spectra were obtained in $CD_2Cl_2$ on a Bruker AMX400 spectrometer; 500 MHz $^{1}H$ and 125 MHz $^{13}C$ NMR spectra were obtained in $CD_2Cl_2$ on a Varian AS500 spectrometer; chemical shifts are reported in parts per million (ppm), referenced to $CD_2Cl_2$ ($^{1}H$: δ=5.32 (t); $^{13}C$: δ=54.00 (quintet)). Molecular weights were measured by gel permeation chromatography (GPC) (Waters model 1515 isocratic pump) equipped with μ-Styragel columns against polystyrene standards. Polymers were eluted with THF using a flow rate of 1.0 mL/min and detected with a UV-vis detector (Waters model 2487) at 254 nm. Elemental analyses were obtained using a Carlo Erba Model 1106 CHN analyzer. Low-resolution mass spectra were measured with a Hewlett Packard 5985 GC-mass spectrometer. Matrix-assisted, laser desorption/ionization, time-of-flight, mass spectra (MALDI-TOF) were recorded on a PerSeptive Biosystems Voyager-DE mass spectrometer using 2,5-dihydroxybenzoic acid as the matrix.

Thermogravimetric analyses (TGA) were performed at 10 °C/min on 3 - 5 mg of polymer sample under ambient atmosphere using a Shimadzu TGA-50

thermogravimetric analyzer. The onset temperature was estimated from the point of intersection of two lines: one extrapolated from the slope of the curve just prior to loss of the THP group and the second from the steepest part of the curve. Mass loss was obtained with ± 1 % error. Infrared spectra were recorded using a Bomem Michelson FTIR (120 series). Polymer samples were spin-cast on sodium chloride disks from chloroform, or from chloroform/THF (80:20 vol%) solution when 5 mol% camphorsulfonic acid (CSA) was added. Thin films were heated to ~185 °C for 3 min, and cooled to ambient temperature.

UV-vis absorption spectra were recorded on a Cary 3E (Varian) spectrophotometer. Photoluminescence (PL) spectra were recorded with a Photon Technology International QuantumMaster model QM-1 equipped with an extra sample compartment containing an integrating sphere. Both solution and solid-state absolute quantum yields (± 10 %) were obtained using an integrating sphere as previously reported.[11] Solutions were de-oxygenated with pre-purified nitrogen (99.9 % $N_2$) prior to fluorescence measurements and the sample compartment was flushed with pre-purified nitrogen for thin film measurements. Fluorescent spectra of thin films, spin cast from $CHCl_3$ on quartz, possessed an optical density of ~0.5. Spectra were recorded 22.5° normal to the incident light.

In the presence of 5 mol% camphorsulfonic acid (5 mol% based on the THP unit), polymer films were spin-cast from chloroform/THF (80:20 vol%) solution. Others were spin-cast from chloroform solution. Acid-catalyzed deprotection was carried out by heating the films in the presence of 5 mol% acid at ~185 °C for 3 min. Films not containing acid were also annealed at ~185 °C

for 3 min for comparison. The photographs of the PDMS stamp and the patterned polyfluorenes were taken using a Nikon D1 camera.

### 2.2.2 PDMS Stamp

An elastomeric stamp of PDMS was molded from a photoresist-patterned template. The template was prepared by spin casting a positive photoresist (Microposit 1813, Shipley) from chloroform on a 4 in. diameter Si (100) wafer at 5000 rpm for 30 s and patterning by photolithography. Photolithography was performed with a 1000 W Xe lamp. The wavelength was selected using a 361 nm broadband filter and was focused to a diameter of 3 cm. The radiation intensity was measured to be 1.8 mW/cm$^2$. Photoresist was exposed to UV light through a direct contact chrome-on-glass mask in ambient air at room temperature. The stamp was molded by pouring a prepolymer of PDMS (Sylgard 184, Dow Corning) and a cross-linker in a 10:1 (w:w) ratio onto the template and curing at 60 °C overnight. Peeling off the template gave the PDMS stamp. The smallest feature size is 150 μm. The height of the template relief structure is ~8 μm, determined by profilometry. The intensity of light was measured using a photometer (IL 1350, International Light). The irradiation dose was calculated from the product of the light intensity and irradiation time.

### 2.2.3 Materials

Fluorene, 2-(2-bromoethoxy)tetrahydro-*2*H-pyran, bis(1,5-cyclooctadiene) nickel (0) (Ni(COD)$_2$), 2,2-bipyridyl (BPY), 1,5-cyclooctadiene (COD), 9,9'-dihexylfluorene-2,7-bis(trimethyleneborate) (diHFTMB), 2,5-thiophenediboronic

acid, and tetrakis(triphenylphosphine)palladium ($Pd(PPh_3)_4$) were purchased from Aldrich and used as received. THF and toluene were dried over Na/benzophenone and freshly distilled prior to use. DMF was dried over BaO and freshly distilled prior to use.

**(i) Synthesis of Poly[9,9'-di(2-(2-tetrahydropyranyloxy)ethyl)fluorene] (PTHPEF, P1).** PTHPEF was synthesized by the following procedure (**Scheme 2.2**). Fluorene was brominated using $Br_2$ and coupled with 2-(2'-bromoethoxy)tetrahydro-*2*H-pyran to afford 2,7-dibromo-9,9'-di(2-(2'-tetrahydropyranyloxy)ethyl)fluorene (diBrTHPEF).[12] As described below, the polymer PTHPEF was prepared by the Yamamoto method.[13]

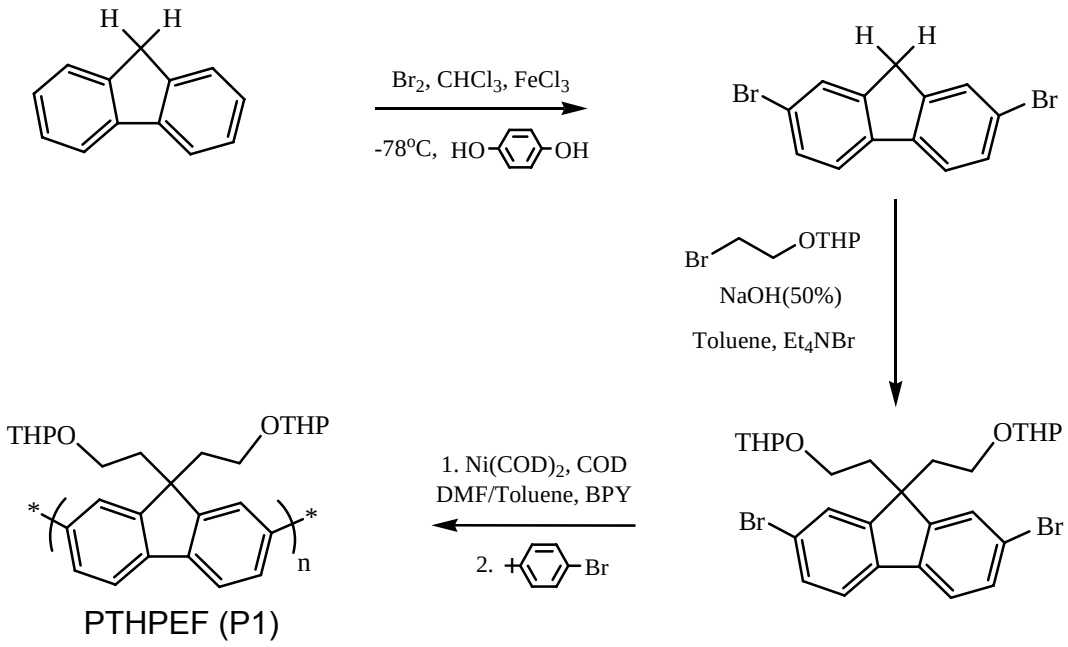


**Scheme 2.2: Synthesis of homopolymer PTHPEF.**

**2,7-Dibromofluorene (diBrF).** Fluorene (10.0 g, 60.2 mmol), $FeCl_3$ (170 mg), and hydroquinone (300 mg) were dissolved in 150 mL of chloroform under nitrogen. In the absence of light, the solution was placed in a dry ice/acetone cooling bath and $Br_2$ (99.5%) (23.1 g, 144 mmol) added dropwise. The reaction mixture was warmed to room temperature and stirred over night. The reaction mixture was quenched with 200 mL water, washed with 10% $NaHSO_3$ and extracted with chloroform. Combined organic phases were washed with water, dried over magnesium sulfate, and concentrated under vacuum. Recrystallization of the crude product from a mixture of ethyl acetate and n-hexane gave 18.0 g (92.3%) of the desired product. $^1$H NMR: (400 MHz, $CD_2Cl_2$) δ 7.69 - 7.47 (m, 6H, aromatic region), 3.88 (s, 2H).

**2,7-Dibromo-9,9'-di(2-(2-tetrahydropyranyloxy)ethyl)fluorene (diBrTHPEF).** To a solution of 5.00 g (15.4 mmol) of 2,7-dibromofluorene, 8.07 g (37.0 mmol) of 2-(2-bromoethoxy)tetrahydro-*2*H-pyran, 15 mL of toluene, and 486 mg of tetraethylammonium bromide as a phase-transfer catalyst was added 7.5 mL of a 50 wt% NaOH aqueous solution. The reaction mixture was refluxed at 90 °C for 48 hours, after which it was cooled to ambient temperature. The resulting mixture was extracted with 100 mL of ethyl acetate, washed with water, dried over anhydrous magnesium sulfate, and concentrated under vacuum. The crude oily product was chromatographed on silica gel with a mixture of ethyl acetate and n-hexane (1/9), and recrystallized in ethanol several times to give 5.50 g (61.5% yield) of the product as colourless crystals: $^1$H NMR: (400 MHz, $CD_2Cl_2$) δ 7.46 - 7.60 (m, 6H, aromatic region), 4.07 (t, 2H), 2.67 - 3.45 (m, 8H),

2.35 (t, 4H), 1.18 - 1.59 (m, 12H). $^{13}C$ NMR (125 MHz, $CD_2Cl_2$) δ 151.9, 139.3, 131.0, 127.5, 122.0, 121.8 (12C, aromatic region), 53.0 (1C, 9,9'-C), 99.1, 62.2, 31.0, 25.9, 19.8 (10C, THP), 40.3 (2C, α-methylene), 63.6 (2C, β-methylene). MS (MALDI-TOF) *m/z* 601 (M + sodium); 603 (M + 2+ sodium); 605 (M + 4 + sodium). Anal. Calcd for $C_{27}H_{32}Br_2O_4$: C, 55.88; H, 5.56; Found: C, 55.71; H, 5.65.

**PTHPEF (P1).** Into a vial were placed bis(1,5-cyclooctadiene) nickel (0) ($Ni(COD)_2$) (660 mg, 2.40 mmol), 2,2-bipyridyl (BPY) (375 mg, 2.40 mmol), 1,5-cyclooctadiene (COD) (0.29 mL, 2.4 mmol), and anhydrous DMF (2.5 mL) in a dry box with nitrogen. This mixture was stirred at 80 °C for 30 min to form active catalyst. The monomer 2,7-dibromo-9,9'-di(2-(2-tetrahydropyranyloxy)ethyl) fluorene (diBrTHPEF) (870 mg, 1.50 mmol) in 9 mL of anhydrous toluene was added to the mixture. The polymerization proceeded at 60 °C for 6 days, and then 1-bromo-4-*tert*-butylbenzene (0.19 mL, 0.10 mmol), as an end-capping agent, was added and the mixture reacted for 24 h. The resulting polymer was purified by aluminum oxide chromatography, precipitated in methanol and dried under vacuum for 24 h. The yield was 387 mg (61.4%). $^{1}H$ NMR: (400 MHz, $CD_2Cl_2$) δ 7.49 - 7.87 (m, 6H, aromatic region), 4.15 (s, 2H), 2.45 - 3.49 (m, 12H), 1.26 - 1.61 (m, 12H). $^{13}C$ NMR (125 MHz, $CD_2Cl_2$) δ 150.9, 141.2, 140.2, 127.2, 122.5, 120.7 (12C, aromatic region); 52.6 (1C, 9,9'-C), 99.2, 62.3, 31.1, 26.0, 19.9 (10C, THP), 40.7 (2C, α-methylene), 64.0 (2C, β-methylene). Anal. Calcd for $C_{27}H_{32}O_4$: C, 77.11; H, 7.67; Found: C, 71.07; H, 7.74.

**(ii) Synthesis of Poly[9,9'-di(2-(2-tetrahydropyranyloxy)ethyl) fluorene-alt-9,9'-dihexylfluorene] (PTHPEF-alt-diHF, P2).** 2,7-dibromo-9,9'-di(2-(2-tetrahydropyranyloxy)ethyl)fluorene (diBrTHPEF) and 9,9'-dihexyl fluorene-2,7-bis(trimethyleneborate) (diHFTMB) were copolymerized by Suzuki coupling[14] to yield an alternating copolymer PTHPEF-alt-diHF (**Scheme 2.3**).

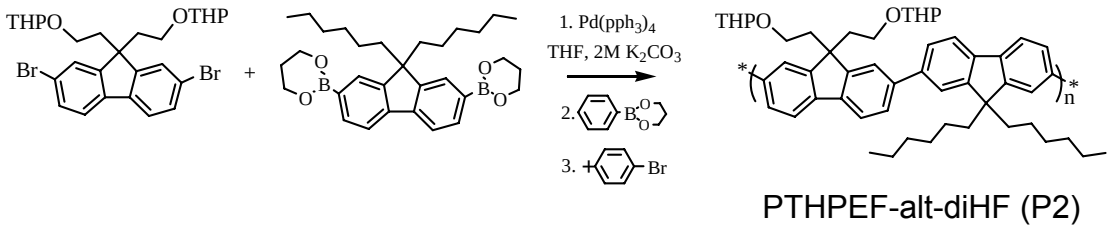


PTHPEF-alt-diHF (P2)

**Scheme 2.3: Synthesis of copolymer PTHPEF-alt-diHF.**

**PTHPEF-alt-diHF (P2).** To a 20 mL Schlenk flask under nitrogen were placed 9,9'-dihexylfluorene-2,7-bis(trimethyleneborate) (diHFTMB) (446 mg, 0.862 mmol), 2,7-dibromo-9,9'-di(2-(2-tetrahydropyranyloxy)ethyl)fluorene (diBrTHPEF) (500 mg, 0.862 mmol), and THF (5 mL). After the solid dissolved completely, 2 M $K_2CO_3$ solution (1.1 mL, 2.16 mmol) and $Pd(PPh_3)_4$ (39.8 mg, 0.0345 mmol) were added and the flask was sealed with a rubber stopper. The mixture was then heated to 60 °C for 6 days. (Trimethyleneborate)benzene as an end-capping agent (10 mg, 0.05 mmol) was added and the mixture allowed to react continually for 24 h, and then 1-bromo-4-*tert*-butylbenzene as another end-capping agent (0.19 mL, 0.10 mmol) was added and the mixture allowed to react continually for another 24 h. THF was removed first by rotary evaporator, and then the reaction mixture was dissolved in chloroform and washed with water 3

times. The organic layer was dried over $MgSO_4$ and the resulting polymer was purified by aluminum oxide chromatography, precipitated in methanol and dried under vacuum for 24 h. The yield was 582 mg (89.7%). $^1$H NMR: (500 MHz, $CD_2Cl_2$) δ 7.50 - 7.89 (m, 12H, aromatic region); 4.18 (s, 2H), 2.88 - 3.53 (m, 8H), 2.60 (br, 4H) (THPEF); 2.17 (br, 4H), 0.77 - 0.82 (t, 10H) (diHF); 1.14 - 1.47 (m, 24H, THPEF and diHF). $^{13}$C NMR (125 MHz, $CD_2Cl_2$) δ 150.8, 141.3, 140.2, 127.1, 122.5, 120.7 (12C, aromatic region), 52.6 (1C, 9,9'-C), 40.7 (2C, α-methylene), 64.1 (2C, β-methylene), 99.2, 62.3, 31.1, 26.0, 20.0 (10C, THP) (THPEF); 152.3, 140.9, 140.7, 126.7, 122.0, 120.5 (12C, aromatic region), 56.0 (1C, 9,9'-C), 41.1, 32.1, 30.3, 24.5, 23.2, 14.4 (12C) (diHF). Anal. Calcd for $C_{52}H_{64}O_4$: C, 82.94; H, 8.57. Found: C, 79.12; H, 8.48.

**(iii) Synthesis of Poly[9,9'-di(2-(2-tetrahydropyranyloxy)ethyl) fluorene-alt-thiophene] (PTHPEF-alt-T, P3).** Using the same method as described above, 2,7-dibromo-9,9'-di(2-(2-tetrahydropyranyloxy)ethyl)fluorene (diBrTHPEF) and 2,5-bis(tetramethylethyleneborate)thiophene (TMEBT) were copolymerized by Suzuki coupling to yield alternating copolymer PTHPEF-alt-T (P3) (**Scheme 2.4**).

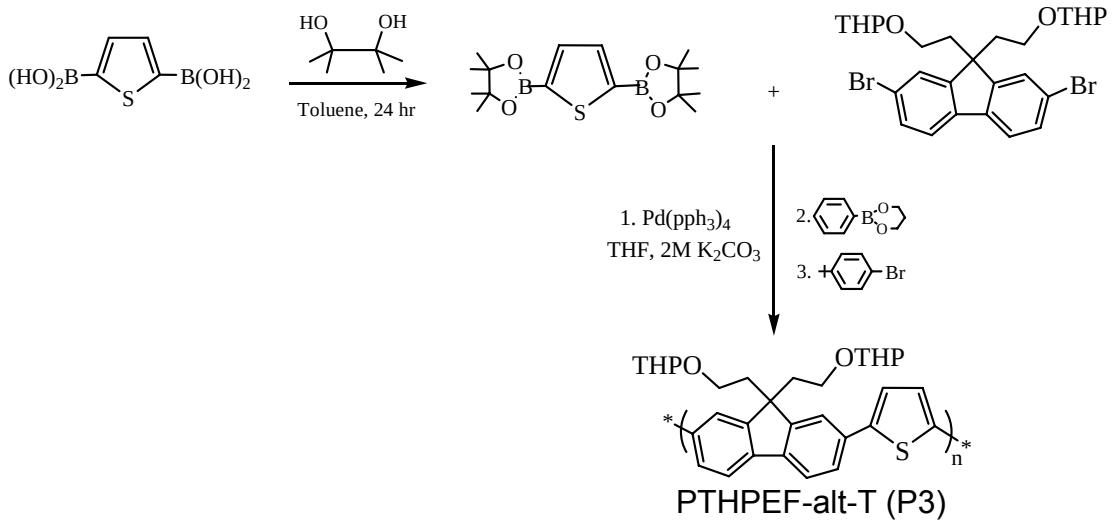


**Scheme 2.4: Synthesis of copolymer PTHPEF-alt-T.**

**2,5-Bis(tetramethylethyleneborate)thiophene (TMEBT).** To a 100 mL two neck round-bottom flask equipped with Dean-Stark trap, molecular sieve and refluxing condenser under nitrogen were placed 2,5-thiophenediboronic acid (0.859 g, 5.00 mmol), pinacol (1.30 g, 5.00 mmol), and toluene (40 mL). The mixture was heated under reflux for 24 h. The organic layer was separated, washed with water 3 - 5 times and dried with anhydrous $MgSO_4$. The solvent was removed under reduced pressure and the product was purified by recrystallization from ether three times to yield a white crystalline product (0.35 g, 20.8% yield). $^1$H NMR: (400 MHz, $CD_2Cl_2$) δ 7.61 (s, 2H); 1.35 - 1.26 (t, 24H, $CH_3$).

**PTHPEF-alt-T (P3).** To a 20 mL Schlenk flask under nitrogen were placed 2,5-bis(tetramethylethyleneborate)thiophene (TMEBT) (290 mg, 0.862 mmol), 2,7-dibromo-9,9'-di(2-(2-tetrahydropyranyloxy)ethyl)fluorene (diBrTHPEF) (500 mg, 0.862 mmol), and THF (5 mL). After the solid dissolved completely, 2

M $K_2CO_3$ solution (1.08 mL, 2.16 mmol) and $Pd(PPh_3)_4$ (39.8 mg, 0.0345 mmol) were added and the flask was sealed with a rubber stopper. The mixture was then heated to 60 °C for 6 days. (Trimethyleneborate)benzene as one end-capping agent (10 mg, 0.05 mmol) was added and allowed to react for 24 h, and then 1-bromo-4-*tert*-butylbenzene as another end-capping agent (0.19 mL, 0.10 mmol) reacted for 24 h. THF was first removed, and the reaction mixture dissolved in chloroform and washed with water 3 times. The organic layer was dried over $MgSO_4$ and the resulting polymer was purified by aluminum oxide chromatography, precipitated in methanol and dried under vacuum for 24 h. The yield was 240 mg (55.4%). $^1$H NMR: (400 MHz, $CD_2Cl_2$) δ 7.12 - 7.77 (m, 8H, aromatic region), 4.12 (t, 2H), 2.74 - 3.48 (m, 8H), 2.49 (br, 4H), 1.23 - 1.56 (m, 12H). Anal. Calcd for $C_{31}H_{34}O_4S$: C, 74.07; H, 6.82. Found: C, 67.72; H, 6.55.

**(iv) Synthesis of Poly[9,9'-di(2-(2-tetrahydropyranyloxy)ethyl) fluorene-co-(2-(2-tetrahydropyranyloxy)ethyl)thiophene] (PTHPEF-co-THPET, P4).**

PTHPEF-co-THPET (50:50) was synthesized by the following procedure (**Scheme 2.5**). 3-(2-Hydroxyethyl)-thiophene was brominated by NBS in DMF and protected by reacting with dihydropyran to afford 2,5-dibromo-3-(2-(2-tetrahydropyranyl-2-oxy)ethyl)thiophene (diBrTHPET).[5] Using the same coupling method as described for PTHPEF, 2,7-dibromo-9,9'-di(2-(2-tetrahydropyranyloxy)ethyl)fluorene (diBrTHPEF) and 2,5-dibromo-3-(2-(2-tetrahydropyranyl-2-oxy)ethyl)thiophene (diBrTHPET) were copolymerized using

a 50:50 feed ratio by the Yamamoto method to yield a statistically random copolymer PTHPEF-co-THPET.

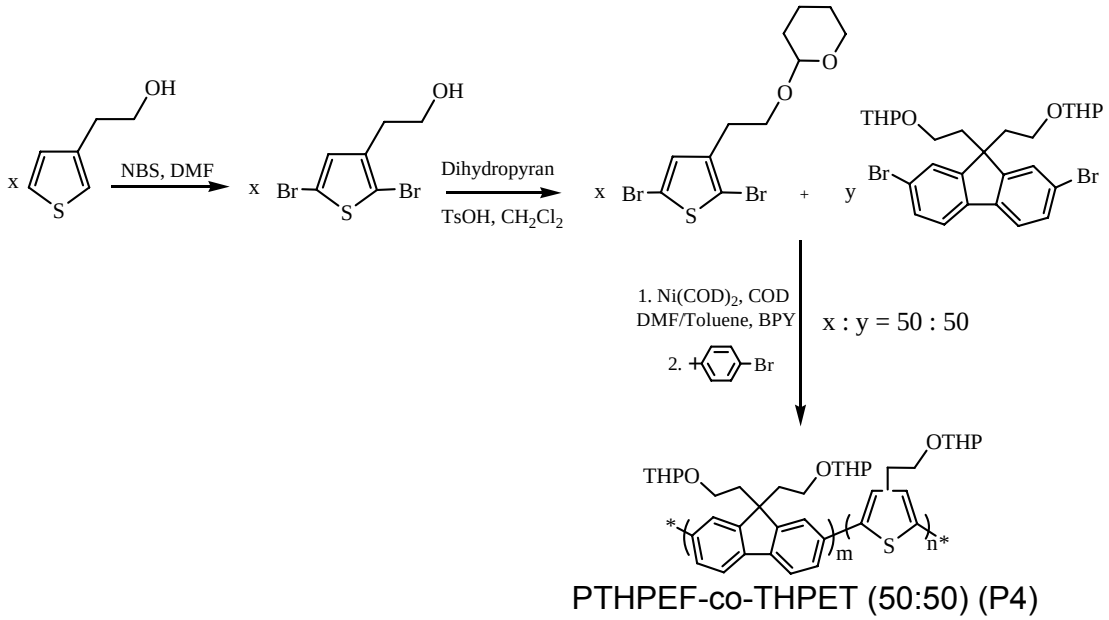


PTHPEF-co-THPET (50:50) (P4)

**Scheme 2.5: Synthesis of copolymer PTHPEF-co-THPET.**

**2,5-Dibromo-3-(2-hydroxy)ethylthiophene (diBrHET).** In the absence of light, a solution of NBS (7.12 g, 40.0 mmol) in DMF (20 mL) was added dropwise to a solution of 3-(2-hydroxyethyl)-thiophene (2.56 g, 20.0 mmol) in DMF (20 mL). After stirring for 3 h, the reaction mixture was quenched with ice-water and extracted with ether. Combined organic phases were washed with water, dried over magnesium sulfate, and concentrated under vacuum. Distillation of the crude product gave 4.46 g (78%) of diBrHET. $^{1}$H NMR: (400 MHz, $CD_2Cl_2$) δ 6.91 (s, 1H), 3.78 (t, 2H), 2.78 (t, 2H), 1.80 (s, 1H). $^{13}$C NMR: (125 MHz, $CD_2Cl_2$) δ 140.2, 132.0, 111.1, 109.8 (4C, thienyl ring), 33.3 (1C, α-methylene), 62.1 (1C, β-methylene). MS *m/z* (based on $^{79}$Br). 284 $M^+$; 286 (M +

2)$^+$; 288 (M + 4)$^+$. Anal. Calcd for $C_6H_6Br_2OS$: C, 25.20; H, 2.11. Found: C, 25.09; H, 2.16.

**2,5-Dibromo-3-(2-(2-tetrahydropyranyl-2-oxy)ethyl)thiophene (diBrTHPET).** To a solution of 2,5-dibromo-3-(2-hydroxy)-ethylthiophene (4.29 g, 15.0 mmol) and freshly distilled dihydropyran (2.52 g, 30.0 mmol) in 80 mL of dry chloroform, cooled to 0 °C, was added 29 mg (0.15 mmol) of *p*-toluene-sulfonic acid monohydrate under $N_2$. After stirring for 10 min at 0 °C, for 2 h at room temperature, the mixture was poured into ice-water and extracted with chloroform. The organic phase was combined, washed with saturated sodium hydrogen carbonate solution and water, and dried over magnesium sulfate. The crude product, obtained by removal of solvent, was chromatographed on silica gel (Silica Gel 60, EM Science) with chloroform to afford 4.16 g (75%) of the desired monomer. $^1$H NMR: (400 MHz, $CD_2Cl_2$) δ 7.25 (s, 1H), 4.60 (s, 1H), 3.91 - 3.48 (m, 4H,), 2.84 (t, 2H), 1.82 - 1.49 (m, 6H). $^{13}$C NMR: (125 MHz, $CD_2Cl_2$) δ 140.7, 132.3, 110.7, 109.5 (4C, thienyl ring), 99.1, 62.5, 31.2, 26.1, 20.0 (5C, THP), 30.6 (1C, α-methylene), 66.4 (1C, β-methylene). MS *m/z* (based on $^{79}$Br). 368 M$^+$; 370 (M + 2)$^+$; 372 (M + 4)$^+$. Anal. Calcd for $C_{11}H_{14}Br_2O_2S$: C, 35.70; H, 3.81. Found: C, 35.72; H, 3.76.

**PTHPEF-co-THPET (50:50) (P4).** Into a vial were placed bis(1,5-cyclooctadiene) nickel (0) ($Ni(COD)_2$) (440 mg, 1.60 mmol), 2,2-bipyridyl (BPY) (250 mg, 1.60 mmol), 1,5-cyclooctadiene (COD) (0.20 mL, 1.6 mmol), and anhydrous DMF (1.5 mL) in a dry box with nitrogen. This mixture was stirred at 80 °C for 30 min to form the active catalyst. The monomers 2,7-dibromo-9,9'-

di(2-(2-tetrahydropyranyloxy)ethyl)fluorene (diBrTHPEF) (290 mg, 0.500 mmol) and 2,5-dibromo-3-(2-(2-tetrahydropyranyl-2-oxy)ethyl)thiophene (diBrTHPET) (185mg, 0.500 mmol) in 6 mL of anhydrous toluene were added to the mixture. The polymerization proceeded at 60 °C for 6 days, and then 1-bromo-4-*tert*-butylbenzene as end-capping agent (0.19 mL, 0.10 mmol) was added and reacted for another 24 h. The resulting polymer was purified by column chromatography ($Al_2O_3$), precipitated in methanol and finally dried under vacuum for 24 h. The yield was 202 mg (64.1%). $^1$H NMR: (400 MHz, $CD_2Cl_2$) δ 7.32 - 7.79 (m, 7H, aromatic region), 4.14 (s, 3H), 2.43 - 3.47 (m, 18H), 1.24 - 1.64 (m, 18H). Anal. Calcd for $C_{38}H_{46}O_6S$: C, 72.38; H, 7.30. Found: C, 67.10; H, 7.33.

## 2.3 Results and Discussion

### 2.3.1 Polymer Structure

The structures of these polymers were confirmed by NMR spectroscopy (shown in the Appendix of Chapter 2). Homopolymer **P1** gave $^1$H NMR resonance peaks at 7.49 - 7.87 and 4.15 ppm assigned to the aromatic protons of the fluorene ring and the methine of the THP group, respectively. $^{13}$C NMR of this homopolymer exhibited fourteen resonance peaks. The six peaks at 150.9, 141.2, 140.2, 127.2, 122.5, and 120.7 ppm were assigned to fluorene carbons.[13b] The observed peaks at 99.2, 62.3, 31.1, 26.0, and 19.9 ppm are characteristic of the THP group.[15] Peaks at 40.7 and 64.0 ppm were assigned to α- and β-methylene carbons, respectively. The peak at 52.6 ppm was assigned to the 9,9'-carbon.

Alternating copolymer **P2** gave resonance peaks at 7.50 - 7.89 ppm assigned to the aromatic protons of the fluorene ring, one resonance peak at 4.18 ppm assigned to the methine of THP group, and two α-methylene resonance peaks at 2.60 and 2.17 ppm corresponding to THPEF and diHF units, respectively. Resonance peaks were observed in the $^{13}C$ NMR spectra of the copolymer **P2** at 99.2, 64.1, 62.3, 40.7, 31.1, 26.0, and 20.0 ppm, assigned to the seven carbons of THPEF unit, and at 41.1, 32.1, 30.3, 24.5, 23.2, and 14.4 ppm, attributed to the six carbons of the hexyl chain. In the aromatic region, peaks were observed at 150.8, 141.3, 140.2, 127.1, 122.5, and 120.7 ppm, and assigned to the fluorene ring carbons of THPEF, and at 152.3, 140.9, 140.7, 126.7, 122.0, and 120.5 ppm, assigned to the fluorene ring carbons of diHF. The two peaks of 9,9'-carbons at 52.6 and 56.0 ppm were attributed to THPEF and diHF respectively.

Alternating copolymer **P3** gave resonance peaks at 7.12 - 7.77 ppm assigned to aromatic protons of the fluorene and thienyl ring, and one resonance peak at 4.12 ppm assigned to the methine of THP group, and one α-methylene resonance peak at 2.49 ppm corresponding to the THP group. Random copolymer **P4** (THPEF:THPET/50:50) gave resonance peaks at 7.32 - 7.79 ppm assigned to aromatic protons of the fluorene and thienyl ring, and one resonance peak at 4.14 ppm assigned to the methine of THP group. The composition of **P4** was determined from the ratio (7.0:3.0) of integrals of the peaks of aromatic protons (6m%+1n%) and methine (2m%+1n%) to yield m : n = 50:50, which is consistent with the feed ratio.

The molecular weight and polydispersity indices of these four polyfluorenes are shown in **Table 2.1**. The molecular weights and the polydispersities of **P1**, **P2** and **P4** are typical of fluorene-based polymers prepared by Yamamoto or Suzuki coupling. However, **P3** possessed a lower molecular weight. This might result from its poor solubility, which was noticeably low because of the absence of a side chain on the thienyl ring. Another reason may be the lower reaction temperature employed. Usually the molecular weights can be increased with reaction temperature, but, in this case, the temperature was limited to 65 °C to prevent cleavage of the THP group.

**Table 2.1: Molecular weight of polyfluorenes.**

| Polymers | $M_n$ | $M_w$ | PDI |
|---|---|---|---|
| **P1** | 23 800 | 34 300 | 1.44 |
| **P2** | 23 800 | 48 200 | 2.02 |
| **P3** | 3 700 | 3 800 | 1.03 |
| **P4** | 10 800 | 26 000 | 2.42 |

### 2.3.2 Thermal Properties and Solid-State Reaction

THP is a relatively thermally stable protecting group. For example, poly(3-(2-(2-tetrahydropyranyloxy)ethyl)thiophene) (PTHPET) was reported stable up to 220-230 °C.[9a, b] For **P1** and **P4**, a significant loss in mass is observed by TGA above this temperature, as shown in **Table 2.2**. **P3** exhibits a lower deprotection

temperature, which is ascribed to its lower molecular weight.[10a] In contrast, **P2** shows quite a high deprotection temperature, owing to its higher molecular weight and the stabilizing effect of the alkyl side chains on the main chain. The incorporation of 9,9'-dihexylfluorene (diHF) groups into the chain might actually increase the rigidity of the polymer and increase molecular interactions by promoting side chain aggregation. This phenomenon has also been observed in a polythiophene copolymer bearing THP groups, as reported in literature.[9b] The THP functionality represents 40 wt% of **P1** and **P4**, 22 wt% of **P2** and 34 wt% of **P3**. The observed losses in mass of **P1**, **P2**, **P3** and **P4** are 40, 20, 34, and 38 wt%, which are consistent with calculated losses of mass due to thermolytic cleavage of the THP group and elimination of dihydropyran.

**Table 2.2: Thermal properties of polyfluorenes.**

| Polymers | Theoretical mass loss (based on removal of THP groups) (%) | In the absence of acid | | In the presence of 5 mol% camphorsulfonic acid | |
|---|---|---|---|---|---|
| | | Onset (°C) | Observed mass loss (%) | Onset (°C) | Observed mass loss (%) |
| **P1** | 40 | 240 | 40 | 120 | 40 |
| **P2** | 22 | 360 | 20 | 150 | 22 |
| **P3** | 34 | 200 | 34 | 110 | 34 |
| **P4** | 40 | 230 | 38 | 140 | 40 |

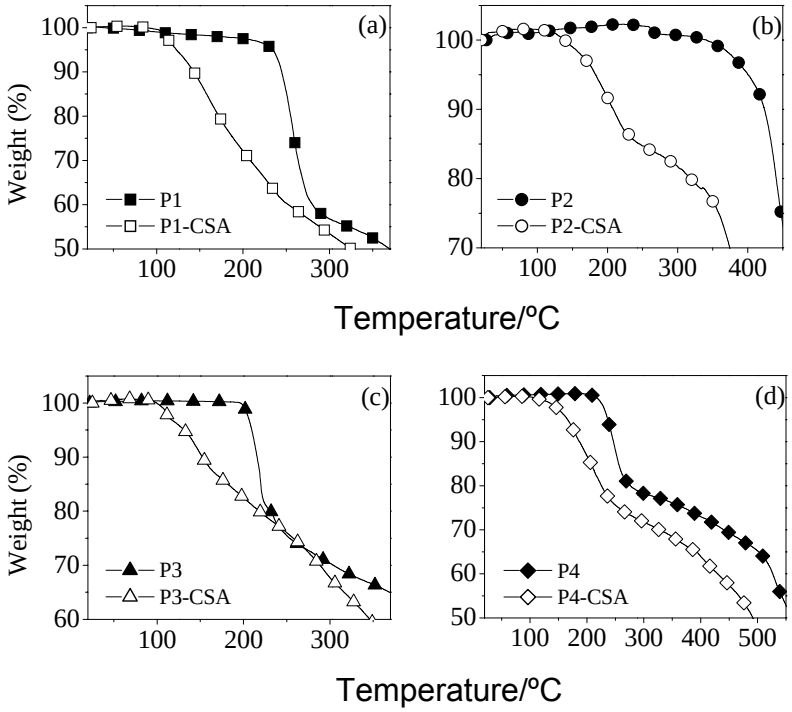
(a)
(b)
(c)
(d)
Weight (%)
P1
P1-CSA
P2
P2-CSA
P3
P3-CSA
P4
P4-CSA
Temperature/ºC

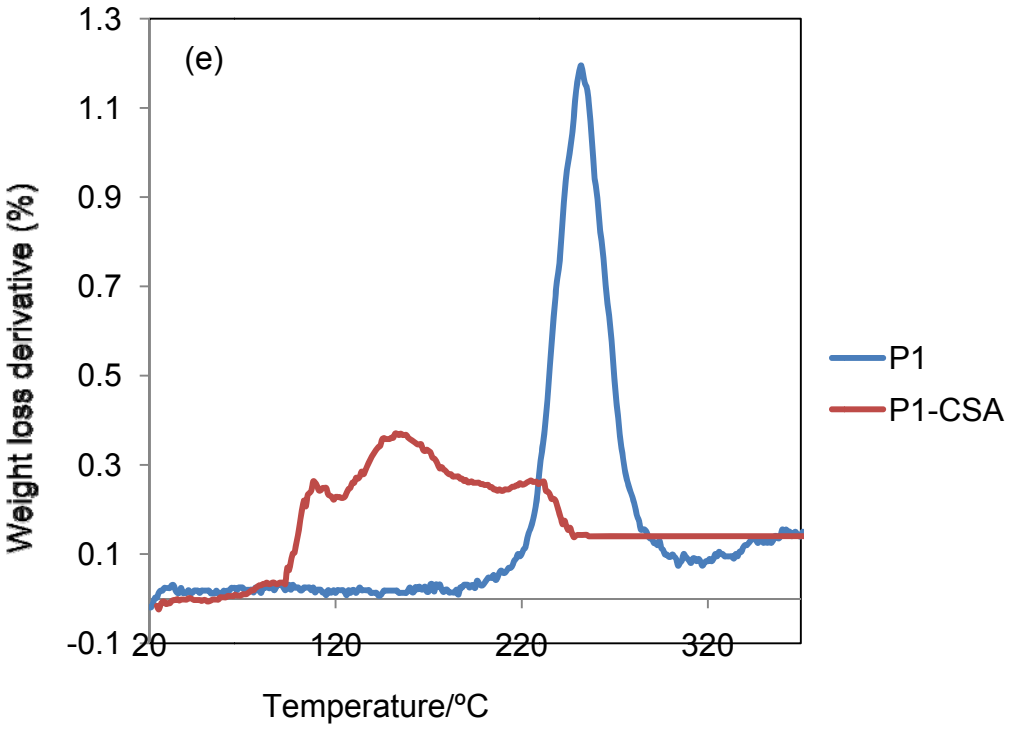
(e)
Weight loss derivative (%)
P1
P1-CSA
Temperature/ºC

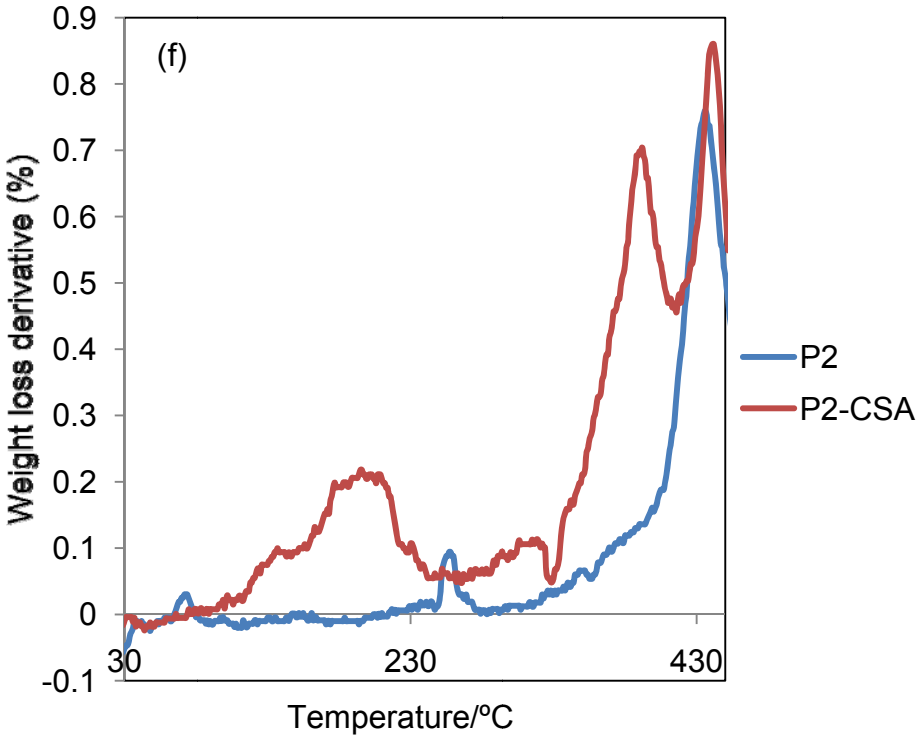
(f)
Weight loss derivative (%)
0.9
0.8
0.7
0.6
0.5
0.4
0.3
0.2
0.1
0
-0.1
30
230
430
Temperature/ºC
P2
P2-CSA

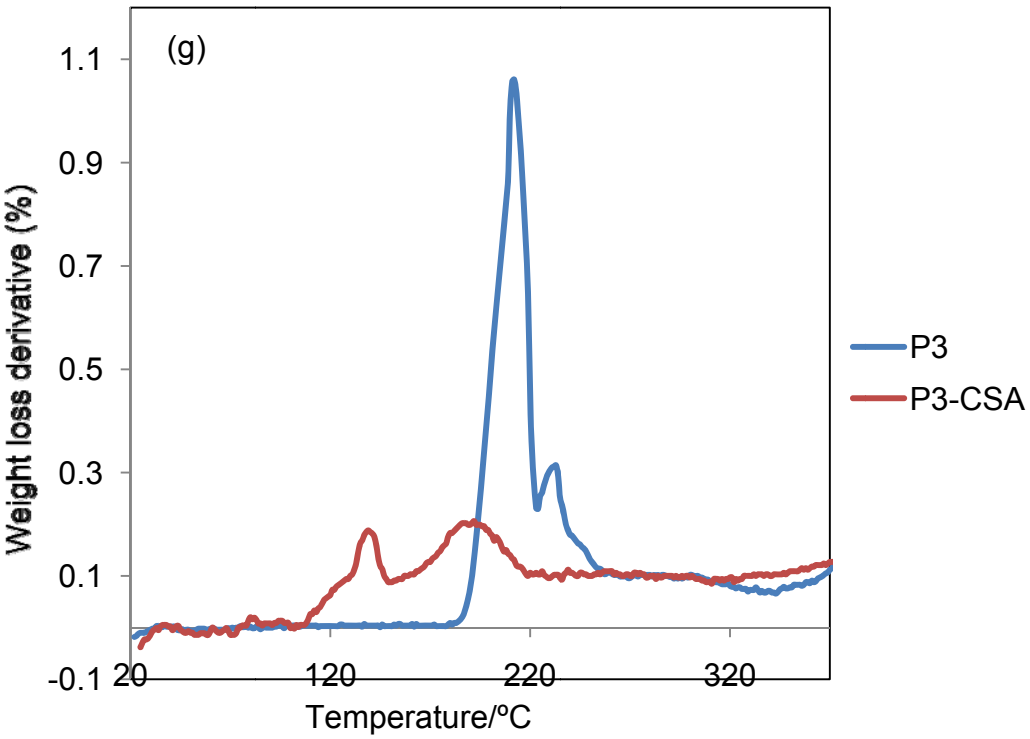
(g)
Weight loss derivative (%)
1.1
0.9
0.7
0.5
0.3
0.1
-0.1
20
120
220
320
Temperature/ºC
P3
P3-CSA

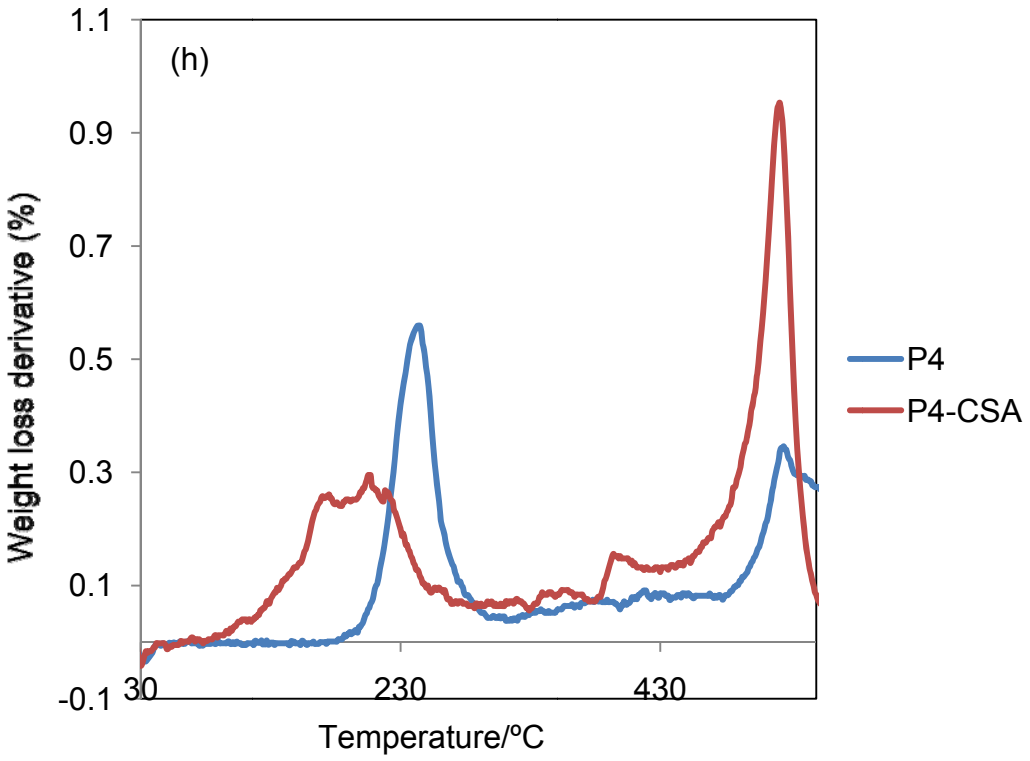


**Figure 2.1: TGA thermograms and derivative plots of polyfluorenes in the absence and presence of 5 mol % camphorsulfonic acid (CSA): (a), (e) P1 (PTHPEF); (b), (f) P2 (PTHPEF-alt-diHF); (c), (g) P3 (PTHPEF-alt-T); and (d), (h) P4 (PTHPEF-co-THPET).**

Using the same scan rate of 10 °C/min, the onset temperatures required to remove the THP group from the polyfluorenes (110-150 °C) are much lower in the presence of 5 mol % camphorsulfonic acid (mol % based on the THP unit), as shown in **Figure 2.1**. The observed losses in mass of **P1**, **P2**, **P3** and **P4** are 40, 22, 34, and 39 wt%, consistent with the theoretical losses in mass. Only 5 mol % acid is needed to promote full deprotection of the THP group, indicating the removal of THP is catalyzed similar to that reported for polythiophenes.[9]

FTIR analysis shows the emergence of a broad signal at ~3450 $cm^{-1}$ at 185 °C due to the formation of the hydroxyl group (**Figure 2.2**). FTIR signals

assigned to the THP group, originally at 1030 - 1130 and 2940 $cm^{-1}$, diminish upon acid-catalyzed reaction. The appearance of one peak at 1742 $cm^{-1}$ is due to the camphorsulfonic acid. The camphorsulfonic acid has another strong peak at ~2940 $cm^{-1}$, which interferes with the peak due to the polymer at 2940 $cm^{-1}$. Furthermore, no obvious new fluorenone peaks were observed at 1717, 1606, and 1457 $cm^{-1}$,[16] although the acid-catalyzed reaction was carried out in the presence of air. This statement is confirmed by PL spectra of deprotected polyfluorenes, which shows the absence of the characteristic, fluoerenone, green emission peak. Therefore, the solid-state reaction can be carried out at lower temperatures to avoid significant oxidation in ambient environment and loss of fine optical properties.

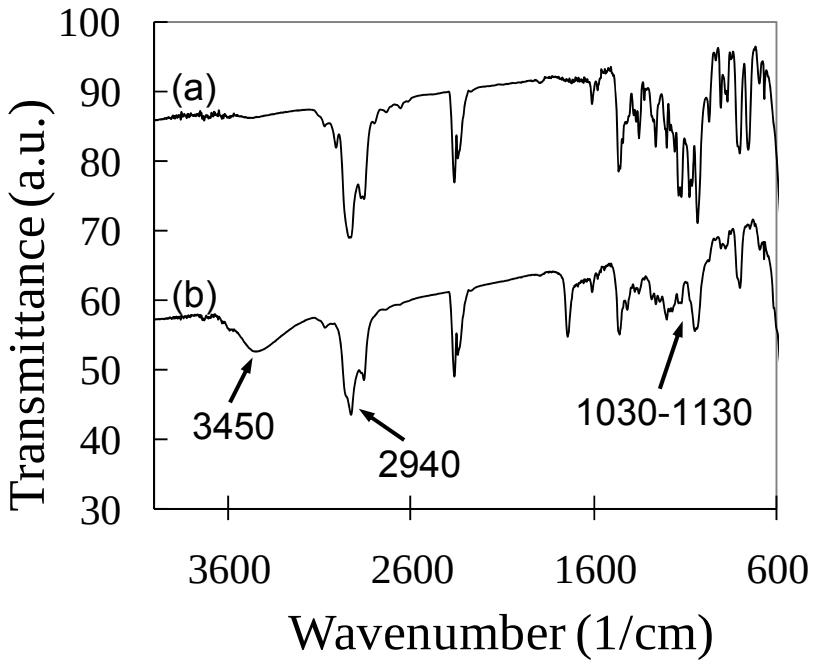


**Figure 2.2: FTIR of P3 (PTHPEF-alt-T) before (a) and after (b) acid-catalyzed deprotection.**

### 2.3.3 Optical properties

The optical properties of the polyfluorenes in THF solution, in the solid state before/after deprotection and after annealing are summarized in **Table 2.3**.

**Table 2.3: Optical properties of polyfluorenes.**

| Polymers | Solution (THF) | | | Solid State | | | Films-Deprotected | | | Films-Annealed | |
|---|---|---|---|---|---|---|---|---|---|---|---|
| | $\lambda_{max}$ Abs, nm | $\lambda_{max}$ Em, nm | $\Phi_{fl}$ | $\lambda_{max}$ Abs, nm | $\lambda_{max}$ Em, nm | $\Phi_{fl}$ | $\lambda_{max}$ Abs, nm | $\lambda_{max}$ Em, nm | $\Phi_{fl}$ | $\lambda_{max}$ Abs, nm | $\lambda_{max}$ Em, nm |
| **P1** | 373 | 414 | 1.00 | 375 | 421 | 0.37 | 380 | 428 | 0.37 | 380 | 431 |
| **P2** | 387 | 416 | 0.96 | 389 | 423 | 0.27 | 389 | 427 | 0.22 | 391 | 427 |
| **P3** | 402 | 465 | 0.76 | 410 | 501 | 0.36 | 412 | 507 | 0.36 | 406 | 501 |
| **P4** | 379 | 502 | 0.62 | 380 | 539 | 0.29 | 381 | 557 | 0.29 | 381 | 540 |

#### 2.3.3.1 UV-vis Absorption and PL Properties of Polyfluorenes prior to Deprotection

The UV-vis and PL spectra of polyfluorenes in THF solution and in the solid state are shown in **Figure 2.3**. Photographs of polyfluorenes in solvent ($CHCl_3$) and in the form of films under visible and UV light are shown in **Figure 2.4**.

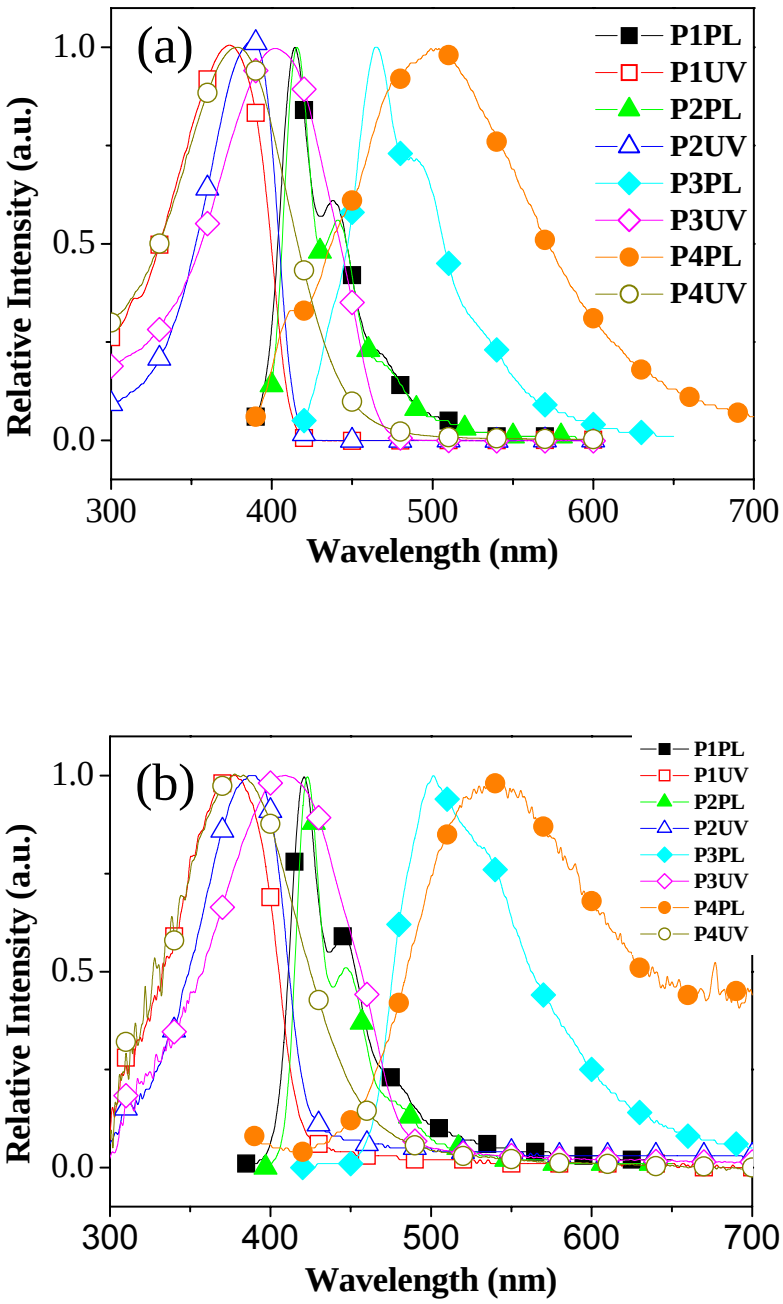


**Figure 2.3: UV-vis and PL spectra of polyfluorenes in solution (a) and the solid state (b): P1 (PTHPEF), P2 (PTHPEF-alt-diHF), P3 (PTHPEF-alt-T), and P4 (PTHPEF-co-THPET).**

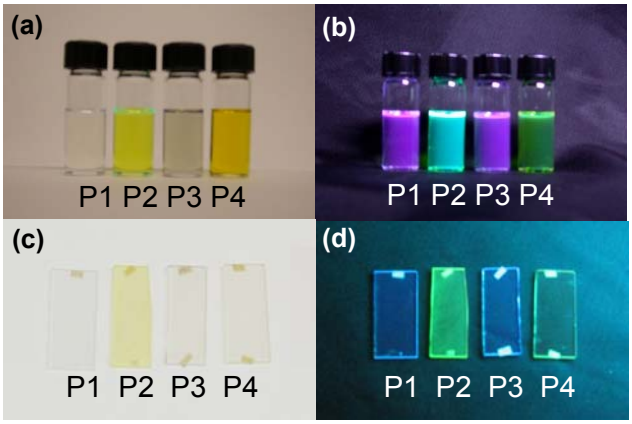


**Figure 2.4: Polyfluorenes in solvent ($CHCl_3$) under visible (a) and UV (b) light (λ=254 nm) and in the form of films under visible (c) and UV (d) light: P1 (PTHPEF), P2 (PTHPEF-alt-diHF), P3 (PTHPEF-alt-T), and P4 (PTHPEF-co-THPET).**

The maximum absorption wavelengths of **P1**, **P2**, **P3**, and **P4** in solution are: 373, 387, 402 and 379 nm; and in the solid state: 375, 389, 410, and 380 nm, respectively. The absorption spectra show a character that $\lambda_{max}$ of films is red shifted compared to that in solution. $\lambda_{max}$ of **P3** in solution and in the solid state are respectively 29 nm and 35 nm higher than those of **P1**, owing to higher electron density of the thienyl ring versus fluorene and the lower band gap of **P3**. $\lambda_{max}$ of **P4**, possessing thienyl rings bearing a THP group, is very close to **P1**, differing by only ~5 - 6 nm. This might be due to the random composition of **P4**. $\lambda_{max}$ of **P4** is expected to be due to the fluorene block. The thienyl block contributes to the lower energy region of the absorption spectra, resulting in a slightly broader full width at half maximum (FWHM) (86 nm for **P4** versus 72 nm for **P1** in solution). The THP side chains on the thienyl ring of **P4** are also

expected to twist the thienyl ring and cause a blue shift of absorption, compared to **P3,** which does not possess a side chain on the thienyl ring. Compared to another alternating polymer, poly[2,7-(9,9'-dihexylfluorene)-alt-2,5-(decylthiophene)], described in the literature, with different side chains on both fluorene and thienyl rings,[17] **P4** possesses a blue-shifted $\lambda_{max}$. The blue-shifted $\lambda_{max}$ was also observed for copolymers of PTHPET-co-P3HT.[9b] With increase of the mole fraction of the bulky THP group, $\lambda_{max}$ is more blue-shifted, because of the group's role in affecting long range structural order. This might also be due to the random composition[18] of **P4** and the less effective conjugation for sterically hindered THP groups. A slightly narrower FWHM (around 66 nm) for the literature polymer supports this explanation.

The maximum emission wavelengths of homopolymer **P1** and alternating copolymer **P2** in solution (414 and 416 nm, respectively, violet-blue colour) and in the solid state (421 and 423 nm, respectively, blue colour) are quite similar and both of their PL spectra are sharp, indicating that the effect of THP versus hexyl side chains attached to the fluorene backbone on the emission spectra is very small. Although both **P1** and **P2** possess almost quantitative absolute quantum yields in solution ($\Phi_{fl}$: 1.00 and 0.96), their quantum yields in the solid state ($\Phi_{fl}$: 0.37 and 0.27) are different. The higher quantum yield for **P1** may indicate that the bulky THP side chain may be more efficient at preventing molecular interaction.[19] The introduction of THP groups to the blue luminescent polyfluorenes on the one hand facilitates patterning of the polymer, but it also improves the emission intensity of the polymer.

The maximum emission wavelengths of alternating copolymer **P3** in solution and in the solid state are 465 nm (blue-green colour) and 501 nm (cyan). Its quantum yields in solution and in the solid state are still high (0.76 and 0.36, respectively). The quantum yield of **P3**, especially in the solid state, is surprisingly high, given that no side chain is present on the thienyl ring to prevent interchain interaction. Other similar copolymers with different side chains on the fluorene in the literature[14a,17,20] have slightly lower values in solutions and very low values in solid films. The reason may be due to the bulky THP side chains, and the contribution of end-capping groups in **P3**. Otherwise, the uncapped end groups may introduce some defects to the emitting structure.[21]

The emission wavelengths of random copolymer **P4** in solution and in the solid state are 502 nm (cyan) and 539 nm (green). Moreover, its emission intensity is high both in solution and in the solid state ($\Phi_{fl}$: 0.62 and 0.29), so that strong emission can be observed under UV light as shown in **Figure 2.4**. In addition, compared to **P3** and to other alternating copolymers with side chains on both fluorene and thienyl rings, **P4** exhibits a red shifted emission wavelength, although its absorption wavelength is blue shifted. The reason may be also attributed to the random structure of copolymer **P4**. The different units of fluorene and thiophene may form two kinds of block, polyfluorene block, polythiophene block, and even graded polymers. The higher energy polyfluorene block might therefore be transferring energy to the lower energy polythiophene blocks to yield enhanced green emission.[20,22]

#### 2.3.3.2 UV-vis Absorption and PL Emission Properties of Polyfluorenes after Deprotection

The UV-vis and PL spectra of the polyfluorenes as a pristine film, after annealing at 185 °C, and after deprotection are shown in **Figure 2.5**. **P1** and **P2** have only fluorene repeat units, their absorption onsets after deprotection are slightly red shifted compared with the pristine films, and their corresponding maximum emission wavelengths are also red-shifted. This phenomenon was reported in polydioctylfluorene (PFO) as a result of extended conjugation, i.e., formation of a β-phase[23] upon extended annealing or upon solvent swelling stress. Absorption and emission spectra of annealed films are similar to that of the deprotected films, indicating that the small variations in spectra of the deprotected polymers are indeed due to the annealing process. **P3** and **P4** both possessed fluorene and thienyl units. Their absorption and emission spectra after annealing are similar to that of the pristine films. This may be related to the polyfluorene structures, which are different from PFO and do not form β-phase such as in the case for polyfluorene with branched side chain.[6d] In our case, the incorporation of thiophene units might prevent the formation of the β-phase. The spectra after deprotection are similar to that of the annealed films, again showing that the removal of THP groups has no obvious effect on the spectra of the polymers. However, the hydroxy groups after the removal of THP induce a small effect on PL spectra, as seen from the broader PL emission peaks for **P3** and **P4**. This effect is not pronounced for all of the deprotected polymers, as also can be inferred by the small variations in quantum efficiency. Pei *et al*.[24] reported a polyfluorene with hydroxy group in the side chain and found that dominating

yellowish-orange emission originates from hydrogen-bonding-induced, self-assembled aggregates in the solid state, due to the formation of entangled nanostructures induced through hydrogen-bonding interactions. Removal of THP in the present case, takes place in the solid state, and self-assembly is difficult to develop during deprotection and thus no obvious emitting aggregates at lower energy are observed. The high emission quantum yields in the solid state were retained, demonstrating that the deprotection process did not damage the emission. Furthermore, the low processing temperature and rather short time of heating reduced the formation of fluorenone, as evidenced by the absence of green emission in the emission spectra of deprotected **P1-4** films.

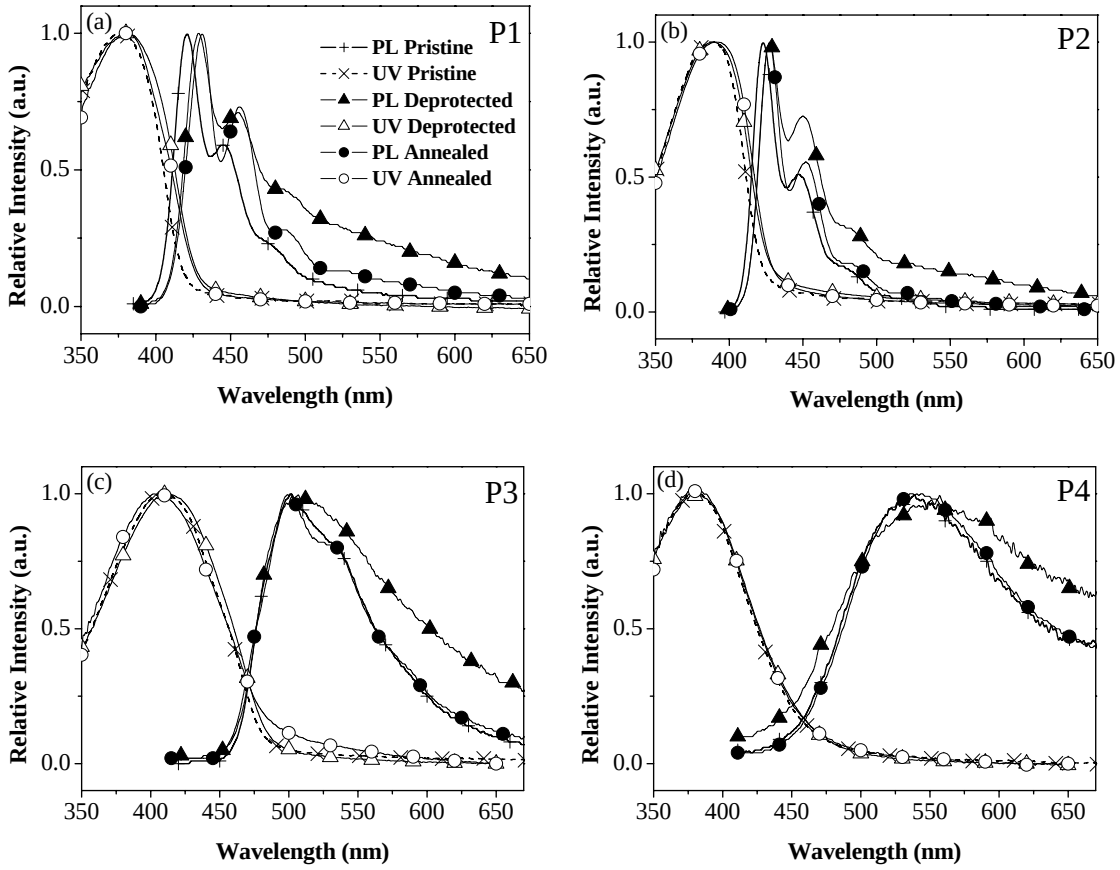


**Figure 2.5: UV-vis and PL spectra of polyfluorenes in the solid state before/after deprotection and after annealing: (a) P1 (PTHPEF), (b) P2 (PTHPEF-alt-diHF), (c) P3 (PTHPEF-alt-T), and (d) P4 (PTHPEF-co-THPET).**

### 2.3.4 Chemically Amplified Soft Lithography

Chemically amplified soft lithography was demonstrated using a copolymer based on 3,4-ethylenedioxythiophene (EDOT) and a thiophene unit bearing a THP group.[10] An insoluble pattern of the polythiophene was fabricated via removal of the THP groups using an acid-catalyzed solid state reaction. The catalytic amount of acid was transferred from an "inked" PDMS stamp to the surface of the polymer. The concentration of the acid affected the quality of the

pattern. A similar procedure was followed for THP-protected polyfluorenes. A higher temperature for the solid state reaction in polyfluorenes was used. A scheme of the procedure is shown in **Figure 2.6 (a)**. All the polymers described in this work were patterned this way. For example, **P2** was spin-cast onto a glass substrate from a chloroform solution to yield a film with thickness ~100 nm. The patterned surface of the PDMS stamp was immersed in a solution of 0.01 M camphorsulfonic acid in THF and hexane (50:50 vol%) for 3 s. A photograph of the stamp pattern is shown in **Figure 2.6 (b)**. The "inked" stamp was dried in air for 30 s and then pressed lightly on top of the polymer film for 10-15 s, thereby transferring the acid to the surface. The resulting film was thermally treated at 185 °C for 15 s under ambient atmosphere. The acid-catalyzed deprotection reaction took place in the solid state and resulted in cleavage of the THP group and elimination of dihydropyran in the regions where acid was deposited. These regions became insoluble by virtue of the residual hydroxyl group and the change in polarity. Development in chloroform provided a positive image of the stamp. **Figure 2.6 (c)** shows emission from the patterned polymer when exposed to UV light.

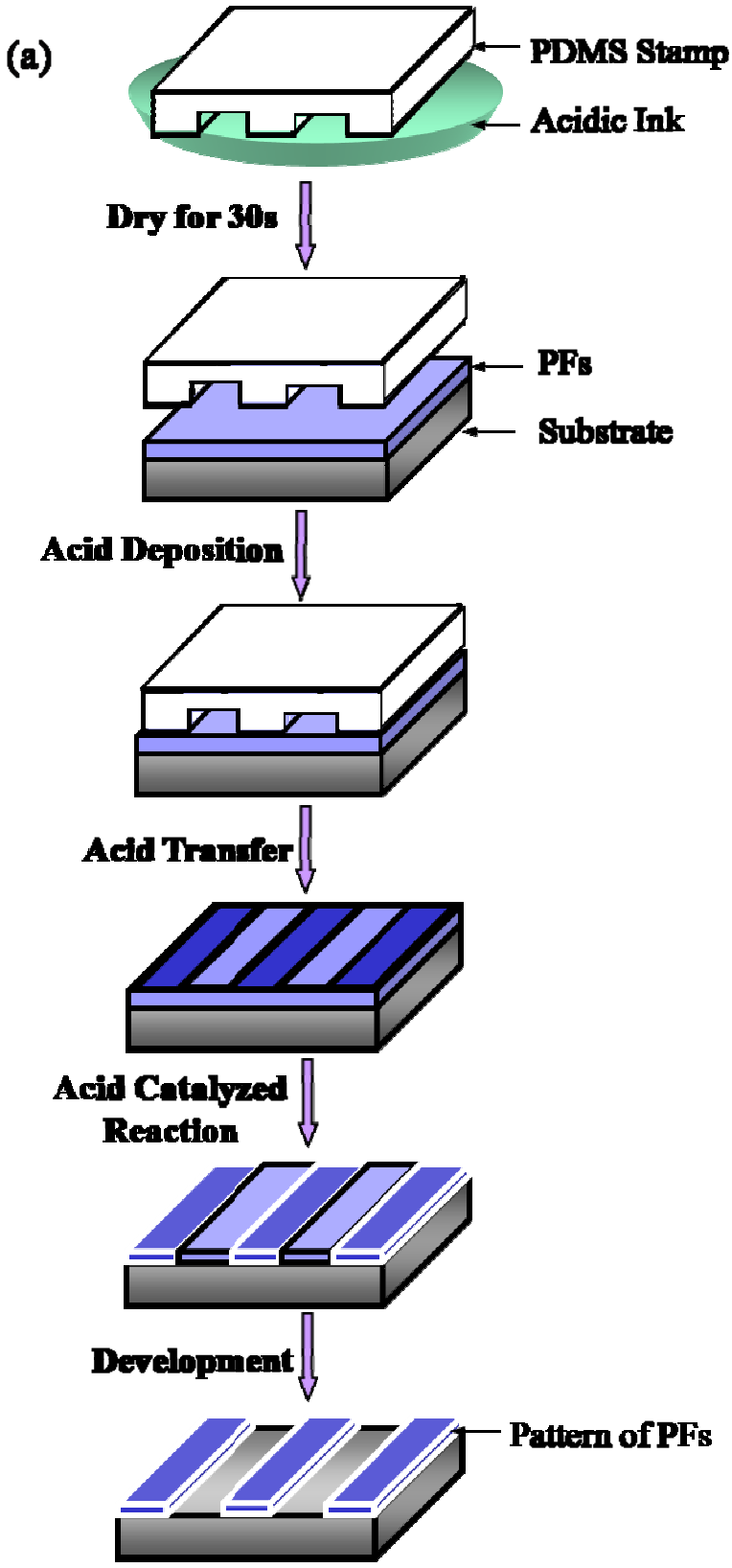
(a)
PDMS Stamp
Acidic Ink
Dry for 30s
PFs
Substrate
Acid Deposition
Acid Transfer
Acid Catalyzed
Reaction
Development
Pattern of PFs

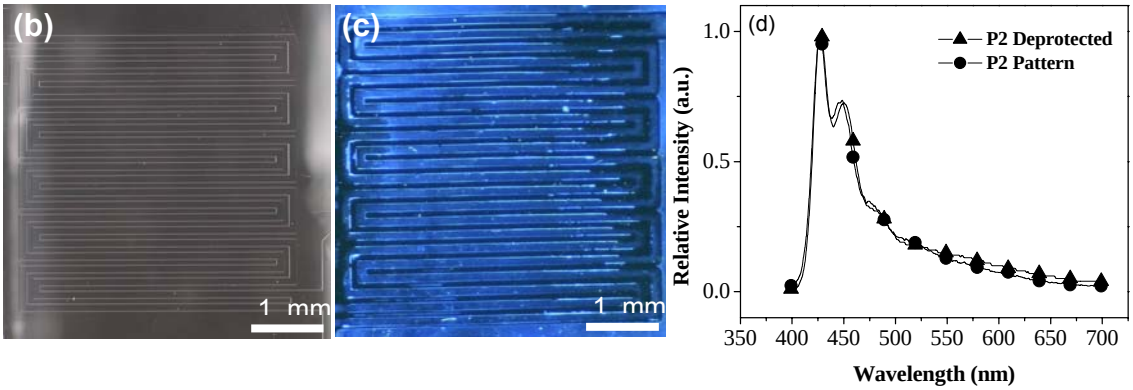


**Figure 2.6: (a) Scheme depicting chemically amplified soft lithographic process, (b) a micrograph of PDMS Stamp, (c) an emission of patterned P2 (PTHPEF-alt-diHF) under UV light, and (d) PL spectra of deprotected and patterned P2.**

**P1** and **P4** possess THP groups on every repeat unit, whereas **P2** and **P3** bear THP groups on 50 % of the repeat units. Nevertheless **P2** and **P3** can be successfully patterned. The removal of the THP functional group from side chains is sufficient to deprotect the polymers and form a patterned image, indicating that other functional groups may be attached to the side chains.

Compared with other methods, such as photolithography, the soft lithographic process eliminates possible damage to the luminescent polymer structure, such as fluorenone formation due to UV irradiation.[25] **Figure 2.5**, showing PL spectra of the **P1-P4** films before and after acid-catalyzed deprotection, indicates the PL spectra are unchanged. The PL spectra of patterned **P2** were measured and were found similar to the PL spectra of the deprotected film as shown in **Figure 2.6 (d)**. Furthermore, the quantum yields of these polymer films exhibited no change after acid-catalyzed deprotection, indicating their potential application in patterned PLEDs.

## 2.4 Conclusions

Blue, green and blue-green colour fluorene-based polymers, PTHPEF, PTHPEF-alt-diHF, PTHPEF-alt-T and PTHPEF-co-THPET, containing THP functional groups, have been synthesized by Yamamoto and Suzuki coupling reactions. The removal of dihydropyran from the side chain was confirmed by thermogravimetric and spectroscopic analysis. The acid-catalyzed cleavage of the THP group in the presence of acid occurred at much lower temperature than homolytic removal of the THP group in the absence of acid. The pristine polyfluorenes exhibit exceptional luminescent properties in solution and in the solid state because the bulky THP group reduces the interchain interaction of the polymers. Moreover, after deprotection, the deprotected polyfluorenes possess optical properties and quantum yields that are similar to the pristine polymers. The slight change of absorption and emission wavelength is attributed to the influence of thermal annealing. Due to the short length of side chains and H-bonding (via terminal hydroxyl groups), the removal of the THP groups causes the polymers to become insoluble. Chemically amplified soft lithography can be used to pattern the luminescent polymers. In summary, the design of conjugated polymers bearing THP groups, or other protecting groups, might be a general method for patterning luminescent polymers. These patternable polyfluorenes with bright blue, green, and blue-green colour emission are promising candidates in the fabrication of multi-colour emitting LED devices.

## 2.5 References


(1) J. H. Burroughes, D. D. C. Bradley, A. R. Brown, R. N. Marks, K. Mackay, R. H. Friend, P. L. Burn, A. B. Holmes, *Nature* **1990,** *347,* 539.

(2) P. E. Burrows, G. Gu, V. Bulovic, Z. Shen, S. R. Forrest, M. E. Thompson, *IEEE Trans. Electron Devices* **1997,** *44,* 1188.

(3) A. Holmes, *Nature* **2003,** *421,* 800.

(4) (a) S. Beaupré, M. Leclerc, *Macromolecules* **2003,** *36,* 8986. (b) S. Beaupré, M. Leclerc, *Adv. Funct. Mater.* **2002**, *12*, 192.

(5) (a) M. *J.* Leclerc, *Polym. Sci., Part A: Polym. Chem.* **2001**, *39*, 2867. (b) S. Panozzo, O. Stephan, J. C. Vial, *J. Appl. Phys.* **2003**, *94*, 1693. (c) P. K. Abhishek, A. J. Samson, *Macromolecules* **2003,** *36,* 5285. (d) D. Neher, *Macromol. Rapid Commun*. **2001**, *22*, 1365. (e) U. Scherf, E. J. W. List, *Adv. Mater*. **2002**, *14*, 477. (f) M. J. Leclerc, D. Sitzky, A. Pogantsch, S. Setayesh, G. Leising, K. Mullen, *Synth. Met*. **2002**, *125*, 73. (g) M. Redecker, D. D. C. Bradley, M. Inbasekaran, E. P. Woo, *Appl. Phys. Lett*. **1998**, *73*, 1565.

(6) N. Stutzmann, R. H. Friend, H. Sirringhaus, *Science* **2003**, *299*, 1881.

(7) C. Winder, N. S. Sariciftci, *J. Mater. Chem*. **2004**, *14*, 1077.

(8) (a) S. Holdcroft, *Adv. Mater*. **2001**, *13*, 1753. (b) S. R. Forrest, *Nature* **2004,** *428,* 911. (c) T. Nyberg, F. L. Zhang, O. Inganas, *Nanotechnology* **2002,** *13,* 205.

(9) (a) J. Yu, M. Abley, C. Yang, S. Holdcroft, *Chem. Commun*. **1998,** 1503. (b) J. Yu, S. Holdcroft, *Macromolecules* **2000,** *33,* 5073. (c) J. Yu, F. P. Orfino, S. Holdcroft, *Chem. Mater*. **2001**, *13*, 526.

(10) (a) J. Yu, S. Holdcroft, *Chem. Mater*. **2002**, *14*, 3705. (b) J. Yu, S. Holdcroft, *Chem. Commun*. **2001,** 1274.

(11) L.-O. Pålsson, A. P. Monkman, *Adv. Mater.* **2002**, *14*, 757.

(12) H.-J. Cho, B.-J. Jung, N. S. Cho, J. Lee, H.-K. Shim, *Macromolecules* **2003,** *36,* 6710.

(13) (a) T. Yamamoto, *Synlett* **2003,** *4,* 425. (b) X. Chen, J. L. Liao, Y. Liang, M. O. Ahmed, H.-E. Tseng, S. A. Chen, *J. Am. Chem. Soc.* **2003,** *125,* 636.

(14) (a) M. Ranger, M. Leclerc, *Can. J. Chem.* **1998,** *76,* 1571. (b) S. Guillerez, G. Bidan, *Synth. Met.*, **1998**, *93*, 123. (c) M. Ranger, D. Rondeau, M. Leclerc, *Macromolecules* **1997**, *30*, 7686. (d) M. Inbasekaran, W. Wu, E. P. Woo, US Patent 5,777,070, 1998. (e) N. Miyaura, A. Suzuki, *Chem. Rev.* **1995,** *95,* 2457.

(15) T. Sakamizu, H. Shiraishi, H. Yamaguchi, T. Ueno, N. Hayashi, *Jpn. J. Appl. Phys.* **1992,** *31,* 4288.

(16) S. Panozzo, J.-C. Vial, Y. Kervella, O. Stéphan, *J. Appl. Phys.* **2002**, *92*, 3495.

(17) B. Liu, W.-L. Yu, Y.-H. Lai, W. Huang, *Macromolecules* **2000**, *33*, 8945.

(18) (a) H. Mao, B. Xu, S. Holdcroft, *Macromolecules* **1993,** *26,* 1163. (b) C. Yang, F. P. Orfino, S. Holdcroft, *Macromolecules* **1996,** *29,* 6510. (c) Q. Pei, H. Järvinen, J. E. Österholm, O. Inganäs, J. Laaksol, *Macromolecules* **1992,** *25,* 4297. (d) M. R. Anderssonl, D. Selse, M. Berggren, H. Järvinen, T. Hjertberg, O. Inganäs, O. Wennerström, J.-E. Österholm, *Macromolecules* **1994,** *27,* 6503.

(19) K.-H. Weinfurtner, H. Fujikawa, S. Tokito, Y. Taga, *Appl. Phys. Lett.* **2000**, *76*, 2502.

(20) G. Vamvounis, S. Holdcroft, *Adv. Mater.* **2004**, *16*, 716.

(21) (a) J. -I. Lee, G. Klaerner, R. D. Miller, *Chem. Mater.* **1999**, *11*, 1083. (b) G. Klarner, J. -I. Lee, V. Y. Lee, E. Chen, A. Nelson, D. Markiewicz, R. Siemens, J. C. Scott, R. D. Miller, *Chem. Mater*. **1999**, *11*, 1800. (c) J. -I. Lee, D. -H. Hwang, H. Park, L.-M Do, H. Y. Chu, T. Zyung, R. D. Miller, *Synth. Met*. **2000**, *111-112*, 195. (d) S. Xiao, M. Nguyen, X. Gong, Y. Cao, H. B. Wu, D. Mosea, A. J. Heeger, *Adv. Funct. Mater.* **2003**, *13*, 25.

(22) (a) K.-Y. Peng, S.-A. Chen, W.-S. Fann, *J. Am. Chem. Soc.* **2001,** *123,* 11388. (b) A. Charas, J. Morgado, J. M. G. Martinho, L. Alcacer, F. Cacialli, *Chem. Commun*. **2001**, 1216.

(23) (a) M. Grell, D. D. C. Bradley, G. Ungar, J. Hill, K. S. Whitehead, *Macromolecules* **1999,** *32,* 5810. (b) A. J. Cadby, P. A. Lane, M. Wohlgenannt, C. An, Z. V. Vardeny, D. D. C. Bradley, *Synth. Met.* **2000,** *111-112,* 515. (c) M. Ariu, D. G. Lidzey, D. D. C. Bradley, *Synth. Met.*

**2000,** *111-112,* 607. (d) M. J. Winokur, J. Slinker, D. L. Huber, *Phys. Rev. B* **2003,** *67,* 184106. (e) M. Ariu, D. G. Lidzey, M. Sims, A. J. Cadby, P. A. Lane, D. D. C. Bradley, *J. Phys.: Condens. Matter* **2002,** *14,* 9975. (f) M. J. Winokur, W. Chunwachirasiri, *J. Polym. Sci., Polym. Phys.* **2003,** *41,* 2630.

(24) J. Pei, X. L. Liu, Z. K. Chen, X. H. Zhang, Y. H. Lai, W. Huang, *Macromolecules* **2003**, *36*, 323.

(25) V. N. Bliznyuk, S. A. Carter, J. C. Scott, R. D. Klärner, R. D. Miller, D. C. Miller, *Macromolecules* **1999**, *32*, 361.

# CHAPTER 3:

# ENHANCEMENT OF OXIDATIVE STABILITY OF POLYFLUORENES FOR NIR DIRECT THERMAL LITHOGRAPHY

## 3.1 Introduction

π-Conjugated polymers (πCPs) are promising materials in application areas such as organic microelectronics, electro-optics, optic-electronics, and photonics. The spatial deposition of πCPs has been extensively studied for the above applications. Three major techniques are: area-selected electropolymerization,[1] photochemical patterning,[2] and non-reactive techniques that include screen printing,[3] inkjet printing,[4] and soft lithography.[5] For example, a patterning method was reported in which photocrosslinking of soluble polymers was used to generate insoluble polymer networks.[6] A RGB, three-colour display was fabricated from three oxetane-functionalized, electroluminescent spirobifluorene-co-fluorene polymers and the patterned polymers were found to retain their electrical and optical properties. In our previous studies in this area,[7] chemically-amplified deposition of πCPs by photolithography, by microcontact printing (μCP), and direct thermal patterning (DTP)[8] have been reported. These techniques have been demonstrated largely with polythiophene derivatives,[9] and, to a lesser degree, polyfluorenes (PFs).[10]

More recently, a novel bilayer approach was reported to pattern fluorescent π-conjugated polymers,[8b] wherein a non-conjugated polymer film of poly(2-hydroxyethylmethacrylate) (p(HEMA)) containing a NIR absorbing dye spin-cast onto a πCP film generates heat upon exposure to 830 nm laser light. The NIR thermal patterning process is shown schematically in **Figure 3.1**. After exposure and subsequent film development, a negative tone image of the fluorescent polymer is obtained. This method of patterning offers the advantage

of single-step film preparation, rapid computer-to-plate direct patterning, and <10 μm resolution imaging.

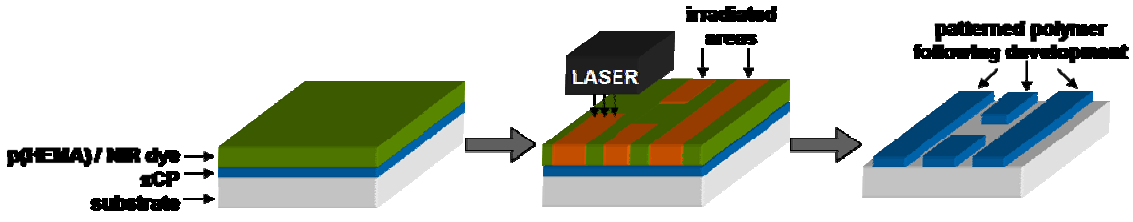


**Figure 3.1: Schematic diagram of direct thermal patterning of thermally-reactive π-conjugated polymers using NIR laser irradiation.**

PFs are currently of wide interest as light-emitting polymers due to their charge transport properties,[11] high luminescent quantum efficiencies, thermal stabilities, and tunable emitting colours by copolymerization with other light-emitting species.[12] However, the majority of polyfluorene derivatives suffer from degradation of fluorescence colour purity caused by the appearance of a broad band, green emission. This low-energy emission band can originate from on-chain impurity units, end-group-enhanced aggregation,[13] and fluorenone defects[14] that may be introduced by photo-oxidation, thermal oxidation, or during device fabrication.[15] Many attempts have been reported to eliminate these defects, and obtain stable blue emission, including purification of monomers, end-capping,[13] and the addition of an electron transport buffer layer in light emitting devices.[15] One of the most effective approaches to decrease the formation of fluorenone defects is substitution of the alkyl side chains at the 9-site carbon with aromatic groups.[16]

In this chapter, thermally-reactive, luminescent, fluorene-based polymers in which (2-tetrahydropyranyloxy)ethyl groups are linked via phenyl groups directly attached to the 9-site carbon are reported. The effect of this mode of coupling was investigated on the thermal oxidative stability and colour stability of the polyfluorenes during the solid-state, acid-catalyzed reaction shown in **Scheme 3.1**. These PFs were investigated for the applicability in NIR thermal patterning using the bilayer approach shown in **Figure 3.1**.[8b] Copolymers were prepared containing 10 mol % of benzothiadiazole and dithienylbenzothiadiazole units. The colour of emission of these copolymers can be tuned by energy transfer from the higher energy fluorene-based block to the benzothiadiazole moieties. The effect of incorporating these low-energy groups on oxidative stability, colour stability, solid-state acid-catalyzed reaction, and NIR patterning is examined.

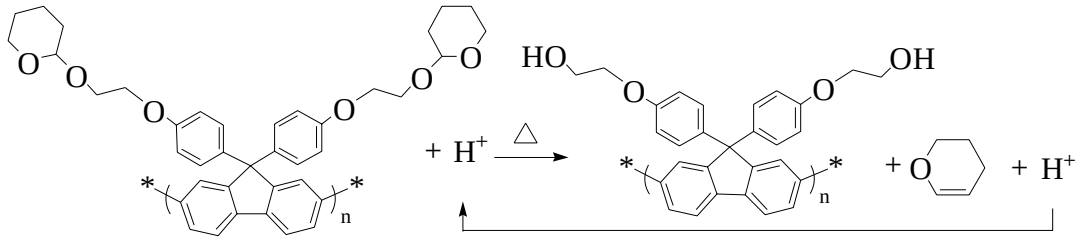


**Scheme 3.1: Acid-catalyzed elimination of dihydropyran from thermally-reactive, fluorene-based homopolymer.**

## 3.2 Experimental

### 3.2.1 Measurements

500 MHz $^{1}H$ and 125 MHz $^{13}C$ NMR spectra were obtained in $CD_2Cl_2$ on a Varian AS500 spectrometer; chemical shifts are reported in parts per million (ppm), referenced to $CD_2Cl_2$ ($^{1}H$: δ=5.32 (t); $^{13}C$: δ=54.00 (quintet)). Molecular weights were estimated by gel permeation chromatography (GPC) (Waters model 1515 isocratic pump) equipped with μ-Styragel columns against polystyrene standards. Polymers were eluted with THF using a flow rate of 1.0 mL/min and detected with a UV-vis detector (Waters model 2487) at 254 nm. Elemental analyses were using a Carlo Erba Model 1106 CHN analyzer.

Thermogravimetric analyses (TGA) were performed at 10 °C/min on 3 - 5 mg of polymer sample under $N_2$ using a HiRes TGA 2950 Thermogravimetric Analyzer (TA Instruments). The onset temperature was estimated from the point of intersection of two lines: one extrapolated from the slope of the curve just prior to loss of the THP group and the second from the steepest part of the curve. Mass loss was obtained with error ± 1 %. Infrared spectra were recorded using a Bomem Michelson FTIR (120 series). Polymer samples were drop-cast on sodium chloride disks from chloroform. 0.01 mol/L HCl solution was drop-cast on the polymer films and dried in air before the thermal treatment. Thin films prepared for FTIR measurement were heated to ~180 °C for 30 min, and cooled to the ambient temperature.

UV-vis absorption spectra were recorded on a Cary 300 Bio (Varian) spectrophotometer. Optical and fluorescent micrographs were obtained with a

Nikon 50i Eclipse series microscope equipped with a 100 W mercury lamp and Q Imaging Qi-Cam 1394 digital camera. A Nikon (V-2A) fluorescence filter cube was employed, consisting of dichromic mirrors that permitted excitation wavelengths in the range of 380 – 420 nm and prevented wavelengths ≤ 430 nm from reaching the detector/camera. Photoluminescence (PL) spectra were recorded with a Photon Technology International Spectrofluorometer QuantumMaster model QM-4 equipped with an extra sample compartment containing an integrating sphere. Both solution and solid-state absolute quantum yields (± 10%) were obtained using an integrating sphere. Solutions were de-oxygenated with high pre-purified nitrogen prior to fluorescence measurements and the sample compartment was flushed with nitrogen for thin film measurements. Fluorescence spectra of thin films, spin cast from $CHCl_3$ on quartz, possessed an optical density of ~0.5. Spectra were recorded 22.5° normal to the incident light.

Polymer films for optical measurements were either prepared by spin-casting the polymer (3 mg/mL) on glass or quartz from chloroform/THF (80:20) solution in the presence of 5 mol % camphorsulfonic acid (CSA); or spin-cast from chloroform solution in the absence of CSA. Acid-catalyzed deprotection was carried out by heating the films in the presence of 5 mol % CSA at ~150 °C for 3 min or at ~180 °C for 30 min.

Bilayer polymer films of **P1** and **P5-P7** were prepared by spin casting from chloroform at 1500 rpm for one min on microscope slides. The microscope slides were rinsed by chloroform prior to use. The polymer solutions consisted of

13 - 15 mg/mL of **P1** and **P5-P7**, and 2.8 - 4.1 mg/mL of thermal acid generator (TAG) in chloroform. The p(HEMA)/NIR dye top-layer was spin cast from methanol at 1500 rpm for one min. The p(HEMA)/dye containing solutions consisted of 11 - 12 mg of p(HEMA) and 48 - 50 mg of NIR dye in 1100 μL of methanol. The absorbance of NIR dye in the bilayer film was > 2.0 absorbance at 830 nm. Films were exposed to 830 nm laser light such that the average laser dosage was ~1300 mJ/cm$^2$. The width of the laser beam was 80 - 90 μm. The NIR laser apparatus has been previously described.[8] Polymer films containing **P1** and **P5-P7** were rinsed with methanol to remove the p(HEMA)/NIR dye top-layer prior to curing or development with THF. Curing was accomplished on a hotplate, under air and subdued light. **P1** was cured at 130 °C for 4 min and **P5** was cured at 120 °C for 30 min. Films were developed by immersion for ~1 min in THF. **P6** and **P7** were developed with THF/hexane (70:30 vol%) without curing. Film thicknesses were determined using an Alpha-Step IQ surface profiler.

### 3.2.2 Materials

2-(2-bromoethoxy)tetrahydro-*2*H-pyran, bis(1,5-cyclooctadiene) nickel (0) ($Ni(COD)_2$), 2,2-bipyridyl (BPY), 1,5-cyclooctadiene (COD), 1-bromo-4-*tert*-butylbenzene, 1,3-bis(diphenylphosphino)propane nickel (II) chloride ($Ni(dppp)Cl_2$), and *N*-bromosuccinimide (NBS), poly(2-hydroxyethylmethacrylate) were purchased from Aldrich and used as received. 4,4'-dimethyldiphenyliodonium hexafluorophosphate, the thermal acid employed in this study, and the NIR dye 2-[2-[2-chloro-3-[2-(1,3-dihydro-1,1,3-trimethyl-2H-

benzo[e]-indol-2-ylidene-ethylidene]-1-cyclohexene-1-yl]-ethenyl]-1,1,3-trimethyl-1-H-benzo[e] indolium 4-methylbenzene-sulfonate (FEW Chemicals), were supplied by Kodak Inc. and used as received under subdued lighting. THF, toluene, and ether were dried over Na/benzophenone and freshly distilled prior to use. DMF was dried over BaO and freshly distilled prior to use.

**(i) Synthesis of Poly[9,9'-di(2-(2-tetrahydropyranyloxy)ethyl) fluorene] (P1).** The homopolymer **P1** was synthesized by the method previously reported,[10] (**Scheme 3.2**). It also has been discussed in Chapter 2. Compared to the method reported in Chapter 2, in this method, the reaction solution was diluted and the reaction temperature was increased to 80 °C for 6 days.

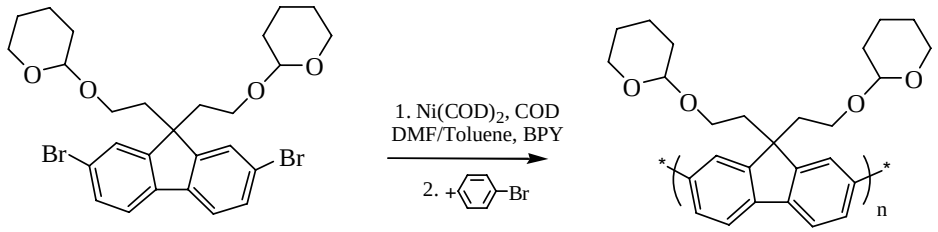


1 P1

**Scheme 3.2: Synthesis of homopolymer P1.**

**Poly[9,9'-di(2-(2-tetrahydropyranyloxy)ethyl)fluorene] (P1).** Into a vial were placed bis(1,5-cyclooctadiene) nickel (0) ($Ni(COD)_2$) (495 mg, 1.80 mmol), 2,2-bipyridyl (BPY) (281 mg, 1.80 mmol), 1,5-cyclooctadiene (COD) (0.22 mL, 1.8 mmol), and anhydrous DMF (4 mL) in a dry box with nitrogen. This mixture

was stirred at 80 °C for 30 min to form active catalyst. The monomer 2,7-dibromo-9,9'-di(2-(2-tetrahydropyranyloxy)ethyl)fluorene (**1**) (696 mg, 1.20 mmol) in 10 mL of anhydrous toluene was added to the mixture. The polymerization proceeded at 80 °C for 6 days, and then 1-bromo-4-*tert*-butylbenzene (0.1 mL, 0.5 mmol), as an end-capping agent, was added and the mixture reacted for 24 h. The resulting polymer was purified by aluminum oxide chromatography, precipitated in methanol and dried under vacuum for 24 h. The yield was 220 mg (43.7%). $^{1}$H NMR (500 MHz, $CD_2Cl_2$): δ 7.73 - 7.87 (m, 6H, aromatic region), 4.16 (s, 2H), 3.50 (s, 2H), 3.22 (s, 4H), 2.84 (s, 2H), 2.58 (s, 2H), 1.26 - 1.54 (m, 12H). $^{13}$C NMR (125 MHz, $CD_2Cl_2$): δ 150.9, 141.3, 140.3, 127.2, 122.6, 120.8, (12C, aromatic region), 52.6 (1C, 9,9'-C), 99.2, 62.3, 31.1, 26.0, 19.9 (10C, THP), 40.7 (2C, α-methylene), 64.0 (2C, β-methylene). Anal. Calcd for $C_{27}H_{32}O_4$: C, 77.11; H, 7.67; Found: C, 76.90; H, 7.64.

**(ii) Synthesis of Poly[9,9'-di[4-(2-(2-tetrahydropyranyloxy)ethoxy) phenyl]fluorene] (P5).**

**P5** was synthesized by the following procedure (**Scheme 3.3**). 2,7-Dibromo-9,9'-bis(4-hydroxyphenyl)fluorene was synthesized according to the literature[17] and coupled with 2-(2'-bromoethoxy)tetrahydro-*2*H-pyran to afford 2,7-dibromo-9,9'-bis[4-(2-(2-tetrahydropyranyloxy)ethoxy)phenyl]fluorene (**2**).[18] The polymer **P5** was prepared by the Yamamoto method.[19]

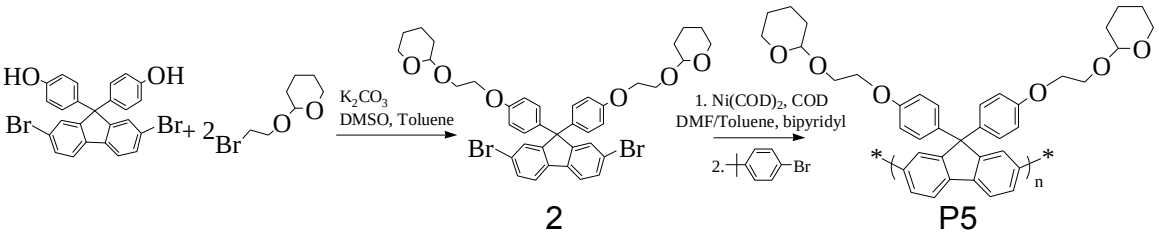


2 P5

**Scheme 3.3: Synthesis of homopolymer P5.**

**2,7-Dibromo-9,9'-bis[4-(2-(2-tetrahydropyranyloxy)ethoxy)phenyl] fluorene (2).** To a solution of 3.00 g (5.90 mmol) of 2,7-dibromo-9,9'-bis(4-hydroxyphenyl) fluorene, 2.96 g (14.2 mmol) of 2-(2-bromoethoxy)tetrahydro-*2*H-pyran, 10 mL of toluene, and 1.96 g of $K_2CO_3$ was added 15 mL of DMSO. The reaction mixture was refluxed at 120 °C for 48 hours, after which it was cooled to ambient temperature. The resulting mixture was extracted with 100 mL of ethyl acetate, washed with water, dried over anhydrous magnesium sulfate, and concentrated under vacuum. The crude oily product was chromatographed on silica gel with a mixture of ethyl acetate and n-hexane (1/1) and recrystallized in ethanol several times to give 2.50 g (55.4% yield) of the product as colourless crystals: $^1$H NMR (500 MHz, $CD_2Cl_2$): δ 7.64 (d, 2H), 7.51 (t, 4H), 7.06 (d, 4H), 6.82 (d, 4H) (aromatic region); 4.65 (d, 2H), 4.10 - 4.12 (m, 4H), 3.98 - 4.02 (m, 2H), 3.83 - 3.88 (m, 2H), 3.74 - 3.78 (m, 2H), 3.47 - 3.51 (m, 2H), 1.20 - 1.83 (m, 12H). $^{13}$C NMR (125 MHz, $CD_2Cl_2$): δ 158.6, 154.2, 138.5, 137.1, 131.3, 129.6, 129.5, 122.3, 122.2, 115.0 (24C, aromatic region), 64.9 (1C, 9,9'-C), 99.4, 62.6, 31.1, 26.0, 20.0 (10C, THP), 68.1 (2C, α-methylene), 66.2 (2C, β-methylene). Anal. Calcd for $C_{39}H_{40}Br_2O_6$: C, 61.27; H, 5.27; Found: C, 61.03; H, 5.43.

**Poly[9,9'-di[4-(2-(2-tetrahydropyranyloxy)ethoxy)phenyl]fluorene]**

**(P5).** To a vial were placed bis(1,5-cyclooctadiene) nickel (0) ($Ni(COD)_2$) (619 mg, 2.25 mmol), 2,2-bipyridyl (BPY) (351 mg, 2.25 mmol), 1,5-cyclooctadiene (COD) (0.28 mL, 2.25 mmol), and anhydrous DMF (3 mL) in a dry box with nitrogen. This mixture was stirred at 80 °C for 30 min to form active catalyst. The monomer 2,7-dibromo-9,9'-bis[4-(2-(2-tetrahydropyranyloxy)ethoxy)phenyl] fluorene (**2**) (1.15 g, 1.50 mmol) in 10 mL of anhydrous toluene was added to the mixture. The polymerization proceeded at 80 °C for 6 days, and then 1-bromo-4-*tert*-butylbenzene (0.02 mL, 0.1 mmol) was added and the mixture reacted for 24 h. The resulting polymer was purified by aluminum oxide chromatography, precipitated in methanol and dried under vacuum for 24 h. The yield was 610 mg (67.3%). $^1$H NMR (500 MHz, $CD_2Cl_2$): δ 7.80 (d, 2H), 7.57 (d, 4H), 7.16 (d, 4H), 6.78 (d, 4H) (aromatic region); 4.63 (t, 2H), 4.07 (s, 4H), 3.95 - 3.97 (t, 2H), 3.80 - 3.84 (m, 2H), 3.70 - 3.74 (m, 2H), 3.45 (t, 2H), 1.47 - 1.77 (m, 12H). $^{13}$C NMR (125 MHz, $CD_2Cl_2$): δ 129.6, 114.9 (8C, aromatic region); 64.9 (1C, 9,9'-C), 99.4, 62.6, 31.1, 26.0, 20.0 (10C, THP), 68.0 (2C, α-methylene), 66.2 (2C, β-methylene). Anal. Calcd for $C_{39}H_{40}O_6$: C, 77.46; H, 6.67; Found: C, 77.27; H, 6.87.

**(iii) Synthesis of Poly[9,9'-di[4-(2-(2-tetrahydropyranyloxy)ethoxy) phenyl]fluorene-co-3,4-benzothiadiazole] (P6).**

**P6** was synthesized by the following procedure (**Scheme 3.4**). 1,4-Dibromo-3,4-benzothiadiazole (**3**) was synthesized according to the literature.[20] 2,7-Dibromo-9,9'-bis[4-(2-(2-tetrahydropyranyloxy)ethoxy)phenyl]fluorene (**2**) and

**3** were copolymerized using a 90:10 feed ratio by the Yamamoto method to yield a statistically random copolymer **P6**.

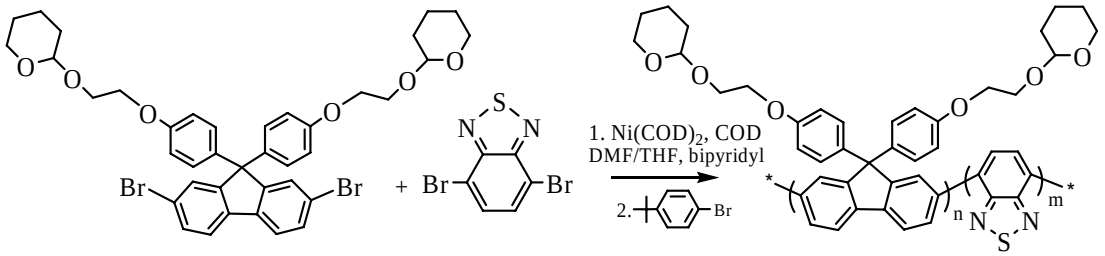


2 3 P6

**Scheme 3.4: Synthesis of copolymer P6 (n:m = 90:10).**

**Poly[9,9'-di[4-(2-(2-tetrahydropyranyloxy)ethoxy)phenyl]fluorene-co-3,4-benzothiadiazole] (P6).** To a vial were placed bis(1,5-cyclooctadiene) nickel (0) ($Ni(COD)_2$) (289 mg, 1.05 mmol), 2,2-bipyridyl (BPY) (164 mg, 1.05 mmol), 1,5-cyclooctadiene (COD) (0.13 mL, 1.05 mmol), and anhydrous DMF (3 mL) in a dry box with nitrogen. This mixture was stirred at 80 °C for 30 min to form active catalyst. The monomers 2,7-dibromo-9,9'-bis[4-(2-(2-tetrahydropyranyloxy) ethoxy)phenyl]fluorene (**2**) (482 mg, 0.630 mmol) and 1,4-dibromo-3,4-benzothiadiazole (**3**) (21mg, 0.070 mmol) in 10 ml of anhydrous THF was added to the mixture. The polymerization proceeded at 70 °C for 6 days, and then 1-bromo-4-*tert*-butylbenzene as end-capping agent (0.1 mL, 0.5 mmol) was added and reacted for another 24 h. The resulting polymer was purified by aluminium oxide chromatography, precipitated in methanol and finally dried under vacuum for 24 h. The yield was 170 mg (43.6%). $^1H$ NMR (500 MHz, $CD_2Cl_2$): δ 6.78 -

7.82 (m, 12.8H, aromatic region), 4.63 (s, 1.8H), 3.47 - 4.08 (m, 10.8H), 1.26 - 1.78 (m, 10.8H). Anal. Calcd for $C_{35.7}H_{36.2}O_{5.4}N_{0.2}S_{0.1}$: C, 76.89; H, 6.54; N, 0.50. Found: C, 73.76; H, 6.56; N, 0.64.

**(iv) Synthesis of Poly[9,9'-di[4-(2-(2-tetrahydropyranyloxy)ethoxy) phenyl]fluorene-co-4,7-di(3(4-n-octylphenyl)-2-thienyl)-2,1,3-benzothiadiazole] (P7).**

**P7** was synthesized by the following procedure (**Scheme 3.5**). Using the same coupling method as described for **P5**, 2,7-dibromo-9,9'-bis[4-(2-(2-tetrahydropyranyloxy)ethoxy)phenyl]fluorene (**2**) and 4,7-bis(3(4-n-octylphenyl)-5-bromo-2-thienyl)-2,1,3-benzothiadiazole (**5**) were copolymerized using a 90:10 feed ratio by the Yamamoto method to yield a statistically random copolymer, **P7**.

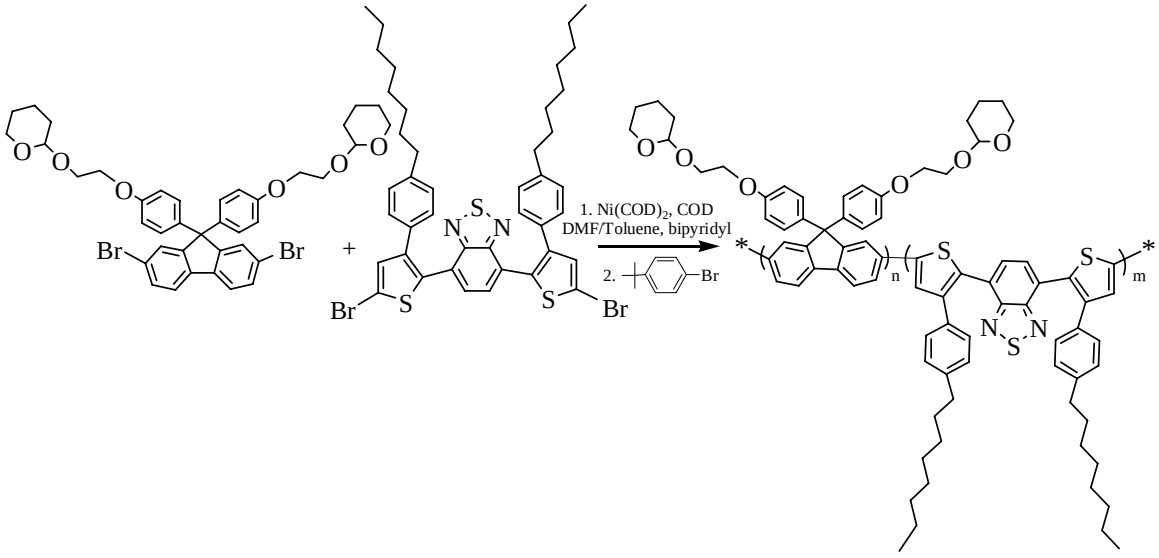


2 5 P7

**Scheme 3.5: Synthesis of copolymer P7 (n:m = 90:10).**

**4,7-Bis(3(4-n-octylphenyl)-2-thienyl)-2,1,3-benzothiadiazole (4).** 2-Bromo-3(4-n-octylphenyl)thiophene (12.0 g, 34.2 mmol) in 20 mL of ether was added dropwise to a mixture of Mg (0.98 g, 41 mmol) in 5 mL ether and refluxed for 3 h. This Grignard reagent was added dropwise to a mixture of $Ni(dppp)Cl_2$ (146 mg, 0.270 mmol) and 1,4-dibromo-3,4-benzothiadiazole (**3**) (4.22 g, 14.4 mmol) in 250 mL ether and stirred overnight. The mixture was poured into cool dilute hydrochloric acid and extracted with ether. It was then washed with saturated sodium carbonate and water and dried. Purification by silica column chromatography gave 9.4 g (yield 96 %) of red, viscous liquid. $^1H$ NMR (500 MHz, $CD_2Cl_2$): δ 7.542 (2 H, d), 7.281 (2 H, s), 7.260 (2 H, d), 7.123 (4 H, d), 7.019 (2 H, d), 2.535 (4 H, t), 1.525 (4H, m), 1.278 (10 H, m), 0.866 (6 H, t). Anal. Calcd for $C_{42}H_{48}N_2S_3$: C, 74.51; H, 7.15; N, 4.14. Found: C, 74.48; H, 7.13; N, 4.24.

**4,7-Bis(3(4-n-octylphenyl)-5-bromo-2-thienyl)-2,1,3-benzothiadiazole (5).** NBS (2.46 g, 13.8 mmol) in 50 mL DMF was added dropwise into a solution of 4,7-bis(3(4-n-octylphenyl)-2-thienyl)-2,1,3-benzothiadiazole (**4**) (4.67 g, 6.90 mmol) in 50 mL of DMF and stirred overnight. The mixture was poured into ice water and extracted with diethyl ether and washed with saturated sodium bisulphate and water, and dried over $Na_2SO_4$. Column purification gave 5.28 g (yield 92 %) red viscous liquid. $^1H$ NMR (500 MHz, $CD_2Cl_2$): δ 7.222 (2 H, s), 7.196 (2 H, s), 7.098 (4 H, d), 7.045 (4 H, d), 2.555 (4 H, t), 1.566 (4H, m), 1.302 (10 H, m), 0.884 (6 H, t). Anal. Calcd for $C_{42}H_{46}Br_2N_2S_3$: C, 60.43; H, 5.55; N, 3.36. Found: C, 60.78; H, 5.90; N, 3.25.

**Poly[9,9'-di[4-(2-(2-tetrahydropyranyloxy)ethoxy)phenyl]fluorene-co-4,7-di(3(4-n-octylphenyl)-2-thienyl)-2,1,3-benzothiadiazole] (P7).** To a vial were placed bis(1,5-cyclooctadiene) nickel (0) ($Ni(COD)_2$) (289 mg, 1.05 mmol), 2,2-bipyridyl (BPY) (164 mg, 1.05 mmol), 1,5-cyclooctadiene (COD) (0.13 mL, 1.05 mmol), and anhydrous DMF (3 mL) in a dry box with nitrogen. This mixture was stirred at 80 °C for 30 min to form active catalyst. The monomers 2,7-dibromo-9,9'-bis[4-(2-(2-tetrahydropyranyloxy)ethoxy)phenyl]fluorene (**2**) (482 mg, 0.630 mmol) and 4,7-bis(3(4-n-octylphenyl)-5-bromo-2-thienyl)-2,1,3-benzothiadiazole (**5**) (59 mg, 0.07 mmol) in 10 ml of anhydrous toluene was added to the mixture. The polymerization proceeded at 80 °C for 6 days, and then 1-bromo-4-*tert*-butylbenzene as end-capping agent (0.1 mL, 0.5 mmol) was added and reacted for another 24 h. The resulting polymer was purified by aluminium oxide chromatography, precipitated in methanol and finally dried under vacuum for 24 h. The yield was 200 mg (46.7%). $^1$H NMR (500 MHz, $CD_2Cl_2$): δ 6.80 - 7.82 (m, 13.8H, aromatic region), 4.64 (s, 1.8H), 3.46 - 4.08 (m, 10.8H), 2.56 (s, 0.4H), 1.27 - 1.77 (m, 13.2H), 0.88 (s, 0.6H). Anal. Calcd for $C_{39.3}H_{40.6}O_{5.4}N_{0.2}S_{0.3}$: C, 77.16; H, 6.69; N, 0.46. Found: C, 77.35; H, 6.64; N, 0.52.

## 3.3 Results and Discussion

### 3.3.1 Synthesis

Homopolymer **P1**, bearing alkyl side chains; homopolymer **P5**, bearing phenyl side chains; and copolymers **P6** and **P7** were synthesized from their corresponding dibrominated monomers using Yamamoto coupling[19] as shown in

**Scheme 3.2 - 3.5**. **Scheme 3.3** also illustrates the synthetic route for preparing monomer 2,7-dibromo-9,9'-bis[4-(2-(2-tetrahydropyranyloxy)ethoxy)phenyl] fluorene (**2**) and its homopolymer, **P5**. To prepare monomer **2**, 2,7-dibromo-9,9'-bis(4-hydroxyphenyl) fluorene was protected by reaction with excess 2-(2-bromoethoxy)tetrahydro-*2*H-pyran. The colorless crystalline monomer, **2**, was polymerized and end-capped with 1-bromo-4-*tert*-butylbenzene for another 24 h to afford **P5**. Monomer 1,4-dibromo-3,4-benzothiadiazole (**3**) was synthesized according to the literature.[20] Compound 4,7-bis(3(4-n-octylphenyl)-2-thienyl)-2,1,3-benzothiadiazole (**4**) was prepared by coupling monomer **3** with the Grignard reagent prepared from 2-bromo-3(4-n-octylphenyl)thiophene. Monomer 4,7-bis(3(4-n-octylphenyl)-5-bromo-2-thienyl)-2,1,3-benzothiadiazole (**5**) was prepared by selectively brominating compound **4** using NBS. Monomer **2** was copolymerized with monomer **3** in a feed ratio 90:10 to yield a statistically random copolymer, **P6**. The structure of these polymers was confirmed by NMR spectroscopy (shown in the Appendix of Chapter 3). Homopolymer **P1** gave $^{1}$H NMR resonance peaks at 7.73 - 7.87 (6H) and 4.16 (2H) ppm, which are assigned to the aromatic protons of the fluorene ring and the methine of the tetrahydropyran (THP) group, respectively. Homopolymer **P5** gave $^{1}$H NMR resonance peaks at 7.57 (4H) and 7.80 (2H) ppm assigned to the aromatic protons of the fluorene ring; at 6.78 (4H) and 7.16 (4H) ppm assigned to the aromatic protons of the phenyl ring; and at 4.63 (2H) ppm assigned to the methine of the THP group. $^{13}$C NMR spectra of **P5** exhibited 10 resonance peaks; fewer than the 18 resonance peaks observed for monomer **2**. The two

peaks at 129.6 (4C) and 114.9 (4C) ppm are assigned to aromatic carbons of the phenyl ring. The observed peaks at 99.4, 62.6, 31.1, 26.0, and 20.0 ppm (10C) are characteristic of the THP group. Peaks at 68.0 (2C) and 66.2 (2C) ppm are assigned to α- and β-methylene carbons, respectively. The peak at 64.9 (1C) ppm is assigned to the 9,9'-carbon.

The random copolymer, **P6**, gave resonance peaks at 6.78 - 7.82 (12.8H) ppm, which are assigned to the aromatic protons of the fluorene, phenyl, and benzothiadiazole ring, and one resonance peak at 4.63 (1.8H) ppm assigned to the methine of THP group. The composition of **P6** was determined from the ratio (12.8:1.8) of integrals of the peaks of aromatic protons (14n%+2m%) and methine (2n%) to yield m:n = 90:10. The random copolymer **P7** (90:10) gave resonance peaks at 6.80 - 7.82 (13.8H) ppm, assigned to the aromatic protons of the fluorene, phenyl, thienyl, and benzothiadiazole ring; one resonance peak at 4.64 (1.8H) ppm, assigned to the methine of THP group; and one α-methylene resonance peak at 2.56 (0.4H) ppm corresponding to octylphenyl side chains. The composition of **P7** was determined from the ratio (1.8:0.4) of integrals of the peaks of methine (2n%) and α-methylene (4m%) to yield m:n = 90:10.

The molecular weights and polydispersity indices of these four polyfluorenes are shown in **Table 3.1**. The molecular weights and the polydispersities of **P1** ($M_w$ = 66 100 Da, PDI = 1.33), **P5** ($M_w$ = 63 900 Da, PDI = 2.04), and **P7** ($M_w$ = 17 000 Da, PDI = 2.86) are typical of fluorene-based polymers prepared by Yamamoto coupling. **P6** ($M_w$ = 10 000 Da, PDI = 2.34) possessed a lower molecular weight, which resulted from its noticeably lower

solubility, due to the absence of a side chain on the benzothiadiazole ring. Alternatively, it may be due to the lower reaction temperature employed, as THF was used as solvent, which has a lower boiling point than toluene.

**Table 3.1: Molecular weight of polyfluorenes.**

| polymers | $M_n$ | $M_w$ | PDI |
|---|---|---|---|
| **P1** | 49 800 | 66 100 | 1.33 |
| **P5** | 31 300 | 63 900 | 2.04 |
| **P6** | 4 300 | 10 000 | 2.34 |
| **P7** | 5 900 | 17 000 | 2.86 |

### 3.3.2 Thermal Properties and Solid-State Reaction

The THP group is reported to be thermally eliminated from conjugated polymers, as dihydropyran, at temperatures, above 220°C.[21] **P1**, **P5**, **P6**, and **P7** are stable up to 240, 330, 270, 280 °C, respectively. **P5**-**4**, which bear phenyl groups exhibit a higher onset temperature compared to **P1**, which bears alkyl side chains. The phenyl groups increase the rigidity of the backbone.[21b] The THP functionality is calculated to 40 wt% of **P1**, 28 wt% of **P5**, 27 wt% of **P6**, and 25 wt% of **P7**. The observed weight losses of 40, 28, 26, and 24 wt% of **P1**, **P5**, **P6**, and **P7**, respectively, indicate that the loss in mass is due to thermolytic cleavage of the THP group and elimination of dihydropyran, as shown in **Table 3.2**.

**Table 3.2: Thermal properties of polyfluorenes P1 and P5-P7 .**

| polymers | theoretical mass loss [a] (%) | in the absence of acid | | in the presence of 5 mol% camphorsulfonic acid | |
|---|---|---|---|---|---|
| | | onset (°C) | observed mass loss (%) | onset (°C) | observed mass loss (%) |
| **P1** | 40 | 240 | 40 | 120 | 40 |
| **P5** | 28 | 330 | 28 | 130 | 28 |
| **P6** | 27 | 270 | 26 | 120 | 28 |
| **P7** | 25 | 280 | 24 | 110 | 26 |

[a] Based on removal of THP groups.

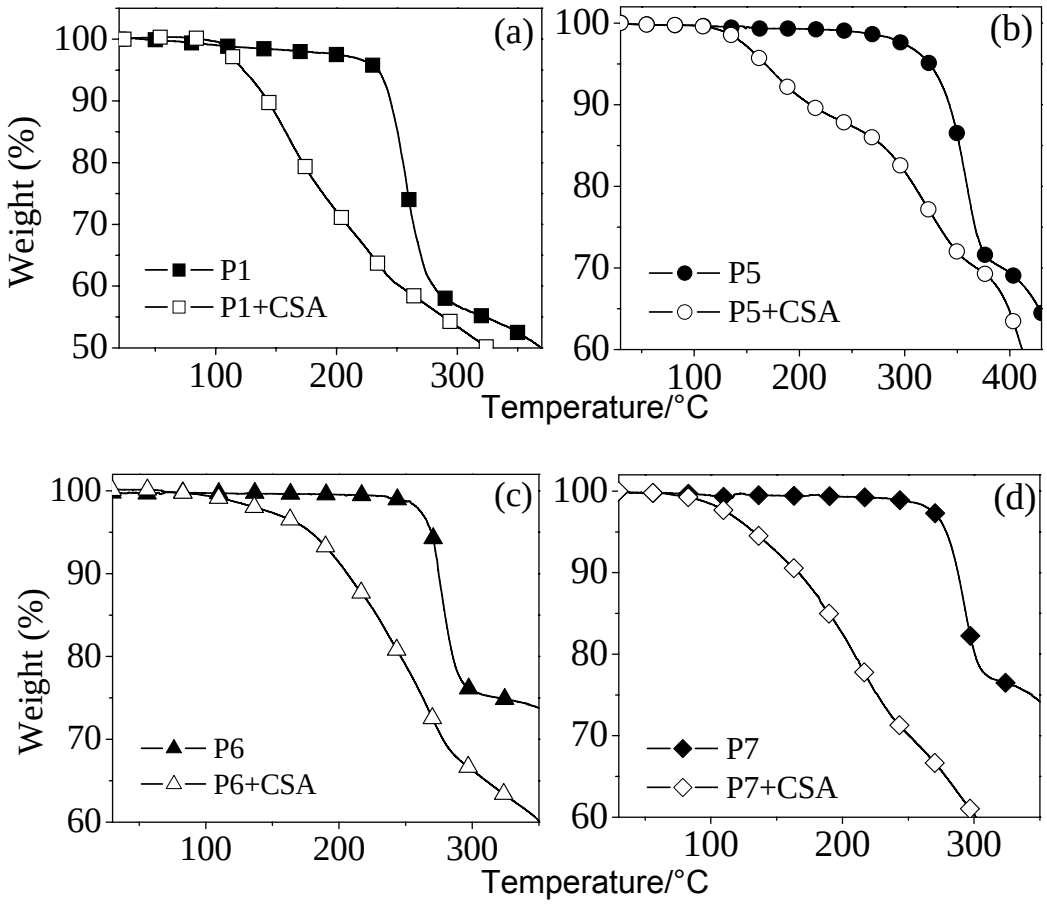


**Figure 3.2: TGA thermograms of pure polymer films and containing 5 mol % camphorsulfonic acid (CSA): (a) P1, (b) P5, (c) P6, and (d) P7.**

TGA of the polymer films containing camphorsulfonic acid (CSA) (5 mol % based on the THP unit) are shown in **Figure 3.2**. The onset temperature required to remove the THP group from the polyfluorenes decreased to 120, 130, 120, and 110 °C for **P1**, **P5**, **P6**, and **P7**, respectively. The observed reduction in mass of **P1**, **P5**, **P6**, and **P7** is 40, 28, 28, and 26 wt%, which is consistent with the theoretical loss of THP.

### 3.3.3 Optical and Luminescent Properties

The absorbance and emission properties of the polymers in THF solution, and in the solid state prior to deprotection are shown in **Figure 3.3** and the data summarized in **Table 3.3**. The maximum absorption wavelengths of **P1** and **P5-P7** in solution are 388, 390, 378, and 378 nm; and in the solid state, 388, 391, 378, and 382 nm, respectively. The main absorbance peak originates from the fluorene block. For **P6**, the lower energy absorption anticipated, due to the contribution of the 10 mol% benzothiadiazole unit, cannot be distinguished from the absorption spectra of the fluorene units. For **P7**, the weak absorption due to the dithienylbenzothiadiazole units can be observed at ~480 nm in both solution and the solid state.

**Table 3.3: Optical properties of polyfluorenes.**

| | solution (THF) | | | solid state | | | film-deprotected* | | |
|---|---|---|---|---|---|---|---|---|---|
| | $\lambda_{max}$(abs) | $\lambda_{max}$(em) | | $\lambda_{max}$(abs) | $\lambda_{max}$(em) | | $\lambda_{max}$(abs) | $\lambda_{max}$(em) | |
| | nm | nm | $\Phi_{fl}$ | nm | nm | $\Phi_{fl}$ | nm | nm | $\Phi_{fl}$ |
| **P1** | 388 | 415 | 1.00 | 388 | 425 | 0.35 | 392 | 433 | 0.35 |
| **P5** | 390 | 418 | 0.96 | 391 | 428 | 0.29 | 392 | 430 | 0.29 |
| **P6** | 378 | 415 | 0.51 | 378 | 421, 526 | <0.01 | 383 | 423, 536 | <0.01 |
| **P7** | 378 | 416, 653 | 0.35 | 382 | 636 | <0.01 | 381 | 654 | <0.01 |

* In the presence of camphorsulfonic acid (CSA), heated at 150 °C for 3 min.

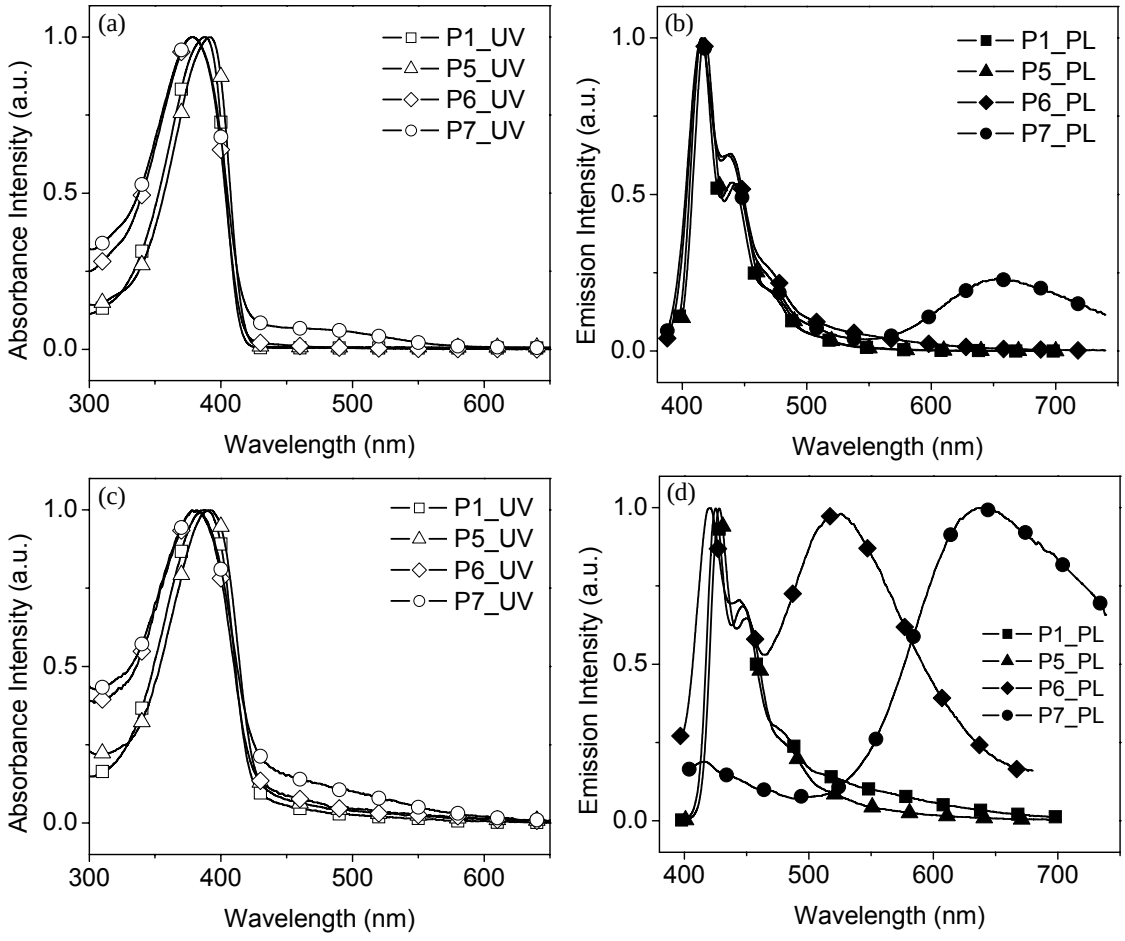


**Figure 3.3: UV-vis and PL spectra of polyfluorenes P1, P5, P6, and P7 in solution, (a) (b); and in the solid state, (c) (d).**

The maximum wavelengths of emission from **P1** and **P5** in solution (415 and 418 nm, respectively, violet-blue in colour) and in the solid state (425 and 428 nm, respectively, blue) are similar, and both of their PL spectra are sharp, indicating that changing the ethyl-THP side chains to phenyl-THP functionality has a minimal effect on the electronic excited state of the polyfluorene backbone. In addition, both **P1** and **P5** possess near-quantitative quantum yields in solution ($\Phi_{fl}$: 1.00 and 0.96), while their quantum yields in the solid state are 0.35 and 0.29. The commission internationale de l'eclairage (CIE)[22] values of emission from **P1** and **P5** films are (X=0.1937, Y=0.1329) and (X=0.1681, Y=0.0863), respectively.

$\lambda_{max}$(em) from copolymer **P6** occurs at 415 nm (violet-blue) in solution. Two peaks are observed (421 and 526 nm, blue and green in colour) in the solid state. Similarly, $\lambda_{max}$(em) from copolymer **P7** possess peaks at 416 and 653 nm (blue and red) in solution and at 626 nm (red) in the solid state. The red-shifted emission provides evidence that energy transfer occurs from the higher energy fluorene-based block to the lower energy benzothiadiazole- or dithienylbenzothiadiazole-based units. The CIE values of emissions from **P6** and **P7** films are (X=0.2751, Y=0.3558) and (X=0.5359, Y=0.3529), respectively. Energy transfer is more efficient in the solid state as evidenced by the relative signals of the high energy (due to fluorene) and low energy (due to benzothiadiazole- or dithienylbenzothiadiazole) emissions. Furthermore, the quantum yields of **P6** and **P7** are 0.51 and 0.35 in solution, respectively, but are very low (<0.01) in the solid state. The low quantum yields are attributed to the

statistical nature of the copolymers that results in longer runs of multiple units of benzothiadiazole, which have a higher propensity to aggregate and quench excitation. In contrast, much higher quantum yields are found in truly, alternating benzothiadiazole-containing copolymers.[23]

To determine whether **P1** and **P5-P7** are susceptible to the formation of ketonic defects induced from thermal oxidation in air, UV-vis and PL spectra of films were recorded after deprotection at 150 °C for 3 min, in the presence of CSA, as shown in **Figure 3.4**. $\lambda_{max}$(abs) of **P1** and **P5-P7** in the solid state after deprotection at 150 °C for 3 min are 392, 392, 383, and 381 nm, respectively; and $\lambda_{max}$(em) after deprotection at 150 °C for 3 min, are 433, 430, 423 (536), and 654 nm, respectively. These values are similar to their pristine films. The quantum yields for emission of **P1** and **P5-P7** before, and after, deprotection at 150 °C for 3 min are identical, demonstrating that the deprotection process does not quench the emission. Furthermore, the low processing temperature and relatively short time of heating (150 °C, 3 min) limits the formation of fluorenone, as evidenced by the absence of green emission in the luminescence spectra of deprotected **P1** and **P5-P7** films.

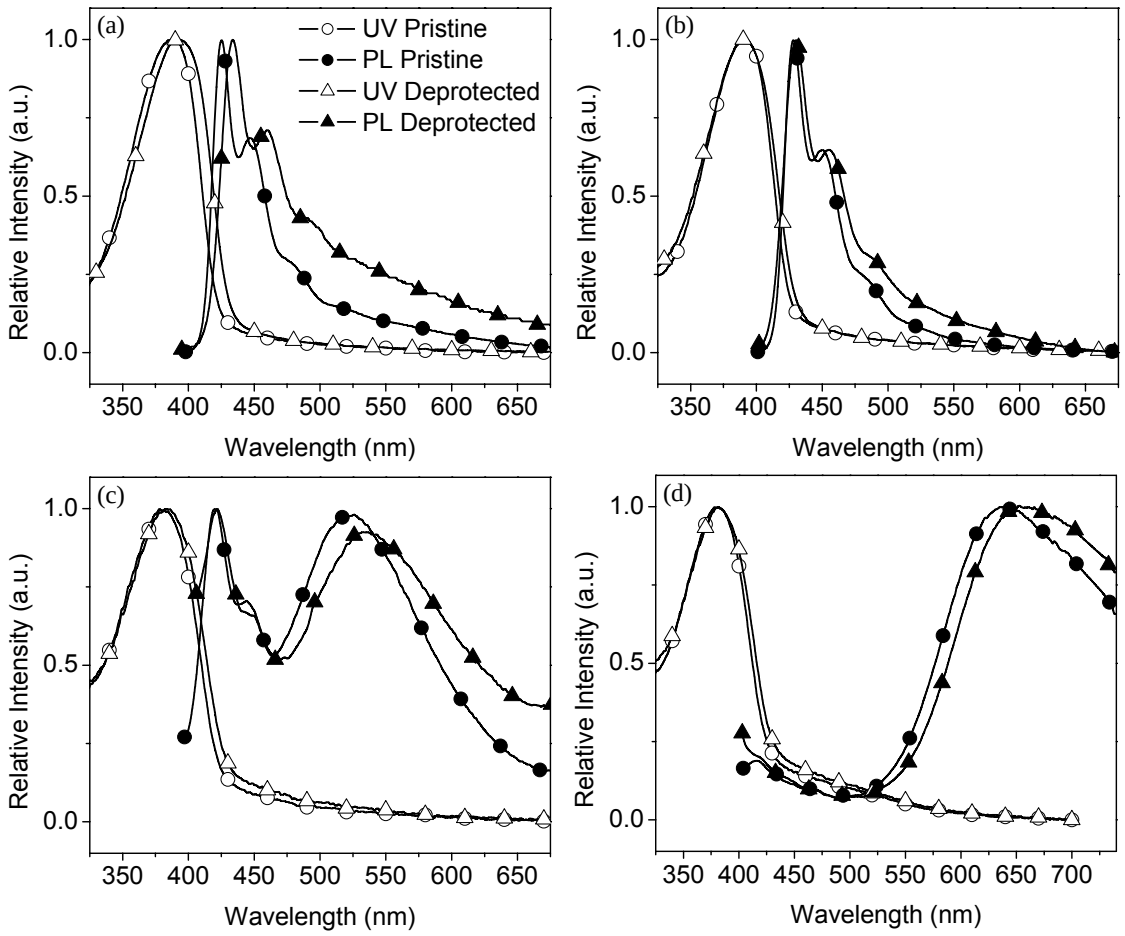


**Figure 3.4: UV-vis and PL spectra of polyfluorenes films before and after acid-catalyzed deprotection in air at 150 °C for 3 min: (a) P1, (b) P5, (c) P6, and (d) P7.**

Films of **P1** and **P5-P7** were also deprotected under the more extreme thermally-oxidative conditions of 180 °C for 30 min in order accelerate degradation. UV-vis and PL spectra are shown in **Figure 3.5**. The UV-vis spectra of deprotected **P1** and **P5-P7** are similar to their pristine films. The PL spectrum of **P1** after deprotection at 180 °C for 30 min exhibits a strong green light emission at ~530 nm, in addition to the original emission peak. This leads to broad emission from 400 to 700 nm. In addition, FTIR of thermally-treated **P1** reveals the emergence of a keto vibration band at ~1708 $cm^{-1}$, as shown **Figure**

**3.6**.[24] This is consistent with the formation of fluorenone groups, as reported by List *et al.*[25] and Sims *et al.*[26] in studies of the origin of green emission from polyfluorene-based conjugated polymers.

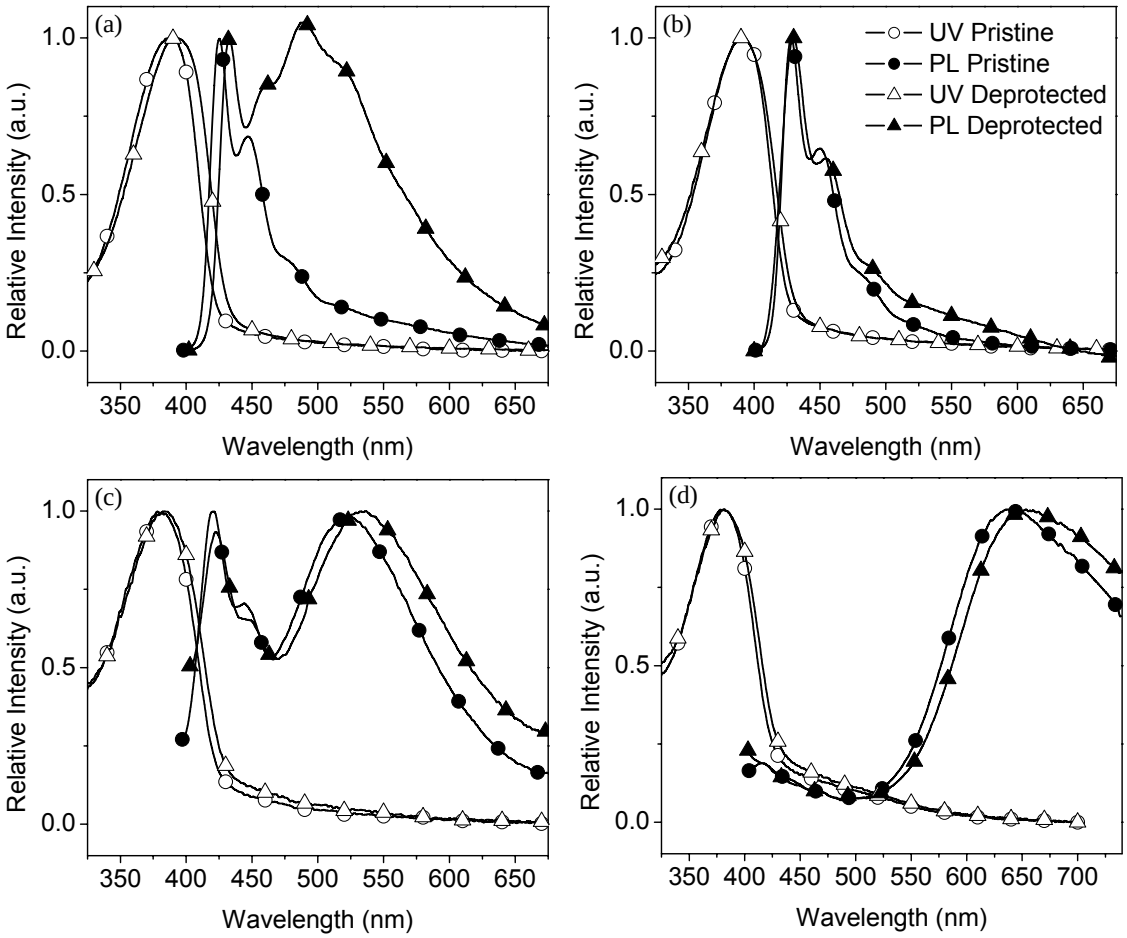


**Figure 3.5: UV-vis and PL spectra of polyfluorenes films before and after acid-catalyzed deprotection in air at 180 °C for 30 min: (a) P1, (b) P5, (c) P6, and (d) P7.**

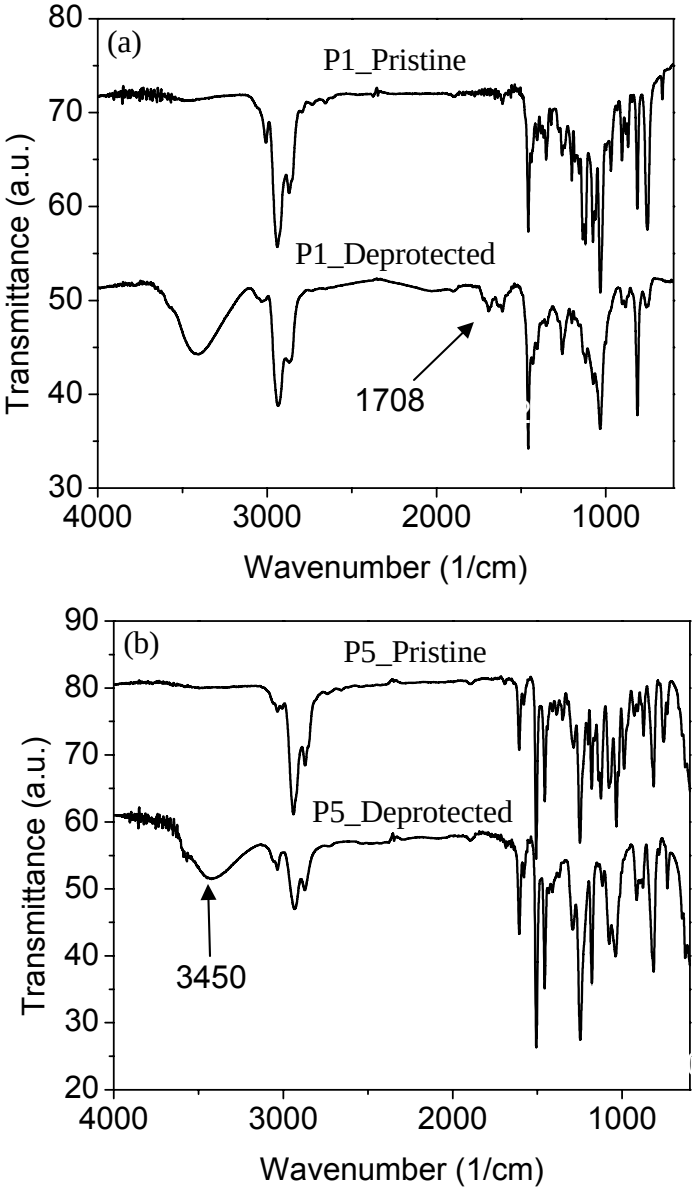


**Figure 3.6: FTIR of (a) P1 and (b) P5 before and after acid-catalyzed deprotection. The emergence of a broad signal at ~3450 $cm^{-1}$ upon deprotection at 180 °C for 30 min is due to the formation of the hydroxyl group.**

In contrast, to **P1**, no green light emission is observed for **P5** exposed to these thermal conditions, nor does a keto band at ~1718 $cm^{-1}$ develop. The PL spectrum of deprotected **P5** is similar to the pristine film. These observations

provide strong evidence that **P5** is more oxidatively stable than **P1**, and that is attributed to the phenyl groups attached directly to the 9-site carbon. Direct evidence for the higher chemical stability of **P5**, compared to **P1**, is provided upon observing the consequence of immersing the deprotected films into 98% $H_2SO_4$. Both films turn pink in colour when immersed in acid, due to acid-doping,[27] but after a few hours **P1** film loses its colour, which is evidence of loss of $\pi$-conjugation; **P5** retains its colour after two months of immersion. A photograph comparing deprotected **P1** with **P5** films prior to and after immersion in strong acid for two days (**P1**) and two months (**P5**) is shown in **Figure 3.7 (a)**. UV-vis spectra were used to verify the presence of **P5** film, as shown **Figure 3.7 (b)**.

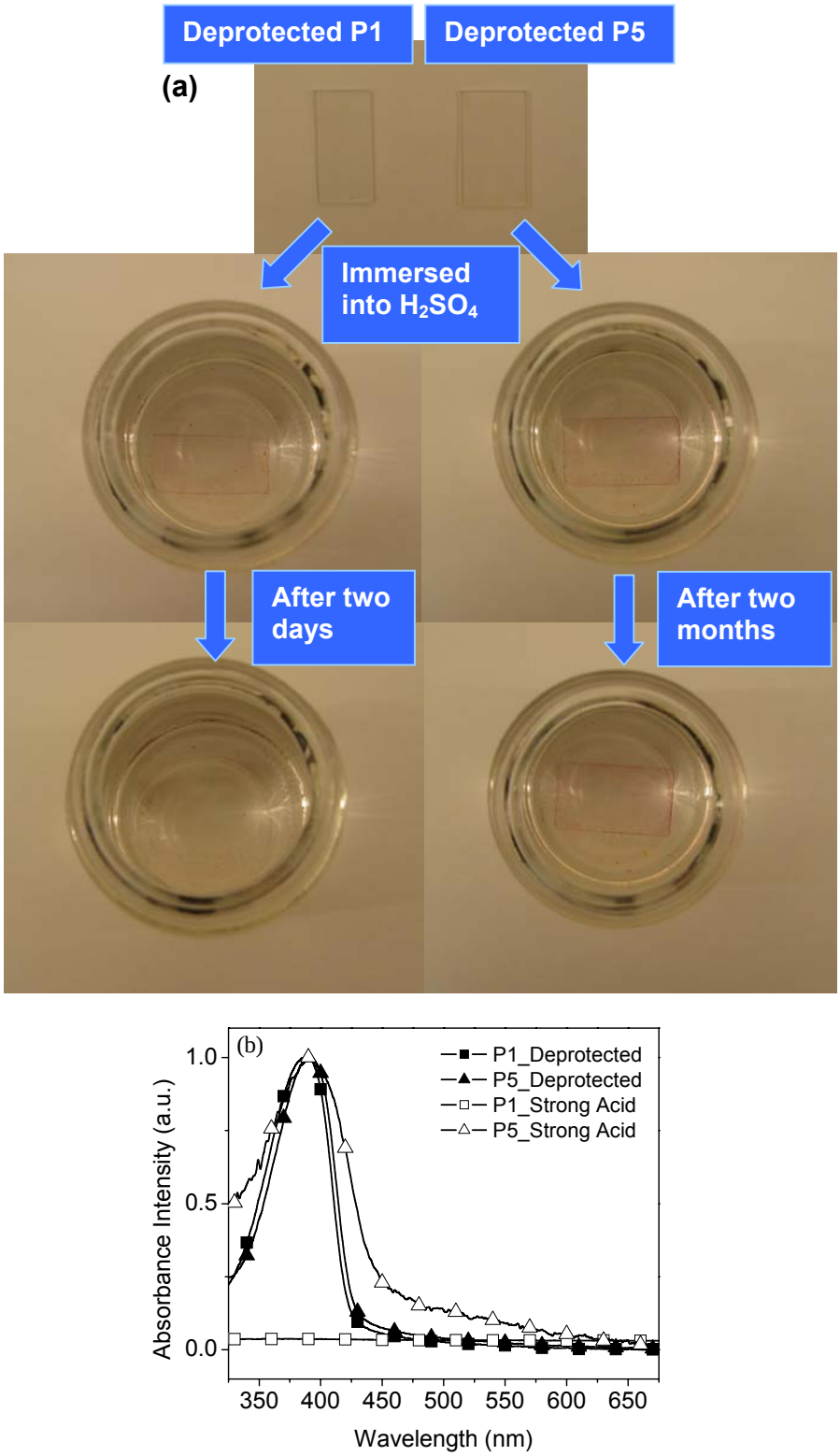


**Figure 3.7: (a) A photograph and (b) UV-vis spectra of deprotected P1 and P5 films prior to, and after, immersion in 98% $H_2SO_4$ for two days (P1) and two months (P5).**

### 3.3.4 Direct Thermal Patterning Analysis

Films of **P1**, ~120 nm thick, containing a thermal acid generator, 4,4'-dimethyldiphenyliodonium hexafluorophosphate (IBPF), were spin cast from $CHCl_3$. On top of these films, a film of poly(2-hydroxyethylmethacrylate) [p(HEMA)] containing a near-infrared dye was spin cast. The optical density of the NIR dye in the film was > 2.0 at 830 nm. The bilayer polymer film was scanned with a 80 - 90 μm wide beam of 830 nm laser light, for a total exposure of ~1300 mJ/cm$^2$. Details of the experimental set up are briefly described in the experimental section and full details are provided in ref [8]. Regions of the film exposed to laser light increase in temperature by virtue of the NIR dye, which absorbs the light and converts it to heat. In these regions of elevated temperature, the thermal acid generator decomposes, and acid is generated spatially. After rinsing the films with methanol to remove the NIR dye-containing layer, and subsequent curing at 130 °C for 4 minutes, the films were developed in THF to remove unexposed π-conjugated polymer. A fluorescence micrograph and the associated line profile of the resultant image are shown in **Figure 3.8**. Line heights were measured to be 60 - 70 nm, and pattern widths were 70 - 80 μm. PL spectra for the pristine and patterned films of **P1** are also shown in **Figure 3.8**. Patterning of **P1** produces an intense emission band centered ~530 nm, which is characteristic of fluorenone formation.

**P5** was patterned in the same manner as described above. The original thickness of the **P5** film was ~140 nm. A longer curing time was necessary (120 °C for 30 min) in order to retain patterns of polymer after development. This is

consistent with the TGA thermograms shown in **Figure 3.2**, which shows that the onset temperature is the highest of the four polymers studied, and is likely due to the higher rigidity of the polymer. Fluorescence micrographs, surface profiles and PL spectra of patterned **P5** are shown in **Figure 3.8**. The emission spectrum of patterned **P5** is similar in profile to the pristine film, and no emission band at ~530 nm is observed as in the case of patterned **P1**. It is inferred that the incorporation of the phenyl groups at the 9,9'-position prevent the formation of fluorenone.

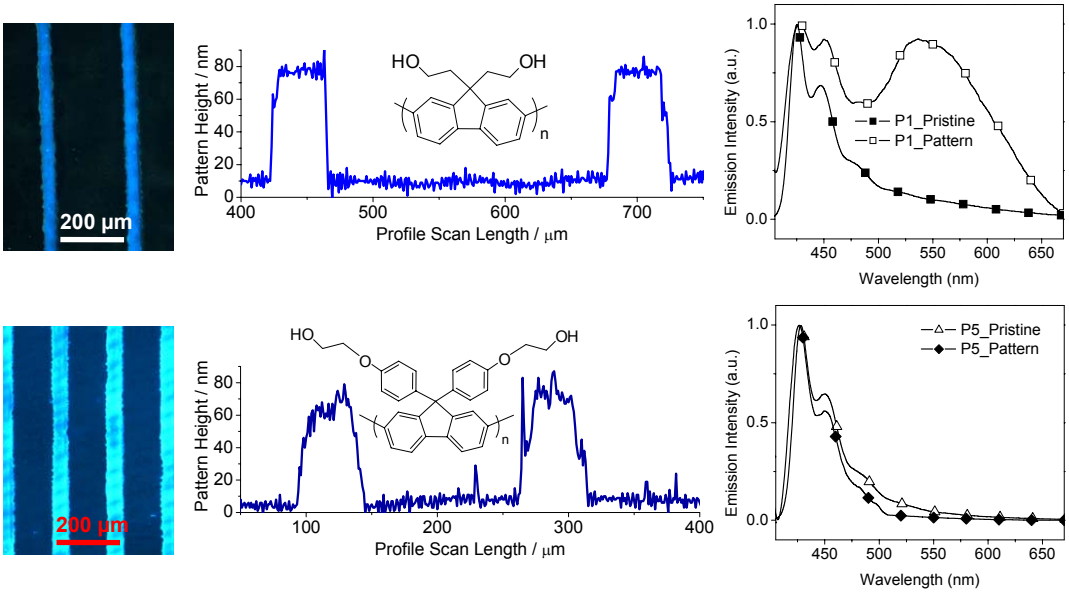


**Figure 3.8: Fluorescence micrograph, surface profile, and normalized PL spectrum of P1 (top) and P5 (bottom) patterned by direct thermal lithography. PL spectra of pristine, non-patterned P1 and P5 are shown for comparison.**

**P6** and **P7** were similarly investigated for patterning. No thermal curing was required for pattern formation, as the onset temperatures for deprotection are lower (see **Figure 3.2**, **Table 3.2**) and the temperature generated upon exposure to the laser is considered high enough to cause sufficient elimination of THP to render the polymer insoluble. Fluorescent micrographs and surface profiles of patterned films, **P6** and **P7**, are shown in **Figure 3.9**. Patterned **P6** and **P7** exhibit green and red emission, respectively. Pattern heights were measured to be 50 - 60 nm and pattern widths were 70 - 90 μm. As with **P5**, no fluorenone formation was evident for the patterned polymers.

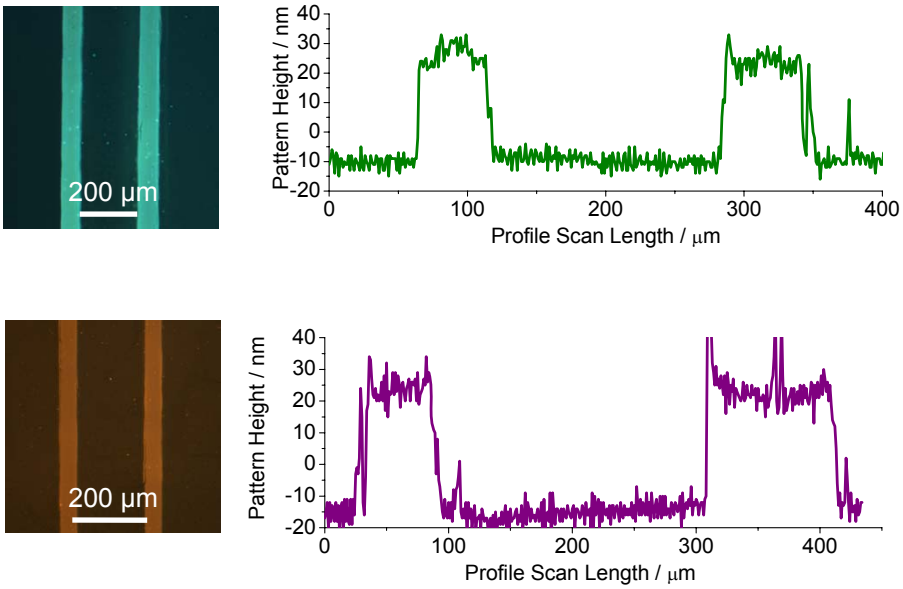


**Figure 3.9: Fluorescence micrograph and surface profile of P6 (top) and P7 (bottom) patterned by NIR direct thermal lithography.**

## 3.4 Conclusions

A series of fluorene-based copolymers were prepared that exhibited blue, green, and red emission, and possessed functionality that can be thermally-eliminated in the solid state to render the film insoluble. The onset for cleavage of the thermally reactive group, THP in this case, is lowered by up to 200 °C when acid is present in the films. Polyfluorenes derivatized directly at the 9-site carbon with (2-tetrahydropyranyloxy)ethyl substituents are susceptible to fluorenone formation, which is responsible for green-emission in the PL spectra. Oxidative stability was enhanced and fluorenone formation mitigated for polymers **P5**-**P7**, possessed by virtue of attaching phenyl groups to the 9-site carbon.

The polymers can be patterned by NIR direct thermal lithography using the bilayer approach. Polymers that do not possess phenyl groups attached to the 9-site carbon are susceptible to fluorenone formation during the laser patterning process. Although the emission quantum yield of the 3,4-benzothiadiazole-based polyfluorenes was low due to energy transfer and quenching, it is demonstrated that the incorporation of phenyl groups at the 9-site carbon of polyfluorene is necessary for oxidative stability during patterning. Polyfluorenes are thus promising candidates for high throughput, high-resolution, RGB three-colour patterning by NIR direct thermal lithography.

## 3.5 References


(1) C. B. Gorman, H. A. Biebuyck, G. M. Whitesides, *Chem. Mater.* **1995**, *7*, 526.

(2) (a) M. S. A. Abdou, S. Holdcroft, in *Encyclopedia of Conductive Molecules and Polymers* (Ed: H. S. Nalwa), Wiley, New York, **1996**, Ch. 4. (b) M. Angelopoulos, in *Handbook of Conducting Polymers*, 2nd ed. (Eds: T. A. Skotheim, R. L. Elsenbaumer, J. R. Reynolds), Marcel Dekker, New York, **1997**. (c) P. I. Clemonson, W. J. Feast, M. M. Ahmad, P. C. Allen, D. C. Bott, C. S. Brown, L. M. Connors, *Polymer* **1992,** *33,* 4711.

(3) (a) Z. Bao, Y. Feng, A. Dodabalapur, V. R. Raju, A. J. Lovinger, *Chem. Mater.* **1997**, *9*, 1299. (b) Z. Bao, J. A. Rogers, H. E. Katz, *J. Mater. Chem.* **1999**, *9*, 1895.

(4) C. C. Wu, D. Marcy, H. Lu, M. J. C. Sturm, *Appl. Phys. Lett.* **1998**, *72*, 519.

(5) (a) Y. Xia, G. M. Whitesides, *Angew. Chem., Int. Ed.* **1998**, *37*, 550. (b) S. Brittain, K. Paul, X.-M. Zhao, G. Whitesides, *Phys. World* **1998**, *11*, 31. (c) T. Granlund, T. Nyberg, L. S. Roman, M. Svensson, O. Inganäs, *Adv. Mater.* **2000**, *12*, 269.

(6) C. D. Muller, A. Falcou, N. Reckefuss, M. Rojahn, V. Wiederhirn, P. Rudati, H. Frohne, O. Nuyken, H. Becker, K. Meerholz, *Nature* **2003**, *421*, 829.

(7) S. Holdcroft, *Adv*. *Mater*. **2001**, *13*, 1753.

(8) (a) T. Gordon, J. Yu, C. Yang, S. Holdcroft, *Chem. Mater*. **2007**, *19*, 2155. (b) T. Gordon, G. Vamvounis, S. Holdcroft, *Adv*. *Mater*. **2008**, *20*, 2486. (c) T. Gordon, Ph. D. Thesis, Simon Fraser University, Burnaby, **2008**, p220.

(9) (a) J. Yu, S. Holdcroft, *Chem. Mater*. **2002**, *14*, 3705. (b) J. Yu, S. Holdcroft, *Chem. Commun*. **2001,** 1274.

(10) X. Han, X. Chen, G. Vamvounis, S. Holdcroft, *Macromolecules* **2005**, *38*, 1114.

(11) A. Babel, S. A. Jenekhe, *Macromolecules* **2003,** *36*, 7759.

(12) X. Chen, J. L. Liao, Y. Liang, M. O. Ahmed, H.-E. Tseng, S. A. Chen, *J. Am. Chem. Soc.* **2003,** *125,* 636.

(13) X. Chen, H.-E. Tseng, J. L. Liao, S. A. Chen, *J*. *Phys*. *Chem*. *B* **2005**, *109*, 17496.

(14) A. P. Kulkarni, X. Kong, S. A. Jenekhe, *J. Phys*. *Chem*. *B* **2004**, *108*, 8689.

(15) X. Gong, P. K. Iyer, D. Moses, G. C. Bazan, A. J. Heeger, S. S. Xiao, *Adv*. *Funct*. *Mater*. **2003**, *13*, 325.

(16) (a) P. E. Keivanidis, J. Jacob, L. Oldridge, P. Sonar, B. Carbonnier, S. Baluschev, A. C. Grimsdale, K. Müllen, G. Wegner, *ChemPhysChem* **2005**, *6*, 1650. (b) D. J. Vak, B. Lim, S.-H. Lee, D.-Y. Kim, *Org*. *Lett*. **2005**, *7*, 4229. (c) J. Jacob, S. Sax, M. Gaal, E. J. W. List, A. C. Grimsdale, K. Müllen,

*Macromolecules* **2005**, *38*, 9933. (d) Y. G. Wu, J. Li, Y. Q. Fu, Z. S. Bo, *Org*. *Lett*. **2005**, *6*, 3485.

(17) L. J. Lindgren, X. Wang, O. Inganas, M. R. Andersson, *Synth. Met.* **2005,** *154,* 97.

(18) H.-J. Cho, B.-J. Jung, N. S. Cho, J. Lee, H.-K. Shim, *Macromolecules* **2003,** *36,* 6710.

(19) T. Yamamoto, *Synlett* **2003,** *4,* 425.

(20) K. Pilgram, M. Zupan, R. Skiles, *J. Heterocycl. Chem.* **1970,** *7,* 629.

(21) (a) J. Yu, M. Abley, C. Yang, S. Holdcroft, *Chem*. *Commun*. **1998**, 1503. (b) J. Yu, S. Holdcroft, *Macromolecules* **2000**, *33*, 5073. (c) J. Yu, F. P. Orfino, S. Holdcroft, *Chem*. *Mater*. **2001**, *13*, 526.

(22) T. Smith, J. Guild, *Trans*. *Opt*. *Soc*. **1931**, *33*, 73.

(23) (a) P. Herguth, X. Z. Jiang, M. S. Liu, A. K.-Y. Jen, *Macromolecules* **2002,** *35*, 6094. (b) Q. Hou, Q. Zhou, *Y*. Zhang, W. Yang, R. Yang, *Y*. *Cao*, *Macromolecules* **2004,** *37*, 6299.

(24) A. P. Kulkarni, X. Kong, S. A. Jenekhe, *J*. *Phys. Chem*. **2004**, *108*, 8689.

(25) E. J. W. List, R. Guentner, P. S. de Freitas, U. Scherf, *Adv*. *Mater*. **2002**, *14*, 374.

(26) M. Sims, D. D. C. Bradley, M. Ariu, M. Koeberg, A. Asimakis, M. Grell, D. G. Lidzey, *Adv*. *Funct*. *Mater*. **2004**, *14*, 765.

(27) C. C. Han, R. L. Elsenbaumer, *Synth*. *Met*. **1989**, *30*, 123.

# CHAPTER 4:

# NANOSTRUCTURED MORPHOLOGIES AND TOPOLOGIES OF Π-CONJUGATED POLYMERS FROM THERMALLY-REACTIVE POLYMER BLENDS

Sections of this chapter have been reproduced in part with permission from:

Xu Han, Xiwen Chen, and Steven Holdcroft,

*Advanced Materials* **2007**, *19*, 1697-1702, Copyright 2007, Wiley-VCH

## 4.1 Introduction

π-Conjugated polymers (πCPs) are of interest due to the combination of their electrical, optical and film-forming properties. They are a class of organic materials with multiple potential applications in organic electronics devices such as full-colour flat panel displays,[1] organic field-effect transistors,[2] and photovoltaic (PV) cells.[3] Considerable effort is being made to optimize device architectures, enhance device efficiencies, and overcome device degradation. In parallel, the development of nano- and micro-fabrication techniques for depositing conjugated polymers is gaining importance as commercialization of organic devices is being realized. Three major techniques for spatial deposition of conjugated polymers are under development: area-selected electropolymerization,[4] photochemical patterning,[5] and non-reactive techniques such as screen printing,[6] inkjet printing,[7] and soft lithography.[8] Coupled to these developments is the need to control the morphology of the active materials, hence, the self-assembly of πCPs and the use of block or graft copolymers or polymer blends add another level of opportunity to organize π-conjugated materials.[9] For example, Widawski *et al.* produced a honeycomb morphology with block copolymers of polystyrene (PS) and poly(*p*-phenylenevinylene) (PPV);[10] and the self-assembly of regioregular poly-3-hexylthiophenes (P3HT) copolymerized with PS, poly(methyl methacrylate) (PMMA), and polyurethane into a cylindrical morphology was achieved by Liu *et al.*[11]

In the context of patterning luminescent materials, Granström *et al.* reported a method to indirectly fabricate luminescent polymers on a conductive

polymer, poly(3,4-ethylenedioxythiophene) (PEDOT), electropolymerized in randomly distributed pores of microfiltration membranes.[12] Iyengar and coworkers studied the morphology of films induced from the compositional evolution of poly(2-methoxy-5-(2'-ethylhexyloxy)-*p*-phenylenevinylene) (MEH-PPV)/PMMA polymer blends.[13] Boroumand *et al.* improved the ordering of polyfluorene nano-patterns by e-beam lithography to indirectly pattern silicon dioxide apertures on top of indium tin oxide (ITO) electrodes.[14] However, reports of well-controlled, segregated patterns of πCPs generated using facile routes, such as solvent casting polymer solutions, are rare.

For polymeric PV cells, the development of novel device architectures is one of the current technical challenges in making more efficient devices. The steps involved in the photovoltaic process, include photon absorption, exciton creation, exciton diffusion, exciton dissociation, carrier separation, carrier transport, and electricity generation.[15] The single layer and bilayer heterojunction organic solar cells exhibit low solar efficiencies partly due to the limited exciton diffusion length, short minority carrier lifetimes, and large series resistance of these organic materials.[16] The exciton diffusion length is the distance over which excitons travel before undergoing recombination and is ~3-10 nm in most organic semiconductors.[17] A method to improve the performance of polymer PV cells is to incorporate a network of internal donor-acceptor bulk heterojunctions.[18] A semiconducting polymer, for example, polythiophene (PT), polyphenylenevinylene (PPV), and their derivatives, can be blended with [6,6]-phenyl $C_{61}$ butyric acid methyl ester (PCBM) to form internal bulk heterojunctions.

The polymer serves as the donor, and PCBM, the acceptor. The process depends upon the transfer of photo-induced electrons from donor to acceptor via the internal donor-acceptor heterojunctions. The bulk heterojunction is the most successful device architecture for polymeric PV devices because exciton harvesting is enhanced. However, the random distribution of electron acceptors in the donors can lead to electron trapping on isolated acceptors unless a large weight fraction of acceptor is used. Thus, more ordered architectures are under investigation. Some methods have been reported using $TiO_2$ hybrid structures,[19] or graft/block copolymers.[20] In addition, both donor and acceptor should have short pathways to the electrode to minimize the carrier transport distance and reduce the probability of back electron transfer. Moreover, each phase of the heterojunction should be in contact with only one of the electrodes to maintain a high shunt resistance through the device and prevent carrier loss at the wrong electrodes.

In this chapter, a novel, facile approach to the creation of morphologically-controlled nano/micro-scale patterns of πCPs is demonstrated. The idea of making nano-patterned πCPs by this approach is suggested by Dr. Xiwen Chen. Acidic solutions of polyfluorene- or polythiophene-bearing, thermally-cleavable, solubilizing tetrahydropyranyl groups, and PMMA are spin-cast onto substrates. Phase separation induced by the chemical dissimilarity of the two polymers gives rise to nano/micro-scale morphology. Thermal elimination of the THP groups renders the conjugated polymer insoluble, enabling PMMA to be removed by dissolution, and thereby leaving a dot matrix of conjugated polymer.

Regioregular poly[3-(2-(2-tetrahydropyranyloxy)ethyl)thiophene] (PTHPET)[21] and poly[9,9'-di(2-(2-tetrahydropyranyloxy)ethyl)fluorene] (PTHPEF)[22] were selected as archetypal conjugated materials for this work: regioregular polythiophenes possess high charge mobilities[23] and relatively low band gaps,[24] while polyfluorenes are of interest in the display technology sector because of their high quantum yields of luminescence.[23] The optical properties of the two polymers are as follows: PTHPET (solid state: $\lambda_{max}$(abs) = 467 nm, $\lambda_{max}$(em) = 603 nm, $\Phi_{fl}$ = 0.11); PTHPEF (solid state: $\lambda_{max}$(abs) = 375 nm, $\lambda_{max}$(em) = 421 nm, $\Phi_{fl}$ = 0.37, CIE coordinates [X=0.1784, Y=0.0890]). The acid-catalyzed, solid state elimination of dihydropyran, as illustrated in **Scheme 4.1**, from either of these polymers renders them insoluble.[21, 22]

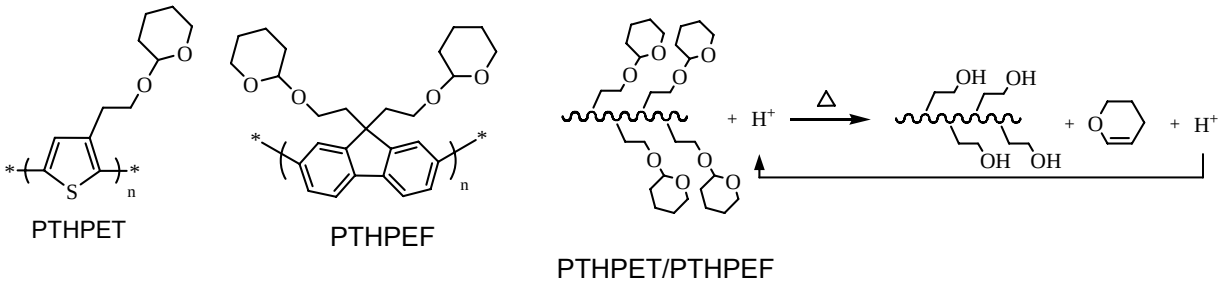


**Scheme 4.1: Thermally-reactive π-conjugated polymers PTHPET and PTHPEF, and acid-catalyzed elimination of dihydropyran from PTHPET and PTHPEF.**

This approach can be used to fabricate nano/micro-sized, donor-acceptor PV cell devices from a patterned πCP active layer, as shown in **Figure 4.1**. The insoluble patterned deprotected πCP (De-πCP) layer is first prepared. A PCBM layer is then spin-cast on top of the patterned layer to form a donor-acceptor heterojunction. Finally, an Al/Ca layer is evaporated on top of the heterojunction.

To investigate the device architecture-performance relationship, PV devices using PTHPET/PCBM bulk heterojunction blends, bilayers, and patterned PTHPET/PCBM as the active polymer layer are fabricated and characterized.

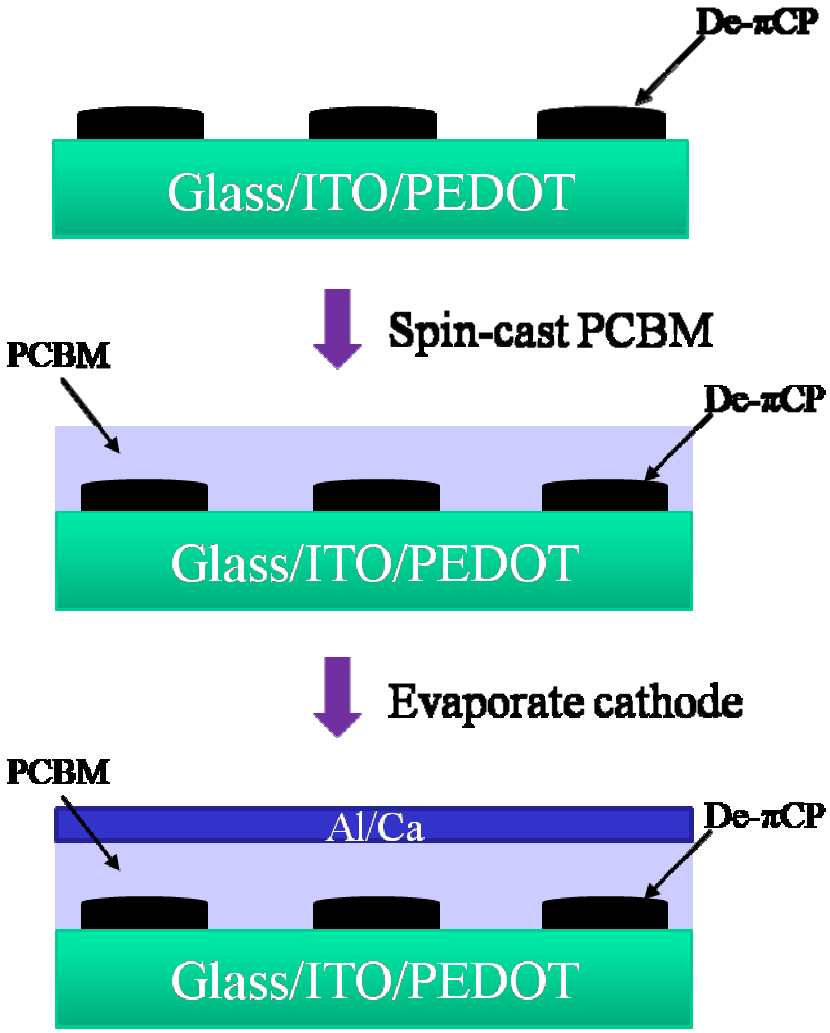


**Figure 4.1: Schematic illustration of the fabrication of a nano/micro-sized, donor-acceptor PV cell device from a patterned πCP active layer.**

## 4.2 Experimental

### 4.2.1 Measurements

Atomic force microscopy (AFM) was performed with an Explorer system (Thermomicroscopes, Sunnyvale, CA, USA) and SPMLabNT software version 5.01 Explorer AFM operating in the tapping mode. Thermogravimetric analyses (TGA) were performed at 10 °C/min on 3 - 5 mg of polymer sample under $N_2$ using a HiRes TGA 2950 Thermogravimetric Analyzer (TA Instruments). The onset temperature was estimated from the point of intersection of two lines: one extrapolated from the slope of the curve just prior to loss of the THP group and the second from the steepest part of the curve. Mass loss was obtained with error ± 1 %. Infrared spectra were recorded using a Bomem Michelson FTIR (120 series). Films of polymer blends were drop-cast onto sodium chloride disks from chlorobenzene/THF (95:5 vol%) solution and contained 5 mol % CSA. Thin films prepared for FTIR measurement were heated to ~160 °C (PTHPET/PMMA) or ~180 °C (PTHPEF/PMMA) for 5 min and cooled to ambient temperature. UV-vis absorption spectra were recorded on a Cary 300 Bio (Varian) spectrophotometer. Photoluminescence (PL) quantum yield measurements were recorded by a Photon Technology International QuantumMaster model QM-4 equipped with an integrating sphere.

### 4.2.2 Materials

Regioregular poly[3-(2-(2-tetrahydropyranyloxy)ethyl)thiophene] (PTHPET) ($M_n$ = 10,700 Daltons) was originally synthesized by Dr. Jianfei Yu.[21] Poly[9,9'-di(2-(2-tetrahydropyranyloxy)ethyl)fluorene] (PTHPEF) ($M_n$ = 23,800 Daltons)

was obtained according to the method reported previously.[22] Poly(methyl methacrylate) (PMMA) ($M_n$ = 48,300 Daltons), camphorsulfonic acid (CSA), chlorobenzene, and THF were purchased from Aldrich and used as received. [6,6]-phenyl $C_{61}$ butyric acid methyl ester (PCBM) were purchased from American Dye Source and used as received.

Blends of PTHPET/PMMA (50:50 wt%) were prepared by casting chlorobenzene solutions of the polymers (24, 4.8, and 2.4 mg/mL). Blends of PTHPET/PMMA (30:70 wt%, 40:60 wt%, 50:50 wt%, 60:40 wt%, and 70:30 wt%), PTHPEF/PMMA (40:60 wt%), and PTHPET/PTHPEF/PMMA (20:20:40 wt%) were prepared by casting chlorobenzene/THF (95:5 vol%) solutions (12 mg/mL). Solutions also contained 5 mol % camphorsulfonic acid (based on the mole percent of THP present). All solutions were mixed ultrasonically for 5 min and filtered (0.2 μm pore size) prior to spin-coating onto glass or silicon wafer substrates at 1500 rpm for 90 s. The resultant films were dried overnight under vacuum to remove any residual solvent. Acid-catalyzed deprotection of the films was carried out by heating the samples for 5 min (PTHPET/PMMA at ~160 °C, PTHPEF/PMMA at ~180 °C). Deprotected films were developed by rinsing with chlorobenzene/hexane (50:50 vol%). The PCBM layer was spin-cast on to the deprotected and developed De-PTHPEF patterns from a 4.8 mg/mL chlorobenzene solution at 1500 rpm for 90 s.

### 4.2.3 Device Fabrication and Characterization

The regioregular PTHPET ($M_n$ = 22,700 Daltons) used in device fabrication was synthesized using the Grignard Metathesis (GRIM) Method.[25]

The synthetic procedure, NMR, GPC, and TGA thermograms are summarized below. The NMR spectrum is shown in the Appendix of Chapter 4.

**Synthesis of PTHPET ($M_n$ = 22,700 Daltons, $M_w$ = 38,200, PDI = 1.68):**

2,5-Dibromo-3-(2-(2-tetrahydropyranyl-2-oxy)ethyl)thiophene (diBrTHPET) (2.56 g, 6.90 mmol) was dissolved in 40 mL of dry THF. Methylmagnesium bromide (6.9 mL, 1.0 M solution in butyl ether) was added and the mixture was heated to reflux for 1 h. Ni(dppp)$Cl_2$ (36 mg) was added and the solution was stirred at reflux for 2 h. The mixture was poured into 300 mL of methanol and filtered into a Soxhlet thimble. Soxhlet extractions were performed with methanol (to remove monomer and salts), hexanes (to remove catalyst and oligomers), and chloroform. The chloroform fraction was reduced and dried in vacuum to afford 1.11 g (76% yield) of the title polymer. $^1$H NMR: (500 MHz, $CD_2Cl_2$) δ 7.19 (s, 1H, aromatic region), 4.64 (s, 1H), 4.03-3.45 (m, 4H,), 3.11 (t, 2H), 1.83-1.1.51 (m, 6H). TGA measurements were carried out in the absence and in the presence of CSA, respectively. The THP functionality represents, in theory, 40 wt% of PTHPET. The observed weight loss values of 35 wt% in the absence of acid and 38 wt% in the presence of acid are consistent with calculated losses of mass due to thermaolytic cleavage of the THP group and elimination of dihydropyran. TGA thermograms of PTHPET are shown in **Figure 4.2**. The onset temperature required to remove the THP group from PTHPET is 230 °C in the absence of acid and 130 °C in the presence of acid, similar to the onset temperature as previously reported. [21]

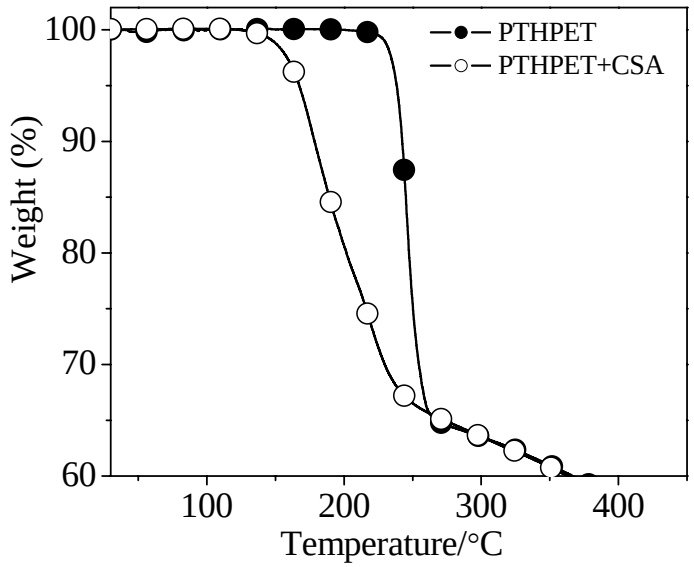


**Figure 4.2: TGA thermograms of PTHPET.**

PTHPET/PCBM bulk heterojunction PV devices were fabricated according to the procedure: indium-tin oxide (ITO) glass (Merck, Taiwan) was patterned and cleaned in a sonicating bath consecutively with deionized water, acetone, isopropanol, and hexane. A layer of highly conducting poly(styrene sulfonic acid)-doped poly(ethylenedioxythiophene) (PEDOT, AI4083, from H. C. Starck.) (~30 nm) was spin-cast at 5000 rpm from aqueous dispersion (after passing a 0.45 μm filter) on top of the ITO glass and heated at 140 °C for 10 min. The substrate was transferred to a $N_2$-filled glove box (< 0.1 ppm $O_2$ and $H_2O$) for spin-casting the photoactive layer. Solutions of polymers blended with PCBM (10.0 mg of PTHPET and 20.0 mg of PCBM in 1.0 mL chlorobenzene) were spin cast on the PEDOT films at 700 rpm for 60 s to produce ~120 nm thick films, as determined by profilometry (KLA Tencor). A layer of calcium (~25 nm), followed

by a layer of aluminum (~100 nm), was thermally deposited under vacuum chamber (~$2\times10^{-6}$ Torr) through a shadow mask, which had a defined active area of ~0.10 $cm^2$. Photovoltaic cells were placed in a custom-built holder and subjected to vacuum prior to PV measurements.

PTHPET/PCBM bilayer PV devices were fabricated according to the procedure of fabrication of bulk heterojunction PV devices, except for the preparation of the photoactive layer: PTHPET layers were prepared by casting chlorobenzene/THF (95:5 vol%) solutions of the polymer (10.0 mg/mL). Solutions also contained 5 mol % camphorsulfonic acid (based on the mole percent of THP present). All solutions were spin-cast at 700 rpm for 60 s on top of the PEDOT:PSS layer. Acid-catalyzed deprotection of the films was carried out by heating the samples for 3 min at ~150 °C. Deprotected films were developed by rinsing with chlorobenzene/hexane (50:50 vol%). A layer of PCBM was spin-cast on top of the deprotected and developed De-PTHPET layer using a 20 mg/mL chlorobenzene solution at 700 rpm for 60 s. The combined thickness of the films was ~90 nm as measured by AFM.

PTHPET/PCBM nano-patterned PV devices were fabricated according to the procedure of fabrication of bulk heterojunction PV devices, except for the preparation of the photoactive layer: blends of PTHPET/PMMA (40:60 wt%) were prepared by casting chlorobenzene/THF (95:5 vol%) solutions of the polymers (25.0 mg/mL). Solutions also contained 5 mol % camphorsulfonic acid (based on the mole percent of THP present). All solutions were spin-cast at 700 rpm for 60 s on top of the PEDOT:PSS layer. Acid-catalyzed deprotection of the films was

carried out by heating the samples for 3 min at ~150 °C. Deprotected films were developed by rinsing with chlorobenzene/hexane (50:50 vol%). PCBM layer was spin-cast on the deprotected and developed De-PTHPET patterned layer using a 20 mg/mL chlorobenzene solution at 700 rpm for 60 s. The combined thickness of the films was ~130 nm in thickness.

Current-voltage characteristics of the PV devices were measured using a Keithley 2400 source meter under illumination with an ozone-free Xenon 500 W lamp through an AM 1.5D filter (Newport Co.). The power was adjusted to be 100 mW/cm$^2$, measured by calibrated Radiant Power Meter (model 70260) combined with the 70268 probe. The incident photon-to-current collection efficiency (IPCE) spectrum was determined by measuring the PV current generated upon exposure to monochromatic light emerging from an Oriel Cornerstone 260 ¼ m monochromator/Xenon 500 W lamp system. The incident light intensity of monochromatic light was measured with a Newport optical power and energy meter (model 841-PE) with a model 818-UV low power detector.

## 4.3 Results and Discussion

### 4.3.1 Nanostructured PTHPET

The formation of ordered micro- or nano-sized separated domains of PTHPET is demonstrated in **Figure 4.3**. Significant efforts have been made to optimize the solution-casting method. The parameters include the selection of polymer matrix and solvent, the concentration of polymer blend solution, the

composition of the blend, the spin speed, the substrate, and the amount of solution applied on the substrate. **Figure 4.3** shows AFM topographical scans and profile scans of PTHPET/PMMA (40:60 wt%) blended films formed from casting a chlorobenzene/THF (95:5 vol%) solution of the polymers (12 mg/mL in total) containing 5 mol % camphorsulfonic acid (CSA) (based on mole percent of the THP group) on a silicon wafer. A two phase morphology of the resultant films is clearly evident, with the PMMA domain forming a continuous phase and the πCP domains scattered within as disc-shape regions ~500 nm in diameter. The thickness of the films is ~100 nm, but the πCP domains are recessed by ~50 nm. Polystyrene (PS) and poly(α-methylstyrene) (PMS) were also used to blend with PTHPET in the same solvent, but the resulting films did not exhibit any obvious phase separation. This may be due to PS and PMS having a solubility more closely aligned to PTHPET. Acid-catalyzed deprotection of the πCP was carried out by heating the films to 160 °C (PTHPET) or 180 °C (PTHPEF) for 5 min. The film was developed by rinsing with solvent to remove PMMA to yield an insoluble dot-matrix of the deprotected πCP (De-πCP). FTIR spectra of the resultant material confirmed the complete removal of PMMA, as shown in **Figure 4.4**. FTIR signals assigned to PMMA, originally at 1150 – 1280, 1470 – 1490, 1730, 2950, and 3000 cm-1, diminished upon solvent development. The AFM topography of the deprotected film after development is shown in **Figure 4.3 (c)**. The domains are ~50 nm thick, as shown in **Figure 4.3 (c)** and **(d)**, and their distribution correlates well to that observed in the pristine, undeveloped film; but

the developed discs are slightly larger in diameter than the exposed, recessed πCP domains observed prior to development.

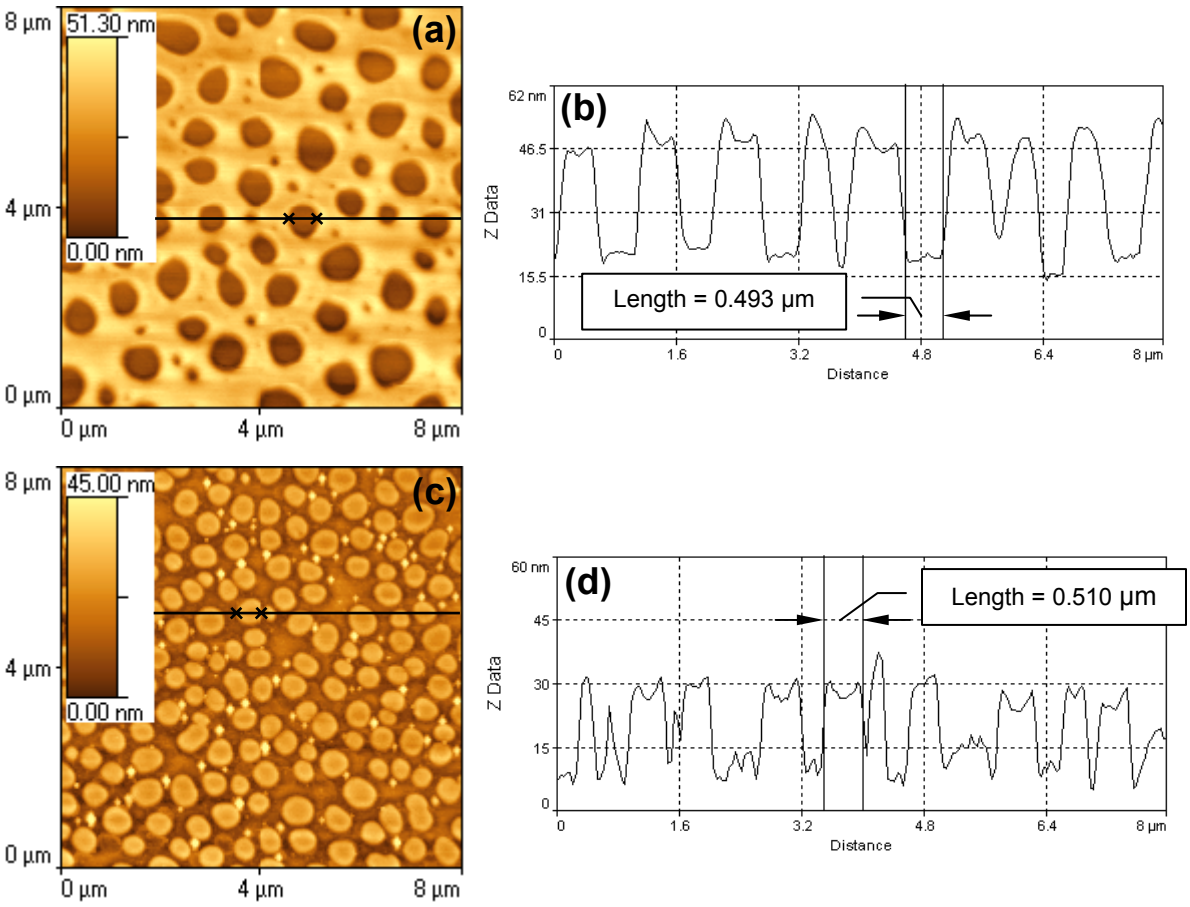


**Figure 4.3: AFM topography scans (a), (c) and profile scans (b), (d) of PTHPET/PMMA (40:60 wt%) blended films, solution cast on silicon wafers: (a), (b) pristine film PTHPET/PMMA (~100 nm thickness) in the presence of acid, and (c), (d) deprotected film De-PTHPET (~50 nm thickness, 500±100 nm sized domains) after rinsing with chlorobenzene/hexane (50:50 vol%). Note: AFM profiles provide a relative, not absolute height. The thickness of the blended films is estimated from the combination of topographies (a) and (c).**

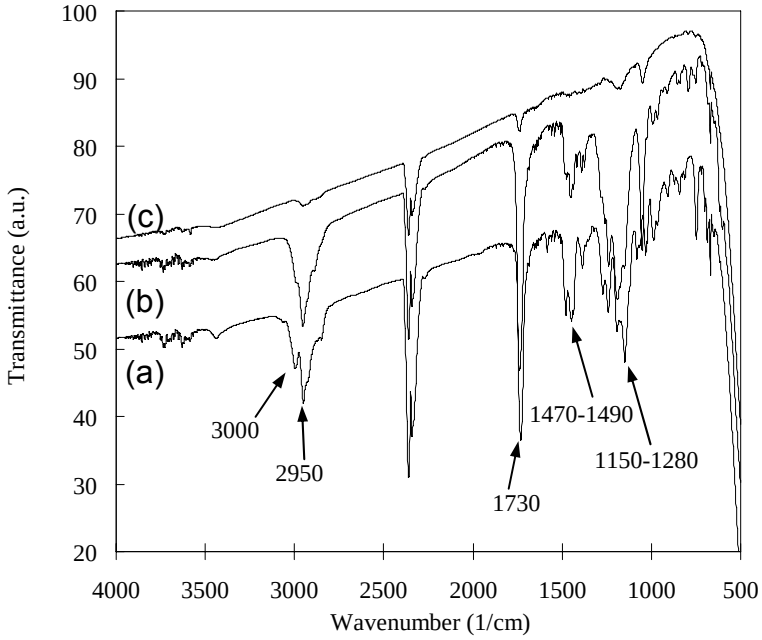


**Figure 4.4: FTIR spectra of PTHPET/PMMA (40/60 wt%) blended films (a) in the presence of acid, (b) the deproteced films prior to, and (c) after rinsing with chlorobenzene/hexane (50:50 vol%).**

A schematic diagram illustrating the formation of ordered domains of πCP is shown in **Figure 4.5**. Following spin casting of the polymer solution and subsequent solvent evaporation a binary thin film is formed in which the PMMA is the continuous phase, of greater thickness, while the πCP domains occupy the lower half of the film and form disc-like shapes that penetrate into the PMMA. The πCP is recessed with respect to the PMMA and a fraction of the domain is not exposed when viewed top-down – this is consistent with other studies of binary polymer mixtures.[26] The driving force for phase separation is the difference in solubility of the two dissimilar polymers. During spin-coating, solvent evaporates and demixing of πCP and PMMA occurs. PMMA is less

soluble in chlorobenzene than the πCP, thus the PMMA phase is more quickly depleted of solvent and begins to solidify before the πCP. In understanding pattern formation in these blends, the three models of the surface segregation and morphology evolution proposed by Ton-That *et al.* are considered, albeit for immiscible PMMA/polystyrene (PS) blends,[27] as shown in **Figure 4.6**. It is found that the πCPs mix well with PS to form homogenous films: by analogy to work described in ref (27) this is evidence that the πCPs used in our studies are immiscible with PMMA. Also, since the less volatile solvent, chlorobenzene was used, this polymer blend is assumed to be described by "model C" using ref (27) designation - in which an extensive dewetting of each phase occurs as a result of the relatively long solvent evaporation time. The πCP domains are slightly concave on their top surface, which may be attributed to the relatively lower surface tension of the πCP solution with respect to the initial solidification of PMMA and the formation of a concave meniscus. The thermally-reactive πCP is insolubilized by acid-catalyzed deprotection upon heating the films for 5 min (**Figure 4.5c**). Following acid catalyzed deprotection of the πCP and development with solvent, disc-shaped domains of πCP remain.

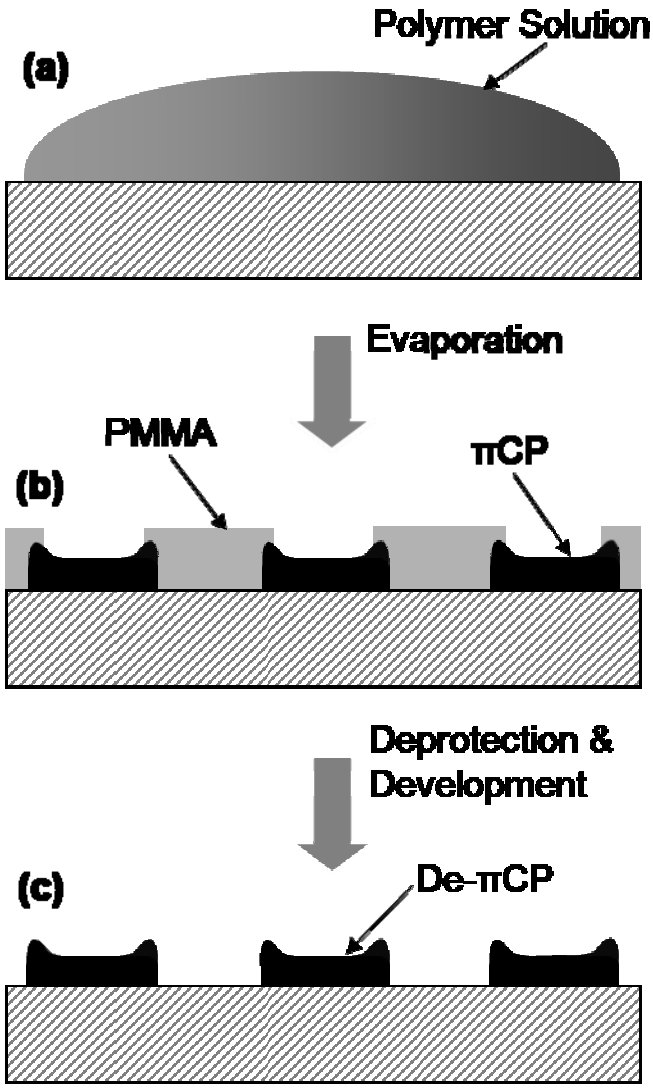


**Figure 4.5: Schematic illustration of the formation of micro/nano-sized πCP features (PTHPET or PTHPEF) by a) solution casting, b) self-organization, c) catalytic reaction and development.**

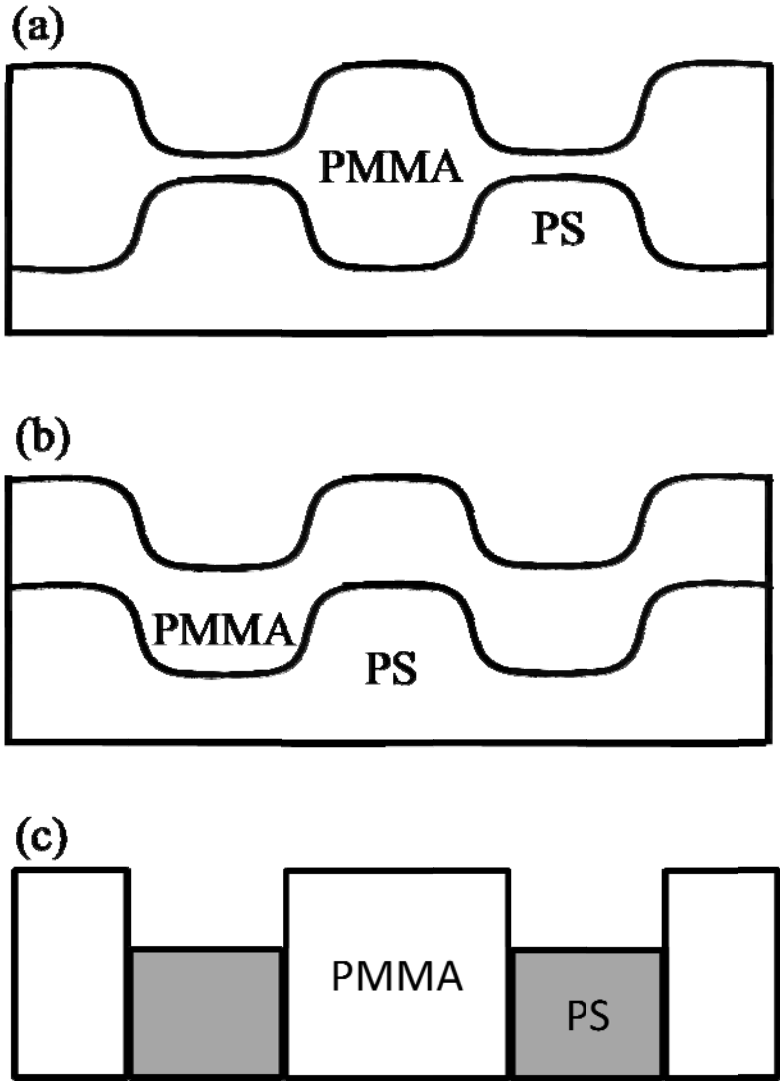


**Figure 4.6: Structural models of PS/PMMA blends: (a) surface pits correspond to hillocks in PS/PMMA interface; (b) surface pits correspond to pits in PS/PMMA interface; and (c) complete dewetting of the PS underlayer from model (a).[27]**

### 4.3.2 Morphology Dependence on Solution Concentration and Polymer Blends Composition

The relationship between the PTHPET/PMMA solution concentration and the resultant morphology of films is illustrated in **Figure 4.7**. Films of binary

composition were spin-cast from polymer solutions of varying concentrations: 24, 12, 4.8, and 2.4 mg/mL. AFM topographies of representative films are shown in **Figure 4.7 (a)**, **(b)**, and **(c)**, respectively. Film thicknesses were ~200, ~100, ~40, and ~20 nm, respectively, and the domain sizes decreased from ~1000, ~500, ~200, to ~100 nm, i.e., a linear relationship between the πCP domain size and the concentration of the casting solution was observed (**Figure 4.7d**). The decrease in domain size is attributed to both diminishing entanglement and intermolecular interaction of πCP chains resulting from a decrease in polymer concentration, and to its effect on the extent of chain coalescence during solvent evaporation, phase separation, and solidification. The influence of polymer concentration, chain coalescence, and the evolution of domain size have been studied in detail by Jose *et al.* for the non-conjugated polymer system, isotactic polypropylene/high density polyethylene.[28] The πCP/PMMA system appears to operate under the same physico-chemical constraints so that both thickness and πCP domain size may be partially controlled by the concentration of the casting solution.

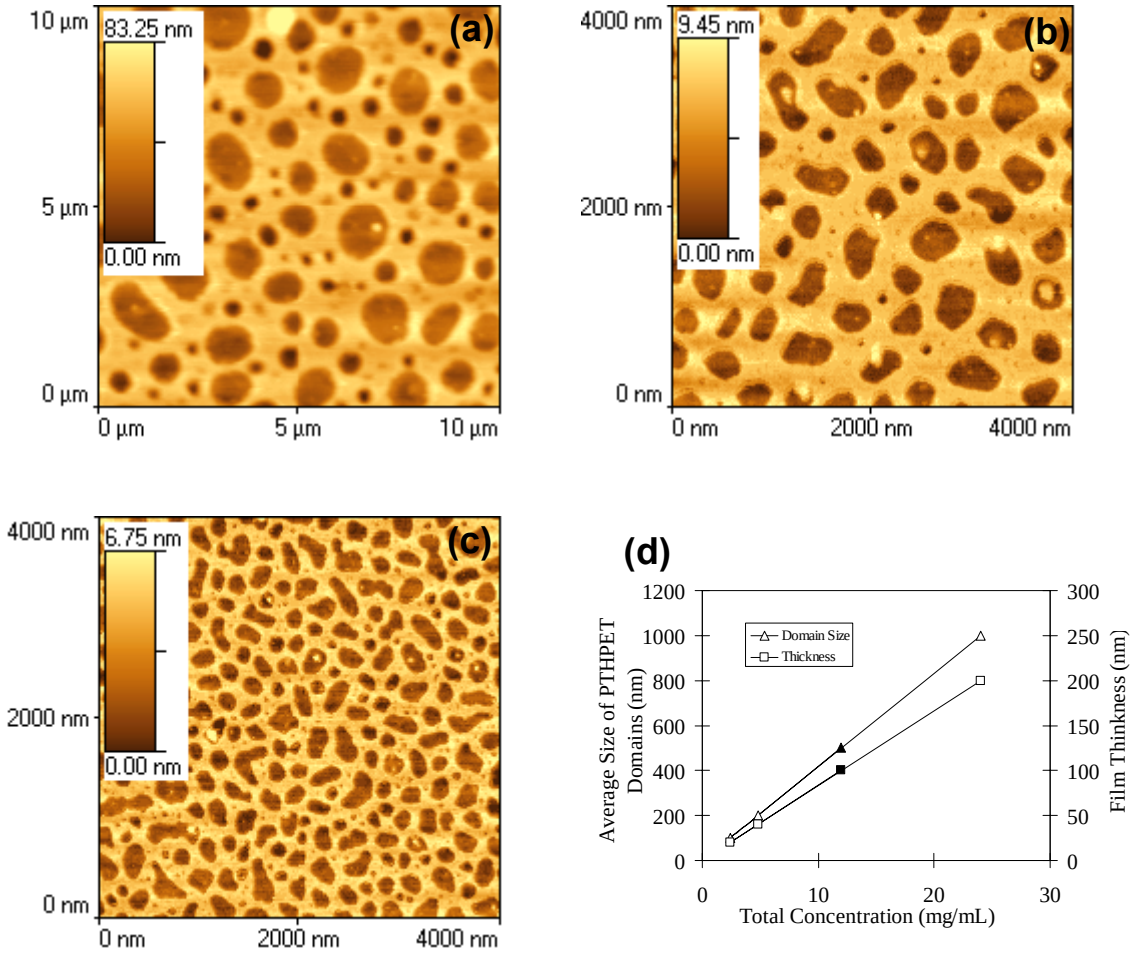


**Figure 4.7: AFM topography scans of PTHPET/PMMA (50:50 wt%) blended films cast from chlorobenzene solution having a total concentration: (a) 24 mg/mL (~200 nm thickness, 1000±200 nm sized PTHPET domains), (b) 4.8 mg/mL (~40 nm thickness, 200±50 nm sized PTHPT domains), (c) 2.4 mg/mL (~20 nm thickness, 100±50 nm sized PTHPET domains), and (d) a plot of film thickness and average size of PTHPET domains versus solution concentration. (▲ and ■ present the sample of PTHPET/PMMA (40:60 wt%) blended film prepared using the same procedure.)**

The relationship between the PTHPET/PMMA polymer blends composition and the resultant morphology of films is illustrated in **Figure 4.8**. Films of binary composition were spin-cast from polymer solutions (12 mg/mL) of varying polymer blends composition: 30:70 wt%, 40:60 wt%, 50:50 wt%, 60:40 wt%, and 70:30 wt%. AFM topographies of pristine blend films in the presence of acid are shown in **Figure 4.8 (a)**, **(c)**, **(e)**, **(g)**, and **(i)**, respectively. In these images, the lighter regions represent PMMA domains and the darker regions represnt PTHPET domains. AFM topographies of the deprotected films, De-PTHPET, from the blends 30:70 wt%, 40:60 wt%, 50:50 wt%, 60:40 wt%, and 70:30 wt%, after rinsing with chlorobenzene/hexane (50:50 vol%) are shown in **Figure 4.8 (b)**, **(d)**, **(f)**, **(h)**, and **(j)**, respectively. In these images, the lighter regions represent De-PTHPET domains and the darker region is mainly the substrate. With a decrease in the weight ratio of PMMA, the PMMA domains become less continuous, covering a small area, and finally break into a discontinuous, worm-shape phase possessing larger height than the PTHPET domains. The original PTHPET domains, which are scattered within as disc-shape regions, 200 - 500 nm in diameter, increase in size and form a more continuous phase with lower height than the PMMA domains. The increase in domain size of the πCP is consistent with the increase of πCP weight ratio in polymer blend solutions, thus πCP domain size may be partially controlled by the blend composition of the casting solution.

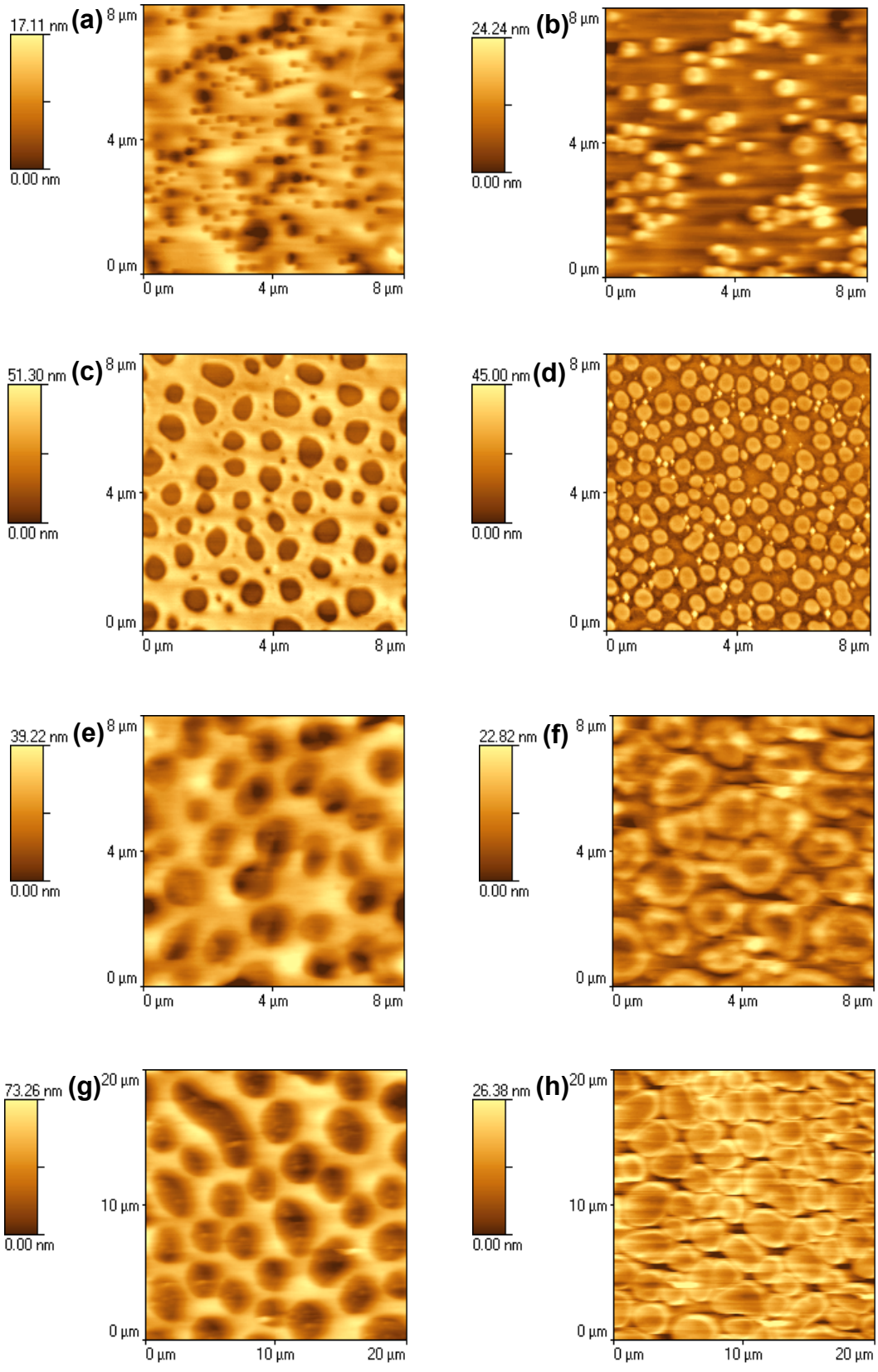
17.11 nm
(a)
8 µm
4 µm
0 µm
0.00 nm
0 µm
4 µm
8 µm
24.24 nm
(b)
8 µm
4 µm
0 µm
0.00 nm
0 µm
4 µm
8 µm
51.30 nm
(c)
8 µm
4 µm
0 µm
0.00 nm
0 µm
4 µm
8 µm
45.00 nm
(d)
8 µm
4 µm
0 µm
0.00 nm
0 µm
4 µm
8 µm
39.22 nm
(e)
8 µm
4 µm
0 µm
0.00 nm
0 µm
4 µm
8 µm
22.82 nm
(f)
8 µm
4 µm
0 µm
0.00 nm
0 µm
4 µm
8 µm
73.26 nm
(g)
20 µm
10 µm
0 µm
0.00 nm
0 µm
10 µm
20 µm
26.38 nm
(h)
20 µm
10 µm
0 µm
0.00 nm
0 µm
10 µm
20 µm

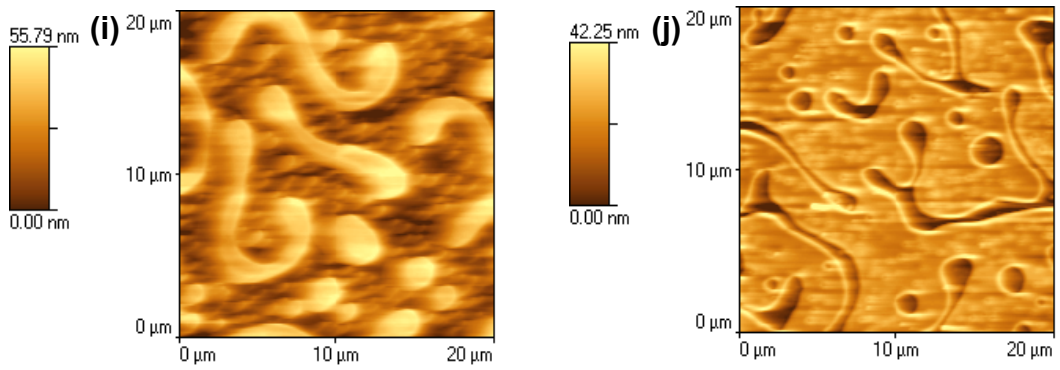


**Figure 4.8: AFM topography scans of PTHPET/PMMA blended films in various weight ratios, solution (12 mg/mL) cast on silicon wafers: pristine film PTHPET/PMMA (a) 30:70 wt%, (c) 40:60 wt%, (e) 50:50 wt%, (g) 60:40 wt%, and (i) 70:30 wt%, in the presence of acid, and deprotected film, De-PTHPET observed from the blends (b) 30:70 wt%, (d) 40:60 wt%, (f) 50:50 wt%, (h) 60:40 wt%, and (j) 70:30 wt%, after rinsing with chlorobenzene/hexane (50:50 vol%).**

### 4.3.3 Nanostructured PTHPEF

The procedure for controlling topography of πCP was also demonstrated with the polyfluorene class of polymer. AFM topography and profile scans of PTHPEF/PMMA (40:60 wt%) blended films formed from casting a chlorobenzene/THF (95:5 vol%) solution of the polymers (12 mg/mL in total) and containing 5 mol % of CSA are shown in **Figure 4.9**. The thickness of the film shown is ~80 nm, the πCP is recessed (by 10 - 20 nm) with respect to the PMMA, and the exposed domain sizes are ~150 nm in size, as shown in **Figure 4.9 (a)** and **(b)**. The topography, a profile scan, and 3-D morphology of the deprotecetd PTHPEF (De-PTHPEF) film after removal of PMMA are shown in **Figure 4.9 (c)-(e)**. Disc-shaped morphologies ~50 nm in height are observed. Notably, the size of the De-PTHPEF domains formed, ~150 nm, are smaller than that for the De-PTHPET film (~500 nm) even though the casting solutions were of

similar concentration. This is due to the differences in immiscibility of the two πCPs with PMMA. Therefore, different conjugated polymers or copolymers, such as polyfluorene, polythiophene, or poly(phenylene vinylene) derivatives bearing similar, removable, solubilizing groups could be selected to achieve various scales of phase separation. Also, it is noted that the domain size of De-PTHPEF pixels are 20 - 30 nm larger than that of the exposed, pristine PTHPEF phase, according to **Figure 4.9 (b)** and **(d)**, which indicates that the PMMA matrix partly covers the edges of the PTHPEF domains, as depicted in **Figure 4.5 (b)**.

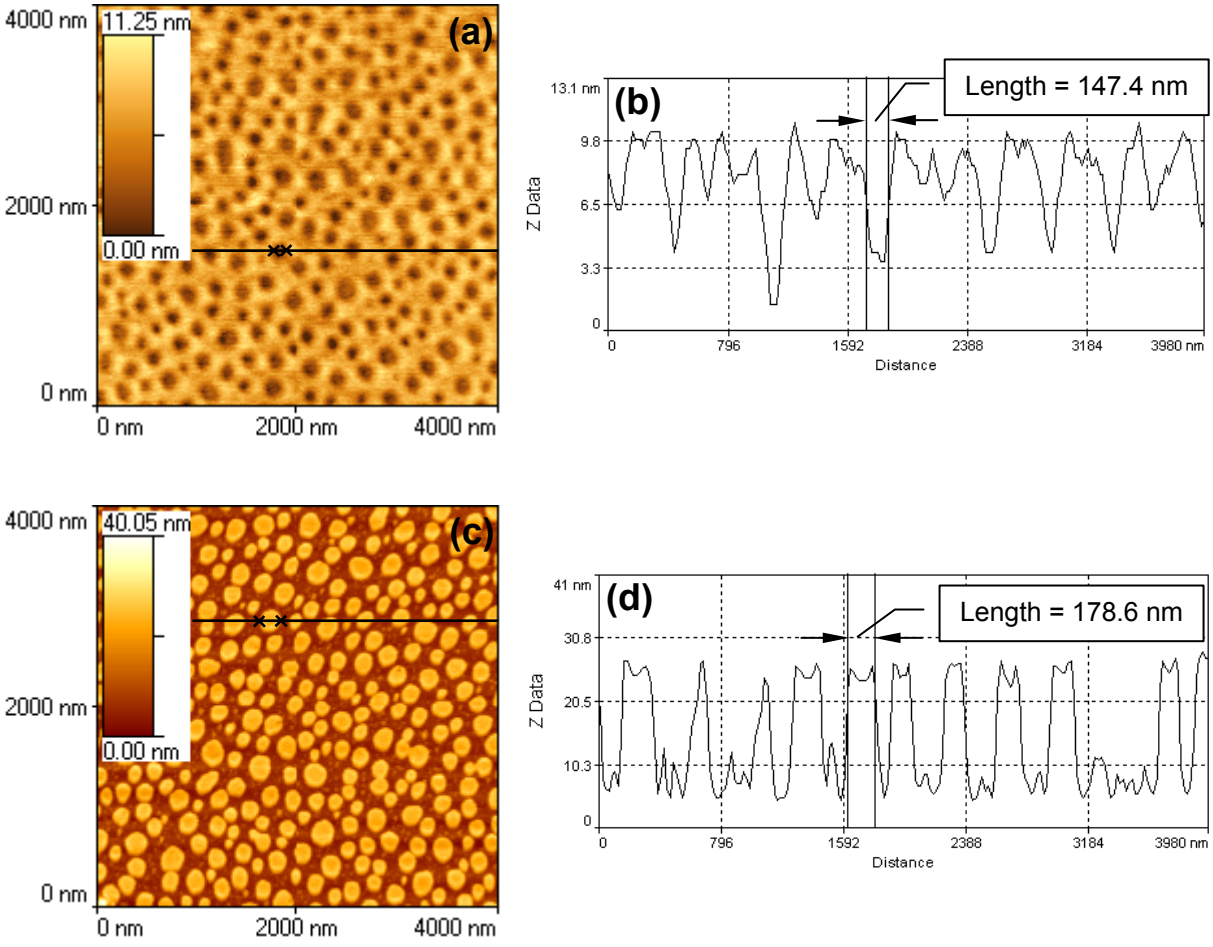

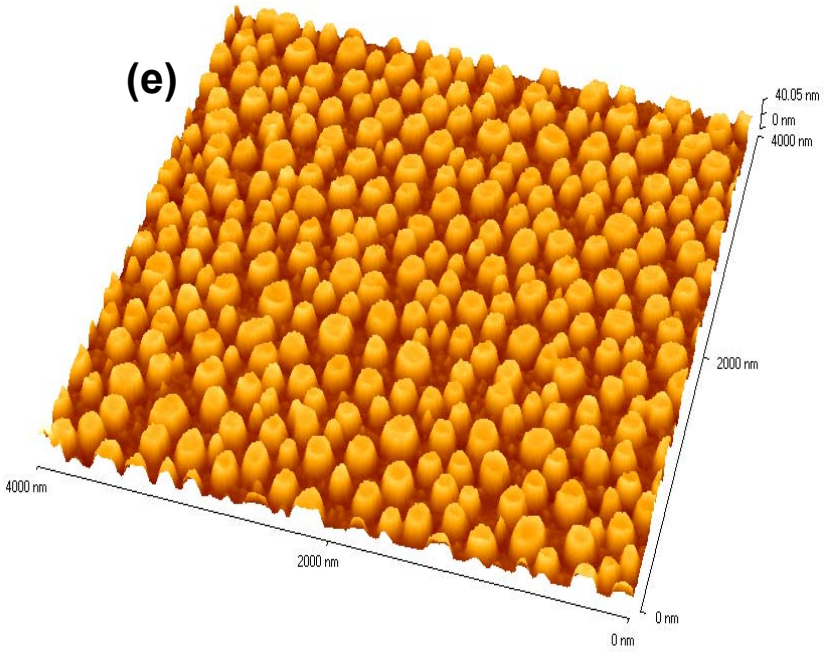


**Figure 4.9: AFM topography scans (a), (c) and profile scans (b), (d) of PTHPEF/PMMA (40:60 wt%) blended films cast from solution (12 mg/mL) on silicon wafers: (a), (b) pristine film PTHPEF/PMMA (50-100 nm thickness) in the presence of acid, (c), (d) deprotected film De-PTHPEF (~50 nm thickness, 100 - 200 nm sized domains) after development with chlorobenzene/hexane (50:50 vol%), and (e) 3-D morphology of (c).**

UV-vis spectra of pristine, as well as deprotected and developed, films of PTHPET/PMMA or PTHPEF/PMMA are shown in **Figure 4.10**. The wavelength of maximum absorption of De-PTHPET film ($\lambda_{max}$ = 460 nm) is very similar to that of the pristine PTHPET/PMMA blended film ($\lambda_{max}$ = 465 nm), as is that of the De-PTHPEF film ($\lambda_{max}$ = 376 nm) and the pristine PTHPEF/PMMA blended film ($\lambda_{max}$ = 371 nm). For both blends, the onset of absorption of the deprotected structures is slightly red-shifted with respect to the pristine films due to the

influence of thermal annealing and the subsequent loss in the bulky THP group, a topic that has been noted and previously discussed.[29]

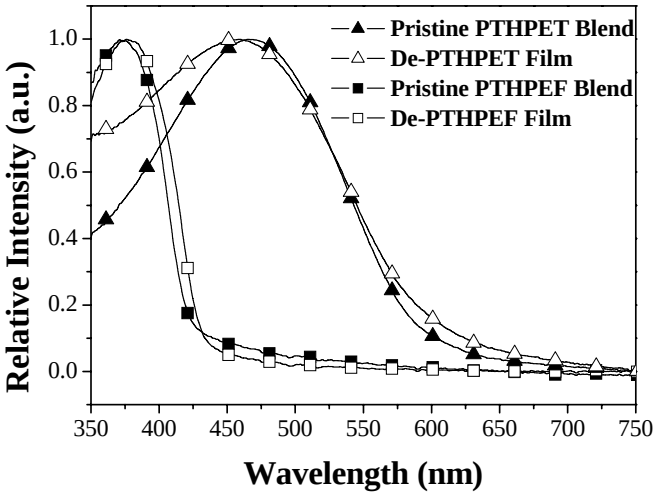


**Figure 4.10: UV-vis spectra of pristine and deprotected PTHPET/PMMA and PTHPEF/PMMA blended films (weight ratio 40:60 wt%) cast from solution (12 mg/mL).**

The procedure for controlling the topography of πCPs has also been demonstrated with ternary blends of PTHPET/PTHPEF/PMMA. AFM topography of PTHPET/PTHPEF/PMMA (20:20:60 wt%) blended films formed from casting a chlorobenzene/THF (95:5 vol%) solution of the polymers (12 mg/mL in total) and containing 5 mol % of CSA are shown in **Figure 4.11**. The thickness of the film shown is ~80 nm, the πCPs are recessed 40 - 50 nm with respect to the PMMA, as shown in **Figure 4.11 (a)**. The topography and 3-D morphology of the deprotected πCPs (De-πCPs) film after removal of PMMA are shown in **Figure 4.11 (b) and (c)**. Worm-shaped morphologies ~40 nm in height with smaller domains on top or beside the worm-shaped domains are observed. Notably, the

size of the De-πCPs domains formed are smaller than that for the De-PTHPET film (~500 nm) and larger than that for the De-PTHPEF film (~150 nm), even though the casting solutions were of similar concentration. This is due to miscibility of these two πCPs and the different immiscibility of the two πCPs with PMMA. Therefore, it is also evident that different conjugated polymers or copolymers bearing similar removable solubilizing groups can be selected to achieve various scales of phase separation. In addition, it is noted that the domain size of De-πCPs phases are much larger than that of the exposed, pristine πCPs phase, according to **Figure 4.11 (a)** and **(b)**, which also indicates that the PMMA matrix partly covers some part of the πCPs domains, as depicted in **Figure 4.5 (b)**.

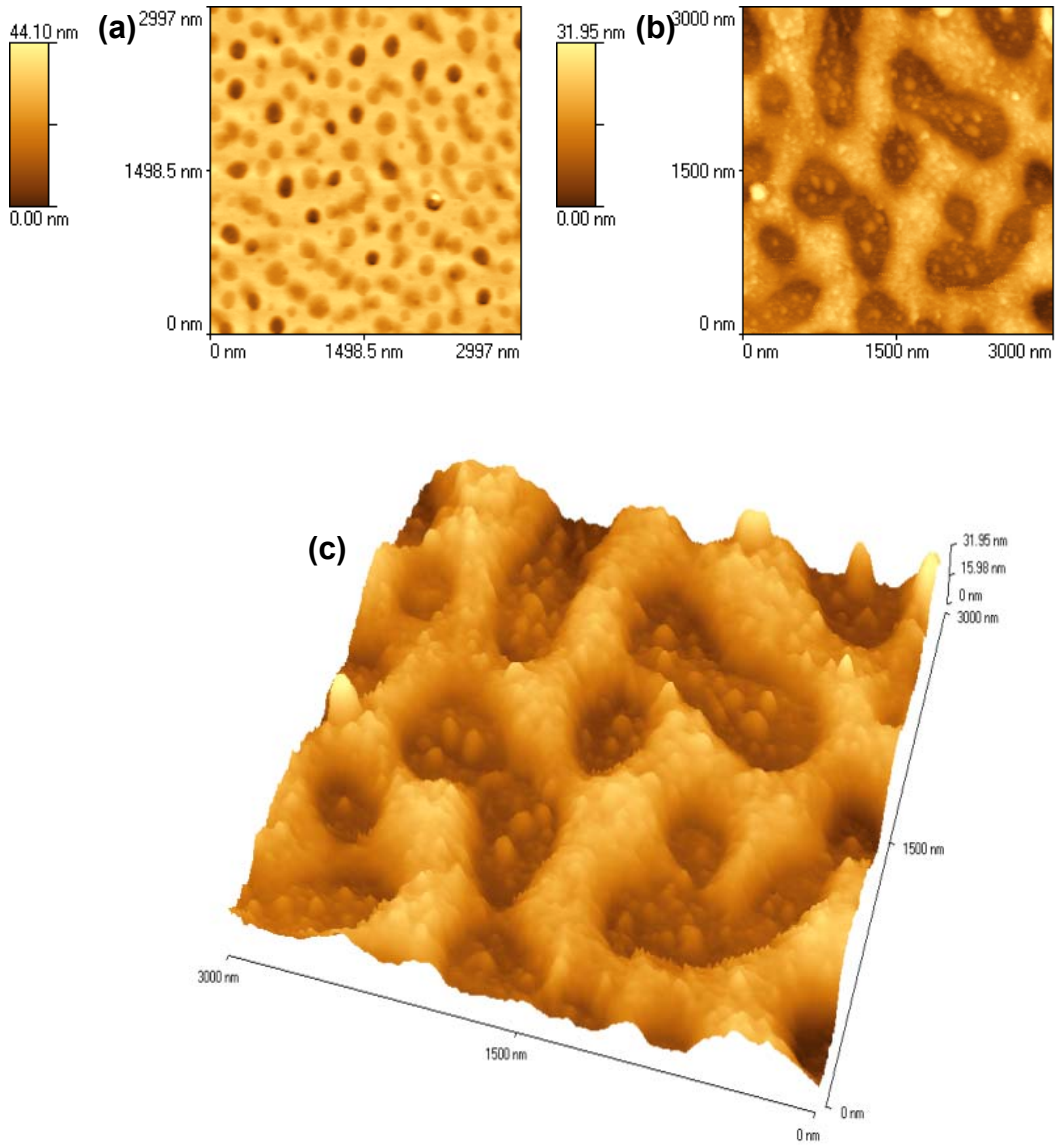


**Figure 4.11: AFM topography scans of PTHPET/PTHPEF/PMMA (20:20:60 wt%) blended films cast from solution (12 mg/mL) on silicon wafers: (a) pristine film PTHPEF/PMMA in the presence of acid, (b) deprotected film De-PTHPET/PTHPEF, and (c) 3-D morphology after development with chlorobenzene/hexane (50:50 vol%).**

This facile method of topographical control may be useful in the patterning of nano-scale morphologies and topographies for PLEDs and modification of the nanostructure for polymer PV cell devices. For example, the insoluble, topographically-structured πCP may be exploited as a donor layer in organic PV cells following simple spin-casting of an electron acceptor layer on top of the donor layer to form a nano/micro-sized, donor-acceptor heterojunction structure. Controlled architectures leading to bulk heterojunctions have been reported by Forrest *et al*. for small molecule PV cells; and Hany *et al*., for polymer PV cells.[30] A unique feature of the present work is that the nano-structured donor layer is rendered insoluble by thermal deprotection so that an electron-acceptor layer can be directly deposited onto the donor layer by solution, thereby avoiding the thermal evaporation process. Single phase structures of electron donor and acceptor, like those demonstrated here, may provide an advantage over simple blended films in that electron acceptor molecules are not isolated in the donor film, and vice versa, which may circumvent charge trapping and thus may improve the device efficiency.[31] These postulations are investigated further in the following section.

### 4.3.4 Devices Performances of PTHPET/PCBM System

PTHPET/PCBM bulk heterojunction (BHJ), bilayer, and nano-patterned PV devices were fabricated and characterized according to the procedure summarized in Section 4.2.3. The measurements of device performance were done many times for each device architecture. **Figure 4.12** shows the J-V characteristics of bulk heterojunction, bilayer, and nano-patterned

PTHPET/PCBM (PTHPET 10 mg/mL, PCBM 20 mg/mL) PV devices under AM 1.5D illumination with an intensity of 100 mW/cm$^2$. The device performance and UV-vis absorbance of these PV devices are summarized in **Table 4.1**. The nano-patterned device shows the best performance with $V_{oc}$ = 0.63 V, $J_{sc}$ = 1.67 mA/cm$^2$, and FF = 51.5 %. The PCE of this device is also the highest value of the series studied (0.54 %). The BHJ device shows moderate performance with $V_{oc}$ = 0.49 V, $J_{sc}$ = 1.34 mA/cm$^2$, FF = 30.6 %, and PCE = 0.2 %. The bilayer device shows the poorest performance with $V_{oc}$ = 0.43 V, $J_{sc}$ = 0.58 mA/cm$^2$, FF = 45.6 %, and PCE = 0.11 %. The low $J_{sc}$ and PCE of the bilayer devices are consistent with the interface between donor layer and acceptor layer being a limiting factor. Excitons formed at a location further from the donor-acceptor interface than the exciton diffusion length have a lower probability of being captured. The BHJ device has a lower fill factor than the nano-patterned device. This is likely due to charge trapping and poor conductivity. However, utilizing the nano-patterned device architecture, the donor-acceptor interface is maximized without the formation of trapped charge. Thus, the nano-patterned device has a better percolation pathway than the BHJ device.

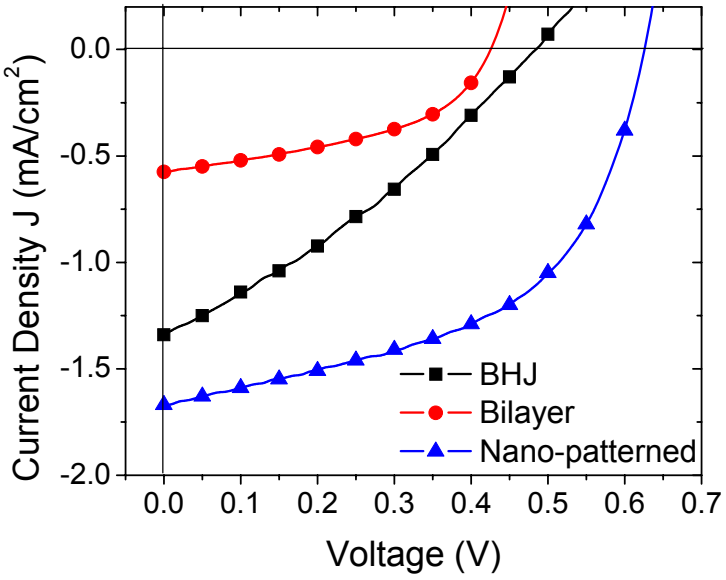


**Figure 4.12: J-V curves obtained from bulk heterojunction (BHJ), bilayer, and nano-patterned PTHPET/PCBM (PTHPET 10 mg/mL, PCBM 20 mg/mL) PV devices under AM 1.5D illumination at an irradiation intensity of 100 mW/cm$^2$.**

**Table 4.1: Summary of device performance, UV-vis absorbance, and transmittance for BHJ, bilayer, and nano-patterned PTHPET/PCBM (PTHPET 10 mg/mL, PCBM 20 mg/mL) PV devices.**

| Device | $J_{sc}$ (mA/cm$^2$) | $V_{oc}$ (V) | FF (%) | PCE (%) | EQE* (%) | IQE* (%) | A* | T* |
|---|---|---|---|---|---|---|---|---|
| BHJ | 1.34 | 0.49 | 30.6 | 0.20 | 10.3 | 26.2 | 0.39 | 0.41 |
| Bilayer | 0.58 | 0.43 | 45.6 | 0.11 | 4.9 | 9.6 | 0.54 | 0.29 |
| Nano-patterned | 1.67 | 0.63 | 51.5 | 0.54 | 12.4 | 24.8 | 0.52 | 0.30 |

* The reported values are at 435 nm.

**Table 4.1** summarizes the results of EQE, IQE, absorbance, and transmittance of these devices at the maximum absorption wavelength of PTHPET (435 nm). The UV-vis spectra and EQE plots are shown in **Figure 4.13** and **Figure 4.14**, respectively. UV-vis spectra of bilayer and nano-patterned devices show stronger absorbance than the BHJ devices in the region 350 - 550 nm. However, the EQE from bilayer devices (4.9 %) is much lower than the BHJ device and nano-patterned devices (10.3 % and 12.4 %, respectively). This observation is consistent with the performance study of $J_{sc}$ from these devices and can be explained by the fact that the efficiency of the bilayer device will be limited by the exciton diffusion length. The nano-patterned device exhibits slightly higher EQE than the BHJ device. However, they have a stronger absorbance than the BHJ device, so that the IQE, absorbed photon-to-current efficiencies are similar, i.e., no apparent improvement in efficiency is observed.

The AM 1.5D solar spectrum and UV-vis absorbance obtained from nano-patterned PTHPET/PCBM device and P3HT film are shown in **Figure 4.15**. The overlap of P3HT with solar spectrum is better than that of the nano-patterned PTHPET/PCBM device with solar spectrum. The red-shifted absorption spectrum of PTHPET compared to that of P3HT may be one of the reasons of the lower PCE (~0.5 %) of PTHPET based devices than the PCE (~ 5 %) of optimized P3HT based devices in literature.[32]

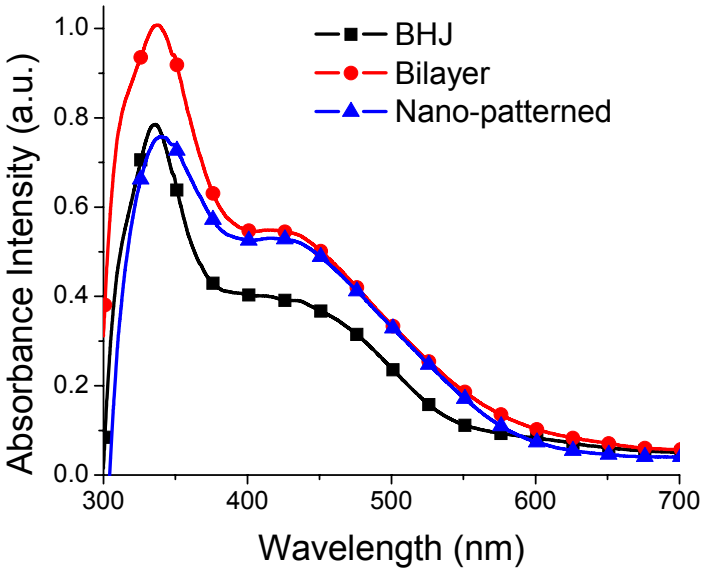


**Figure 4.13: UV-vis absorbance obtained from BHJ, bilayer, and nano-patterned PTHPET/PCBM (PTHPET 10 mg/mL, PCBM 20 mg/mL) PV devices.**

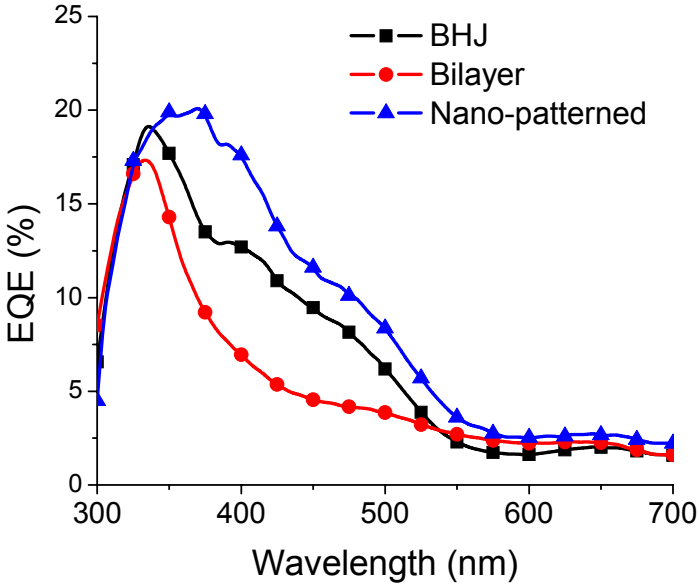


**Figure 4.14: EQE obtained from BHJ, bilayer, and nano-patterned PTHPET/PCBM (PTHPET 10 mg/mL, PCBM 20 mg/mL) PV devices under AM 1.5D illumination at an irradiation intensity of 100 mW/cm$^2$.**

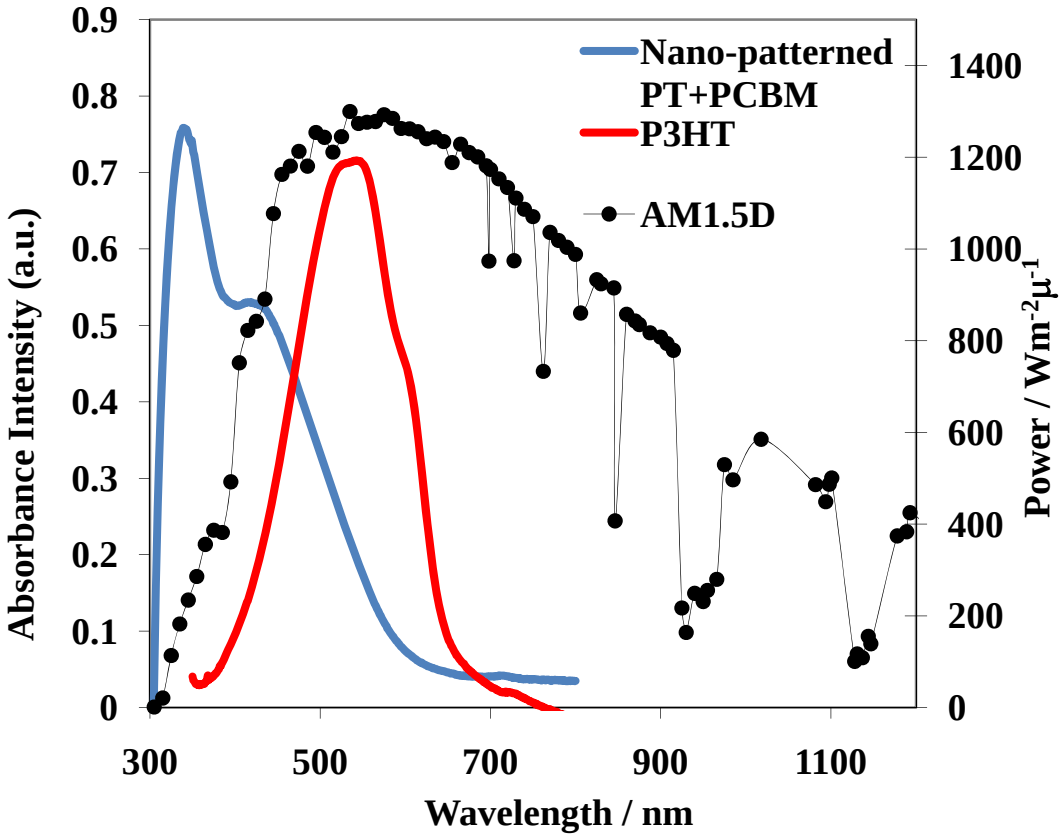


**Figure 4.15: AM 1.5D solar spectrum and UV-vis absorbance obtained from nano-patterned PTHPET/PCBM PV device and P3HT.**

## 4.4 Conclusions

In summary, a facile method for preparing nano/micro-sized topologies of π-conjugated polymers from πCP bearing thermally-cleavable, solubilizing groups is reported. The feature size of the πCP formed is dependent on several parameters including solvent, solution concentration, polymer blends composition, and the nature of the polymer(s) used. Features as small as 150 nm are demonstrated, and much smaller features are likely possible with further optimization of conditions. With a clearer understanding of the entropies of mixing between polymers and solvents employed, more accurate control of the morphologies is anticipated. Patterned films were found to exhibit optical properties that are similar to the pristine polymer blend thin films. The unique feature of the present work is that the nano-structured donor layer is rendered insoluble by thermal deprotection so that an electron-acceptor layer can be directly deposited onto the donor layer by solution. The insoluble nano/micro-structured πCP has been exploited as a donor layer in polymeric PV cells following spin-casting of an electron acceptor layer on top of the donor layer to form a nano/micro-sized donor-acceptor heterojunction. The device architecture-performance relationship was studied. The patterned πCP devices exhibit a higher power conversion efficiency and external quantum efficiency than the bilayer and bulk heterojunction devices. This is attributed to the patterned architecture, which improves the donor-acceptor interface, reduces trapping, and improves the pathway for electrons and holes to reach their respective electrodes.

## 4.5 References

(1) P. E. Burrows, G. Gu, V. Bulovic, Z. Shen, S. R. Forrest, M. E. Thompson, *IEEE Trans. Electron Devices* **1997**, *44*, 1188.

(2) N. Stutzmann, R. H. Friend, H. Sirringhaus, *Science* **2003**, *299*, 1881.

(3) C. Winder, N. S. Sariciftci, *J. Mater. Chem*. **2004**, *14*, 1077.

(4) C. B. Gorman, H. A. Biebuyck, G. M. Whitesides, *Chem. Mater.* **1995**, *7*, 526.

(5) (a) M. S. A. Abdou, S. Holdcroft, in *Encyclopedia of Conductive Molecules and Polymers* (Ed: H. S. Nalwa), Wiley, New York, **1996**, Ch. 4. (b) M. Angelopoulos, in *Handbook of Conducting Polymers*, 2nd ed. (Eds: T. A. Skotheim, R. L. Elsenbaumer, J. R. Reynolds), Marcel Dekker, New York, **1997**. (c) P. I. Clemonson, W. J. Feast, M. M. Ahmad, P. C. Allen, D. C. Bott, C. S. Brown, L. M. Connors, *Polymer* **1992,** *33,* 4711.

(6) (a) Z. Bao, Y. Feng, A. Dodabalapur, V. R. Raju, A. J. Lovinger, *Chem. Mater.* **1997**, *9*, 1299. (b) Z. Bao, J. A. Rogers, H. E. Katz, *J. Mater. Chem.* **1999**, *9*, 1895.

(7) C. C. Wu, D. Marcy, M. H. Lu, J. C. Sturm, *Appl. Phys. Lett.* **1998**, *72*, 519.

(8) (a) Y. Xia, G. M. Whitesides, *Angew. Chem. Int. Ed.* **1998**, *37*, 550. (b) S. Brittain, K. Paul, X.-M. Zhao, G. Whitesides, *Phys. World* **1998**, *11*, 31. (c) T. Granlund, T. Nyberg, L. S. Roman, M. Svensson, O. Inganäs, *Adv. Mater.* **2000**, *12*, 269.

(9) (a) F. J. M. Hoeben, P. Jonkheijm, E. W. Meijer, A. P. H. J. Schenning, *Chem. Rev.* **2005**, *105*, 1491. (b) U. H. F. Bunz, *Adv. Mater.* **2006**, *18*, 973.

(10) G. Widawski, M. Rawiso, B. François, *Nature* **1994**, *369*, 387.

(11) J. Liu, E. Sheina, T. Kowalewski, R. D. McCullough, *Angew. Chem., Int. Ed.* **2002**, *41*, 329.

(12) M. Granström, M. Berggren, O. Inganäs, *Science* **1995**, *267*, 1479.

(13) N. A. Iyengar, B. Harrison, R. S. Duran, K. Schanze, J. R. Reynolds, *Macromolecules* **2003**, *36*, 8978.

(14) F. A. Boroumand, P. W. Fry, D. G. Lidzey, *Nano. Lett.* **2005**, *5*, 67.

(15) R. H. Bube (ed.), in *Photovoltaic Material*, Imperial College Press, London, **1998**, p. 2 and p. 219.

(16) H. Hoppe, N. S. Sariciftci, *J. Mater. Res.* **2004**, *19*, 1924.

(17) (a) P. Peumans, A. Yakimov, S. R. Forrest, *J. Appl. Phys.* **2003**, *93*, 3693. (b) S. R. Scully, M. D. McGehee, *J. Appl. Phys.* **2006**, *100,* 034907.

(18) G. Yu, J. Gao, J. C. Hummelen, F. Wudl, A. J. Heeger, *Science* **1995,** *270*, 1789.

(19) K. M. Coakley, M. D. McGehee, *Chem. Mater.* **2004**, *16*, 4533.

(20) (a) U. Scherf, A. Gutacker, N. Koenen, *Acc. Chem. Res*. **2008**, *41*, 1086. (b) X. Chen, B. Gholamkhass, X. Han, G. Vamvounis, S. Holdcroft, *Macromol. Rapid Commun.* **2007**, *28*, 1792.

(21) J. Yu, M. Abley, C. Yang, S. Holdcroft, *Chem. Commun*. **1998,** 1503.

(22) X. Han, X. Chen, G. Vamvounis, S. Holdcroft, *Macromolecules* **2005**, *38*, 1114.

(23) H. Sirringhaus, P. J. Brown, R. H. Friend, M. M. Nielsen, K. Bechgaard, B. M. W. Langeveld-Voss, A. J. H. Spiering, R. A. J. Janssen, E. W. Meijer, P. Herwig, D. M. de Leeuw, *Nature* **1999**, *401*, 685.

(24) H. Mao, B. Xu, S. Holdcroft, *Macromolecules* **1993**, *26*, 1163.

(25) R. S. Loewe, S. M. Khersonsky, R. D. McCullough, *Adv. Mater.* **1999**, *11*, 250.

(26) S. Walheim, M. Böltau, J. Mlynek, G. Krausch, U. Steiner, *Macromolecules* **1997**, *30*, 4995.

(27) C. Toh-That, A. G. Shard, D. O. H. Teare, R. H. Bradley, *Polymer* **2001**, *42*, 1121.

(28) S. Jose, A. S. Aprem, B. Francis, M. C. Chandy, P. Werner, V. Alstaedt, S Thomas, *Eur. Polym. J.* **2004**, *40*, 2105.

(29) J. Yu, S. Holdcroft, *Macromolecules* **2000**, *33*, 5073.

(30) (a) F. Yang, M. Shtein, S. R. Forrest, *Nature Mater.* **2005**, *4*, 37. (b) F. A. Castro, H. Benmansour, C. F. O. Graeff, F. Nüesch, E. Tutis, R. Hany, *Chem. Mater.* **2006**, *18*, 5504.

(31) J. J. Dittmer, E. A. Marseglia, R. H. Friend, *Adv. Mater.* **2000**, *12*, 1270.

(32) (a) W. Ma, C. Yang, X. Gong, K. Lee, A. J. Heeger, *Adv. Funct. Mater.* **2005**, *15*, 1617. (b) J. Peet, J. Y. Kim, N. E. Coates, W. L. Ma, D. Moses, A. J. Heeger, G. C. Bazan, *Nat. Mater.* **2007**, *6*, 497. (c) J. Y. Kim, K. Lee, N. E. Coates, D. Moses, T-Q. Nguyen, M. Dante, A. J. Heeger, *Science* **2007**, *317*, 222. (d) M. J. Currie, J. K. Mapel, T. D. Heidel, S. Goffri, M. A. Baldo, *Science* **2008**, *321*, 226.

# CHAPTER 5: SUMMARY AND FUTURE WORK

## 5.1 Summary

A homopolymer of 9,9'-di(2-(2-tetrahydropyranyloxy)ethyl)fluorene and copolymers based on 9,9'-dihexylfluorene, thiophene and 3-(2-(2-tetrahydropyranyloxy)ethyl)thiophene repeat units, were obtained as thermally-reactive luminescent polymers. Thermolytic removal of tetrahydropyran (THP) groups from polymer films rendered the films insoluble due to the formation of hydroxyl groups on the termini of side chains. The acid-catalyzed deprotection removal of THP groups from the polymers can be carried out at temperature of 100 - 200 °C lower than the thermolytic deprotection in the absence of acid. The effect of the acid-catalyzed deprotection of these polyfluorenes on the photoluminescent properties was studied. Prior to deprotection, the polyfluorenes show fluorescence in different colour and high emission intensity both in solution and in the solid state. After deprotection at 150 °C for 3 min, their optical properties quantum yields were retained, but their solubility was reduced due to the formation of hydroxyl groups. The decrease in solubility allows for their spatially-controlled deposition using chemically amplified, maskless, soft lithography. However, it was shown that these polyfluorenes suffered from a degradation of colour purity of fluorescence due to fluorenone formation.

A new series of polyfluorenes with enhanced oxidative stability were investigated to eliminate fluorenone formation. A homopolymer of 9,9'-bis[4-(2-(2-tetrahydropyranyloxy)ethoxy)phenyl]fluorene and its copolymers with 3,4-benzothiadiazole and 4,7-di(3(4-n-octylphenyl)-2-thienyl)-2,1,3-benzothiadiazole

were synthesized to produce a series of thermally-reactive blue, green, and red luminescent polymers with enhanced oxidative stability. Thermal removal of the THP was lowered by up to 200 °C when acid is present in the films. The fluorescence quantum yield of the benzothiadiazole-containing copolymers was low due to energy transfer and quenching. These polymers were found applicable to patterning by NIR direct thermal lithography, in conjunction with a NIR dye and thermal acid generator. The presence of the phenyl groups at the 9-site carbon was found to necessary to eliminate fluorenone formation and enhance the colour purity of the material.

A facile method for preparing nano/micro-sized topologies of π-conjugated polymers (πCPs) from πCP blends is also reported. πCPs bearing thermally-cleavable, solubilizing, THP groups were blended with PMMA in the presence of camphorsulfonic acid to yield micro- and nano-phase separated thin films of thickness ~100 nm. A thermally-induced, acid-catalyzed solid-phase reaction, in which the bulky THP group is eliminated, renders the conjugated polymer insoluble. The induced dissimilarity in solubility and subsequent removal of PMMA by dissolution affords retention of the conjugated polymer in the form of micro/nano-sized architectures. Domains of conjugated polymer, 100 - 500 nm in diameter and 40 - 50 nm in depth, maintained their optical properties. The insoluble patterned πCP has been exploited as a donor layer in polymeric PV devices following spin-casting an electron acceptor layer on top of the donor layer to form a nano/micro-sized donor-acceptor heterojunction. The performance study of these PV devices demonstrated that the patterned πCP

architecture may circumvent charge trapping and thus improve device efficiency. This method offers a potential strategy for further improvement of polymer-based PV cells.

## 5.2 New Directions

The thermally-reactive π-conjugated polymers (πCPs) are promising candidates for use in polymer-based electronics, because of the combination of their electrical properties, optical properties, and controllable solubility via thermally-induced solid phase reaction. These materials can be patterned by various methods of lithography, such as photolithography, chemically amplified soft lithography, and thermal laser lithography. Thermal laser lithography is of particular interest for deposition of the polymeric active materials for the fabrication of organic electronics. This method provides many unique features, such as large area, high throughput, high-resolution, and prevention of damage to the optical and electronic properties. Thermal laser patterning of thermally-reactive fluorene-based polymers has been demonstrated using a NIR dye and thermal acid generator. One future direction may be employing the method in the fabrication of devices such as PLEDs. The process would involve deposition and patterning of the active material on a PEDOT-coated ITO glass, followed by the deposition of the electrode via metal evaporation through an appropriate mask. However, the requirements of the appropriate mask are very strict; the mask must have the same shape and size as the patterned polymer. In addition, the position of the mask must be controlled so that the metal electrode can be deposited at the exact location on the pattern without contaminating neighbouring

patterns. An alternative method of post-fabrication patterning may also be investigated with the combination of patterning and deposition of metal electrodes. The process of this device fabrication method is shown schematically in **Figure 5.1**. Here, a layer of active material, containing a thermal acid generator, is spin cast on a PEDOT-coated ITO glass, followed by the deposition of the electrode via metal evaporation. The second layer of p(HEMA) containing a NIR dye is spin cast on top of the electrode. After exposure and subsequent film development, a negative tone image of the active material with the electrode on top can be obtained. This method offers two advantages over the previous method: it is maskless. No mask of special shape and size is required, and no alignment is necessary. Measurements of the device properties could be conducted using conventional LED testing methods.

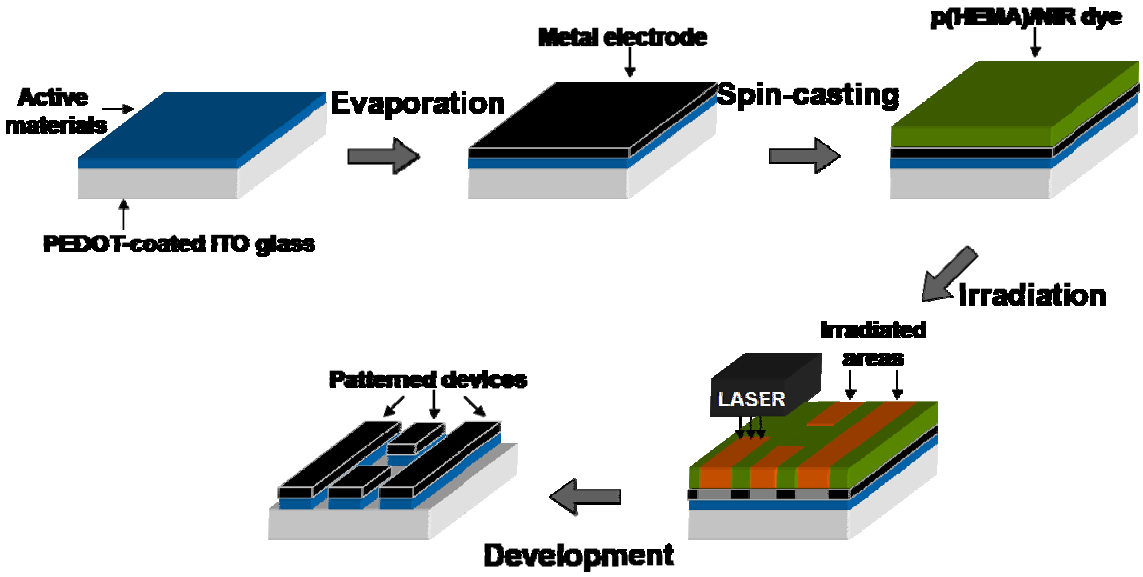


**Figure 5.1: Schematic diagram of device fabrication via thermal laser patterning of thermally-reactive π-conjugated polymers.**

For the application of polymeric PV devices, a future direction may be the synthesis of new copolymers, such as P3HT-co-hexylthiophene(THP) and polyfluorene(THP)-co-bithiophene, as shown in **Figure 5.2**. These polymers can be considered as the donor materials. Compared to P3HT, PTHPET is blue-shifted in absorption. P3HT has good charge mobility and optical density, thus the copolymer P3HT-co-hexylthiophene(THP) can be optimized to retain the crystalline structure and optical, electronic properties. The domain size of De-PTHPEF from polymer blends is observed to be 100-150 nm. However, fluorene-based homopolymers are not likely to be used for PV applications because of their UV light absorption. However, fluorene bearing THP groups can be copolymerized with bithiophene to tune the donor band gap. The structure-morphology relationship can be investigated. Due to the nature of these

polymers, different morphologies and domain size are expected, and this is expected to affect the device performance. Very recently, Schulz *et al.* reported a high band gap polyfluorene-alt-bithiophene/PCBM device with 2.7% PCE. It is promising to improve the device performance of this type of amorphous polyfluorene copolymer using the nano-patterning method.

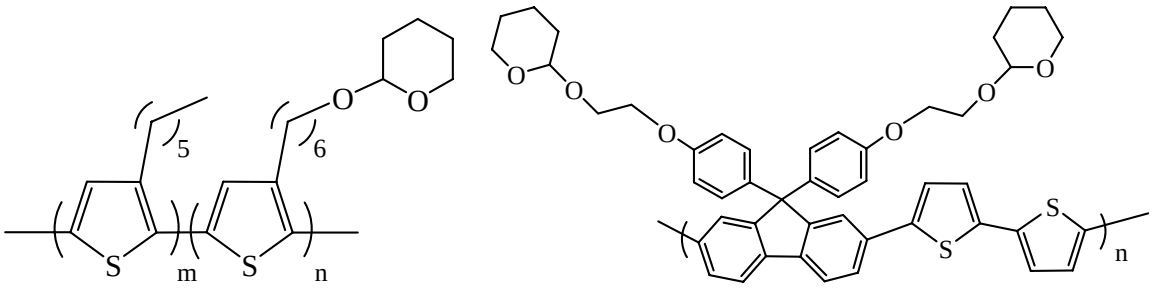


P3HT-co-hexylthiophene(THP) polyfluorene(THP)-co-bithiophene

**Figure 5.2: Structures of P3HT-co-hexylthiophene(THP) and polyfluorene (THP)-co-bithiophene.**

## 5.3 References

(1) G. Schulz, X. Chen, S. Holdcroft, *Appl*. *Phys*. *Lett*. **2009**, *94*, 023302.

# APPENDIX

**Supporting Information of Chapter 2.**

**NMR spectra of P1-P4.**

**Figure S1. $^{1}H$ NMR spectrum of P1 (PTHPEF) in $CD_2Cl_2$.**

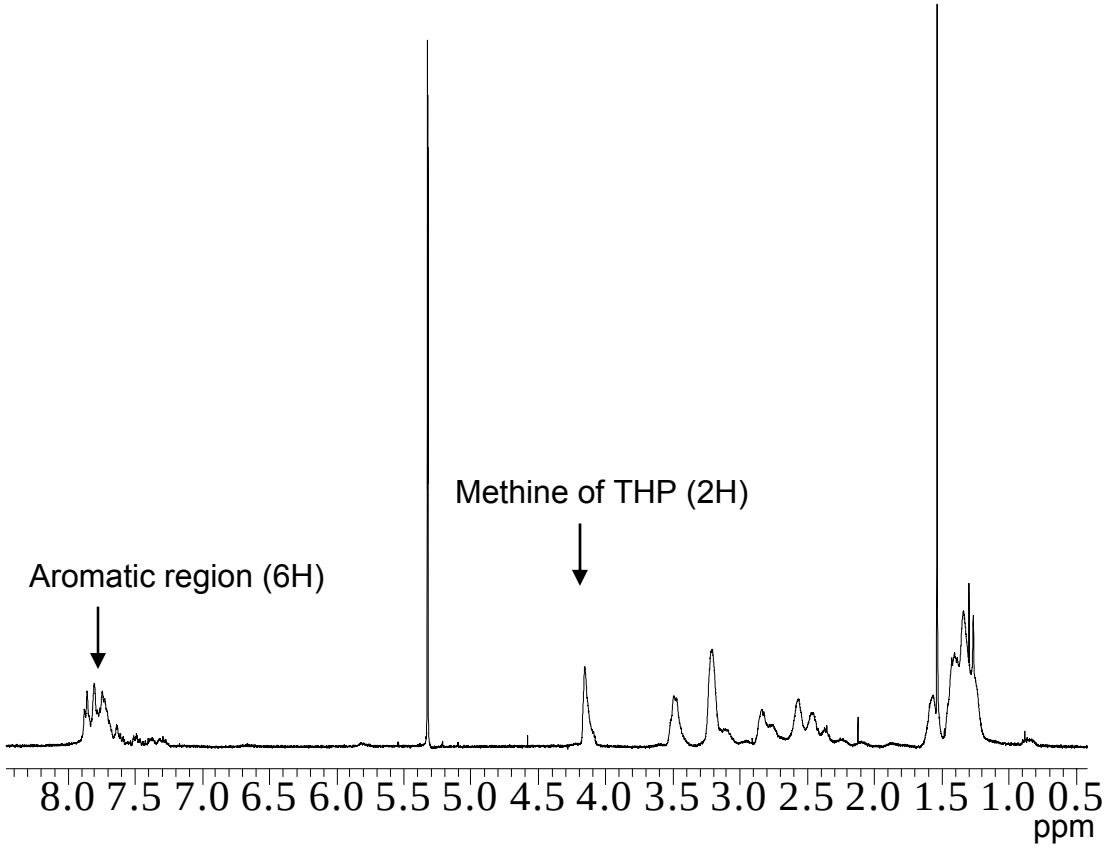

**Figure S2. $^{13}C$ NMR spectrum of P1 (PTHPEF) in $CD_2Cl_2$.**

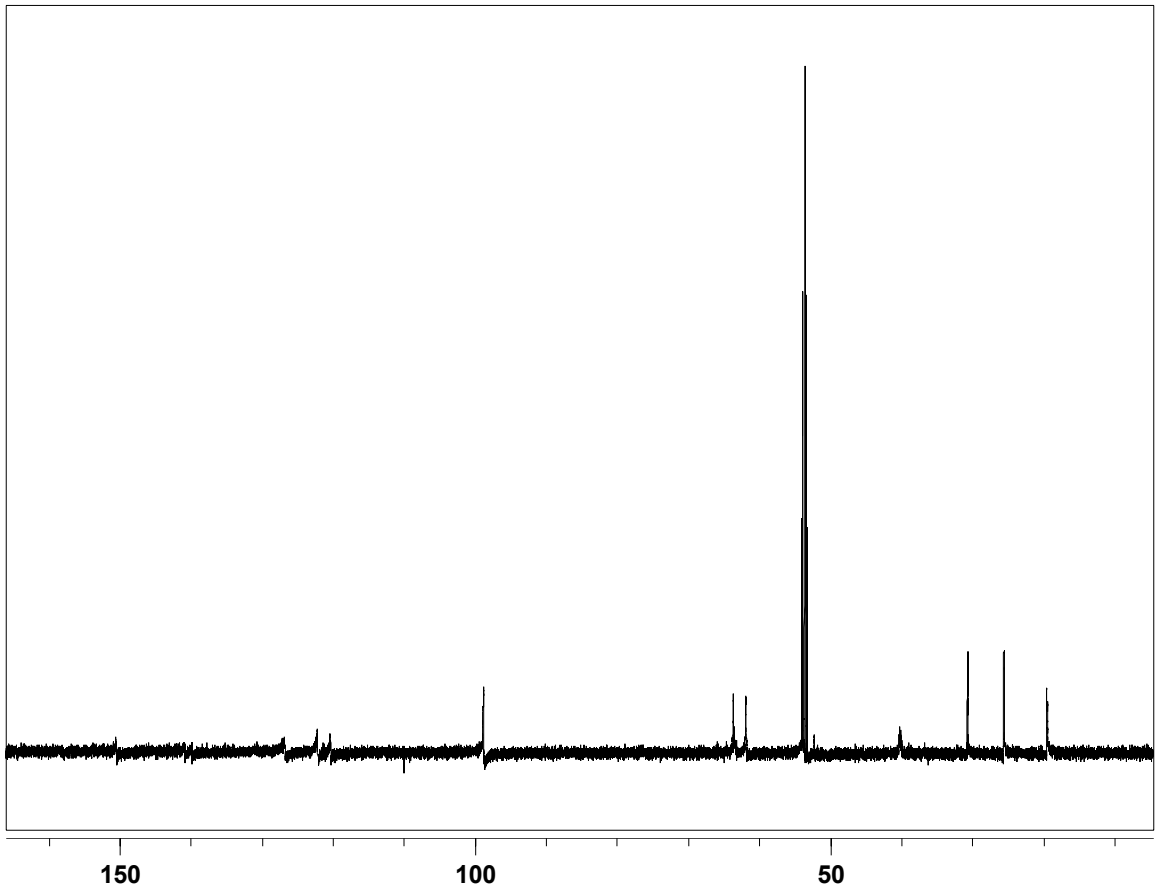

**Figure S3. $^{1}$H NMR spectrum of P2 (PTHPEF-alt-diHF) in $CD_2Cl_2$.**

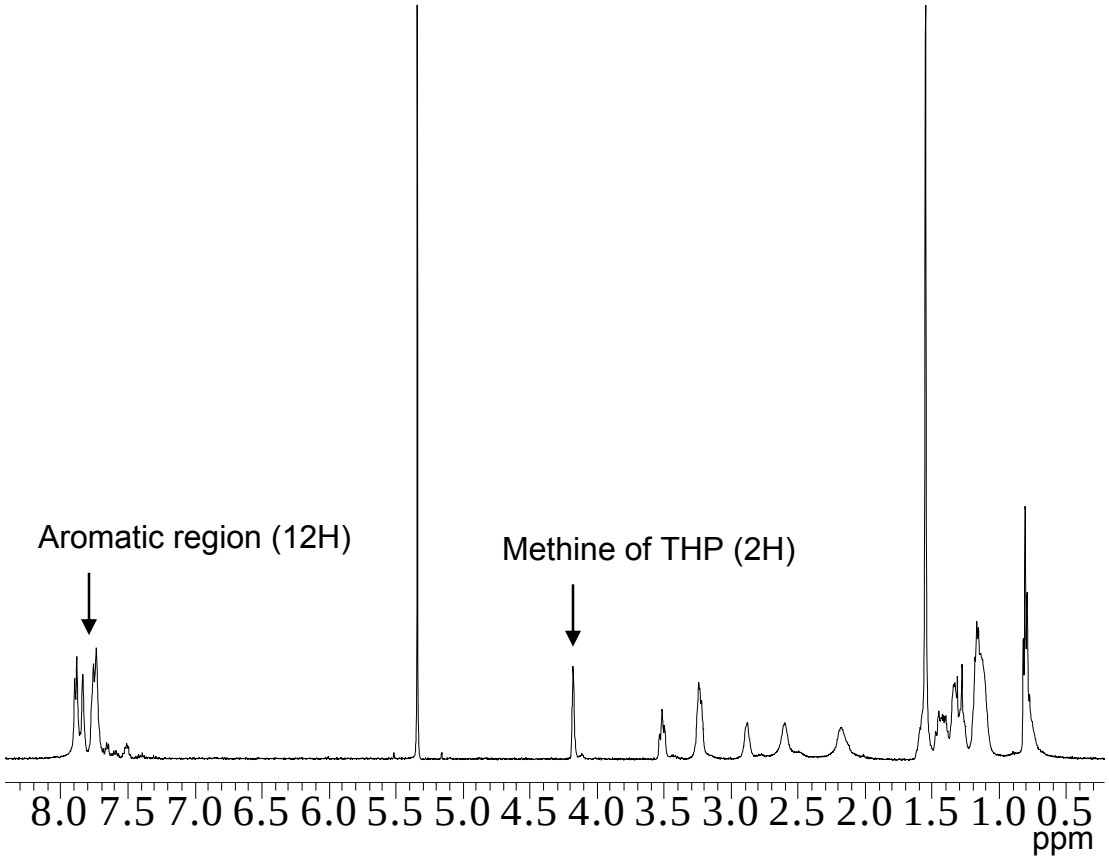

**Figure S4. $^{13}C$ NMR spectrum of P2 (PTHPEF-alt-diHF) in $CD_2Cl_2$.**

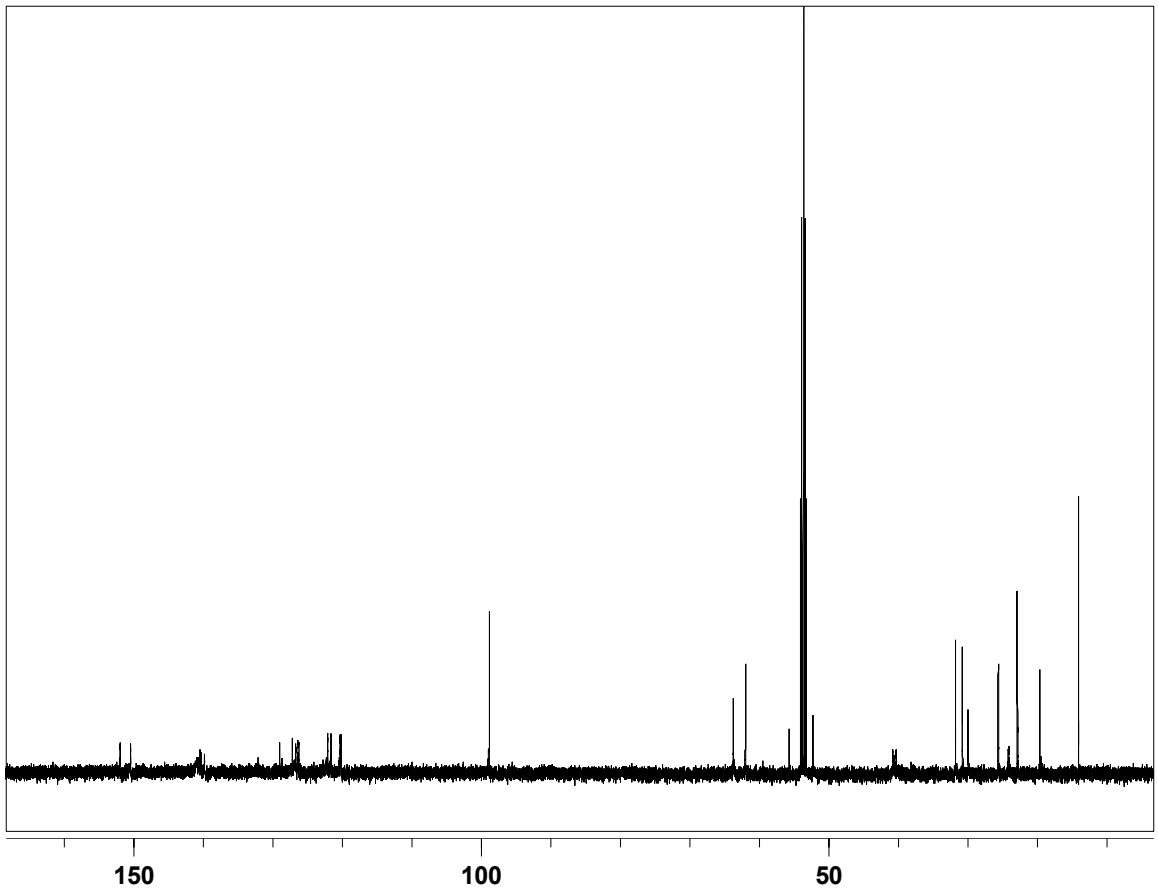

**Figure S5. $^{1}$H NMR spectrum of P3 (PTHPEF-alt-T) in $CD_2Cl_2$.**

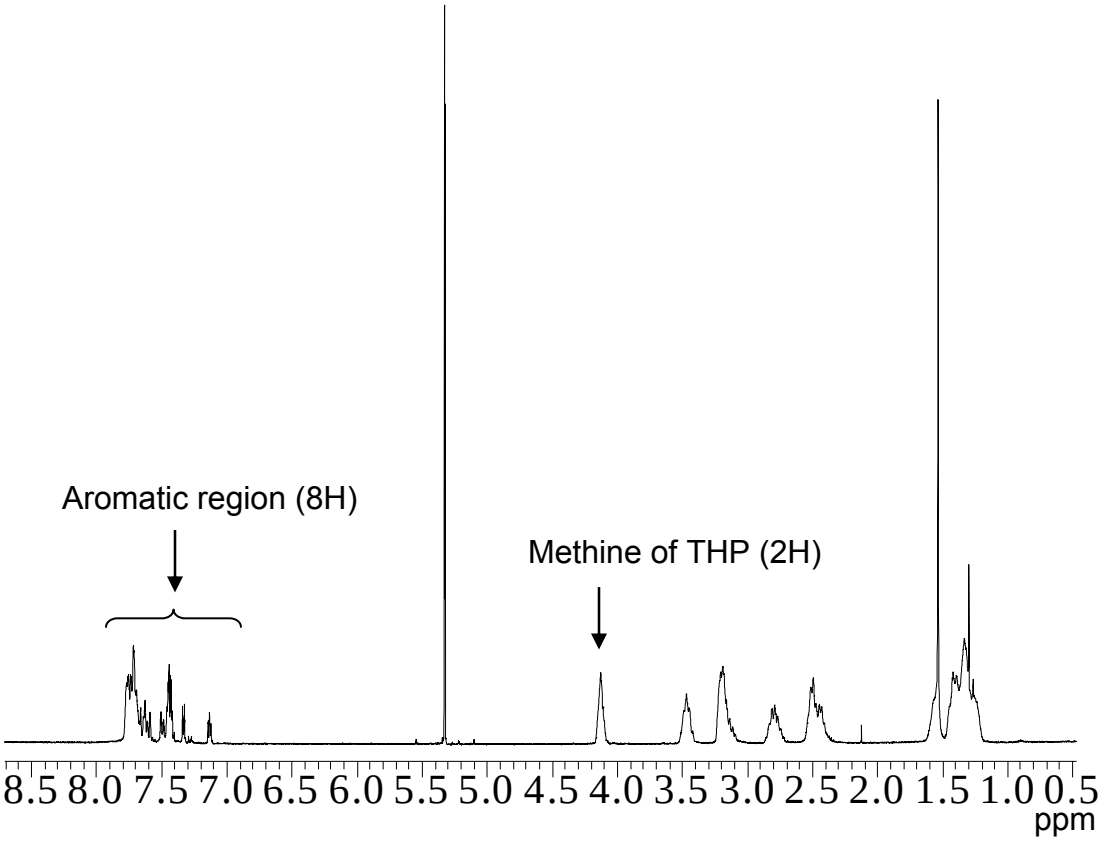

**Figure S6. $^{1}$H NMR spectrum of P4 (PTHPEF-co-THPET) in $CD_2Cl_2$.**

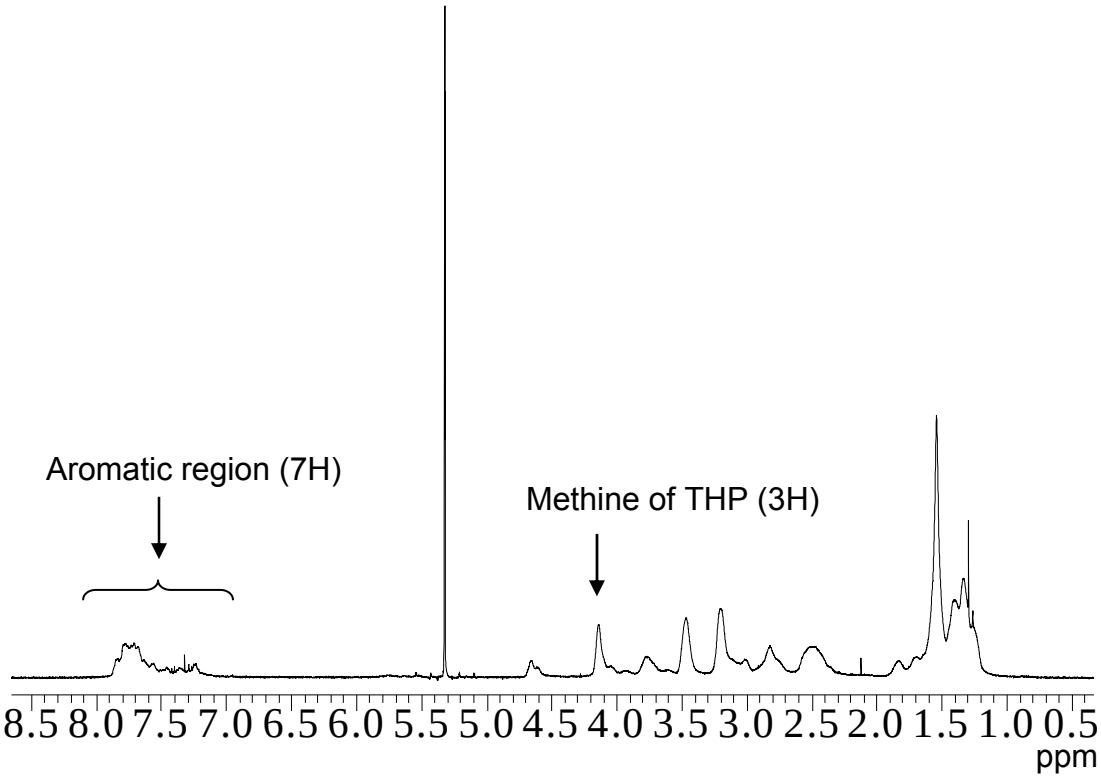

**Supporting Information of Chapter 3.**

**NMR spectra of P1-P4.**

**Figure S7. $^{1}H$ NMR spectrum of P1 in $CD_2Cl_2$.**

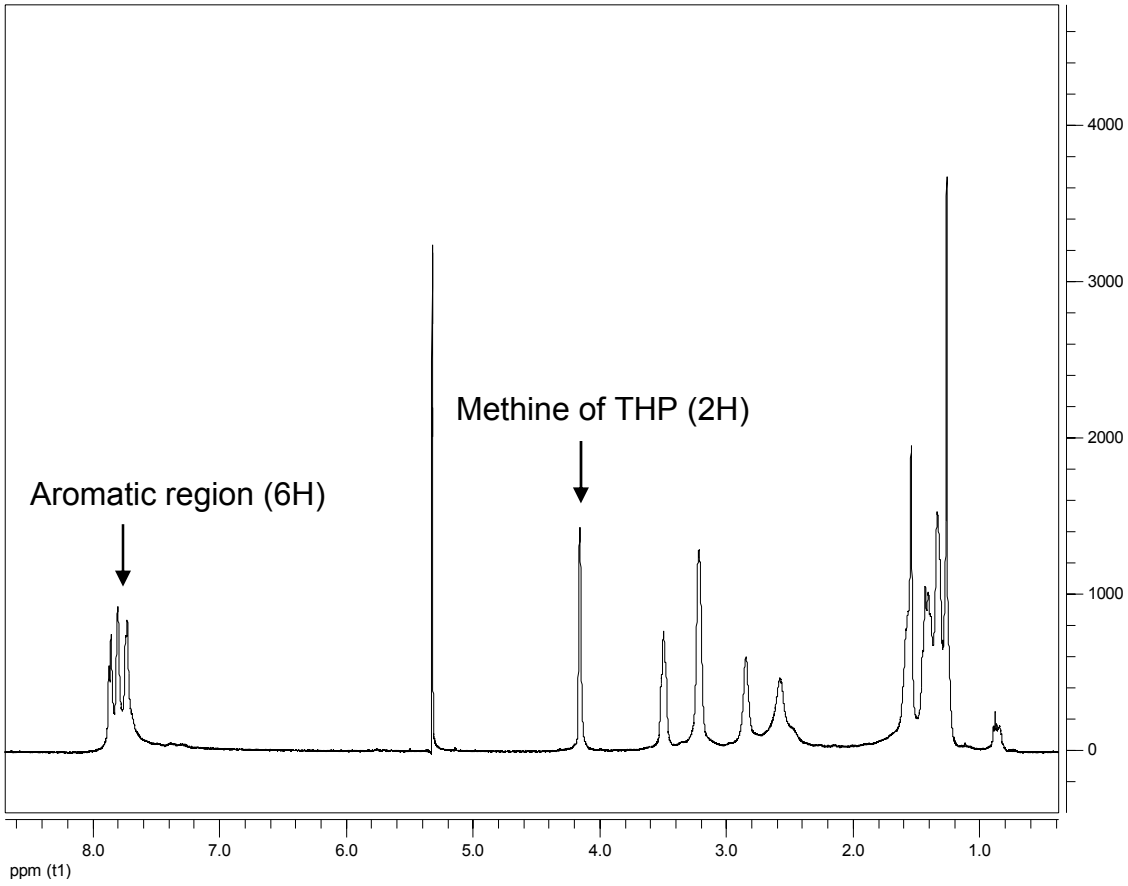

**Figure S8. $^{13}C$ NMR spectrum of P1 in $CD_2Cl_2$.**

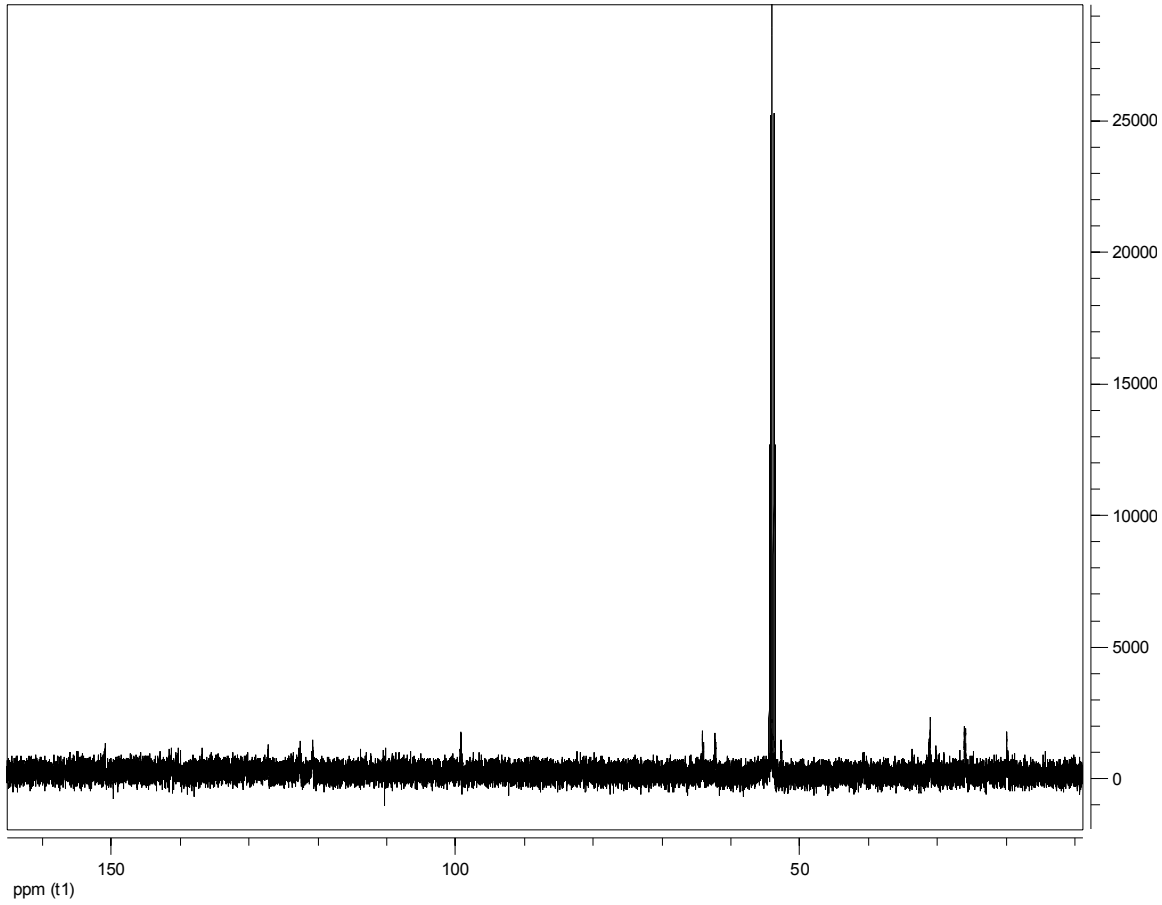

**Figure S9. $^{1}H$ NMR spectrum of P5 in $CD_2Cl_2$.**

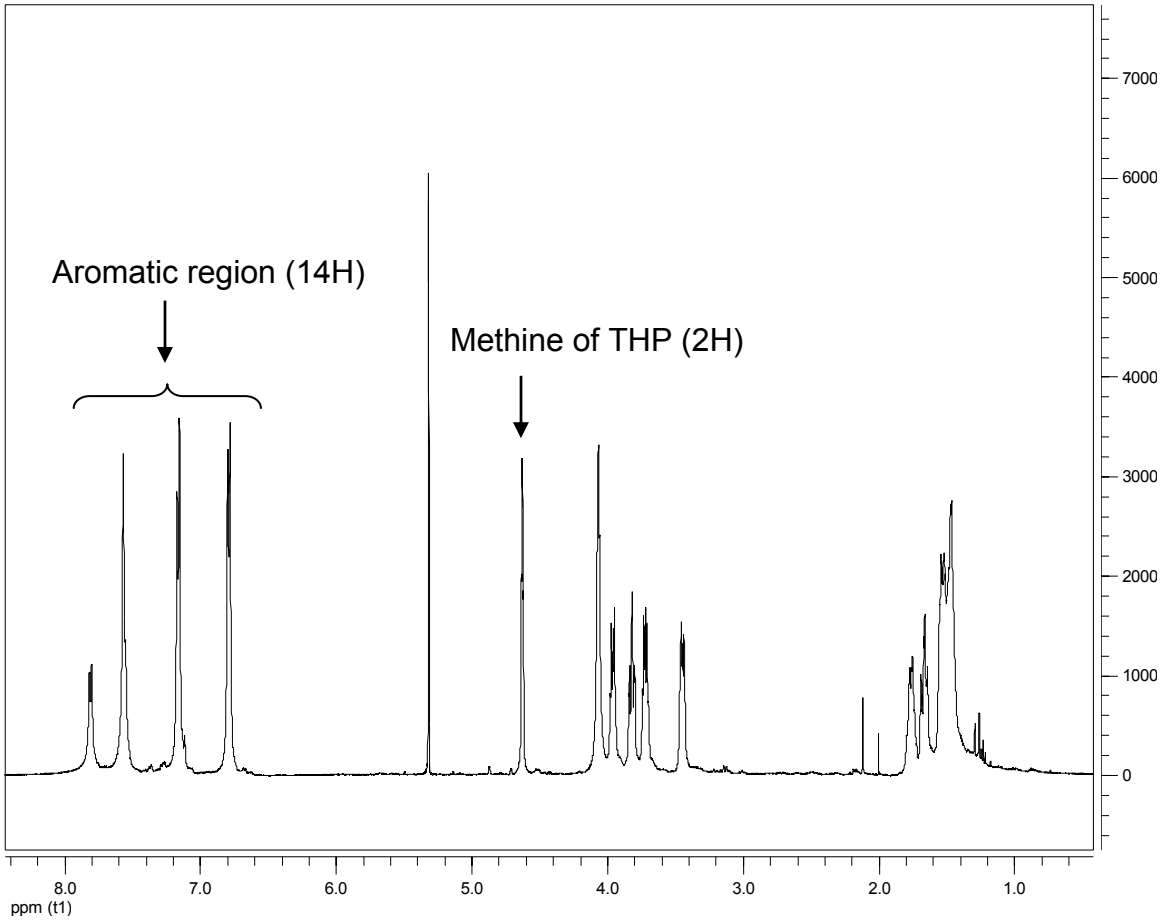

**Figure S10. $^{13}C$ NMR spectrum of P5 in $CD_2Cl_2$.**

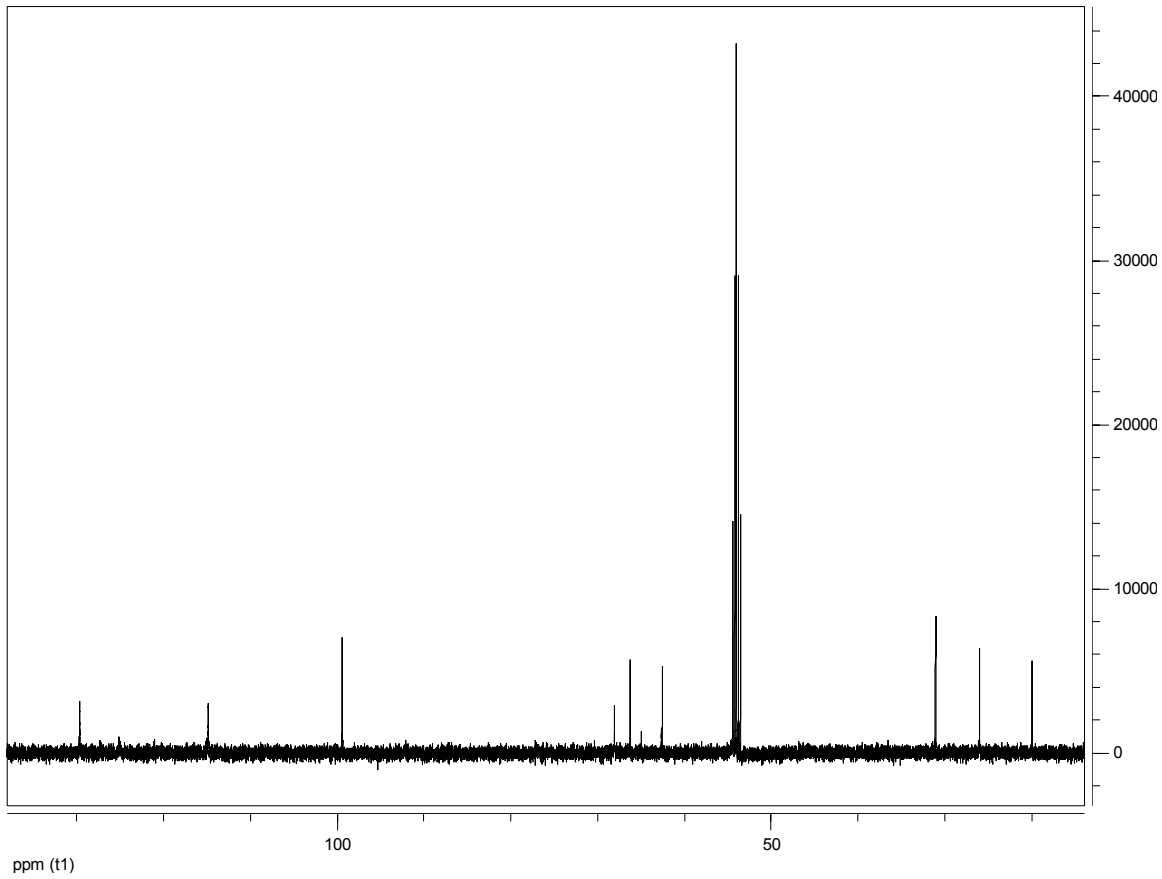

**Figure S11. $^{1}H$ NMR spectrum of P6 in $CD_2Cl_2$.**

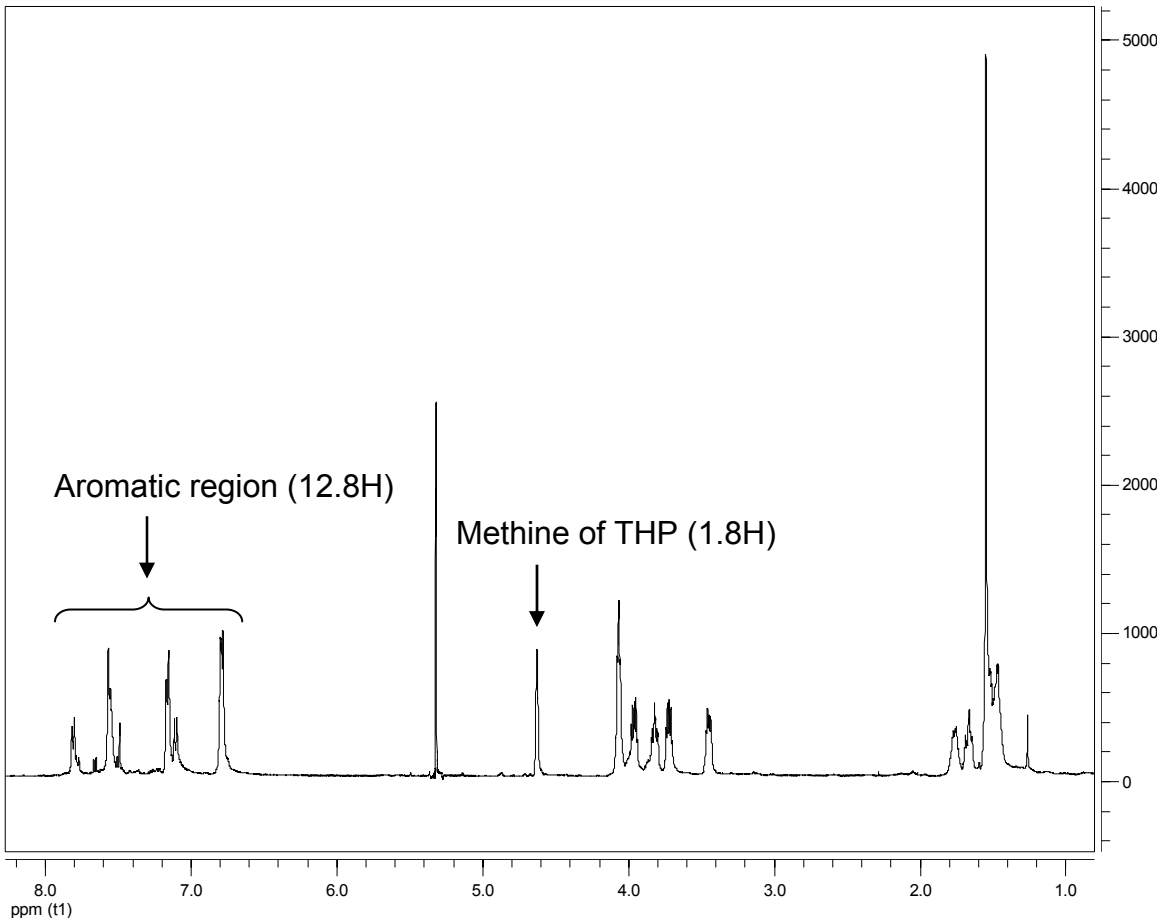

**Figure S12. $^{1}H$ NMR spectrum of P7 in $CD_2Cl_2$.**

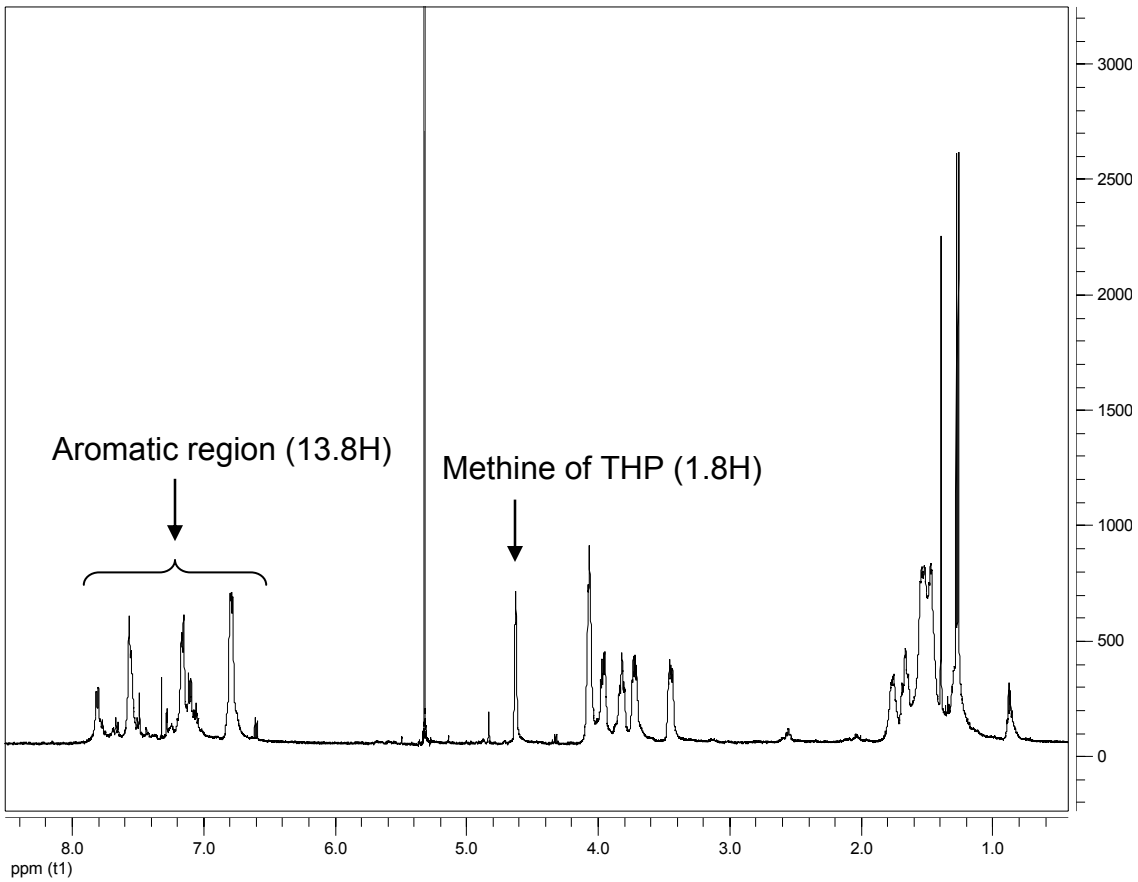

**Supporting Information of Chapter 4.**

**NMR spectrum of PTHPET.**

**Figure S13. $^{1}H$ NMR spectrum of PTHPET in $CD_2Cl_2$.**